

Doctoral thesis

Doctoral theses at NTNU, 2023:81

Chiara Zarna

Producing floor and side panels from biocomposites

NTNU
Norwegian University of Science and Technology
Thesis for the Degree of
Philosophiae Doctor
Faculty of Engineering
Department of Mechanical and Industrial
Engineering



Norwegian University of
Science and Technology

Chiara Zarna

Producing floor and side panels from biocomposites

Thesis for the Degree of Philosophiae Doctor

Trondheim, March 2023

Norwegian University of Science and Technology
Faculty of Engineering
Department of Mechanical and Industrial Engineering



Norwegian University of
Science and Technology

NTNU

Norwegian University of Science and Technology

Thesis for the Degree of Philosophiae Doctor

Faculty of Engineering

Department of Mechanical and Industrial Engineering

© Chiara Zarna

ISBN 978-82-326-5670-7 (printed ver.)

ISBN 978-82-326-5224-2 (electronic ver.)

ISSN 1503-8181 (printed ver.)

ISSN 2703-8084 (online ver.)

Doctoral theses at NTNU, 2023:81

Printed by NTNU Grafisk senter

Preface

This PhD thesis is submitted to the Norwegian University of Science and Technology (NTNU) in partial fulfilment of the requirements for the degree of Philosophiae Doctor, under the supervision of Prof. Andreas T. Echtermeyer and co-supervision of Dr. Gary Chinga Carrasco. This doctoral work has been carried out at the Department of Mechanical and Industrial Engineering at NTNU, Trondheim and in close collaboration with RISE PFI AS, between January 2020 and January 2023. This work was performed within the ALLOC innovation project (Grant no. 282310), co-funded by the Research Council of Norway and owned by Alloc AS. The consortium participants besides the already mentioned were Norske Skog Saugbrugs AS, Thor Magne Hansen og Sønn AS, Ranheim Paper & Board AS and Åbo Akademi (Finland).

Abstract

High pressure laminates for floor and wall coverings mainly consist of wood fibres and resins. Such laminates are made of a high density fibre board core and several paper sheets glued to the core to obtain a decorative, strong, and durable panel. Disposal or reuse of multi-material composite structures is challenging because the materials might not be separable. Interest in more sustainable products and industrial solutions have increased in the recent years, and similarly, regulations and laws are becoming stricter, for example on formaldehyde emissions in building materials. The present thesis aims to develop a way of producing floor and wall coverings from biocomposites by replacing, reusing and reducing material. This is to create biocomposite flooring that is more sustainable and lighter while maintaining critical properties of the current flooring laminates.

To address the mentioned issues, a biocomposite formulation, a core panel design and a manufacturing method considered to be suitable for the application were developed. Requirements for the biocomposite core were established to design the core accordingly. Biocomposite formulations of poly(lactic acid), different weight fractions of thermomechanical pulp fibres and an industrial side stream from laminate production were prepared and assessed. Different sandwich structure designs with in-plane and out-of-plane oriented cells were manufactured by 3D printing and mechanically tested. The 3D-printed core design was developed using finite element analysis. A bimodular material model was applied and fitted to capture the elastic/plastic behaviour of the 3D-printed parts under bending.

Additionally, a proof of concept of biocomposite core panels with unidirectional core stiffeners manufactured in profile extrusion was performed. Promising alternatives for the biocomposite material, core design and manufacturing method were weighted against each other using an approach adapted from systems engineering. Finally, a biocomposite core made of poly(lactic acid) and 30 wt.% thermomechanical pulp fibres, with an arched core design and manufactured in profile extrusion was demonstrated and considered to be a suitable replacement for the currently used laminate core.

Acknowledgment

Not everyone can claim that their work is pleasant. I'm grateful to be able to say that about my time at MTP and it's because of the lovely people around me. Shared doubts are half the doubts.

Therefore, I would like to thank my supervisor Prof. Andreas T. Echtermeyer (NTNU) for giving me the opportunity to do my PhD in his research group and for sharing his deep knowledge in the field of composite materials. Andreas great experience in mechanical characterisation and modelling of composite materials helped me to accomplish my goals in a well-founded way. A very special thank you also applies to my supervisor Dr. Gary Chinga Carrasco (RISE PFI) who guided and supported me constantly with his creativity and innovative thinking. He shared his great experience as a researcher in multidisciplinary projects and expanded my knowledge towards biocomposite materials and on how to do scientific research. Importantly, he always took care of me achieving my goals efficiently and in alignment with current research trends. Besides that, I am very grateful for that he not only supported me as a PhD student but also in learning Norwegian and becoming a part of RISE PFI.

I would also like to thank the laboratory technicians who contributed to my work. Their experiences were of great value for any kind of laboratory tasks. Especially Johnny K. Melbø (RISE PFI) and Børge Holen (NTNU) had an open ear and creative and practical ideas.

I thank the project partners of the ALLOC project for their kind comments and suggestions that helped me to stay on track, for the support with materials and knowledge and for providing me insights into the production of decorative laminates, paper and biocomposites.

Additionally, I am thankful for the kind and efficient administration at MTP. Among them, Ingjerd Strand, Natalia Trotsenko and Linn-Cecilie Felle Brattheim enhanced the social interaction between employees, for example by actively contributing to the Female Network MTP, an initiative launched in March 2021. Mentioning the Female Network MTP, I would also like to thank all the employees involved for making it possible to create such a network and for taking part in the activities.

Importantly, I wish to thank my great colleagues and friends who made working at MTP and living in Trondheim such a cheerful and happy time: My office mates from the Composite group Shaoquan Wang, Sondre Østli Rokvam, Victor Maneval for active support concerning work related questions. Ambra Celotto and Saveria Spiller for always having an open ear and balancing out the office work with physical training together. Pietro Foti, Emanuele Solfiti, Sara Esmaeilian, Magdalena S. Müller, Marco Maurizi, Maria L. Casasin, Nora Nyholm, Loker Xu, Anni Cao, Kinga Somló, Gabor Sziebig, Aldo Milone, Anna Ermakova and many more for having the best

coffee breaks, lunches and weekends together. Sandra Rodríguez-Fabià (RISE PFI) for spending many hours with me in the lab to get things working and sharing her experiences as a PhD student. My friends at home who remain despite long distances and make me feel like I have never left when we see each other.

A very special thanks goes to Victor André, who constantly helped me with many professional concerns and was the driving force to start this PhD studies. He is an important support and example for me and brings a lot of joy and variety to my everyday life.

Last but not least, I am grateful for my family, who always stood behind me, saw the positive side in challenging times and got me to where I am now.

Abbreviations and Symbols

Abbreviations

AR	Arched cell shape	PHA	Poly(hydroxyalkanoate)
CH	Circular-cored hexagonal cell shape	PhD	Philosophiae Doctor
CNF	Cellulose nano fibrils	PLA	Poly(lactic acid)
CO	Corrugated cell shape	S	Industrial side stream
CS	Circular-cored squared cell shape	SEM	Scanning Electron Microscopy
DMA	Dynamic Mechanical Analysis	SQ	Squared cell shape
DSC	Differential Scanning Calorimetry	T	Triangular cell shape
FE-analysis	Finite Element-analysis	TGA	Thermogravimetric Analysis
H	Hexagonal cell shape	TMP	Thermomechanical pulp
HDF	High Density Fibreboard	TMPg	TMP fibre granulate
HPL	High Pressure Laminate	TMPm	Milled TMP fibres
MEX	Material Extrusion	TR	Trapezoid cell shape
MFI	Melt Flow Index	UMAT	User Material Subroutine
MOE	Measures of Effectiveness	X- μ CT	X-ray micro-computed tomography
PBAT	Poly(butylene-adipate-terephthalate)		

Symbols

Cell wall angle	a	Cell pillar thickness	p
Sandwich panel width	b	Distance between face sheet mid planes	m
Load acting on face sheets under bending	C	Cell radius	R
Cell wall distance	d	Face sheet thickness	s
Bending rigidity	D	Cell wall thickness	t
Young's modulus	E_i	Poisson's ratio	ν_i
Bending stress	f_i	Yield stress	σ_i
Force	F	Yield strain	ε_i
Shear modulus	G_{ij}	Normal stress along the x-, y-, z-axis	$\sigma_{x,y,z}$
Sandwich thickness	h	Normal strain along the x-, y-, z-axis	$\varepsilon_{x,y,z}$
Bending deflection constant	K_b	Normal shear stress	$\tau_{xy,yz,zx}$
Shear deflection constant	K_s	Normal shear strain	$\gamma_{xy,yz,zx}$
Cell wall length	l	Relative density	$\rho_{rel,i}$
Span length	L	Extensional stiffness matrix	A_{ij}
Deflection	Δ		
Indicator for materials, components, properties or material direction:	i,j		
<i>Sandwich core</i>	c	0° raster orientation	1
<i>Face sheets</i>	s	90° raster orientation	2
<i>Compressive property</i>	C	<i>Out-of plane direction</i>	3
<i>Tensile property</i>	T		

Table of Contents

Preface	i
Abstract	iii
Acknowledgment	v
Abbreviations and Symbols	vii
Contents	ix
1 Introduction	1
1.1 Context and motivation	1
1.2 State of the art	3
1.2.1 Laminate flooring	3
1.2.2 Sandwich structures	5
1.2.3 Biocomposites with lignocellulosic reinforcements for 3D printing	10
1.2.4 Numerical modelling of biocomposite parts fabricated in material extrusion 3D printing	14
1.3 Problem statement	18
1.3.1 Problem description	18
1.3.2 System boundaries	19
1.3.3 Research objectives and expected results	21
2 Research methodology	23
2.1 Materials	23
2.2 Biocomposite core panel design	24
2.3 Biocomposite processing methods	25
2.4 Characterisation and analysis	29

3	Results	31
3.1	I - Reinforcement ability of lignocellulosic components in biocomposites and their 3D printed applications - A review	31
3.2	II - Influence of compounding parameters on the tensile properties and fibre dispersion of injection moulded poly(lactic acid) and thermomechanical pulp fibre biocomposites	33
3.3	III - Preparation and characterisation of biocomposites containing thermomechanical pulp fibres, poly(lactic acid) and poly(butylene-adipate-terephthalate) or poly(hydroxyalkanoates) for 3D and 4D printing	35
3.4	IV - Bending properties and numerical modelling of cellular panels manufactured from wood fibre/PLA biocomposite by 3D printing	36
3.5	V - Wood fibre biocomposite sandwich panels with unidirectional core stiffeners - 3-point bending properties and considerations on 3D printing and polymer extrusion as a manufacturing method	37
3.6	Compression tests	38
4	Discussion	39
4.1	Biocomposite material	39
4.2	Biocomposite core design	41
4.3	Manufacturing process	41
5	Conclusions	44
6	Suggestions for future work	46
	References	47
	Appendices	57
A. I	Publication I	57
A. II	Publication II	77
A. III	Publication III	97

A. IV Publication IV	113
A. V Publication V	127
A. VI List of presentations at international conferences	141

1 Introduction

The present thesis is part of the ALLOC innovation project for the industrial sector owned by Alloc As (Lyngdal, Norway). The PhD work aims to develop a core for light-weight decorative laminates with a greener profile and cost-effective processes by making use of bio-based materials. Hence, thermomechanical pulp (TMP) fibres from the pulp and paper industry and a side stream (S) from the flooring industry were assessed as reinforcement and filler, respectively. Additionally, biocomposites were developed with the intention to be used for prototyping laminate cores in 3D printing.

In the following subsections the context and motivation of the present thesis and its scope inside the ALLOC innovation project is described. The current state of the art of decorative laminates for floor and wall coverings and the use of cellular sandwich panels in this sector is provided. Additionally, a brief overview on thermoplastic biocomposites with lignocellulosic reinforcements for 3D printing applications and current numerical modelling approaches for predicting mechanical properties of biocomposite structures fabricated by 3D-printing are given.

1.1 Context and motivation

Nowadays plastics are ubiquitous because they offer many benefits concerning manufacturing and usage. Plastics in general are lightweight, stable, durable, versatile, and offer a high degree of design freedom. In 2019, 368 million tons of plastic were produced globally. 50.7 million tons of the plastic were demanded in Europe and 20.4% of this in the building and construction industry [1]. The building and construction industry is accordingly the second-biggest end-marked user of plastics after the packaging industry. After the product-life-time plastic waste is either collected and used for energy recovery, recycled, stored in landfills or enters the environment. Indeed, the amount of recycled plastics increased in the last few years but in 2018, 25% of collected plastic waste was still stored in landfills [1] and uncertain amounts entered the environment. Therefore, new and innovative manufacturing methods and materials are required for durable products fabricated in large quantities with limited prospects for disposal.

In the construction sector, plastics are used for pipes, window frames, furniture, doors, floor and wall coverings, such as laminates, and much more [2]. Decorative laminates must meet high everyday requirements and must have high durability. Particularly important are the scratch and impact resistance, bending stiffness, thermal insulation capacity and acoustic properties [3].

Laminates essentially consist of a composition of wood fibres and resin, paper sheets and a dec-

orative top layer. A typical build up of a high pressure laminate (HPL) is shown in Section 1.2.1 (Figure 1). The number of paper sheets, type of resin and grade and type of wood fibres can vary according to the desired properties of the laminate [4].

Such multi-layer laminate structures made of several different materials make recycling difficult as the materials are not separable. Interest in more sustainable products and industrial solutions has increased in the recent years, and similarly, regulations and laws are becoming stricter, for example on formaldehyde emissions in building materials [5]. Another important concern of environmental impact is the emission of greenhouse gases, like carbon dioxide. For example, during the on-site construction process the carbon emission is mostly contributed by fuel consumption in the transport of heavy materials or products. The impact on the environment is influenced by several factors and is a shared responsibility. However, the selection of material and construction systems is an important challenge for designers, engineers and architects, to continuously make products and processes more environmentally friendly [1].

Resin-based products are mostly recycled by grinding them to a powder and reusing it in small amounts as fillers in new products. However, due to the energy required and the low proportion of filler in the end-product, this recycling process offers no economic or ecological benefits [6]. In contrast, thermoplastic waste of known origin and composition is much more worthwhile to recycle by its producer or specialised reprocessing companies because it is re-shapeable upon heating [6, 7]. Recycling management of the containing wood fibres is equally important and there are already successful strategies, like adding recycled paper flakes [8] or waste panel chips [9] to new manufactured fibre boards.

As mentioned above, the goal is not only to manufacture HPL from more environmentally friendly material, but also to use less material and end up with a lighter end-product. To achieve this, hollowed or porous structures can be a useful approach. Many lightweight structures are inspired by nature and especially the honeycomb structure is widely used because it offers maximum cell space with minimal use of material. The structure has evolved into many different cell shapes to meet specific requirements for certain applications, for example squared, triangular or circular shapes [10].

To manufacture thermoplastic structures, plates or profiles, common methods are for example 3D printing, injection moulding, compression moulding or extrusion. 3D printing is particularly suitable for prototyping, since it allows a high degree of design freedom and flexibility. In comparison to extrusion or injection moulding, 3D printing does not need any dies or customised tools. The major disadvantage of 3D printing compared to the other two mentioned methods is the relatively

time-consuming printing process and the decreased quality in terms of mechanical, haptic, and optical properties, caused by the layer-by-layer build-up [10].

1.2 State of the art

1.2.1 Laminate flooring

Flooring laminates are mainly composed of wood fibres and different types of resins to bind the fibres and glue the different layers together. In Figure 1, the layered structure of a typical HPL is shown. A high density fibre board (HDF) is the core of the laminate. The HDF core is placed in between layers of phenol formaldehyde-impregnated kraft paper. On top is a décor paper. The décor paper is printed with a decorative look, mostly wood or stone looks. It usually contains CaCO_3 particles that provide whiteness, and smoothness and reduce the cost of the paper [11]. The décor paper is covered by an overlay. This is a melamine-based wear layer which is visually and haptic appealing and highly resistant to scratches and stains. The overlay contains ceramic particles (*e.g.*, Al_2O_3) to provide mechanical surface protection [11, 12].

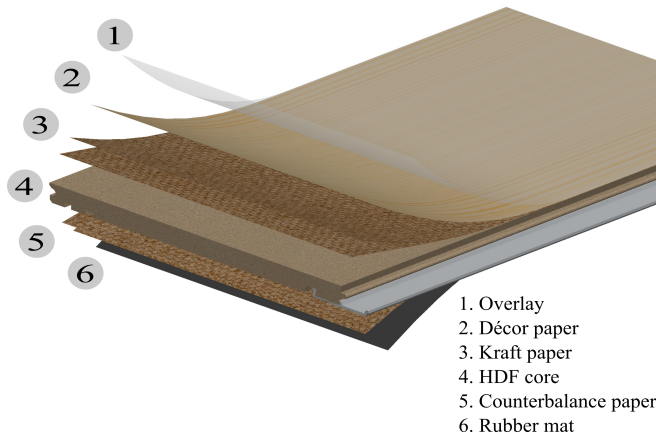


Figure 1: Schematic view of a HPL and its multi-material structure.

In the manufacturing process, the various layers are pressed at relatively high temperature and pressure (*e.g.*, 110-150 °C and 75 kg/cm²) to form a strong and durable HPL. The pressing process ensures wear resistance and secures a good appearance and topography that should be pleasant to look and feel for the end-users [11]. Afterwards, the laminate is cut to the correct size and sent to a profiling section. The HDF core of the laminate is profiled by sawing. Each of these steps yields a side stream. In the case of BerryAlloc[®] HPLs, an aluminium lock is attached through sheet

roll forming. The profiled edges and the aluminium lock ensure easy assembling and a tight and secure fit of the mounted panels [13]. The HDF and HPL production process is shown a simplified form in Figure 2. In the following, a laminate made of overlay, decorative paper and several kraft papers, which was produced by pressing, is referred to as the décor layer.

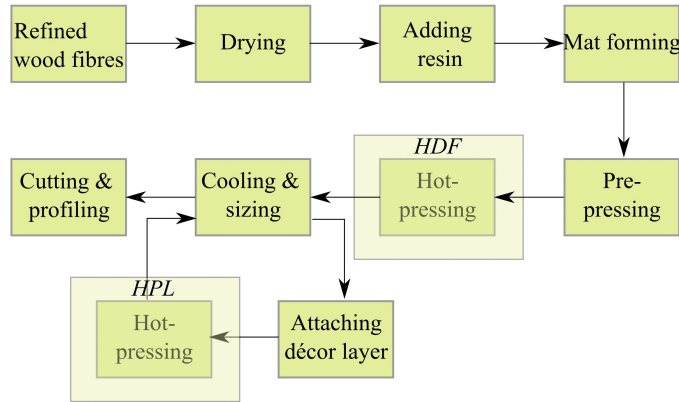


Figure 2: Flowchart of a HDF and HPL production process.

Current trends in laminate flooring point towards low or no formaldehyde emissions and high water resistance. A study on consumer preferences for wooden and laminate flooring, conducted in Sweden in 2008, suggested enhanced marketing of environmental attributes [14]. Besides, cost and look were pointed out as the most important aspects for the customers [14]. To replace resins or petroleum-based thermoplastic polymers, one of the most used bioplastics is poly(lactic acid) (PLA). This is because PLA can be mass-produced from agricultural sources, is applicable to a wide range of industries and products, and might be considered as an alternative to polypropylene or polyethylene [15]. Most of the PLA-based products in the construction industry are related to flooring. PLA involves fewer toxic substances during processing than other greatly used polymers for flooring (e.g. PVC). Ideally, PLA products can be disposed without causing adverse effects to the environment at the end of life [16].

The construction industry is one of the largest consumers of biocomposites world wide [17]. A composite can be defined as a material composed of two or more components having distinct morphology and chemistry, and giving synergetic effects. Additionally, the term biocomposite also refers to materials having at least one bio-component. Here, a component is considered a bio-component if it is obtained from natural resources and/or is considered to be biodegradable (e.g., biopolymer, lignocellulosic pulp fibres, lignin or cellulose nano-fibrils (CNFs)) [18]. Terrace flooring is the most important sales market for thermoplastic biocomposites [19].

1.2.2 Sandwich structures

Sandwich structures generally are composite structures which consist of two thin, dense, and strong face sheets and a thick, lightweight core. One well-known lightweight core design consist of periodic hexagonal honeycomb cells. It is inspired by the honeycombs found in nature. Honeycomb structure panels find their application in the automotive and aerospace industry, the construction and building industry and sports and leisure equipment. Honeycombs are closed-cell pores, often formed from thin sheets of material that are attached to each other [20].

The first patent for manufacturing a honeycomb core from kraft paper was issued in 1905 in Germany by Budwig. In 1919 sandwich panels with a honeycomb core made from balsa wood were used on the pontoons of seaplanes. From the late 1930s kraft paper honeycomb sandwich panels were also manufactured for the use in furniture. The first aluminium sandwich panels were produced around 1945, driven by the development of sufficient adhesives for the attachment of core and face sheets [20]. A typical honeycomb sandwich panel construction is shown in Figure 3.

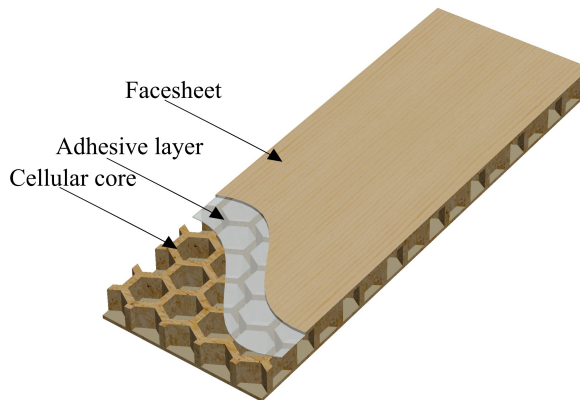


Figure 3: Illustration of a honeycomb sandwich panel.

The major reason for using honeycomb structures is to save weight and material. Hexagonal cellular structures provide a maximum cell space, by using a minimum amount of material [21]. Other reasons are to maintain smooth skin surfaces under load [20].

A cellular sandwich panel can be stronger and stiffer than a solid panel having a similar weight. However, sandwich panel constructions are often more costly than a solid panel of the same material. Honeycomb cores are worthwhile to consider whenever lightweight is a design criterion and when the skin sheets have a buckling problem [20].

Besides a hexagonal cell shape several other configurations, such as triangular, squared, or circular,

can be found in sandwich panels. For example the triangular cell structure is known for higher in-plane strength and stiffness compared to the hexagonal or squared cells [21]. Not only the cell shape influences the core plate properties, but also the cell size and the thickness of the cell walls. These attributes are often referred to as the relative density of a honeycomb core panel [22]. Relative density is the ratio of the density of a structured or porous material and the corresponding solid material density. It can be calculated considering geometric unit cells. The area of the struts is then divided by the full cell area. Examples of typical unit cells and the corresponding equations to calculate their relative density are provided in Figure 4 [21].

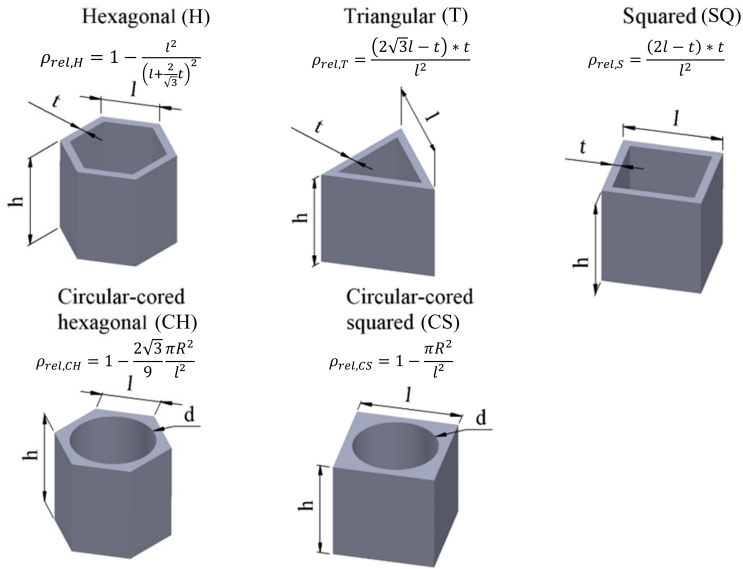


Figure 4: Relative density of different unit cell configurations for in- plane-oriented cellular structures.

Honeycomb cells in sandwich core panels are usually in-plane-orientated [23]. If these cores are rotated 90° about their horizontal axis, they become prismatic out-of-plane-orientated structures. Such structures are often called corrugated structures or longitudinal core stiffeners. A few examples of longitudinal core stiffener unit cells are shown in Figure 5.

A huge variety of cell configurations can be found in the literature [21, 24]. The here presented cell configurations are a limited selection of the most common and basic ones.

$$\rho_{rel,AR} = 1 - \frac{\pi r^2}{4h \cdot (p + R)}$$

$$\rho_{rel,CO} = 1 - \frac{\sin(\alpha) \cdot l \cdot (\cos(\alpha) + d)}{h \cdot (\cos(\alpha) \cdot l + d) + \frac{t}{\tan((180^\circ - \alpha)/2)}}$$

$$\rho_{rel,TR} = \frac{2s}{h} + \frac{t(h - 2s)}{h \cdot (\sin(\alpha) \cdot (2d + \cos(\alpha) \cdot l) + t)}$$

Figure 5: Relative density of different unit cell configurations for longitudinal core stiffeners.

The resistance to bending loads of cellular cores increases with increasing relative density provided that the skins are not changed. Additionally, the differences in load-bearing capacity of different cellular configurations get less with increasing relative density. Thus, different cell configurations might be beneficial for different relative densities [25]. Comparing panels having hexagonal and circular-cored cells, the ones consisting of hexagonal cells resist higher bending-loads when having a lower relative density (0.1), while the panels consisting of circular-cored cells resist higher bending-loads when having a higher relative density (0.6) [25]. Some typical sandwich constructions with different core types and materials are compared on their relative bending strength and rigidity in Table 1. All sandwich configurations are 2.5 mm thick and have the same density (7 g/cm³). Compared to the honeycomb panel, the foam shows greater deflection and has a lower load-bearing capacity. The stringer and extrusion panel type have thin skins which tend to buckle [20].

Core design	Designation	Relative strength	Relative rigidity
	Honeycomb sandwich	100%	100%
	Foam sandwich	26%	68%
	Structural extrusion	62%	99%
	Sheet stringer	64%	86%
	Plywood	3%	17%

Table 1: Relative bending strength and rigidity of different sandwich panel types in relation to a typical honeycomb sandwich. Modified and reproduced from [20].

The traditional ways of manufacturing hexagonal sandwich structures from sheet metal, kraft paper or fibre reinforced composites are the expansion or the corrugation process in combination with adhesive bonding, resistance welding, brazing, diffusion bonding or thermal fusion [23]. Ther-

moplastic hexagonal cell cores can be produced in several ways, including injection moulding or bonding extruded tubes to each other [26].

The expansion process (Figure 6a) is applicable for metallic and non-metallic materials. Glue lines are placed on a sheet material which is then stacked up to a certain height. The stacked block is expanded whereby the sheets are attached to each other through adhesive lines and form a hexagonal cell shape. The corrugation method (Figure 6b) is mainly applicable to metallic cores. In this process the sheets are corrugated through rolls and then stacked up into a hexagonal block. Here, thicker adhesive as in the expansion process is needed because no high-pressure loads can be applied to the corrugated sheet block. The corrugation method is further more time-consuming than the expansion method and thus more costly (Figure 6) [23].

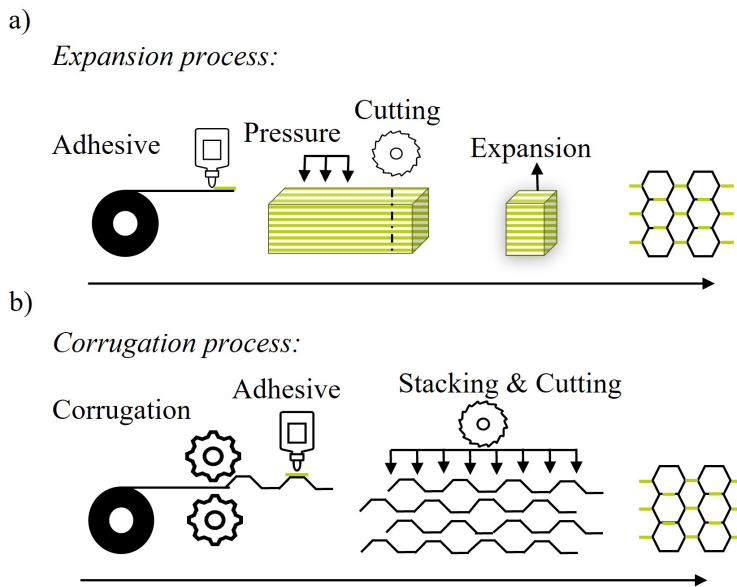


Figure 6: Schematic visualisation of manufacturing hexagonal cores. a) Expansion process and b) corrugation process.

Thermoplastic honeycomb cores can also be produced by the expansion or corrugation process in combination with heat fusion [23]. An innovative process was patented by EconCore N.V. in Leuven, Belgium [27, 28]. It is a continuous production process for thermoplastic hexagonal cores. A flat thermoplastic film is extruded, shaped to corrugated sheets via thermoforming and finally folded to honeycombs. The skin sheets are attached in-line.

In designing sandwich panels, it is assumed that the bending loads are taken by the face sheets and the shear loads by the core. It is further assumed that the facing stresses are evenly distributed and the core bending modulus is equal to zero.

A simple approach to estimate the bending stresses, rigidity, and deflection of cellular sandwich panels having two equal face sheets is presented in Figure 7 [29].

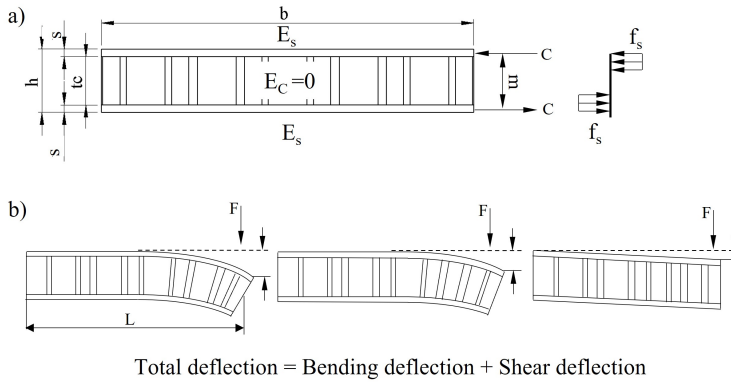


Figure 7: Illustration of a sandwich panel subjected to bending loads with the approximate bending stress distribution (a), rigidity and deflection (b) of cellular sandwich cores.

The bending stress for the upper and lower face sheet can be calculated by [29]:

$$f_s = \frac{C}{sb} \quad (1)$$

The bending rigidity of sandwich panels with facings of the same material and thickness is calculated by [29]:

$$D = \frac{E_s s_s h^2}{2(1 - \nu_s^2)} \quad (2)$$

In Equation 2 E_s is the elastic modulus of the face sheet material and ν_s is the Poisson's ratio of the face sheet material. The maximum bending deflection can be described by the sum of bending deflection and shear deflection [29]:

$$\Delta_{max} = K_b \frac{FL^3}{D} + K_s \frac{PL}{dG_c} \quad (3)$$

In Equation 3 K_b and K_s are a bending deflection and shear deflection constant. Both depend on the boundary and loading conditions of the panel and can be found in [29]. G_c is the shear modulus of the sandwich core.

Concluding, the main reason to work with cellular sandwich panels as a structural material is their high stiffness-to-weight and strength-to-weight ratio. Other reasons to use honeycomb sandwich materials are, if very smooth surface appearance is desired, for energy absorbing reasons, for air directionalisation, thermal or acoustic insulation and in some cases also for economic reasons [30].

1.2.3 Biocomposites with lignocellulosic reinforcements for 3D printing

In the following biocomposites are defined as having a bioplastic matrix and lignocellulosic reinforcements. Bioplastics are considered thermoplastic polymers that are derived from biomass and/or biodegradable *e.g.*, poly(lactic acid) (PLA), bio-polyethylene (BioPE), poly(hydroxyalkanoates) (PHA), and poly(butylene-adipate-terephthalate) (PBAT) [31, 32]. Further, a strong focus is placed on lignocellulosic wood fibres, especially thermomechanical pulp (TMP) fibres.

The exploitation of the full potential of lignocellulosic fibres as reinforcement of bioplastics depends on uniform fibre distribution and sufficient stress transfer between fibres and matrix. These aspects are addressed by modification of the fibre surface, modification of the matrix and development of adequate processing methods. The strength of a biocomposite will always be limited by its weakest point. Hence, care must be taken not to weaken or damage the reinforcing fibres and fibre-matrix-interface, as may be the case during thermoplastic processing, such as *e.g.*, compounding, extruding, and pelleting [33]. Since lignocellulosic fibres have a higher aspect ratio than lignocellulosic particles, these fibres have been extensively studied for their utility as biocomposite components [34–36]. Such fibres are well implemented as a reinforcement for bioplastics and contribute some beneficial properties, such as *e.g.*, higher stiffness, strength increment, weight reduction, cost reduction, and increased sustainability [37–39]. Besides thermomechanical pulping, pulp fibres can be obtained by chemi-thermomechanical pulping or chemical pulping. Depending on the pulping process, the pulp fibres differ greatly with respect to the fibre morphology and chemistry, as seen in Figure 8 [18].

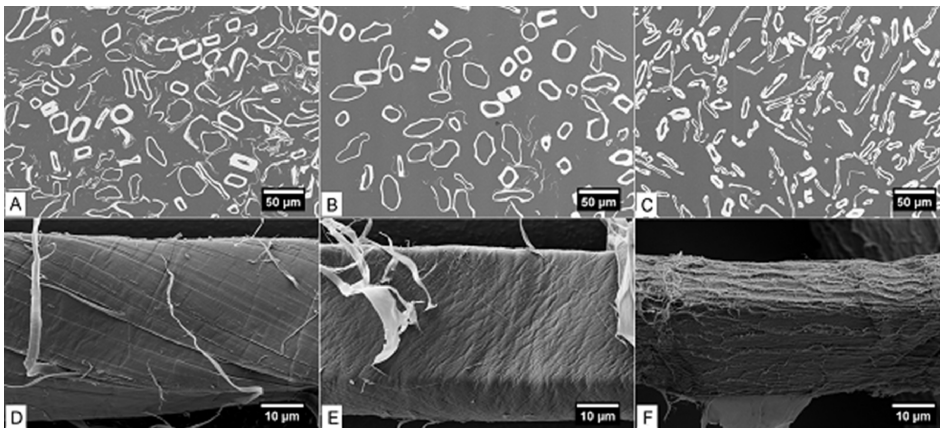


Figure 8: Transversal (upper panel) and longitudinal (lower panel) scanning electron microscopy (SEM) images of lignocellulosic pulp fibres. A and D thermo-mechanical pulp fibres. B and E chemi-thermomechanical pulp fibres. C and F chemical pulp fibres. Reproduced with permission from Jhon Wiley and Sons [40], license number: 5500650538727. Copyright (2009) John Wiley & Sons, Inc.

TMP fibres are shorter, stiffer, have a lower aspect ratio and contain more lignin compared to chemical pulp fibres [41]. Peltola et al. [41] demonstrated that TMP fibres can offer a greater reinforcing potential for PLA than chemical pulp, due to lignin on the TMP fibres surface that might act as a compatibiliser.

In biocomposite processing one major challenge is to avoid agglomeration, caused by *e.g.*, fibre-fibre interaction, fibre entanglement and the non-compatibility between hydrophilic fibres and hydrophobic matrices [42]. The compounding temperature, speed, mixing elements, repetitions of compounding and the pre-treatment of the raw materials can be varied to achieve a given biocomposite quality [18]. Lignocellulosic fibres start degrading above 200°C [43] which limits the processability of lignocellulosic fibre-reinforced biocomposites [33, 44, 45]. In general, the fibres orient according to the flow direction when *e.g.*, extruding or injection moulding. The melt flow can be influenced by temperature, speed and mould geometry [46]. This is common for various processing techniques.

To process biocomposites additive manufacturing, or 3D printing is a method for creating a physical object by layering material. It is widely used for customised production, and prototyping and when it comes to complex geometry build-ups. There exist several 3D-printing techniques that apply to polymers, composites, metals, ceramics, gels, etc. [47, 48].

Material extrusion (MEX) [49] is one out of many 3D printing techniques which is mainly used to process thermoplastic polymers and composites. MEX is probably the most affordable and most used 3D printing technique. In MEX a polymer-based material in the form of granulates or in the shape of a filament is heated to a semi-liquid phase and layer-wise deposited along a pre-defined extrusion path [48]. Figure 9 illustrates MEX 3D printing using filaments.

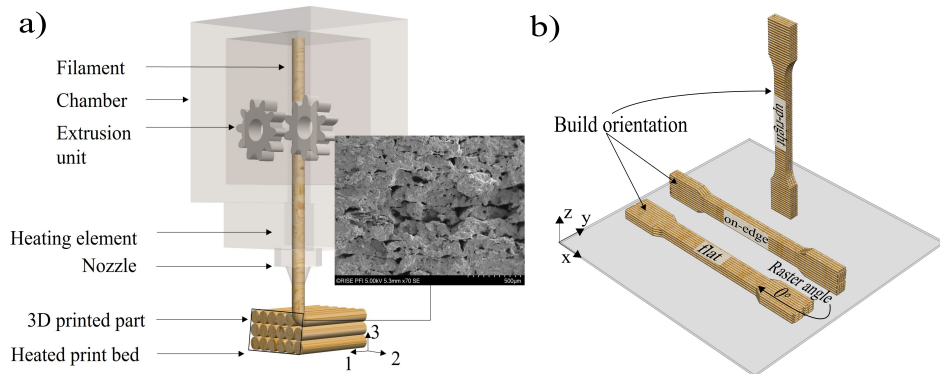


Figure 9: Schematic illustration of a) MEX 3D printing process and microscopy images with a 70x magnification of a fracture surface of a 3D-printed biocomposite part and b) different 3D printing build orientations.

The physical characteristics of MEX 3D-printed parts are highly dependent on feedstock material properties and the printing parameters: [50]:

Gap size between strands: Can be negative or positive, depending on whether the strands overlap or not.

Build orientation: Defines the direction of layer-stacking with respect to the x-, y- and z-axis (Figure 9b).

Extrusion temperature: Temperature to which the input material is heated to turn it into a semi-liquid phase.

Bed temperature: Temperature of the printing bed.

Infill density: The outer layers of a 3D-printed part are solid, but the inside can be filled with differently structured patterns in different densities. Infill density is given in percent as the ratio of material volume to part volume.

Infill pattern: Structure pattern inside the 3D-printed part, *e.g.*, hexagonal, linear, grid, triangular, etc.

Layer thickness: Height of the deposited layers along the z-axis.

Print/extrusion speed: Travel speed along the x-, y-plane while extruding the melted polymer strand.

Raster width: The width of the extruded strands that is depending on the nozzle diameter, extrusion speed and layer height.

Raster angle: Defines the strand orientation with respect to the x-axis of each layer (Figure 9b).

3D-printed parts generally yield poor mechanical properties compared to other polymer processing techniques, such as extrusion or injection moulding. This is mainly attributed to porosity caused by the layering process. Additionally, 3D-printed parts show anisotropic material behaviour, depending on the raster (polymer strand) orientation [51]. The mechanical properties of a 3D-printed part can be determined by the material properties of the filament, the void density (porosity) and the bonding strength between the deposited polymer strands [51]. The void density and bonding strength are influenced by the printing parameters: extrusion temperature, extrusion speed, layer height, raster width and gap size between the strands [18, 47].

Thermoplastic biopolymers in general show viscoelastic material behaviour. Thus, the stiffness is dependent on the strain rate. This means a thermoplastic part, exposed to higher strain rates will show greater stiffness and strength [52]. Similar observations can be drawn when a thermoplastic is exposed to colder temperatures [53]. Some physical and mechanical properties of biopolymers used in 3D printing are presented in Table 2. PLA generally has a relatively low toughness, depending on its crystallinity. Introducing wood fibres to PLA additionally reduces the toughness by creating local defects [18, 54, 55]. To enhance the toughness of wood fibre-reinforced PLA filaments, aliphatic polyesters such as PHA are commonly introduced to the biocomposite [56–59]. Amorphous PHA shows rubbery behaviour and commonly has a lower tensile strength and stiffness,

but higher elongation than PLA [56]. PBAT, a biodegradable aliphatic/aromatic copolyester, was also found to enhance the fracture toughness and processability of PLA [60–62]. It was further stated that PBAT might not lead to a drastic loss in tensile strength and stiffness [19] and showed to increase the melt flow index (MFI) of neat PLA [62].

Property	PLA [63]	PHA [64, 65]	PBAT [66, 67]
Specific gravity	1.24	1.23	1.25-1.27
Glass transition temperature	55-60 °C	-	-
Melting temperature	145-160 °C	140-160 °C	110-120 °C
Melt flow index	6 g/10 min	4 g/10 min	2.7-4.9 g/10 min
Tensile strength	60 MPa	15-40 MPa	12-45 MPa
Elastic modulus	3.6 GPa	1-2 GPa	0.7 GPa
Elongation at break	~6%	~30%	~600 %

Table 2: Physical and mechanical properties of selected biopolymers used in MEX 3D printing.

Fibre-reinforced filaments for 3D printing can strengthen a 3D-printed part but might also promote void formation due to an inadequate fibre-matrix interface and rough filament surface [47]. A high-quality biocomposite filament needs to be well compounded, and can only contain a limited amount of fibres and a limited fibre size. Otherwise the melt viscosity will increase significantly which can lead to nozzle blockage. In addition, the filament may become relatively brittle, the quality of the surface finish gets worse, and the dimensional accuracy can be reduced [18, 68]. Commercial biocomposite filaments contain up to 40 wt.% fibre loading [69]. Amorphous polymers, such as amorphous PLA are affected by warping. Warping is the dimensional change of a solidified 3D-printed part, due to residual stresses induced through rapid cooling. To reduce warping in 3D printing, process parameter optimisation is essential. Warpage is also correlated with the thermal expansion coefficient, and the difference between glass transition and heat chamber temperature [70]. Lignocellulosic fillers have been reported to reduce warping [71]. This was attributed to an increase in viscosity [18, 68, 72, 73]. A comprehensive review of the reinforcement ability of lignocellulosic components in biocomposites and their 3D-printed applications is provided in the Appendix I.

When it comes to dimensional accuracy, shrinkage is observed in the x-y-directions, while expansion is observed in the z-direction (Figure 9b). Thus, build orientation has an impact on the accuracy. It was observed that high dimensional accuracy can be achieved by setting a low layer thickness. However, many process parameters have not yet been examined for their influence on the part properties. The surface roughness can also be reduced by setting a low layer thickness.

Additionally, low extrusion temperature and print speed do contribute to a smoother surface appearance [50]. Regarding the tensile strength of 3D-printed parts, the raster orientation turned out to have a great effect. A 0° flat/or on-edge raster orientation results in the highest tensile strength. Apart from this, a low layer thickness, high infill density, high extrusion temperature and low extrusion speed are recommended to achieve the highest possible tensile strength [50]. The stiffness of 3D-printed parts is also highly dependent on the raster orientation. In accordance with laminate theory [74], a raster orientation of 0° yields a higher elastic modulus along the 0° direction than other orientations [75]. In contrast to the so far discussed part properties, the compressive strength can be maximised by increasing the layer thickness. In general, it can be stated that a higher infill density contributes to resisting higher compressive loads [50].

As mentioned previously, a 3D-printed part is generally a layout of melted filament strands, which is comparable to a composite made of lamina ply stocks. Compared to solid parts, the strength of a 3D-printed part is reduced due to bonding defects between the strands. Under the assumption of isotropic material behaviour of the filament material, the actual 3D-printed part can be regarded as orthotropic [18, 76]. Orthotropic means that a material has different properties along three axes, perpendicular to each other (1-, 2- and 3-axis). In contrast to an anisotropic material, orthotropic materials have three planes of symmetry. Note that 1, 2, 3 refer to the local material coordinate system and x, y, z to the global component coordinate system. One approach to characterise the elastic properties of 3D-printed parts, is to apply laminate theory [77]. Here, for example the modulus of elasticity is described by a weighted function of the modulus of the individual layers printed in different raster orientations. For example, if a MEX part is printed in flat build orientation (x-, y-plane) in a $0^\circ/90^\circ$ layout, the longitudinal elastic modulus (along the x-axis) will be different for the 0° layers and the 90° layers [74]. Here, the raster orientation angle is always referring to the x-axis. However, since 3D-printed parts are porous materials, the void density ρ_1 (1-, 2, plane) and ρ_2 (2-, 3-plane) must be considered. The void densities can be calculated under the assumption of a perfect geometric shape of the strands and by analysing cross-sectional microscopic images of the 3D-printed part (Figure 9). For more detailed information see [75].

1.2.4 Numerical modelling of biocomposite parts fabricated in material extrusion 3D printing

Several analytical models attempt to predict the mechanical properties of 3D-printed parts based on the void density and classical laminate theory. These models require experimental measurements, *e.g.* scanning electron microscope (SEM) images to estimate the void density, and may be restricted to specific printing parameters [51, 77, 78].

Numerical simulations can be used to estimate the mechanical properties of 3D-printed parts, based on printing parameters and material properties [51, 78–80]. Finite element (FE) analysis is a tool to simulate experiments virtually by using a numerical method. FE-analysis is widely used in *e.g.*, product development to optimise designs, processes and materials. One advantage of FE-analysis compared to experimental investigations is the potential of saving resources, such as time, costs, material, etc. However, it is necessary to validate FE models through physical experiments to make sure that the simulation provides sufficient results [81].

Various numerical analysis approaches for modelling 3D-printed parts can be found in the literature [51, 78, 82, 83], showing the high interest of many researchers in this field. An overview of some important methods and approaches is presented in this section. The focus is placed on material modelling for simulating quasi-static mechanical tests and is limited to elastic and perfectly plastic material behaviour.

An isotropic and linear elastic model can be designed based on tensile tests of 3D-printed specimens with different raster orientation angles [82]. One approach is to print tensile test specimens in flat build orientation and different raster orientations *e.g.*, 0° , 30° , 45° , 60° and 90° . As input data for the model, the mean value of Young’s modulus and Poisson’s ratio of all tested raster orientations were applied [82].

To increase the models accuracy, it might be beneficial to consider anisotropic material behaviour. For 3D-printed parts it can be assumed that the material behaviour is similar along two of the three axes, perpendicular to each other. Thus, the part can be considered as transversely isotropic (or special orthotropic). The symmetry of material properties is valid for the two transverse planes normal to the vertical axis. For example, a part, printed in flat build orientation and a 0° raster angle, is assumed as having different properties along the raster orientation (1-axis) and the directions in which the layers are stacked (2- and 3-axis in Figure 9a). In this case five elastic constants are needed to describe the constitutive material model. The Young’s modulus along the vertical axis E_1 , the Young’s modulus along the transverse axis $E_2 = E_3$, the Poisson’s ratios $\nu_{12} = \nu_{13}$, $\nu_{22} = \nu_{23}$ and the shear modulus $G_{12} = G_{23}$. The generalised Hook’s Law is written in the following matrix for 3D modelling of transversely isotropic material:

$$\begin{bmatrix} \varepsilon_x \\ \varepsilon_y \\ \varepsilon_z \\ \gamma_{xy} \\ \gamma_{yz} \\ \gamma_{zx} \end{bmatrix} = \begin{bmatrix} \frac{1}{E_1} & -\frac{\nu_{21}}{E_2} & -\frac{\nu_{31}}{E_3} & 0 & 0 & 0 \\ -\frac{\nu_{12}}{E_1} & \frac{1}{E_2} & -\frac{\nu_{32}}{E_3} & 0 & 0 & 0 \\ -\frac{\nu_{13}}{E_1} & -\frac{\nu_{23}}{E_2} & \frac{1}{E_3} & 0 & 0 & 0 \\ 0 & 0 & 0 & \frac{1}{G_{12}} & 0 & 0 \\ 0 & 0 & 0 & 0 & \frac{1}{G_{23}} & 0 \\ 0 & 0 & 0 & 0 & 0 & \frac{2(1+\nu_{12})}{E_1} \end{bmatrix} \cdot \begin{bmatrix} \sigma_x \\ \sigma_y \\ \sigma_z \\ \tau_{xy} \\ \tau_{yz} \\ \tau_{zx} \end{bmatrix} \quad (4)$$

In Equation 4 ε_i is the strain in x-, y- or z-direction, respectively and γ_{ij} is the shear strain. Transversely isotropic material behaviour for modelling 3D-printed parts has been used by several researches [51, 79, 82, 83].

One method to determine all five independent elastic constants is to perform tension tests of two specimen sets with different printing configurations [83]. The authors defined the elastic properties to be equal in the 1- and the 2-direction. One specimen set was printed in the x-y-plane (flat build orientation and $0^\circ/90^\circ$ raster orientation) to determine $E_1 = E_2$, ν_{12} and G_{12} . The other specimen set was printed normal to the x-z-plane (up-right build orientation and 0° raster orientation) to determine E_3 , ν_{13} and G_{13} [83]. The elements orientated parallel to the x-y-plane were referred to as the material data obtained from the specimens printed in flat build orientation, while the elements orientated along the z-axis were referred to as the data obtained from the specimens printed in up-right orientation.

Considering a 3D-printed part as construction of thin layers, plane stress can be used to model one single material layer in a local coordinate system (1, 2, 3) [79]. The independent constants of the stiffness matrix are then reduced to E_1 , E_2 , ν_{12} and G_{12} (compare Equation 4). The authors performed three uni-axial tensile tests numerically. One with the 0° raster orientation to determine E_1 and ν_{12} , one with a 90° raster orientation to determine E_2 and a third test with a raster orientation of 45° to determine G_{12} . Considering a symmetric layup (identical lamina thickness and raster orientation above and below the mid-plane), the elastic modulus along the x-axis of a laminate (or 3D-printed part) can be calculated from [84]:

$$E_x = \frac{A_{11} - \frac{A_{12}^2}{A_{22}}}{h} \quad (5)$$

In Equation 5, A_{ij} is one of the extensional stiffness matrices, containing information about the raster orientation of each lamina and h is the lamina layer thickness. For more detailed information regarding the calculations and laminate theory see [74] and [79].

Another way to obtain the five elastic constants is to model the mesostructure of a 3D-printed layer and perform mechanical tests numerically. In this approach, an isotropic material model for the filament material can be used. This is a two-step modelling process. Firstly, one lamina was modelled from a periodic pattern of elements, representing the mesostructure of the 3D-printed part (Figure 10), considering isotropic material behaviour. Secondly, five elastic constants were determined by applying different strain conditions to the 3D mesostructure model [79, 80]. The output data from the mesostructure analysis was used for creating a transversely isotropic and homogeneous material model [79].

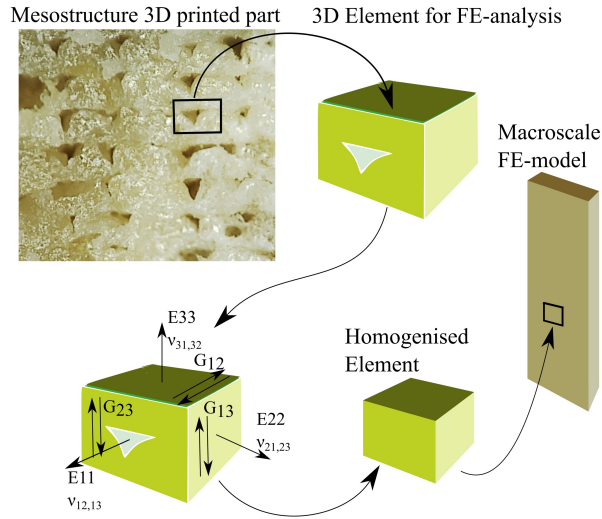


Figure 10: Mesostructure of a 3D-printed part and representative volume element for FE-analysis.

Thermoplastic materials are known for having non-linear elastic behaviour, due to their viscoelasticity. Viscoelastic material shows elastic and viscous characteristics under deformation which can be described by the storage and loss modulus [51]. Models for simulating the response of a hyper-elastic material, such as semi-crystalline thermoplastic polymers are for example, the Yeoh model, Ogden model or Marlow model. The Marlow model is calculated based on experimental uni-axial tensile test data. Thus, no curve fitting needs to be done by the user. The Marlow model was shown to not only give good results for uni-axial load cases but also for more complex ones such as for example 3-point bending on injection moulded parts [85]. An overview and comparative study of these models is presented in [85].

Additionally, 3D-printed parts were shown to have elastic asymmetry [86, 87]. Elastic asymmetry means, that there is a difference between the elastic behaviour of a material when it is exposed to tensile or compressive loads. It was observed that on specimens printed in flat build-orientation

with a $\pm 45^\circ$ raster orientation, the Young's modulus was about 37% higher in tension than in compression. This was assumed to be related to voids, caused by the layer-by-layer construction. The voids get reduced under compression, which changes the load capacity of the material and may lead to softer material behaviour than observed under tensile loads [86]. To model such a material, a bimodular elasticity model can be applied [86]. For numerical modelling of isotropic bimodular elasticity, three elastic constants were needed: The elastic modulus in tension, the elastic modulus in compression and the Poisson's ratio. The compliance matrix in Equation 4 is then written with $E_1 = E_2 = E_3$, $\nu_{12} = \nu_{13} = \nu_{23}$ and $G_{12} = G_{13} = G_{23}$ for an isotropic material. Depending on the sign (negative or positive) of the hydrostatic strain, the compressive, or tensile elastic modulus was applied [87]:

$$\begin{aligned} &\text{for } \varepsilon_i \geq 0; E = E_T, \sigma = \sigma_T, \nu = \nu_T \\ &\text{for } \varepsilon_i < 0; E = E_C, \sigma = \sigma_C, \nu = \nu_C \end{aligned} \tag{6}$$

The presented modelling methods are only valid for specific process parameters. The part properties may change drastically with other raster orientations or void densities. The influence of the printing parameters is still partially uncertain and difficult to capture.

1.3 Problem statement

As mentioned above, a HPL is a structure composed of several different materials. Reusing composite materials is generally not a straightforward process because the composed materials need to be separated to be fed back into a product life cycle. In the HDF core of the HPL, phenol formaldehyde resin is used to bind its components together, separation of materials after the HPL life-time is not possible. Phenol formaldehyde resins undergo a non-reversible curing process which limits the options for the materials to be reused [6, 88]. Furthermore, formaldehyde may be emitted from the panel and might be hazardous at higher concentrations [89]. Today, formaldehyde emission of dry wood based panels (inculding HDF) should be limited to under 8 mg/100g (EN 13986, class E1). A life-cycle-analysis on wooden floor coverings from Nebel et al. [90] showed that mainly energy consumption and the use of solvents have a great impact on the environment and that these topics offer the potential for improvement.

1.3.1 Problem description

The overall problem, addressed by the present thesis, is to replace, reduce and reuse materials that are used for producing a core for a HPL, while maintaining some properties of the HDF core currently being produced. There are three major approaches for contributing to the problem

solution:

1. Replacing resin with non-toxic thermoplastic material.
2. Reducing the amount and the number of differed raw materials involved.
3. Reusing material side streams.

To solve the problem of replacing, reducing and reusing materials used to produce HPL and to apply alternative solution approaches, knowledge, and technologies must be developed, transferred and adapted from other industries or applications. The success of the approaches can be measured based on the properties of the current HPL. Additionally, involving new materials and modifying the design of the core plate requires modifications of the nowadays production process. The problem statement is visualised in Figure 11.

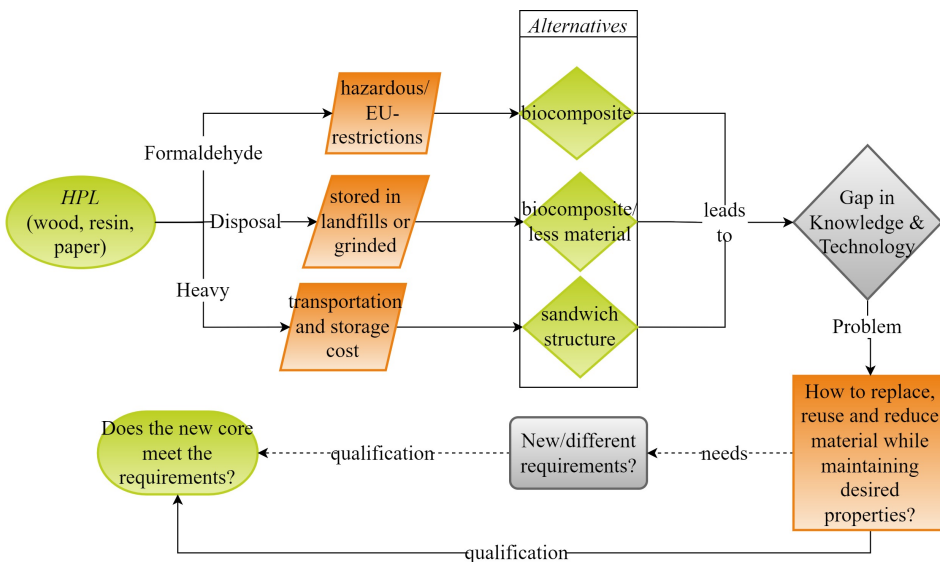


Figure 11: Problem statement of the "ALOC PhD project".

1.3.2 System boundaries

Projects are based on requirements that can change during solution finding, and new requirements can be developed while others are discarded. To evaluate requirements frequently, an understanding of the interaction between the sources of requirements and their environment should be gained [91]. A visualisation of the contextual environment of the ALOC project is shown in Figure 12. This thesis is limited to the "ALOC PhD project" and is dependent on data and information about production and accessible material from the organisational environment as well as from the external

environment. The organisational environment provides general standards and specifications which can be regarded as baseline requirements for the new biocomposite core. Further, the fibre material selection is limited to TMP fibres, and the manufacturing process is required to be as efficient as possible. In this context efficient means time and cost-efficient and integrable into the HPL manufacturing process. When looking at the production process of HPL (Figure 2), the HDF core is affected by "Attaching décor layer" and "Cutting and profiling". The "ALLOC PhD project" is limited to the processing steps directly affecting the HDF core.

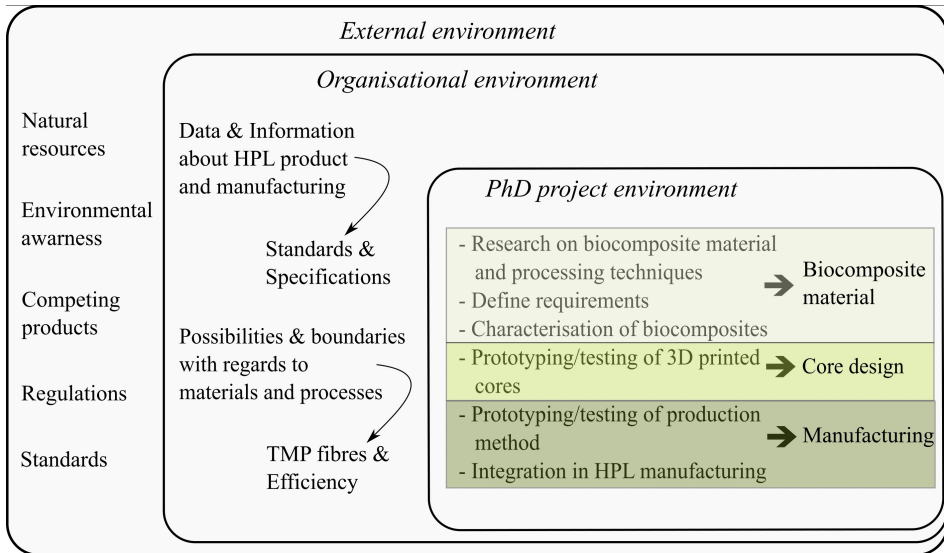


Figure 12: Visualisation of context for the ALLOC project.

The boundary conditions given through the organisational environment are presented in more detail in Table 3. They also serve as general requirements for the biocomposite core developed in the "ALLOC PhD project". The actions to fulfil the research objectives, discussed in the following section, are based on the here presented requirements.

Source	Characteristic	Requirement
Adapted from specification	Bending (EN 310)	Strength \geq 50 MPa Stiffness \geq 4500 MPa
	Core thickness	8 mm
Additional requirements	Relative density	50 % of current HDF
	Compression	Cell size \leq \varnothing 10 mm Strength \geq 13 MPa (EN 12369)
		3D printing
	Producibility	Injection moulding Extrusion

Table 3: General characteristics and requirements of the biocomposite core.

1.3.3 Research objectives and expected results

To evaluate the success of fulfilling objectives, Measures of Effectiveness (MOE) serve as a measurement or standard [92]. MOEs are specific properties that must be present in any potential solution to consider the solution a success. They are independent of any solution and should be able to be quantified [92, 93]. In the case of the "ALLOc PhD project", the major request is placed by the organisational environment, but also by standards and regulations from the external environment. Critical operational issues refer to the properties the system must have to function [92]. The critical operational issues are pointed out in Figure 13, such as finding a suitable biocomposite material and core design, and assessing its producibility. Solving these three issues is the expected result of the described project. Actions to address the research objectives are mentioned in the grey boxes in Figure 13. MOEs can be drafted out of the objectives and requirements (Table 4). Drafting, evaluating, applying, and revising or adding of MOEs is meant to be a circular process.

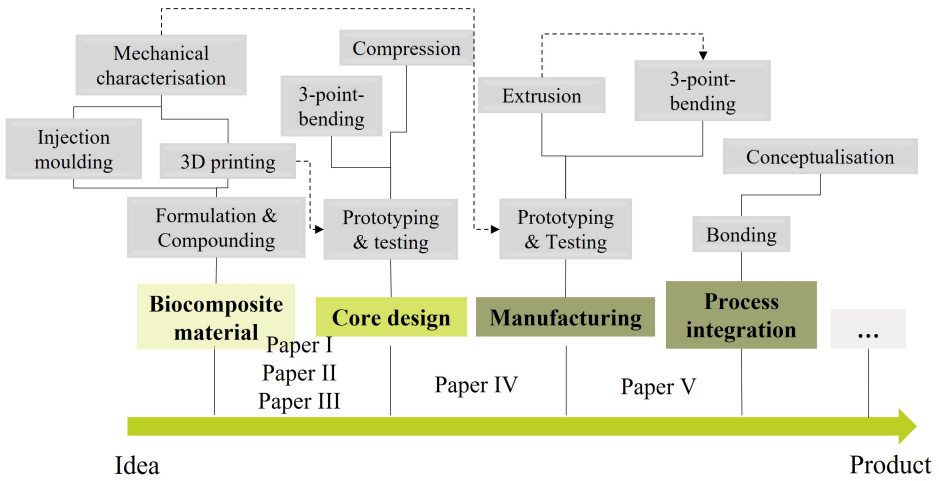


Figure 13: Critical operational issues to be solved in order to fulfil the research objectives.

The "values to achieve" in Table 4 are based on the current HDF panel characteristics and its manufacturing process. In addition, the number of research articles is a measurement of the research contribution.

Objective	Measure	Values to achieve
Suitable biocomposite material	Workable	Below 200 °C
	Mechanical properties	As stated in Table 3
	Producibility	≤ 40 sec per panel
Suitable core design	Relative density of the panel	50 % of HDF
	Mechanical properties	As stated in Table 3
Suitable manufacturing process	Efficiency	≤ 40 sec per panel
Publications	Number of written articles	≥ 3

Table 4: MOEs for the presented research objectives.

2 Research methodology

In the following the overall research method to procure the expected results outlined in Section 1.3 is presented. The materials, processes and methods used in this study are described to provide a concise overview of the research work. The cell shapes used to design the different core panels are shown in Figure 4 and Figure 5. In Figure 14 a comprehensive overview of the conducted work inside the "ALLOC PhD project" is shown. The research objectives of finding a suitable "biocomposite material", "cellular structure" and "manufacturing method" are split into several work packages that might interact with each other. Finally, these packages were evaluated based on the requirements in Table 3 that led to their rejection or acceptance.

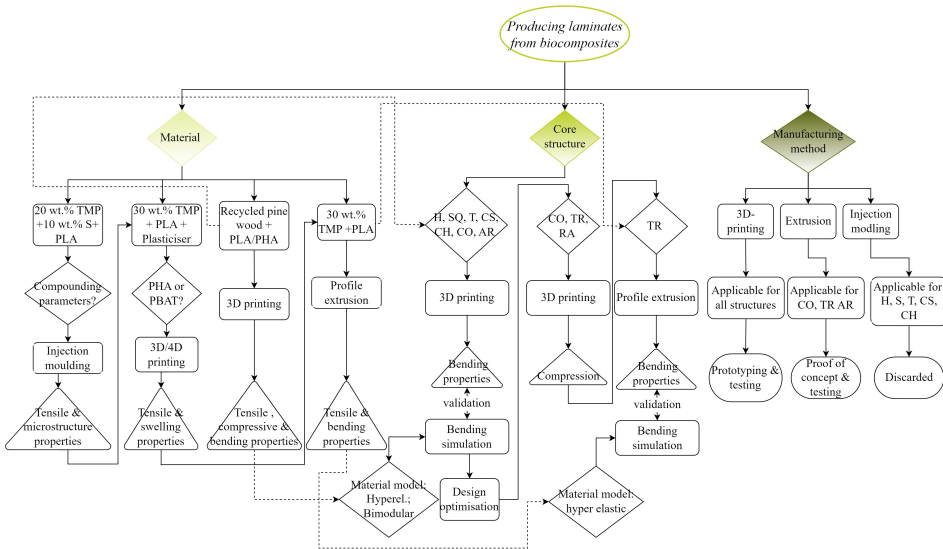


Figure 14: Flowchart to illustrate the applied research strategy.

2.1 Materials

The raw materials used in this study are presented in Table 5. PLA is used as the matrix material of all biocomposites prepared and used in this study. PHA or PBAT are added as plasticisers to increase the toughness of the biocomposite and make it 3D-printable. PLA was chosen because of its comparatively high tensile strength and stiffness and moderate processing temperature between 150 °C and 200 °C (Table 2). A blend of PLA and PHA is used in commercial wood fibre-filled filaments, such as woodFill[®] from colorFab BV (Belfeld, The Netherlands). However, the tensile strength of PHA is considerably lower than those of PLA and thus the resulting biocomposite exhibits comparatively low tensile strength as well [56]. Therefore, PBAT was chosen to be

investigated as an alternative plasticiser for wood fibre-filled filaments for 3D printing.

TMP fibres are greatly available in Norway. Considering sustainability aspects, such as energy and chemical consumption, transportation and cost-efficiency, TMP fibres are most favourable. Additionally, TMP fibres might have the potential to act as reinforcement in PLA without using any compatibilisers. This has been suspected to be due to the presence of lignin on the TMP fibres surface [41]. The side stream (S) was collected from the production plant at Alloc AS (Lyngdal, Norway). A chemical characterisation of this side stream can be found in [11].

Component	Raw material	Source	Publications
Matrix	PLA Ingeo 4043D	NatureWorks (Minnetonka, USA)	II, III, V
	PHA granulate	GoodFellow Cambridge Limited (Huntingdon, United Kingdom)	III
	PBAT ecoflex [®]	B-Plast2000 (Aurich, Germany)	III
Fibres	Spruce TMP fibre granulate (TMPg)	Norske Skog Saugbrugs (Halden, Norway)	II, III, V
	Spruce TMP fibre milled (TMPm)	Norske Skog Saugbrugs (Halden, Norway); Milled with Thomas Wiley Mini-Mill, 30 mesh.	III
Filler	Industrial side stream (S)	Sawing section Alloc AS (Lyngdal, Norway)	II
3D printing filament	PLA/PHA + recycled pine fibre woodFill [®]	colorFabb BV (Belfeld, The Netherlands).	IV, V

Table 5: Materials used in the present thesis.

2.2 Biocomposite core panel design

The biocomposite core, proposed in this thesis, is a sandwich structure consisting of a cellular core and two face sheets. In total eight different cellular core designs (Figure 4 and Figure 5) were manufactured, tested and evaluated. The design was based on the requirements given in Table 3. An overall core thickness of 8 mm, a relative density of 50 % and a maximum inner cell diameter of 10 mm to prevent imprints from point loads were required to be maintained. For calculating the relative density of the biocomposite core, the equations from Figure 4 and Figure 5 were used. However, since the biocomposite core panel is not only a cellular core but a sandwich structure the solid face sheets had to be taken into account:

$$\rho_{rel,c} = 1 - \frac{h}{h - 2s}(1 - \rho_{rel}) \quad (7)$$

To design the cellular sandwich core towards an overall biocomposite core relative density ρ_{rel} , the relative density of the cellular sandwich core $\rho_{rel,c} = 0.5$ had to be reduced to compensate for the solid face sheets. Considered examples are shown in Table 6.

Parameter	Face sheet thickness s [mm]			
	0.5 mm	1 mm	1.5 mm	2 mm
Targeted relative density ρ_{rel}	0.50	0.50	0.50	0.50
Core fraction with saving potential $\frac{h-2s}{h}$	0.88	0.75	0.63	0.50
Relative density cellular core $\rho_{rel,c}$	0.43	0.33	0.20	0.00

Table 6: Considerations on the skin thickness for the biocomposite core.

Generally, thicker face sheets would increase the bending strength and stiffness of a sandwich structure (Equations 1 and 2). Therefore, thicker face sheets were considered favourable for the biocomposite core. However, when the face sheets are 2 mm thick, the cellular sandwich core would need to have a relative density of zero to achieve the goal of an overall biocomposite core density of 0.5. This means that the face sheet thickness had to be less than 2 mm. A face sheet thickness of 1.5 mm would result in quite large cell diameters (greater than 10 mm), especially for the CS configuration. When choosing a skin thickness of 1 mm, the cell diameters of the configurations H, S, T and CH were around 10 mm (Appendix IV). Based on that a skin thickness of 1 mm and a core thickness of 6 mm were applied to all biocomposite sandwich panel configurations. The exact dimensions of the cells can be found in Appendix IV and V.

2.3 Biocomposite processing methods

Generally, four biocomposite processing methods were used (Table 7). MEX 3D printing was used for prototyping and 3-point bend testing of core designs and for producing test specimens used for mechanical characterisation of the 3D printing materials (Appendices III and IV). Specimens for tensile and compression testing were printed in the same way as the ones for 3-point bend testing with the parameters shown in Figure 15d. The 3-point bending specimen size was (42 x 6 x 8) mm (width x depth x height). Batch compounding was used for the preparation and characterisation of different biocomposite formulations that were later used in 3D printing and for preparing injection moulded tensile test specimens (Appendix II). Filament extrusion was used for preparing biocomposite filaments for 3D printing (Appendix III) and profile extrusion was used to prepare core prototypes and proof the final manufacturing concept (Appendix V).

Method	Type and Manufacturer	Publications
3D printing	Original Prusa MK3 (Prague, Czech Republic)	III, IV, V
Batch compounding	Micro compounder 15HT Xplore Instruments BV (Sittard, The Netherlands)	II, III
Injection moulding	Micro moulder Xplore Instruments BV (Sittard, The Netherlands)	II, III, V
Filament extrusion	3devo Precision 350 filament maker (Utrecht, The Netherlands)	III
Profile extrusion	ZSK 25 WLE Coperion (Stuttgart, Germany)	V

Table 7: Biocomposite processing methods used in the present thesis.

In Figure 15 the processing techniques for compounding, injection moulding, filament extrusion and 3D printing are shown. The presented parameters for batch compounding were found by performing an analysis of variance of different compounding parameters on the tensile properties of injection moulded dogbone specimens (Appendix II). In 3D printing, the commercial woodFill[®] filament was extruded with an extrusion temperature of 200 °C as recommended by the manufacturer. The filaments for 3D printing, prepared from PLA, 20 wt.% PBAT and 15 wt.% granulated or milled TMP fibres (B+TMPg or B+TMPm), was extruded at 210 °C (Appendix III). A visual assessment revealed that 210 °C yielded a smoother surface finish than 190 °C, 200 °C or 220 °C.

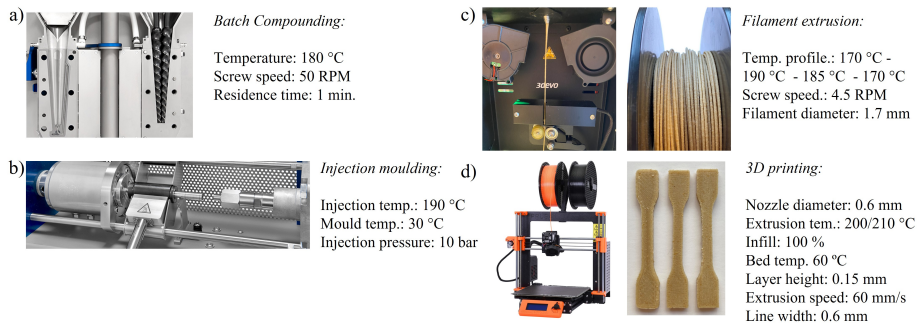


Figure 15: Biocomposite processing techniques used in this thesis a) batch compounding, b) injection moulding, c) filament extrusion and d) 3D printing strategy.

Profile extrusion was done on a twin-screw extruder. PLA and TMP fibres were compounded twice as illustrated in Figure 16. The compounding parameters were chosen based on a previous study by Le Baillif [94]. Finally, the profile extrusion was performed at a constant temperature of 150 °C for 20 wt.% fibre loading and at 170 °C for 30 wt.% fibre loading. The parameters were found by performing several extrusion iterations with different settings. Starting from the parameters used in the second compounding and systematically reducing temperature and screw speed until

a satisfying panel shape was obtained.

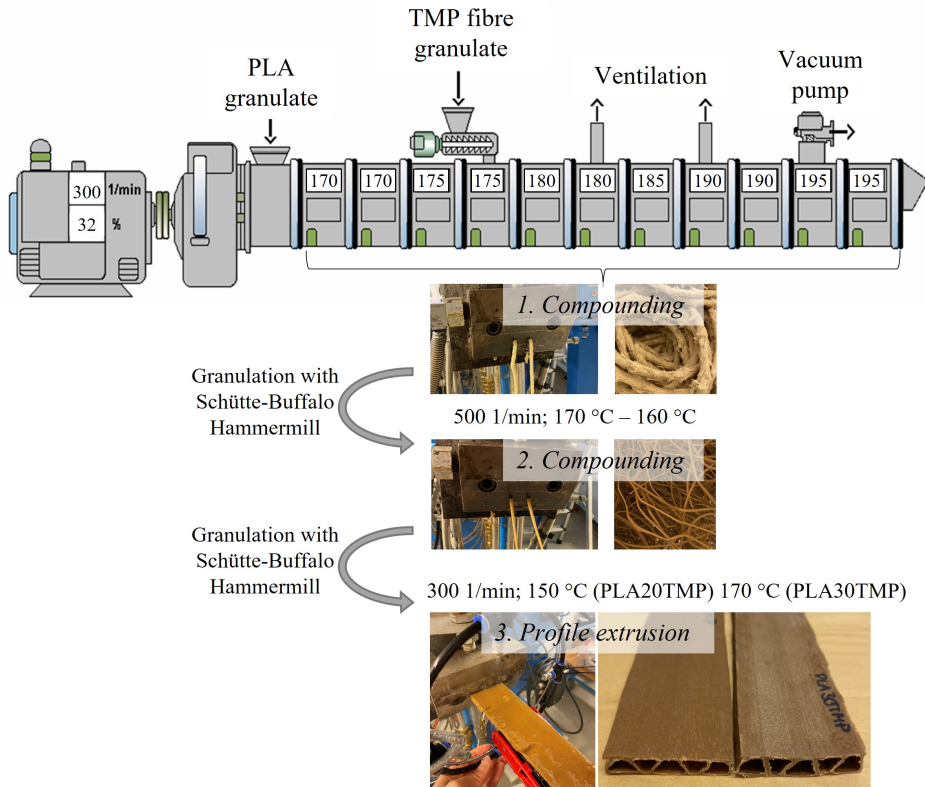


Figure 16: Profile extrusion strategy.

The extrusion tool (Figure 17) was designed after assessing the bending properties of panels having different cellular shapes, and concluding that TR resulted in the highest bending strength and stiffness (Appendix V). The tool design was based on other available tools for the ZSK 25 WLE Coperion extruder and consulting experts in this field. The decision-making will be further explained in Section 4. Additionally, a circular water misting system was implemented at the tool outlet for quick cooling and freezing of the shape of the extruded biocomposite panel.

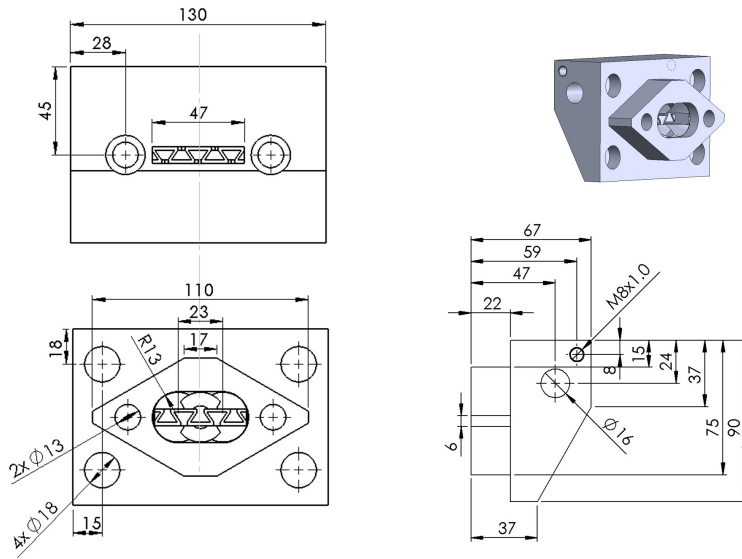


Figure 17: Extrusion tool design.

The biocomposite formulations prepared, characterised, and evaluated as potential material for the biocomposite core are presented in Table 8.

Designation	PLA [wt.%]	PHA [wt.%]	PBAT [wt.%]	TMPm [wt.%]	TMPg [wt.%]	S [wt.%]	Methods	Publi- cations
P20TMP10S	70	-	-	-	20	10		II
P+PHA	80	20	-	-	-	-		
P+PHA+TMPm	50	20	-	30	-	-	Batch com- pounding, injection moulding	
P+PHA+TMPg	50	20	-	-	30	-		
P+PBAT	80	-	20	-	-	-		III
P+PBAT+TMPm	50	-	20	30	-	-		
P+PBAT+TMPg	50	-	20	-	30	-		
B+TMPm	65	-	20	15	-	-	Filament extrusion, 3D printing	
B+TMPg	65	-	20	-	15	-		
P20TMP	80	-	-	-	20	-	Profile extrusion, injection moulding	
P30TMP	80	-	-	-	30	-		V

Table 8: Biocomposite formulations prepared and characterised in the present thesis.

2.4 Characterisation and analysis

Selected material and structural characterisation methods were used to evaluate the performance of the potential biocomposite core designs. Biocomposite materials were mechanically tested in tension and partially in compression. The melt flow index (MFI) was measured to compare the flow properties of the biocomposite formulations. MFI is an important measure to verify the suitability of a biocomposite for injection moulding, 3D printing or extrusion. Scanning electron microscopy (SEM) and X-ray micro-computed tomography (X- μ CT) were used to assess the fracture surfaces of the mechanically tested biocomposite specimens and to analyse the fibre morphology and distribution. To analyse the thermal stability of the prepared biocomposite formulations thermogravimetric analysis (TGA) and differential scanning calorimetry (DSC) were used. Dynamic mechanical analysis (DMA) was used to identify the glass transition region and viscoelasticity of selected biocomposites.

The biocomposite core panels were mechanically characterised in 3-point bending and partially in compression. This was done to evaluate if the biocomposite core fulfils the requirements summarised in Table 3. Additionally, finite element (FE) analysis was applied in order to optimise the core design towards the given requirements. This was done using the 3D-printed woodFill[®] material (Appendix IV) and extruded P20TMP (Appendix V). All materials were modelled as perfectly plastic and no damage was included. This was because in the case of the presented biocomposite

cores, yielding is considered as failure of the structure. Predicting elastic deformation and stiffness were considered to be the most critical aspects for the present application. Since additional testing would have been required to identify the yield point in thermoplastic composites and the final formulation had yet to be found, the maximum stress was assumed to be the initial yield strength in the FE analysis. The material models were validated on 3-point bending tests on different types of sandwich panels. The applied characterisation and analysis techniques and the corresponding publications are presented in Table 9.

Compression tests on 3D-printed biocomposite core specimens were not part of any publication and are therefore described separately. The tests were done on an Instron Electropulse test system (Nordwood, United States) with a 10 kN load cell. The specimens had a width of 41 mm, a depth of 30 mm and height of 8 mm. The configurations CR, AR and TR were tested with 5 repetitions each. The test speed was 1 mm/min and digital image correlation (DIC) with a system from Correlated Solutions Europe (Kassel, Germany) was used to capture the failure mode.

Method	Type and Manufacturer	Publications
Tensile testing	MTS Creterion 42 503E, 5 kN (Eden Prairie, United States)	II
	Gabo Eplexor 150, 1.5 kN (Selb, Germany)	III
	MTS Series 809, 50 kN (Eden Prairie, United States)	IV
Compression testing	Zwick Roell Zmart.Pro, 2.5 kN (Ulm, Germany)	V
	MTS Series 809, 50 kN (Eden Prairie, United States)	IV
	Instron Electropulse, 10 kN (Nordwood, United States)	
DMA	Gabo Eplexor 150, 1.5 kN (Selb, Germany)	II
MFI	Melt Flow Index - Deluxe (Faridabad, India)	II, III
TGA and DSC	Netzsch Jupiter F3 (Selb, Germany)	III
SEM	Hitachi SU3500 (Tokyo, Japan)	II, III
X- μ CT	Xradia MicroXCT-400 tomograph (Concord, California, United States)	II, III
3-point bending	METEK CS2-225, 899 N (Beijing, China)	IV
	Instron Electropulse, 10 kN (Nordwood, United States)	V
FE-analysis	Abaqus 2017 (Vélizy-Villacoublay, France)	IV, V
Statistical analysis	Minitab [®] 19.2020.1 (State College, Pennsylvania, United States)	II

Table 9: Characterisation and analysis methods used in the present thesis.

3 Results

In this section the results of the previously mentioned studies are presented briefly. The complete results and comprehensive discussions can be found in the Appendices I - V. Furthermore, compression test results of 3D printed CO, AR and TR are presented in Section 3.6 and a list of presentations at international conferences in Appendix VI.

3.1 I - Reinforcement ability of lignocellulosic components in biocomposites and their 3D printed applications - A review

Authors: Chiara Zarna, Mihaela Tanase Opedal, Andreas T. Echtermeyer, Gary Chinga-Carrasco

Journal: Composites Part C Volume 6, October 2021

Biocomposites based on lignocellulosic components (e.g. pulp fibres, nanocellulose and lignin) are of interest as sustainable replacements for thermoplastic fossil-based materials, which find their application in household items, construction, automotive, 3D-printing, etc. (Figure 18). Nanocellulose, a nano-structural component of pulp fibres, is considered having potential as a high-performance reinforcement for bioplastics, due to its high aspect ratio and potentially strong mechanical properties. Lignin, a biodegradable polymer isolated from pulp fibres, can be considered as an essential bioresource for the production of biocomposites, due to the aromatic structure and functional groups.

In this review the reinforcing ability of selected lignocellulosic components and their applicability in 3D printing is presented, considering their mechanical properties. At this point, there are challenges in processing nanocellulose that may reduce its attractiveness as a reinforcement in thermoplastic biocomposites. The objective of the review is to identify current challenges and opportunities for the application of 3D-printed lignocellulosic biocomposites.

Optimisation of 3D printing process parameters are considered to be a key to further improve the mechanical properties of the end-product. Importantly, this review revealed that greater efforts in mechanical fatigue research may contribute to assess and improve the potential of lignocellulosic reinforcements for structural applications. Details and extensive discussions can be found in Appendix I.

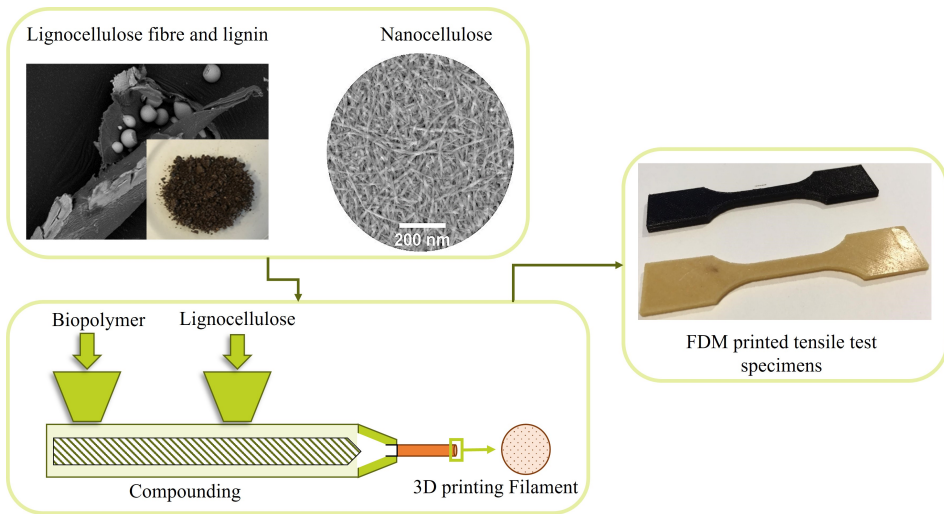


Figure 18: Lignocellulosic components as reinforcement for thermoplastic polymers used in 3D printing.

3.2 II - Influence of compounding parameters on the tensile properties and fibre dispersion of injection moulded poly(lactic acid) and thermomechanical pulp fibre biocomposites

Authors: Chiara Zarna, Sandra Rodríguez-Fabià, Andreas T. Echtermeyer, Gary Chinga-Carrasco

Journal: Polymers Volume 14, October 2022

TMP fibres can serve as renewable, cost-efficient and lightweight reinforcement for thermoplastic polymers such as PLA. The reinforcing ability of TMP fibres can be reduced due to various factors, *e.g.*, insufficient dispersion of the fibres in the matrix material, fibre shortening under processing and poor surface interaction between fibres and matrix.

A two-level factorial design was created and PLA together with TMP fibres and an industrial and recyclable side stream were processed in a twin-screw micro-compounder accordingly. From the obtained biocomposites, dogbone specimens were injection moulded. These specimens were tensile tested, and the compounding parameters statistically evaluated. Additionally, the analysis included melt flow index (MFI), dynamic mechanical analysis (DMA), scanning electron microscopy (SEM) and three-dimensional X-ray micro tomography (X- μ CT). The assessment provided insight into the micro structure that could affect the mechanical performance of the biocomposites.

The temperature turned out to be the major influence factor on tensile strength and elongation, while no significant difference was quantified for the tensile modulus. A temperature of 180 °C, screw speed of 50 rpm, and compounding time of 1 minute turned out to be the optimal setting (Figure 19). Details and extensive discussions can be found in Appendix II.

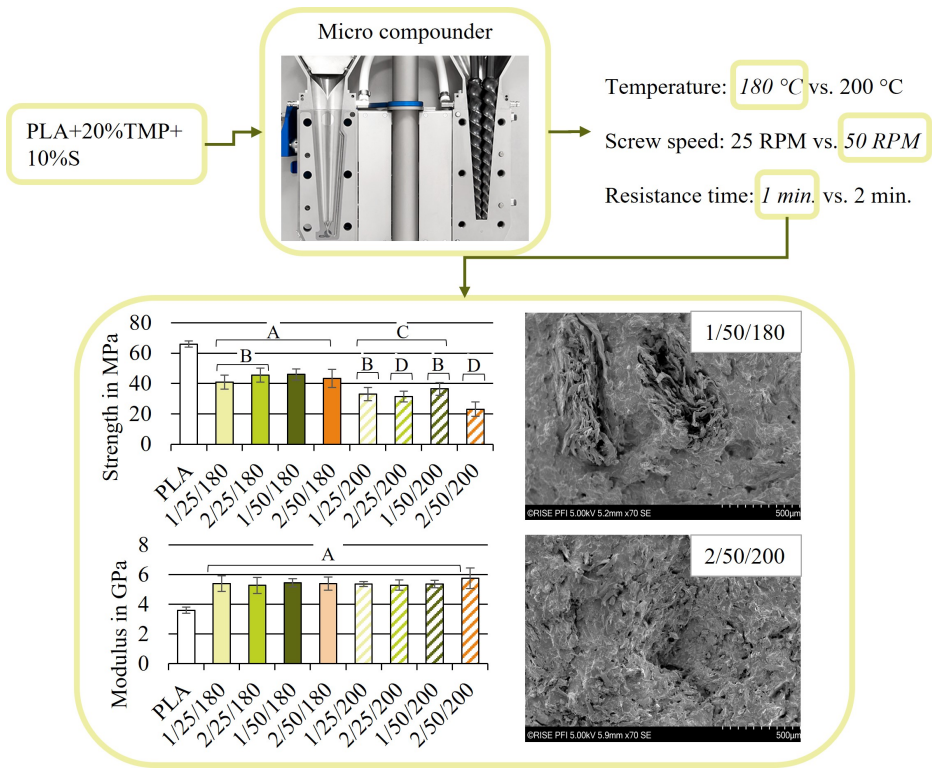


Figure 19: Tensile properties and SEM images of fracture surfaces of biocomposite specimens of PLA, 20 wt.% TMP fibres and 10 wt.% side stream compounded using different parameter settings.

3.3 III - Preparation and characterisation of biocomposites containing thermomechanical pulp fibres, poly(lactic acid) and poly(butylene-adipate-terephthalate) or poly(hydroxyalkanoates) for 3D and 4D printing

Authors: Chiara Zarna, Sandra Rodríguez-Fabià, Andreas T. Echtermeyer, Gary Chinga-Carrasco

Journal: Additive Manufacturing Volume 59, November 2022

Wood fibres are hygroscopic and swell when immersed in water. This effect can be used to create shape-changing structures in 3D printing. Hence, wood fibre reinforced filaments have the potential to be used in four-dimensional (4D) printing.

In this work, biocomposites based on granulated or milled TMP fibres and PLA were prepared and evaluated based on their tensile properties. PHA or PBAT were included in the biocomposite recipes to assess their effect on the MFI and tensile properties. Clear effects of the TMP fibre morphology on MFI were quantified. Biocomposites containing 20 wt.% PBAT turned out to be stronger and tougher than the ones containing PHA. Based on that, filaments for 3D and 4D printing were manufactured.

Interestingly, the tensile strength of 3D printed specimens containing milled TMP (TMPm) fibres was about 33% higher compared to those containing TMP fibre granulate (TMPg). Using hot water as the stimulus, the 3D printed specimens containing TMPg showed a greater reactivity and shape change compared to TMPm specimens (Figure 20). Details and extensive discussions can be found in Appendix III.

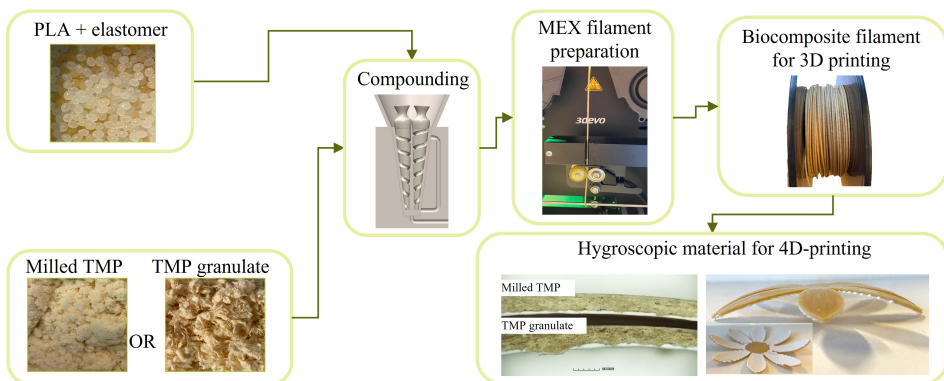


Figure 20: Compounding and filament preparation of PLA, 20 wt.% PBAT and 15 wt.% TMP fibres for 3D and 4D printing.

3.4 IV - Bending properties and numerical modelling of cellular panels manufactured from wood fibre/PLA biocomposite by 3D printing

Authors: Chiara Zarna, Gary Chinga-Carrasco, Andreas T. Echtermeyer

Journal: Composite Part A Volume 165, February 2023

The major advantage of cellular structures is the saving of material, energy, cost, and weight. Biocomposites are strong, lightweight materials and offer a high degree of design freedom. The purpose of this study was to characterise and compare the bending properties of various cellular structures for utilisation in panels made of a wood fibre/PLA biocomposite. Material extrusion (MEX) 3D printing is a highly flexible manufacturing method and well-suited for prototyping. Hence, MEX was applied to manufacture five different cell configurations that were mechanically tested.

Additionally, numerical simulations were carried out to present a tool for optimising the structures for future requirements. Two material modelling approaches, a hyperelastic and a linear elastic, bimodular model were created and validated based on 3-point bending tests. It is shown that a linear elastic, bimodular and perfectly plastic material model can adequately capture the elastic/plastic bending behaviour of the corresponding 3D-printed sandwich panels (Figure 21). Details and extensive discussions can be found in Appendix IV.

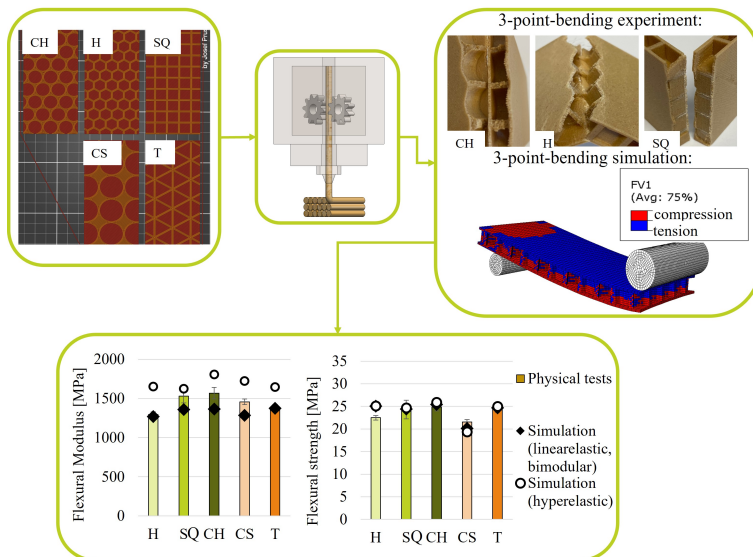


Figure 21: 3-point bending experiments and simulations of 3D-printed biocomposite core prototypes.

3.5 V - Wood fibre biocomposite sandwich panels with unidirectional core stiffeners - 3-point bending properties and considerations on 3D printing and polymer extrusion as a manufacturing method

Authors: Chiara Zarna, Gary Chinga-Carrasco, Andreas T. Echtermeyer

Journal: Composite Structures Volume 313, March 2023

Sandwich panels with unidirectional core stiffeners are known for their relatively high bending stiffness at low weight, stability under compressive and shear loads and energy absorption capability. In this study, 3D printing was used to screen biocomposite sandwich panels easily and preliminarily with different unidirectional core stiffener designs. Thermomechanical pulp (TMP) fibre-reinforced poly(lactic acid) (PLA) was used in this study.

A corrugated, trapezoid and arched cell structure were tested experimentally and numerically using a bimodular material model, accounting for different behaviour in tension and compression. The trapezoid structure showed the best flexural properties of the three 3D-printed sandwich beams. It was chosen to be explored further, manufacturing it by extrusion. Extrusion is a production process likely to be used in industry on a larger scale.

Basic material properties of the extruded sandwich were obtained from injection moulded dogbone specimens. The flexural properties of the extruded panels were measured experimentally and simulated using finite element analysis. Simulations were done with a hyperelastic material model. Predictions and experiments were in adequate agreement, allowing these kinds of simulations to be used for extruded biocomposite sandwich panels. (Figure 22). Details and extensive discussions can be found in Appendix V.

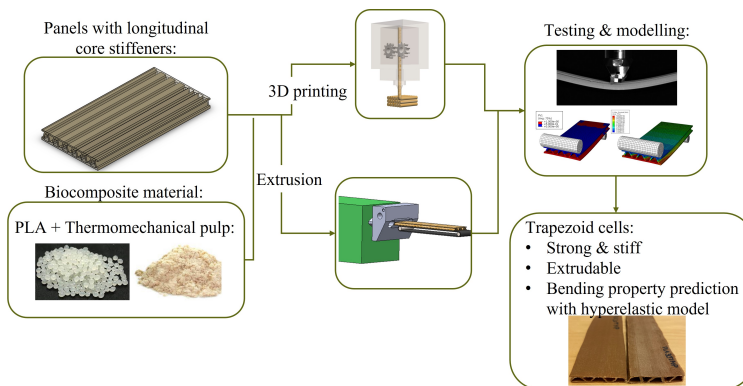


Figure 22: Preparation and testing of biocomposite sandwich panels with longitudinal core stiffeners by 3D printing and profile extrusion.

3.6 Compression tests

The results of compression tests on 3D-printed biocomposite core panels of the structures CO, AR and TR are presented in Figure 23. As already presented in Figure 14, only the three core types with unidirectional core stiffeners were chosen to be compression tested. This was because they outperformed the cellular panels from Figure 4 in 3-point bending and might offer advantages in terms of manufacturing since these structures are continuously extrudable. This will be discussed in more detail in Section 4.

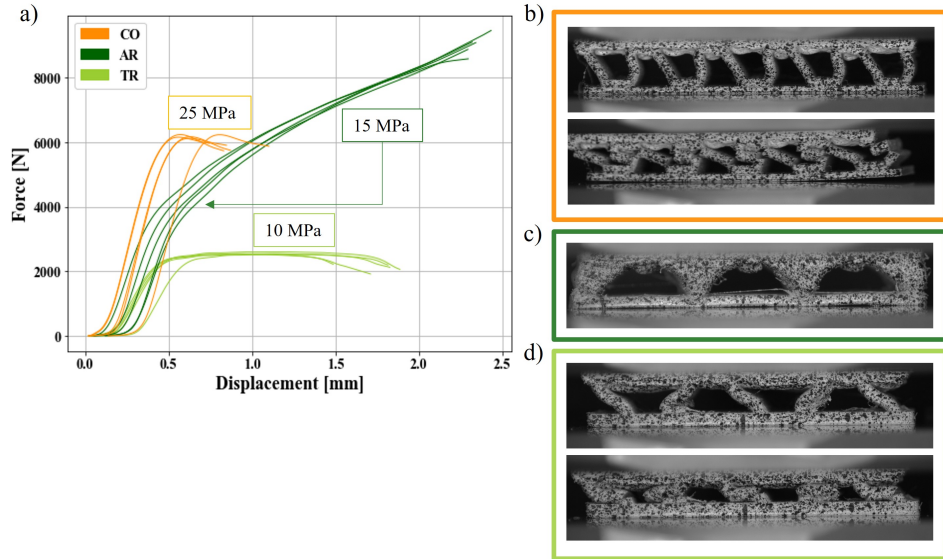


Figure 23: Results of compression tests on 3D-printed biocomposite cores. a) Force-displacement curves, b) corrugated (CO) core at failure, c) arched core at densification and d) trapezoid core at failure.

As seen in Figure 23a and b, CO resisted the highest compression loads compared to the other tested biocomposite cores. However, after reaching the maximum load the struts buckled and collapsed. TR (Figure 23d) was the weakest core configuration with a maximum compressive strength of 10 MPa. The failure was similar to CO, but since the struts of TR were longer and the angle α was less, the struts formed a sort of "S-shape" and sustained more deflection before collapsing than CO. AR did not collapse but densified after reaching its maximum compression load bearing capacity. The minimum required compressive strength of the biocomposite core is 13 MPa (Table 3). CO and AR 3D printed from woodFill[®] met this requirement. AR did not collapse due to its arched cells. The pillars were not angled and were wider than the struts of CO and TR. The arch shape improved the stress distribution along the cell walls, while in CO and TR stress concentrations might have arisen at the connection areas between core and face sheets.

4 Discussion

In this section, the process of decision-making to find a suitable solution for producing floor and side panels from biocomposites is discussed. Several biocomposite materials were investigated, potential biocomposite core structures were tested and a proof of concept for manufacturing of panels with unidirectional core stiffeners in profile extrusion was presented. Considering all obtained results, decisions must be made that are a comparison between alternatives and then choosing the option providing the most desirable outcome. Thus, a trade-off is always done when deciding [95]. The trade-off process can be described through the following steps [96]:

- Identification of alternatives: Providing a set of alternative candidates that potentially meet the essential requirements (Section 2).
- Sensitivity analysis: Prioritisation of MOEs (Table 4) and candidate ratings.
- Decision making: Documentation of data and reasoning.

4.1 Biocomposite material

According to Table 4, the biocomposite material for the core is desired to be more sustainable than the current material, have sufficient mechanical properties to meet the previously presented requirements, and it must be processable with conventional polymer processing techniques. Among the assessed recipes, three material alternatives were considered to meet the objectives: P20TMP10S, P+PBAT+TMPg, P30TMP (Figure 14). Only these three biocomposite formulations were considered for the decision-making because they had the highest fibre loading (30 wt.%) which is expected to increase the sustainability, decrease the weight, and increase the stiffness of the material. Further, only granulated TMP fibres were considered because milling is an additional process. Avoiding additional processing steps might be beneficial with respect to manufacturing time, and the sustainability of the final product. The alternatives then require an assignment of value ratings and can be compared in a trade-off matrix (Table 10) [96]. The score is rated from 1 to 5, where 1 is the lowest and 5 is the highest score.

Criteria	Weight	P20TMP10S		P+PBAT+TMPg		P30TMP	
		Score	Weighted score	Score	Weighted score	Score	Weighted score
Sustainability	3	4	12	3	9	5	15
Mechanical properties	5	2	10	3	15	4	20
Processability	4	4	16	3	12	3	12
Sum			38		36		47

Table 10: Trade-off matrix for the manufacturing process.

The mechanical properties were assigned the highest rating followed by processability and sustainability. This was because the biocomposite quality, including the resistance to loads, was considered most important because this requirement directly affects the customer. The highest tensile strength and stiffness were measured for P30TMP (69 MPa and 6.7 GPa). However, the material is relatively brittle with an elongation at break below 2%. Adding plasticiser such as PBAT (P+PBAT+TMPg) improved the toughness (elongation at break \sim 3%) but decreased the tensile strength and stiffness (40 MPa and 4 GPa). P20TMP10S had an intermediate tensile strength but the lowest toughness (elongation at break \sim 1%) and therefore got the lowest score for its mechanical properties.

The material must be processable with a conventional method such as profile extrusion. To evaluate the processability the MFI was measured, and profile extrusion trials were conducted. Extrusion of P30TMP was challenging since the TMP fibre reinforcement inhibited the flow properties (Appendix V). The MFI of P30TMP was measured to be below 1 g/10min [11]. Higher MFI values may not be of major concern in profile extrusion, but are desirable since formulations with a higher MFI require less energy to be processed and might therefore be less susceptible to degradation [97]. The highest MFI (\sim 5 g/10min) was found for P20TMP10S (Appendix II). Therefore, P20TMP10S got the highest score in processability.

Both, P30TMP and P20TMP10S got the highest score for sustainability because TMP fibre and S are obtained from local resources and in combination with PLA, no compatibiliser is necessarily required [41]. In P+PBAT+TMPg, PBAT is added as a plasticiser. Blending multiple materials includes additional processes when preparing the biocomposite. Additionally, the side stream in P20TMP10S might not always be consistent and may lead to inconsistent biocomposite properties. Therefore, the sustainability score is lower than for the other biocomposite formulations.

4.2 Biocomposite core design

The core design was required to aim for a relative density of 0.5, it must be producible in an efficient way and meet the required mechanical properties. In Table 11 the two design alternatives sandwich with cellular core (H, S, T, CS, CH (Appendix IV)) and sandwich with unidirectional core stiffeners (CO, TR, AR (Appendix V)) are compared to each other.

Criteria	Weight	Cellular core		Unidirectional core stiffeners	
		Score	Weighted score	Score	Weighted score
Producibility	4	3	12	5	20
Relative density	3	5	15	5	15
Mechanical properties	5	4	20	4	20
Sum			31		55

Table 11: Trade-off matrix for biocomposite core design.

In terms of mechanical properties, both designs received the same score, as the cores with unidirectional stiffeners had a higher flexural strength (~ 30 MPa) and stiffness (~ 2 GPa) than the cellular core panels (~ 25 MPa strength and ~ 1.5 GPa stiffness), but they were potentially more sensitive to compressive loads. The bending properties were obtained from 3D-printed specimens.

The main advantage of the core with unidirectional core stiffeners over the sandwich with the cellular core was its producibility. Such biocomposite panels were shown to be producible using continuous profile extrusion (Appendix V). It was assumed that profile extrusion is one of the most efficient methods to manufacture biocomposite sandwich panels. Sandwich panels with the core designs H, T, S, CH or CS cannot be produced in profile extrusion. Injection moulding could be an option, but at least one of the face sheets would need to be attached in the following production step. The desired relative density can be achieved with both designs.

4.3 Manufacturing process

The objective was to find a manufacturing method to produce a biocomposite sandwich core. The manufacturing method is desired to be efficient and yield the required mechanical properties of the product. Three feasible alternatives to meet the requirements were considered: 3D printing, injection moulding and profile extrusion (Table 12).

Criteria	Weight	3D printing		Injection moulding		Extrusion	
		Score	Weighted score	Score	Weighted score	Score	Weighted score
Efficiency	4	1	4	3	12	5	20
Mechanical properties	5	2	10	5	25	5	25
Sum			14		37		45

Table 12: Trade-off matrix for the manufacturing process.

The mechanical properties considered to score the manufacturing techniques in Table 12 were obtained from physical experiments and simulations on 3D-printed and extruded cores. The flexural strength of the extruded TR core from P30TMP (44 MPa) was about 27% higher than the 3D-printed TR core. The flexural stiffness of the extruded TR core (4.5 GPa) was more than doubled compared to the 3D-printed one. No injection moulded samples could be produced and tested. However, it can be expected that the mechanical properties of injection moulded panels will differ to some extent from extruded panels depending on the polymer flow direction and corresponding TMP fibre alignment. Since in injection moulding additional bonding of the face sheets and the core would be necessary, this could be a potential weak spot in the structure.

Taking into account the different designs of sandwich cores with unidirectional core stiffeners (TR, AR, and CO) and their compression properties (section 3.6), AR is considered to be the most favourable design for the biocomposite core. The current design does not meet the required flexural strength and stiffness, but the required compressive strength was achieved. The current AR core solidified rather than collapsed when overloaded. This failure mechanism is considered favourable for floor and wall coverings.

Finally, it can be concluded that the proposed biocomposite core would be made from P30TMP, with the AR design and manufactured by profile extrusion. It can further be proposed to use a hot-press to attach the décor layer to the biocomposite core. At the current state, hot-pressing should be done at 170 °C, with a pressure of 70 kg/cm² and with a duration of 15 sec. These parameters were determined through trial and error, followed by a visual assessment of the 3D-printed AR panel and décor sheet bonding. The developed and manufacturing process is illustrated in Figure 24.

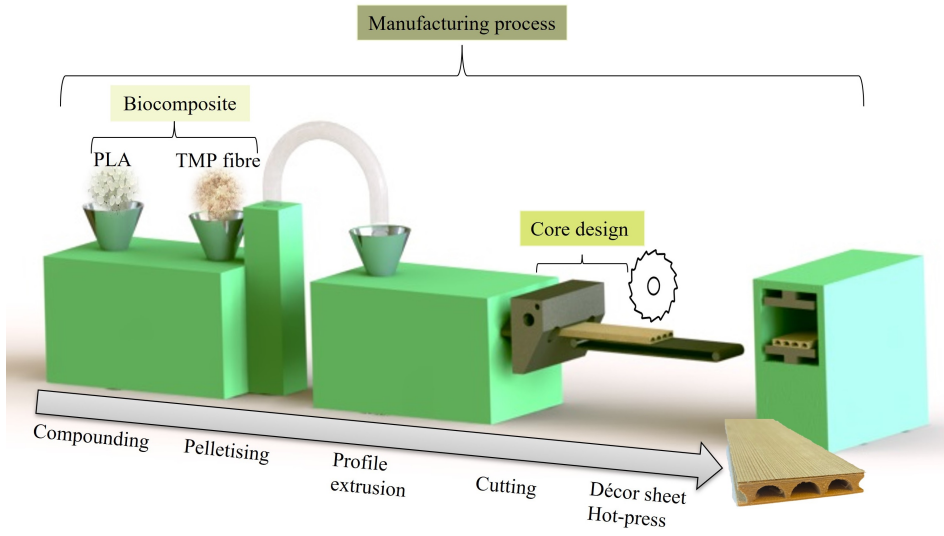


Figure 24: The proposed way of producing floor and side panels from biocomposites.

5 Conclusions

For producing floor and side panels from biocomposites, three objectives were placed; i) Developing a suitable biocomposite material, ii) Designing and optimising a biocomposite sandwich core, and iii) Assessing a suitable manufacturing method for future flooring products. Requirements that the biocomposite core should meet were collected to evaluate the biocomposite core performance constantly.

Different formulations mainly consisting of PLA and TMP fibres were considered as biocomposite material. Extensive literature research on the reinforcement ability of lignocellulosic components in biocomposites and their 3D-printed applications was conducted. To maximise the performance of the biocomposite formulations prepared in this study, the influence of compounding parameters on the tensile properties and fibre dispersion of injection moulded biocomposites was studied. A temperature of 180 °C, screw speed of 50 rpm and residence time of 1 min was found to yield the highest tensile properties of a biocomposite prepared from PLA, 20 wt.% TMP and 10 wt.% industrial side stream. Importantly, the side stream was shown to be a potential MFI enhancer. Since biocomposites from PLA and TMP were generally low in toughness formulations with the plasticisers PHA or PBAT were prepared and characterised. A biocomposite made from PLA, 20 wt.% PBAT and 15 wt.% milled TMP was found to be well-suited for 3D and 4D printing. The tensile properties of 3D-printed parts from such material turned out to be slightly better than parts printed from the commercial woodFill® filament.

Five potential sandwich designs with hexagonal, squared, triangular or circular shaped cells were designed to meet a relative density of 0.5 and were manufactured in 3D printing using the woodFill® filament. 3-point bending tests revealed that with the chosen design and relative density the differences in flexural strength and stiffness between the different designs were negligible except for the CS design. The flexural strength of CS was slightly lower compared the other designs. That was most probably related to the comparatively large cell diameter and limited test specimen size. To optimise the core design, numerical modelling using different elastic material modelling approaches was applied. Finally, a bimodular model based on tensile and compression tests of 3D-printed specimens was found to be the most accurate. Using this model numerical 3-point bending tests of potential core designs could be performed in a more efficient way. To increase the bending strength and stiffness of the biocomposite core the sandwich design with in-plane oriented cells was adapted to out-of-plane-oriented core stiffeners. 3-point bending tests on the 3D-printed panels confirmed the results obtained through simulations. Based on experiments and simulations, the biocomposite core design with unidirectional trapezoidal core stiffeners was chosen to be manufactured by profile

extrusion from PLA and 30 wt.% TMP fibres. The extruded biocomposite panels met the flexural stiffness requirements but failed to meet the flexural strength requirements by 10 %. Compression tests showed that both the arched and the corrugated core designs could meet the required compressive strength, with the arched design showing the most favourable failure mode.

A biocomposite core made from PLA and 30 wt.% TMP fibres, with the arched core design and manufactured by profile extrusion was considered a potentially suitable solution for a floor and wall cladding panel. The decisions were based on a trade-off strategy using weighted scores to meet predefined criteria. Additionally, hot-pressing was proposed to bond a décor sheet to the biocomposite core.

In summary, a way of producing floor and side panels of biocomposites was demonstrated successfully. The proposed biocomposite core was shown to meet most of the assigned requirements. Not meeting flexural strength requirements, was most likely due to the relatively poor processing conditions of the profile extrusion, which can be significantly improved in an industrial set-up.

6 Suggestions for future work

For future work, it can be suggested to perform trials with the proposed biocomposite material and core design on an industrial extrusion line. Such industrially manufactured panels could be evaluated in a similar way as described in the present thesis. Besides 3-point bending and compression properties, moisture absorption, acoustic and insulation properties would need to be tested. The resistance against point loads from *e.g.*, furniture could also be an important factor to assess and optimise the core design and biocomposite material accordingly. Further, the biocomposite core production process needs to be integrated into the overall process of manufacturing flooring laminates. This means implementing a locking system and find a solution for attaching the décor sheet. Hot-pressing has been suggested, but the bond strength between core and décor sheet would need to be measured.

Additionally, it could be interesting to investigate the differences in mechanical properties between 3D-printed and extruded biocomposite structures to a greater extent. This could support the usage of 3D printing in early development stages for prototyping and testing. Further, more research efforts to scale up from a laboratory to an industrial extruder could be useful. It might be of interest to develop a model for predicting the mechanical properties of a biocomposite produced on industrial plants from data generated on a laboratory scale.

Finally, it would be of high relevance to investigate the long term properties of biocomposite materials. Especially as application in products meant to last for decades as *e.g.*, floor and side panels. In such cases longevity and durability must be considered and balanced with attributes such as biodegradability and recyclability.

References

- [1] I. M. Ahmed and K. D. Tsavdaridis, 'Life cycle assessment (LCA) and cost (LCC) studies of lightweight composite flooring systems', *Journal of Building Engineering*, vol. 20, pp. 624–633, 2018, ISSN: 2352-7102.
- [2] C. Arkin *et al.*, *Plastic Atlas*, L. Fuhr and M. Franklin, Eds. Berlin, Germany: Heinrich Böll Foundation, and Break Free From Plastic, 2019, ISBN: 978-3-86928-211-4.
- [3] M. Brodin *et al.*, 'THE BIOCOMPOSITE STRUCTURE OF DECORATIVE LAMINATES', in *10th International Conference on Composite Science and Technology*, 2015.
- [4] A. G. Buekens, 'Some observations on the recycling of plastics and rubber', *Conservation & Recycling*, vol. 1, no. 3, pp. 247–271, 1977, ISSN: 0361-3658.
- [5] A. Bayatkashkoli *et al.*, 'Investigation on the production possibilities of high pressure laminate from borax and recycled papers as a cleaner product', *Journal of Cleaner Production*, vol. 192, pp. 775–781, 2018, ISSN: 0959-6526.
- [6] Y. Yang *et al.*, 'Recycling of composite materials', *Chemical Engineering and Processing: Process Intensification*, vol. 51, pp. 53–68, 2012, ISSN: 0255-2701.
- [7] M. E. Grigore, 'Methods of Recycling, Properties and Applications of Recycled Thermoplastic Polymers', *Recycling*, vol. 2, no. 4, 2017.
- [8] A. Nourbakhsh and A. Ashori, 'Particleboard made from waste paper treated with maleic anhydride', *Waste management & research : the journal of the International Solid Wastes and Public Cleansing Association, ISWA*, vol. 28, pp. 51–55, Jul. 2009.
- [9] G. Mantanis *et al.*, 'A New Process for Recycling Waste Fiberboards', in *38th International Wood Composites Symposium*, Apr. 2004.
- [10] D. Filgueira *et al.*, 'Enzymatic-Assisted Modification of Thermomechanical Pulp Fibers To Improve the Interfacial Adhesion with Poly(lactic acid) for 3D Printing', *ACS Sustainable Chemistry & Engineering*, vol. 5, no. 10, pp. 9338–9346, Oct. 2017.
- [11] G. Chinga-Carrasco *et al.*, 'Side streams from flooring laminate production – Characterisation and recycling in biocomposite formulations for injection moulding', *Composites Part A: Applied Science and Manufacturing*, vol. 153, p. 106723, 2022, ISSN: 1359-835X.
- [12] C. L. Rusu *et al.*, 'The Potential of Functionalized Ceramic Particles in Coatings for Improved Scratch Resistance', *Coatings*, vol. 8, no. 6, 2018, ISSN: 2079-6412.
- [13] 'BerryAlloc. Accessed: 20.08.2022'. (2022), [Online]. Available: <https://www.berryalloc.com/global/en/high-pressure-floors/original>.

- [14] A. Roos and M. Hugosson, 'Consumer preferences for wooden and laminate flooring', *Wood Material Science & Engineering*, vol. 3, no. 1-2, pp. 29–37, Mar. 2008, ISSN: 1748-0272.
- [15] L. T. Sin, A. R. Rahmat and W. A. Rahman, '2 - Overview of Poly(lactic Acid)', in *Plastics Design Library*, S. Ebnesajjad, Ed., Boston: William Andrew Publishing, 2013, pp. 11–54, ISBN: 978-1-4557-2834-3.
- [16] L. T. Sin, A. R. Rahmat and W. A. Rahman, '3 - Applications of Poly(lactic Acid)', in *Plastics Design Library*, S. Ebnesajjad, Ed., Boston: William Andrew Publishing, 2013, pp. 55–69, ISBN: 978-1-4557-2834-3.
- [17] M. Fan and F. Fu, '1 - Introduction: A perspective – natural fibre composites in construction', in *Advanced High Strength Natural Fibre Composites in Construction*, M. Fan and F. Fu, Eds., Woodhead Publishing, 2017, pp. 1–20, ISBN: 978-0-08-100411-1.
- [18] C. Zarna *et al.*, 'Reinforcement ability of lignocellulosic components in biocomposites and their 3D printed applications – A review', *Composites Part C: Open Access*, vol. 143, p. 100 171, 2019, ISSN: 2351-9789.
- [19] M. Carus and C. Gahle, 'Injection moulding with natural fibres', *Reinforced Plastics*, vol. 52, no. 4, pp. 18–25, 2008, ISSN: 0034-3617.
- [20] T. Bitzer, 'Honeycomb and sandwich testing', in *Honeycomb Technology: Materials, Design, Manufacturing, Applications and Testing*, Dordrecht: Springer Netherlands, 1997, pp. 149–192, ISBN: 978-94-011-5856-5.
- [21] Q. Zhang *et al.*, 'Bioinspired engineering of honeycomb structure – Using nature to inspire human innovation', *Progress in Materials Science*, vol. 74, pp. 332–400, Oct. 2015, ISSN: 00796425.
- [22] J. Zhang and M. F. Ashby, 'The out-of-plane properties of honeycombs', *International Journal of Mechanical Sciences*, vol. 34, no. 6, pp. 475–489, 1992, ISSN: 0020-7403.
- [23] T. Bitzer, 'Honeycomb core', in *Honeycomb Technology: Materials, Design, Manufacturing, Applications and Testing*, Dordrecht: Springer Netherlands, 1997, pp. 10–42, ISBN: 978-94-011-5856-5.
- [24] Y. Feng *et al.*, 'Creative design for sandwich structures: A review', *International Journal of Advanced Robotic Systems*, vol. 17, no. 3, p. 1 729 881 420 921 327, May 2020, ISSN: 1729-8806.
- [25] H. Araújo *et al.*, 'The effect of geometry on the flexural properties of cellular core structures', *Proceedings of the Institution of Mechanical Engineers, Part L: Journal of Materials: Design and Applications*, vol. 233, no. 3, pp. 338–347, 2019.

- [26] J. Grünewald, P. Parlevliet and V. Altstädt, 'Manufacturing of thermoplastic composite sandwich structures: A review of literature', *Journal of Thermoplastic Composite Materials*, vol. 30, no. 4, pp. 437–464, Sep. 2015, ISSN: 0892-7057.
- [27] I. Verpoest and J. Pflug, 'KU Leuven Research Development. Half closed thermoplastic honeycomb, their production process and equipment to produce. Belgium, EP1824667B1', 2010.
- [28] J. Pflug *et al.*, 'Thermoplastic Folded Honeycomb Cores - Cost Efficient Production of All Thermoplastic Sandwich Panels', in *ICCM 13*, 2001.
- [29] T. Bitzer, 'Honeycomb processes', in *Honeycomb Technology: Materials, Design, Manufacturing, Applications and Testing*, Dordrecht: Springer Netherlands, 1997, pp. 70–79, ISBN: 978-94-011-5856-5.
- [30] T. Bitzer, 'Sandwich design', in *Honeycomb Technology: Materials, Design, Manufacturing, Applications and Testing*, Dordrecht: Springer Netherlands, 1997, pp. 43–69, ISBN: 978-94-011-5856-5.
- [31] L. Jiang and J. Zhang, '6 - Biodegradable Polymers and Polymer Blends', in *Plastics Design Library*, S. Ebnesajjad, Ed., Boston: William Andrew Publishing, 2013, pp. 109–128, ISBN: 978-1-4557-2834-3.
- [32] A. Neubert. 'Die Alternative "Biokunststoffe"'. Accessed: 20.08.2022'. (2019), [Online]. Available: <https://www.biooekonomie-bw.de/fachbeitrag/dossier/die-alternative-biokunststoff>.
- [33] T. Joffre *et al.*, 'X-ray micro-computed tomography investigation of fibre length degradation during the processing steps of short-fibre composites', *Composites Science and Technology*, vol. 105, pp. 127–133, 2014, ISSN: 0266-3538.
- [34] K. L. Pickering, M. G. A. Efendy and T. M. Le, 'A review of recent developments in natural fibre composites and their mechanical performance', *Composites Part A: Applied Science and Manufacturing*, vol. 83, pp. 98–112, 2016, ISSN: 1359-835X.
- [35] M. Delgado-Aguilar *et al.*, 'Bio composite from bleached pine fibers reinforced polylactic acid as a replacement of glass fiber reinforced polypropylene, macro and micro-mechanics of the Young's modulus', *Composites Part B: Engineering*, vol. 125, pp. 203–210, 2017, ISSN: 1359-8368.
- [36] P. Nygård *et al.*, 'Extrusion-based wood fibre-PP composites: Wood powder and pelletized wood fibres – a comparative study', *Composites Science and Technology*, vol. 68, no. 15, pp. 3418–3424, 2008, ISSN: 0266-3538.

- [37] D. Dai and M. Fan, '1 - Wood fibres as reinforcements in natural fibre composites: structure, properties, processing and applications', in *Natural Fibre Composites*, A. Hodzic and R. Shanks, Eds., Woodhead Publishing, 2014, pp. 3–65, ISBN: 978-0-85709-524-4.
- [38] S. R. Djafari Petroudy, '3 - Physical and mechanical properties of natural fibers', in *Advanced High Strength Natural Fibre Composites in Construction*, M. Fan and F. Fu, Eds., Woodhead Publishing, 2017, pp. 59–83, ISBN: 978-0-08-100411-1.
- [39] C. Neagu, K. Gamstedt and F. Berthold, 'Stiffness Contribution of Various Wood Fibers to Composite Materials', *Journal of Composite Materials*, vol. 40, pp. 663–699, Apr. 2006.
- [40] G. Chinga-Carrasco, 'Exploring the multi-scale structure of printing paper – a review of modern technology', *Journal of Microscopy*, vol. 234, no. 3, pp. 211–242, 2009.
- [41] H. Peltola, E. Laatikainen and P. Jetsu, 'Effects of physical treatment of wood fibres on fibre morphology and biocomposite properties', *Plastics, Rubber and Composites*, vol. 40, no. 2, pp. 86–92, Mar. 2011, ISSN: 1465-8011.
- [42] S. Ebnesaajad, *Handbook of Biopolymers and Biodegradable Plastics: Properties, Processing and Applications* (Plastics Design Library). Elsevier Science, 2012, ISBN: 9781455730032.
- [43] W. G. Glasser *et al.*, 'Fiber-reinforced cellulosic thermoplastic composites', *Journal of Applied Polymer Science*, vol. 73, no. 7, pp. 1329–1340, 1999.
- [44] A. Dufresne, '8 - Cellulose-Based Composites and Nanocomposites', in *Plastics Design Library*, S. Ebnesaajad, Ed., Boston: William Andrew Publishing, 2013, pp. 153–169, ISBN: 978-1-4557-2834-3.
- [45] M. D. Stanciu *et al.*, 'Mechanical and Rheological Behaviour of Composites Reinforced with Natural Fibres', *Polymers*, vol. 12, no. 6, 2020.
- [46] B. D. Agarwal, L. J. Broutman and K. Chandrashekhara, *Analysis and Performance of Fiber Composites, 4th Edition*. John Wiley & Sons, Ltd, 2017, p. 576, ISBN: 978-1-119-38998-9.
- [47] T. D. Ngo *et al.*, 'Additive manufacturing (3D printing): A review of materials, methods, applications and challenges', *Composites Part B: Engineering*, vol. 143, pp. 172–196, 2018, ISSN: 1359-8368.
- [48] N. Shahrubudin, T. C. Lee and R. Ramlan, 'An Overview on 3D Printing Technology: Technological, Materials, and Applications', *Procedia Manufacturing*, vol. 35, pp. 1286–1296, 2019, ISSN: 2351-9789.
- [49] 'ISO/ASTM 52900: Additive manufacturing - General principles - Fundamentals and vocabulary', 2021.

- [50] A. Dey and N. Yodo, 'A Systematic Survey of FDM Process Parameter Optimization and Their Influence on Part Characteristics', *Journal of Manufacturing and Materials Processing*, vol. 3, no. 3, 2019.
- [51] S. Garzon-Hernandez *et al.*, 'Design of FDM 3D printed polymers: An experimental-modelling methodology for the prediction of mechanical properties', *Materials & Design*, vol. 188, p. 108 414, 2020, ISSN: 0264-1275.
- [52] O. Volgin and I. Shishkovsky, 'Material modelling of FDM printed PLA part', *Engineering Solid Mechanics*, pp. 153–160, Jan. 2021.
- [53] M. Grasso *et al.*, 'Effect of temperature on the mechanical properties of 3D-printed PLA tensile specimens', *Rapid Prototyping Journal*, vol. 24, Oct. 2018.
- [54] M. S. Huda *et al.*, 'Wood-fiber-reinforced poly(lactic acid) composites: Evaluation of the physicomechanical and morphological properties', *Journal of Applied Polymer Science*, vol. 102, no. 5, pp. 4856–4869, 2006.
- [55] L. Gallagher and A. McDonald, 'The effect of micron sized wood fibers in wood plastic composites', *Maderas. Ciencia y tecnología*, vol. 15, pp. 357–374, 2013.
- [56] S. Rodríguez-Fabià and G. Chinga-Carrasco, 'Effects of a poly(hydroxyalkanoate) elastomer and kraft pulp fibres on biocomposite properties and three-dimensional (3D) printability of filaments for fused deposition modelling', *Journal of Bioresources and Bioproducts*, 2022, ISSN: 2369-9698.
- [57] N. Ehman *et al.*, 'Biocomposites of Polyhydroxyalkanoates and Lignocellulosic Components: A Focus on Biodegradation and 3D Printing BT - Bioplastics for Sustainable Development', in *Bioplastics for Sustainable Development*, M. Kuddus and Roohi, Eds., Singapore: Springer Singapore, 2021, pp. 325–345, ISBN: 978-981-16-1823-9.
- [58] A. Le Duigou *et al.*, '3D printing of wood fibre biocomposites: From mechanical to actuation functionality', *Materials & Design*, vol. 96, pp. 106–114, 2016, ISSN: 0264-1275.
- [59] V. Kumar, R. Sehgal and R. Gupta, 'Blends and composites of polyhydroxyalkanoates (PHAs) and their applications', *European Polymer Journal*, vol. 161, p. 110 824, 2021, ISSN: 0014-3057.
- [60] V. Gigante *et al.*, 'Rubber Toughening of Polylactic Acid (PLA) with Poly(butylene adipate-co-terephthalate) (PBAT): Mechanical Properties, Fracture Mechanics and Analysis of Ductile-to-Brittle Behavior while Varying Temperature and Test Speed', *European Polymer Journal*, vol. 115, pp. 125–137, 2019, ISSN: 0014-3057.

- [61] J. Andrzejewski *et al.*, ‘Development of Toughened Blends of Poly(lactic acid) and Poly(butylene adipate-co-terephthalate) for 3D Printing Applications: Compatibilization Methods and Material Performance Evaluation’, *ACS Sustainable Chemistry & Engineering*, vol. 8, no. 17, pp. 6576–6589, May 2020.
- [62] P. Chaiwutthinan *et al.*, ‘Composites of poly(lactic acid)/poly(butylene adipate-co-terephthalate) blend with wood fiber and wollastonite: Physical properties, morphology, and biodegradability’, *Journal of Applied Polymer Science*, vol. 136, no. 21, p. 47 543, 2019.
- [63] Nature Works. ‘Ingeo™ Biopolymer 4043D Technical Data Sheet. Accessed: 20.08.2022’. (2022), [Online]. Available: https://www.natureworkslc.com/~ / media / Files / NatureWorks / Technical- Documents / Technical- Data- Sheets / TechnicalDataSheet_4043D_3D- monofilament_ pdf.pdf.
- [64] GoodFellow. ‘PH32-GL-000101 Technical Data Sheet. Accessed: 20.08.2022’. (2022), [Online]. Available: <https://www.goodfellow.com/uk/en-gb/displayitemdetails/p/ph32-gl-000101/polyhydroxyalkanoate-biopolymer-granule>.
- [65] A. Z. Naser, I. Deiab and B. M. Darras, ‘Poly(lactic acid) (PLA) and polyhydroxyalkanoates (PHAs), green alternatives to petroleum-based plastics: a review’, *RSC Adv.*, vol. 11, no. 28, pp. 17 151–17 196, 2021.
- [66] BASF SE. ‘ecoflex® F Blend C1200 Technical Data Sheet. Accessed: 20.08.2022’. (2021), [Online]. Available: <https://plastics-rubber.basf.com/global/en/performance-polymers/products/ecoflex.html>.
- [67] C. Pavon *et al.*, ‘Improvement of PBAT Processability and Mechanical Performance by Blending with Pine Resin Derivatives for Injection Moulding Rigid Packaging with Enhanced Hydrophobicity.’, eng, *Polymers*, vol. 12, no. 12, Dec. 2020.
- [68] V. Mazzanti, L. Malagutti and F. Mollica, ‘FDM 3D Printing of Polymers Containing Natural Fillers: A Review of their Mechanical Properties’, *Polymers*, vol. 11, no. 7, 2019, ISSN: 2073-4360.
- [69] T.-C. Yang and C.-H. Yeh, ‘Morphology and Mechanical Properties of 3D Printed Wood Fiber/Poly(lactic acid) Composite Parts Using Fused Deposition Modeling (FDM): The Effects of Printing Speed’, *Polymers*, vol. 12, no. 6, 2020, ISSN: 2073-4360.
- [70] A. Armillotta, M. Bellotti and M. Cavallaro, ‘Warping of FDM parts: Experimental tests and analytic model’, *Robotics and Computer-Integrated Manufacturing*, vol. 50, pp. 140–152, 2018, ISSN: 0736-5845.

- [71] M. A. Morales *et al.*, ‘Development and Characterization of Rice Husk and Recycled Polypropylene Composite Filaments for 3D Printing’, *Polymers*, vol. 13, no. 7, 2021, ISSN: 2073-4360.
- [72] A. Le Duigou *et al.*, ‘A review of 3D and 4D printing of natural fibre biocomposites’, *Materials & Design*, vol. 194, p. 108911, 2020, ISSN: 0264-1275.
- [73] D. Filgueira *et al.*, ‘3D Printable Filaments Made of Biobased Polyethylene Biocomposites’, *Polymers*, vol. 10, no. 3, 2018.
- [74] R. F. Gibson, *Principles of composite material mechanics*. CRC press, 2016, ISBN: 1498788246.
- [75] L. Li *et al.*, ‘Composite Modeling and Analysis for Fabrication of FDM Prototypes with Locally Controlled Properties’, *Journal of Manufacturing Processes*, vol. 4, no. 2, pp. 129–141, 2002, ISSN: 1526-6125.
- [76] R. Sayre III, ‘A comparative finite element stress analysis of isotropic and fusion deposited 3D printed polymer’, *Masters of Engineering Thesis, Rensselaer Polytechnic Institute, Troy, New York*, 2014.
- [77] P. Kumar Mishra and S. P., ‘Prediction of in-plane stiffness of multi-material 3D printed laminate parts fabricated by FDM process using CLT and its mechanical behaviour under tensile load’, *Materials Today Communications*, vol. 23, p. 100955, 2020, ISSN: 2352-4928.
- [78] M. Somireddy, A. Czekanski and C. V. Singh, ‘Development of constitutive material model of 3D printed structure via FDM’, *Materials Today Communications*, vol. 15, pp. 143–152, 2018, ISSN: 2352-4928.
- [79] M. Somireddy and A. Czekanski, ‘Mechanical Characterization of Additively Manufactured Parts by FE Modeling of Mesostructure’, *Journal of Manufacturing and Materials Processing*, vol. 1, no. 2, 2017.
- [80] M. S. Anoop and P. Senthil, ‘Homogenisation of elastic properties in FDM components using microscale RVE numerical analysis’, *Journal of the Brazilian Society of Mechanical Sciences and Engineering*, vol. 41, no. 12, p. 540, 2019, ISSN: 1806-3691.
- [81] R. Hambali *et al.*, ‘Effect of Build Orientation on FDM Parts: A Case Study for Validation of Deformation Behaviour by FEA’, in *International Conference on Design and Concurrent Engineering*, Sep. 2010.
- [82] R. Zou *et al.*, ‘Isotropic and anisotropic elasticity and yielding of 3D printed material’, *Composites Part B: Engineering*, vol. 99, pp. 506–513, 2016, ISSN: 1359-8368.
- [83] M. Scapin and L. Peroni, ‘Numerical Simulations of Components Produced by Fused Deposition 3D Printing’, *Materials*, vol. 14, no. 16, 2021.

- [84] A. Nettles, 'Basic Mechanics of Laminated composite plates', *NASA Reference Publication*, Oct. 1994.
- [85] D. A. Serban, L. Marsavina and V. Silberschmidt, 'Behaviour of semi-crystalline thermoplastic polymers: Experimental studies and simulations', *Computational Materials Science*, vol. 52, no. 1, pp. 139–146, 2012, ISSN: 0927-0256.
- [86] M.-M. Pastor-Artigues *et al.*, 'Elastic Asymmetry of PLA Material in FDM-Printed Parts: Considerations Concerning Experimental Characterisation for Use in Numerical Simulations', *Materials*, vol. 13, no. 1, 2020.
- [87] T. Vukasovic *et al.*, 'Characterization of the mechanical response of thermoplastic parts fabricated with 3D printing', *The International Journal of Advanced Manufacturing Technology*, vol. 104, no. 9, pp. 4207–4218, 2019, ISSN: 1433-3015.
- [88] N. Reynolds and M. Pharaoh, '1 - An introduction to composites recycling', in *Woodhead Publishing Series in Composites Science and Engineering*, G. Recycling and V. B. T. -. M. Reuse of Waste Composites, Eds., Woodhead Publishing, 2010, pp. 3–19, ISBN: 978-1-84569-462-3.
- [89] M. Z. M. Salem *et al.*, 'Evaluation of formaldehyde emission from different types of wood-based panels and flooring materials using different standard test methods', *Building and Environment*, vol. 49, pp. 86–96, 2012, ISSN: 0360-1323.
- [90] B. Nebel, B. Zimmer and G. Wegener, 'Life Cycle Assessment of Wood Floor Coverings - A Representative Study for the German Flooring Industry (11 pp)', *The International Journal of Life Cycle Assessment*, vol. 11, no. 3, pp. 172–182, 2006, ISSN: 1614-7502.
- [91] INCOSE, *INCOSE Systems Engineering Handbook: A Guide for System Life Cycle Processes and Activities*. Jun. 2015, ISBN: 9781118999400.
- [92] N. Sproles, 'Formulating measures of effectiveness', *Systems Engineering*, vol. 5, no. 4, pp. 253–263, Jan. 2002, ISSN: 1098-1241.
- [93] A. Kossiakoff *et al.*, *Needs Analysis* (Wiley Online Books). Apr. 2011, pp. 139–164, ISBN: 9781118001028.
- [94] M. Le Baillif, 'Extrusion of Cellulose Fibers Polypropylene Composites', Ph.D. dissertation, NTNU, Department of Mechanical and Industrial Engineering, Trondheim, 2008.
- [95] C. Haskins, 'Systems engineering analyzed, synthesized, and applied to sustainable industrial park development', Ph.D. dissertation, NTNU, Department of Industrial Economics and Technology Management, Trondheim, 2008.

-
- [96] A. Kosiakoff *et al.*, ‘Decision Analysis and Support’, *Systems Engineering Principles and Practice*, Wiley Online Books, pp. 255–313, Apr. 2011.
- [97] O. Mysiukiewicz *et al.*, ‘Correlation between Processing Parameters and Degradation of Different Polylactide Grades during Twin-Screw Extrusion’, *Polymers*, vol. 12, no. 6, 2020.

Appendices

A. I Publication I

Reinforcement ability of lignocellulosic components in biocomposites and their 3D printed applications - A review





Reinforcement ability of lignocellulosic components in biocomposites and their 3D printed applications – A review

Chiara Zarna^a, Mihaela Tanase Opedal^b, Andreas T. Echtermeyer^a, Gary Chinga-Carrasco^{b,*}

^a Department of Mechanical and Industrial Engineering, NTNU, Richard Birkelandsvei 2B, 7491 Trondheim, Norway

^b RISE PFI, Hogskoleringen 6b, 7491 Trondheim, Norway

ARTICLE INFO

Keywords:

Cellulose
Nano-cellulose
3D Printing
Bio-composites
Lignin
Biocomposites
Nanocellulose

ABSTRACT

Biocomposites based on lignocellulosic components (e.g. pulp fibers, nanocellulose and lignin) are of interest as sustainable replacements for thermoplastic fossil-based materials, which find their application in household items, construction, automotive, 3D-printing, etc. Nanocellulose, a nano-structural component of pulp fibers, is considered having potential as a high-performance reinforcement for bioplastics, due to its high aspect ratio and potentially strong mechanical properties. Lignin, a biodegradable polymer isolated from pulp fibers, can be considered as an essential bioresource for the production of biocomposites, due to the aromatic structure and functional groups. In this review the reinforcing ability of selected lignocellulosic components and their applicability in 3D printing is presented, considering their mechanical properties. At this point, there are challenges in processing nanocellulose that may reduce its attractiveness as a reinforcement in thermoplastic biocomposites. The objective of the review is to identify current challenges and opportunities for the application of 3D printed lignocellulosic biocomposites. Optimization of 3D printing process parameters are considered to be a key to further improve the mechanical properties of the end-product. Importantly, this review revealed that greater efforts in mechanical fatigue research may contribute to assess and improve the potential of lignocellulosic reinforcements for structural applications.

1. Introduction

The utilization of lignocellulosic fibers and their nanomaterials has gained major interest during the last years. Lignocellulosic fibers and nanocelluloses have been proposed as reinforcement in bioplastics [1–5]. Particularly, nanocelluloses have been considered as promising candidates for bionanocomposites, based on several characteristics such as mechanical properties (tensile strength and stiffness), low weight and biodegradability [6]. In this review, bioplastics are considered as thermoplastic materials derived from biomass, e.g. poly-lactic acid (PLA), bio-based polyethylene (BioPE), bio-based polypropylene (BioPP), and poly-hydroxyalkanoates (PHA). For a detailed overview of bioplastic production see e.g. Brodin et al. [5].

A composite can be defined as a material composed of two or more components having distinct morphology and chemistry, and giving synergetic effects. Additionally, the term biocomposite also refers to materials having at least one bio-component (e.g. bioplastic, lignocellulosic pulp fibers, lignin or cellulose nanofibrils (CNFs)). One of the reasons for combining nanocellulose and polymers is to improve the

mechanical properties of a given polymer, which strongly depend on the type and fraction of nanocellulose and the dispersion and adhesion between the matrix and the nanocellulose. In this respect, CNFs and cellulose nanocrystals (CNCs) have been proposed as most adequate materials, with excellent mechanical properties [7–9]. However, nanocellulose reinforcements have mostly shown modest improvement of strength in physical tensile tests of biocomposites [8,10–13]. Major challenges are inhomogeneous dispersion, poor interfacial adhesion, low thermal stability, kinking and curling under processing [8,11,13,14]. To overcome these issues, surface modifications and adjustments of melting and mixing processes have been proposed and will be briefly presented in the following sections [11,15,16]. There seems to be a knowledge gap concerning the challenges and benefits of using nanocellulose as reinforcement, compared to lignocellulosic fibers. Long-term investigations regarding mechanical fatigue of biocomposites are also of major importance, if materials are considered for structural applications. However, to the best of our knowledge, such studies are currently lacking in literature about biocomposites reinforced with nanocellulose.

* Corresponding author.

E-mail address: gary.chinga.carrasco@rise-pfi.no (G. Chinga-Carrasco).

<https://doi.org/10.1016/j.jcom.2021.100171>

Received 22 January 2021; Received in revised form 6 July 2021; Accepted 8 July 2021

Available online 12 July 2021

2666-6820/© 2021 The Authors.

Published by Elsevier B.V. This is an open access article under the CC BY-NC-ND license

(<http://creativecommons.org/licenses/by-nc-nd/4.0/>).

Three-dimensional (3D) printing as an application for biocomposites has been in focus for some years. Reviews have been written about several techniques for 3D printing, including fused deposition modelling, selective laser sintering, stereo-lithography and bio-plotting [17–20]. Some of the commercially available technologies that seem adequate for biocomposites containing short fibers, nanocelluloses and lignin are briefly described in Table 1. This includes the technology Fused Deposition Modelling (FDM), which will be focused on in the present review. In addition to Table 1, direct ink writing (DIW), inkjet printing, digital light processing (DLP) and laminated object manufacturing (LOM) can also be used to 3D print bio-derived materials [21]. These methods are not considered in this review, since the focus is placed on thermoplastic biocomposites for structural applications. However, further information on several 3D printing techniques, suitable for biocomposites, can be found in [11,20,21].

The present work reviews the latest advances in research and development of biocomposites containing lignocellulosic fibers, lignin and nanocelluloses with a special focus on 3D printing of the corresponding biocomposites. Firstly, a general overview of lignocellulosic pulp fibers, nanocelluloses and lignin will be given. Secondly, the potential of analytical modelling for predicting the mechanical tensile properties of biocomposites will be discussed. Thirdly, the applicability of lignocellulosic materials for reinforcing bioplastics will be explored, with a critical focus on the potential of nanocellulose as reinforcement for bioplastics, compared to lignocellulosic pulp fibers. Finally, mechanical fatigue characteristics of biocomposites will be discussed, considering its importance on structural applications.

2. Lignocellulosic components in biocomposites

Exploitation of the full potential of lignocellulosic fibers as reinforcement of bioplastics depends on uniform fiber distribution and sufficient stress transfer between fibers and matrix. These aspects are addressed by modification of the fiber surface, modification of the matrix and development of adequate processing methods. The strength of a biocomposite will always be limited by its weakest point. Hence, care has to be taken not to weaken or damage the reinforcing fibers during modification and processing, as may be the case during thermoplastic processing, such as e.g. melt blending, extruding, pelleting [30].

2.1. Lignocellulosic fibers

The interest for lignocellulosic-based biocomposites has increased over the last years due to environmental concerns. In addition, biocomposites could potentially obtain better mechanical strength and stiffness properties if the reinforcement has a greater length-to-diameter

ratio (aspect ratio). Since lignocellulosic fibers have a higher aspect ratio than lignocellulosic particles, these fibers have been extensively studied for their utility as biocomposite components [1,3,31]. They are well implemented as a reinforcement for bioplastics and contribute some beneficial properties, e.g. higher stiffness, strength increment, weight reduction and cost reduction [32–34]. Lignocellulosic fibers can be of various origins including flax, hemp, jute, sisal, bamboo, wood, etc [35–38]. In this review the focus is placed on lignocellulosic wood fibers, as these have been widely used as reinforcement in biocomposite materials for several years. Wood is also the main source of lignin and nanocellulose [39,40].

There are various lignocellulosic pulp fibers that can be used to reinforce thermoplastics, e.g. Thermo-Mechanical Pulp (TMP), Chemi-thermo-mechanical pulp and chemical pulp fibers [1,3,41]. Depending on the pulping process, the pulp fibers differ greatly with respect to the fiber morphology and chemistry (Fig. 1).

TMP fibers are shorter, stiffer, have a lower aspect ratio and contain more lignin compared to chemical pulp fibers [41]. Peltola et al. [41] demonstrated that TMP fibers can offer a greater reinforcing potential for PLA than chemical pulp, due to lignin on the TMP fibers surface that might act as a compatibilizer. For PP and PE matrixes, the addition of TMP or chemi-thermo-mechanical pulp fibers together with maleic anhydride compatibilizers showed promising results regarding the reinforcement of polyolefins [1,43]. The polymeric matrix of biocomposites typically contains about 0–8 wt.% of coupling agent and 10–50 wt.% of fibers [43–45].

2.2. Nanocelluloses

Cellulose is a structural component in plants, embedded in a polymeric matrix of lignin and complex sugars. Cellulose appears as a hierarchical structure of cellulose molecules which are linked to form elementary fibrils (Fig. 2). Fibrils in nanofiber size are named as cellulose nanofibrils (CNF, Fig. 3A and B). CNF are a composition of highly ordered cellulose nanocrystals (CNC, Fig. 3C) and amorphous parts [46].

Chemical pulping includes several processes to extract cellulose fibers by dissolving the lignocellulosic matrix [48]. Chemical pulp fibers have been one of the most used raw materials for production of nanocellulose, mainly based on two types of chemical pulping, i.e. sulphite and kraft pulping. For details on the chemical pulping see [49]. For more information about various methods applied to obtain different nanocelluloses see [50].

To obtain CNFs, a cellulose suspension can be treated mechanically through high-pressure homogenization, microfluidizers [51], grinding [52], ball milling, ultra-sonication [53] and cryocrushing [54, 55]. Producing mechanical CNFs (Fig. 3A) requires high amounts of energy

Table 1
3D printing techniques for biocomposites

3D printing technique	Materials	Principle	Advantages	Disadvantages
Fused deposition modelling (FDM)	Lignocellulosic fibers and fillers in thermoplastic filaments (10–40 wt.%) [22]	Melted filament is extruded through a nozzle and deposited layer-wise on a heated table [22]	<ul style="list-style-type: none"> - Affordable - Accessible/ simple - Rapid prototyping - Multi material capability [23,24] 	<ul style="list-style-type: none"> - Poor quality/ warping and shrinking - Relatively slow - Limited for large unsupported sections or sharp external corners [20,24,25]
Selective laser sintering (SLS)	Lignocellulosic fillers blended with thermoplastic powder (5–10 wt.%) [26, 27]	Laser fuses powder particles to impose a selective fused pattern on a powdered surface [26]	<ul style="list-style-type: none"> - Complex geometries possible (no support required) - Ability to process multiple materials in one bed - High accuracy [20,24] - Smooth surface finish - High accuracy - Wide range of materials [24,29] 	<ul style="list-style-type: none"> - Expensive (high machine costs and requires special knowledge) - Requires large amount of material - Slow (long cooling time and cleaning process) [20,24,25]
Stereolithography (SLA)	UV-resin filled with nanoclay, nanocellulose crystals [28]	- Resin is cured layer by layer via UV-light [28]		<ul style="list-style-type: none"> - Supports are required - Post-processing to remove supports - Eventually post curing required - Poor mechanical properties [24,25,28]

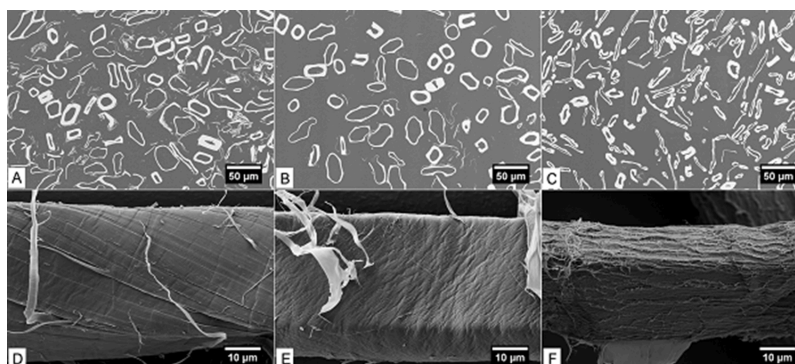


Fig. 1. Transversal (upper panel) and longitudinal (lower panel) SEM images of lignocellulosic pulp fibers. A) and D) thermo-mechanical pulp fibers. B) and E) chemi-thermomechanical pulp fibers. C) and F) chemical pulp fibers. Reproduced with permission from Jhon Wiley and Sons [[42], P.212], license number: 5006530754958. Copyright (2009) John Wiley & Sons, Inc.

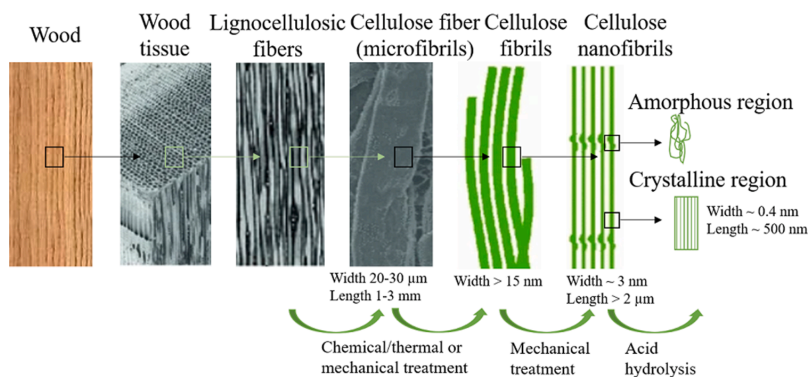


Fig. 2. Hierarchical structure from lignocellulose to crystalline nanocellulose. Reproduced and modified from Springer-Verlag ([47], P.450), no permission required. Copyright (2013) The Japan Wood Research Society.

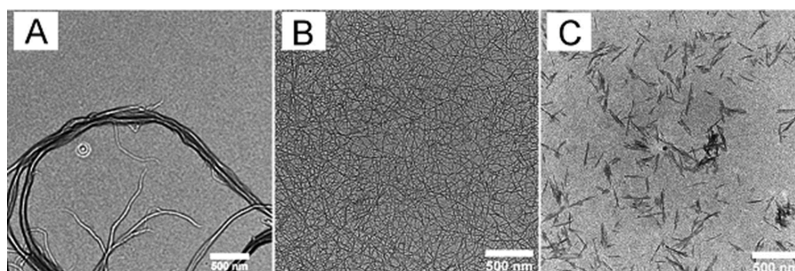


Fig. 3. Transmission electron microscopy images of some typical nanocelluloses. (A) Mechanical grade CNF. (B) TEMPO mediated oxidized CNF. (C) CNC. Reproduced and modified with permission from American Chemical Society [65]. Copyright (2014) American Chemical Society.

(over 25 000 kWh per ton of CNFs obtained from high-pressure homogenization) [56,57]. Therefore, enzymatic [51] and chemical [58] pre-treatments (e.g. TEMPO mediated oxidation, (Fig. 3B)) have been implemented to reduce energy consumption. However, the TEMPO process involves chemicals which may be harmful to the environment, if not treated adequately [56,57]. The result after TEMPO mediated oxidation is highly homogeneous CNF (widths of 3.5 nm), which is composed of crystalline and amorphous zones [58]. Alternatively, cellulose fibers can directly be the source of CNC by applying acid

hydrolysis, enzymatic hydrolysis or ion liquid methods to remove the amorphous zones and obtain highly crystalline nano-objects (Fig. 3C) [55–57].

CNFs have typical diameters in the nanometre scale (<100 nm) and lengths in the micrometre scale [58–61]. CNFs produced without chemical pre-treatment are relatively coarse (Fig. 3A). Chemical pre-treatments facilitate the production of structurally homogeneous nanofibrils (Fig. 3B). The morphology and surface chemistry can be widely tailored with chemical and enzymatic pre-treatments, as well as

with processing variables (Fig. 3) [58–64].

As an example, for the mechanical properties of lignocellulosic fibers and nanocellulose, measured and theoretically estimated strength and stiffness values, collected from literature, are presented in Table 2. Additional tensile strength and stiffness values of natural fibers can be found in [31,66].

However, caution has to be taken when interpreting mechanical tensile properties obtained from theoretical estimations and numerical simulations, since these are based on individual nanofibrils with optimum physical characteristics [67,69,70], which seems to be difficult to obtain and use in current processing conditions. In theory, nanofibrils offer a much better reinforcing ability than lignocellulosic fibers (Table 2). This is due to the high aspect ratio of nanofibrils [74]. To make use of these properties in a biocomposite, coupling agents must be added to ensure sufficient interaction between fibrils or fibers and the matrix. Uniform dispersion is equally important for obtaining an entire wetting of each individual fiber with matrix material.

It has been expected, that nanocellulose with a suitable morphology and nanofibrillation degree and an adequate surface chemistry would be beneficial for improving the mechanical properties of a given biocomposite material. However, the full utilization of nanocellulose mechanical properties as reinforcing component in biocomposites has been demanding and is still challenging and uncertain, mainly due to challenges such as dewatering without causing agglomeration of the nanomaterials and the implied production costs [67,74]. The agglomeration of nanofibers due to dewatering/drying may impair the dispersion of the material in the polymer matrix and most probably limit the reinforcing potential.

2.3. Lignin

In the last years, research on biomass valorisation has focused on pretreatment processes that yield fermentable sugars for bioethanol production, while lignin (Fig. 4) has been collected as a low value by-product and used for cogeneration of heat and electricity [75–78]. Each year, over 50 million tons of lignin are produced worldwide as a biorefinery side-product, of which 98% are burned to generate energy. Only 2% is currently used for other purposes, mainly in applications such as dispersants, adhesives, and fillers [75–78].

Recent studies have demonstrated that lignin, a currently underutilized renewable aromatic polymer can be incorporated into biocomposite products, both as a filler or as a polymer matrix [79–81]. However, there are some challenges that require attention in order to facilitate the utilization of lignin in high-value products, e.g. lignin extraction and isolation method and complex lignin structure for given

Table 2

Theoretically estimated or measured values of tensile strength and stiffness for nanocellulose films, nanofibrils and other lignocellulosic fiber, collected from literature

	Tensile strength [MPa]	Tensile stiffness [GPa]
Nanocellulose films obtained through high-pressure homogenization (measured)	> 200 [67,68]	> 10 [67,68]
Nanofibrils obtained through high-pressure homogenization and acid hydrolysis (estimated)	300–22000 [67]	60–300 [2, 67,69,70]
Spruce lignocellulosic fiber obtained through kraft pulping (measured/estimated)	500–1700 [71, 72]	40 [32]
Birch lignocellulosic fiber obtained through sulphite pulping	300–1500	30–80 [35]
Cotton	287–800	6–13 [35, 36]
Flax	344–1500	26–80 [35, 36]
Hemp	389–690	35 [35]
Sisal	287–913	9–28 [35, 36]
Bamboo	450–800	11–35 [73]

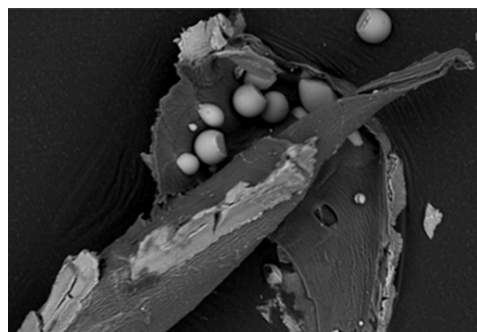


Fig. 4. Lignin particles precipitated on lignocellulosic fibers. The lignin particles appear bright compared to the grey-colored lignocellulosic pulp fiber surface. Image: Per Olav Johnsen, RISE PFI AS.

applications [82]. Attempts to use lignin in thermoplastics have resulted in applying lignin as a filler (up to 40 wt.%), however without providing mechanical improvement [39,78,79]. The adequate and sustainable modification of lignin to be used as thermoplastic matrix seems to remain as an interesting challenge. This could make it possible to produce thermoplastic wood-based biocomposites, i.e. fiber- or nanocellulose-reinforced lignin materials.

The raw material and the fractionation method determine the reactivity of lignin, which is represented by the occurrence of hydroxyl and aromatic functional groups. Lignin tends to depolymerize and re-polymerize with itself, leading to formation of additional C-C linkages. As a result, the number of hydroxyl groups is reduced and the molecular weight is increased. The formation of C-C linkages can also reduce the possibilities for further functionalization, which is important to make lignin compatible with other thermoplastics or fibers. Therefore, controlling the condensation and re-polymerization reactions is important in lignin valorisation, e.g. application of lignin in biocomposite products. Moreover, chemical functionalization of lignin is often a necessity to introduce new functional groups compatible with the final material. Different (chemical) reactants have been described in the literature to functionalize lignin towards different properties [76,83]. Modification of the aliphatic and aromatic hydroxyl groups of lignin via esterification is a typical approach [84].

3. Dispersion of lignocellulosic components in thermoplastic polymers

Uniform dispersion of fibers, nanofibers and lignin in thermoplastic biopolymers (e.g. PLA, BioPE, Poly-Butylene Succinate (PBS), acrylonitrile-butadiene-styrene (ABS)) is required to ensure sufficient component interaction and desired biocomposite properties. One major challenge in dispersion processes is to avoid agglomeration, caused by e.g. fiber-fiber interaction, fiber entanglement and the non-compatibility between hydrophilic fibers and hydrophobic matrixes [85].

To disperse lignocellulosic fibers in a bioplastic matrix, one common procedure is to mix dry polymer and compatibilizer powder first and then add fibers. Fibers may be pretreated by chemical and/or mechanical procedures to functionalize them. Since lignocellulosic fibers are water absorbents, it can be necessary to dry them before processing. The dried and mixed biocomposite powder can either be fed directly into a melt extruder, or processed into pellets beforehand by melt compounding, pressing and chopping. Through melting and mechanical shearing inside the extruder, the mixture will be further compounded. The steps of pelleting and melt extrusion can be repeated several times, but it should be considered that fiber damage occurs during this procedure [86–88].

The extrusion temperature, speed, mixing elements, repetitions of

compounding and the pretreatment of the raw materials can be varied in order to achieve a given biocomposite quality. Different mixing elements e.g. kneading blocks, conveying elements or tooth mixing elements are connected in series to accomplish certain objectives [89]. Lignocellulosic fibers start degrading above 200°C, whereas lignin has a broader degradation temperature range (200–500°C) [90]. Therefore, it is recommended to maintain a melting temperature that does not exceed this temperature range [88]. In general, the fibers orient according to the flow direction when extruding the biocomposite into a mold. The mold flow can be influenced by temperature, speed and mold geometry [91].

In [86] the authors investigated different dispersion processes for lignocellulosic fibers and polyethylene (PE). Drying the lignocellulosic fibers makes them brittle and fragile. That leads to fiber damage and shortening during the extrusion process. Wet lignocellulosic fibers are not that susceptible to damage development during extrusion, but they agglomerate and cannot be compounded properly. As shown in [86], the agglomeration of wet fibers provides the least increase of the flexural strength and modulus compared to neat PE. The greatest improvement of flexural strength was gained with dried and pelleted fibers. Thus, agglomeration of the fibers affects the mechanical properties of the biocomposite more negatively than fiber shortening.

Boran et al. [92] investigated the effect of different mixing strategies on the mechanical properties of cellulose and high-density polyethylene (HDPE). The authors concluded that the master batch method and extensional flow mixing provided reasonable dispersion [92].

Blending and dispersion of nanocelluloses in a bioplastic matrix is more demanding than for lignocellulosic pulp fibers. That is because the resulting product after deconstructing lignocellulose fibers to nanocellulose is usually a translucent and highly viscous dispersion of more than 95% water and nanocellulose fibrils [42,54]. The nanocellulose fibrils must be separated from water before mixing them with bioplastic polymer, which causes the nanocellulose fibrils to agglomerate, thus forming strong structures that are difficult to disperse in a bioplastic matrix. Dried lignocellulosic pulp fibers on the other side are relatively easy to disperse during melt-compounding in e.g. twin-screw extruders. Water affects a given biocomposite by i) causing fiber swelling, ii) affecting the dimensional stability, iii) disabling the fiber-matrix-interaction and iv) causing voids in the matrix [93–95]. In addition, some polymers (e.g. PLA) degrade in the presence of water [96–98].

Igarashi et al. [99] reported about a process the authors termed the “Pulp Direct-Kneading Method”. The process simultaneously fibrillates dried pulp into nanoscale fibers with a diameter of 10–100 nm and uniformly disperses the resulting CNFs in HDPE. The pulp fibers were previously modified by alkenyl succinic anhydride (ASA), which suppresses the hydrogen bonding between dried CNFs and afterwards kneaded in a melt extruder to fibrillate the fibers and disperse them in HDPE. The authors aim was to increase the attractiveness of CNFs for commercialization by the “Pulp Direct-Kneading Method” [99].

However, Wang et al. [100] pointed out that screw designs still need to be optimized to generate higher shear forces to obtain CNFs that are homogeneously dispersed in thermoplastic matrix and suitable for large-scale production. In addition, better understanding of the relations between extrusion parameters, such as e.g. temperature settings, screw speed, residence time, and dispersion of CNFs is required [100]. Bourmaud et al. [101] investigated the property changes of plant fibers (including lignocellulosic fibers) during processing of biocomposites and presented the importance of selecting suitable processing parameters to take full advantage of lignocellulosic fiber reinforcements.

Tanase et al. (2019) [79] demonstrated that PLA can be compounded with lignin and the biocomposites performed well in 3D printing operations. No sign of phase separation was observed and X-ray analysis revealed that lignin increased the crystallization, indicating that lignin acted as nucleating agent. However, lignin did not improve the mechanical properties of the biocomposite which suggests that an

additional reinforcement (e.g. lignocellulosic fibers) may be adequate for tailoring the mechanical performance [102–104].

4. Compatibilizers and fiber surface treatments

The well-known poor interaction between lignocellulosic fibers and e.g. polyolefins, is related to the highly different polarities of the matrix (hydrophobic) and the lignocellulosic fibers (hydrophilic). Therefore, it is important to include coupling agents and/or fiber sizing, which compensates the polarity difference between fiber and matrix to improve the adhesive strength between the two phases and contribute to an even distribution of the fibers in the matrix.

Fibers can be modified physically to change their surface properties and enhance mechanical adhesion, or chemically to improve adhesion through chemical reactions. Physical treatments include corona, plasma and ultraviolet (UV). Chemical modifications include alkaline, silane [105–109], acetylation, oxidation, maleated coupling agents [110,111], grafting and others. More detailed information on fiber treatments can be found in [15].

Widely used coupling agents for lignocellulosic fibers and thermoplastic polymers are maleated coupling agents, for example maleated polypropylene (MAPP) or maleated polyethylene (MAPE) [112,113]. It is worth to mention that in most cases MAPE and MAPP are based on polyolefins derived from petroleum. However, recent developments have also introduced maleated polyolefins where the PE fraction was derived from biomass resources [114]. In addition, maleic anhydride can also be obtained from carbohydrates, e.g. from 5-hydroxymethylfurfural [115], which makes it possible to produce 100% bio-based compatibilizers.

As an alternative to chemical modifications, Filgueira et al. [116] focused on the enzymatic modification of thermo-mechanical pulp (TMP) fibers by grafting phenolic compounds, which rendered the TMP fibers hydrophobic and with better compatibility with the used PLA matrix. The authors demonstrated that the compatibilization with octyl gallate by enzymatic grafting improved the tensile strength and simultaneously reduced the water uptake of the biocomposite. Although a clear, positive fiber-reinforcing effect was demonstrated, the tensile strength of the 3D printed specimens with reinforcement was low. This was most probably due to the processing parameters selected for 3D printing.

Approaches to reduce hydrophilicity of lignocellulosic fiber and CNFs surfaces include the use of relatively simple methods that are usually applied to paper sizing, e.g. hydro-phobization with ASA or alkyl ketene dimers (AKD). Sato et al. (2016) [117] applied ASA to modify the surface of mechanically produced CNFs in order to improve the reinforcement potential of HDPE. The use of unmodified CNFs increased the tensile strength and modulus and the hydrophobized CNFs (18.8 wt.%) potentiated this effect, achieving strength and modulus levels of 43.4 MPa and 1.97 GPa, respectively. Lepetit et al. (2017) [118] confirmed this approach by modifying mechanically produced CNFs with ASA and testing the modified CNFs as reinforcement of low-density PE. The effect of the surface modification led to a significant increase of the tensile strength and modulus. Three main aspects can be drawn from this approach, i) the CNFs grade was a relatively coarse quality which avoid chemical pre-treatment and reduces production costs, ii) the modification can be performed in the wet state of the CNFs which may ease part of the processing and iii) mechanically produced CNFs (Fig.3A) seem to provide an acceptable level of mechanical improvement. However, it remains an open question whether the additional processing steps and energy, to produce the CNFs and compound with PE, are necessary considering that the reported levels of mechanical improvement can be achieved with more reasonable and abundant lignocellulosic pulp fibers, such as thermo-mechanical pulp fibers (see e.g. [119]).

Surface modification through acetylation of CNFs contributed to better dispersion of CNFs in PLA for low fiber loadings up to 0.5 wt.% - 5 wt.% [120]. However, no increment in tensile strength or modulus could

be achieved [121]. For decylamine-modified CNCs in PLA, similar outcomes were reported [122].

According to Olonisakin et al. [109] the currently most used surface modification techniques are silane treatments. Prior maceration of fiber by NaOH causes a rough surface, so that both chemical and mechanical adhesion is promoted. It was stated that a combination of adding compatibilizers to the matrix and treating the fiber with NaOH is an efficient way to compatibilize lignocellulosic fibers and bioplastics.

Lignin has also been proposed as coupling agent in biocomposite filaments [123]. The effect of esterified lignin was comparable to the commercial coupling agent used in these experiments. According to the authors, the lignin esterified with maleic anhydride provided the best specific tensile strength of biocomposite filaments (7.71 MPa), which was comparable to a commercial coupling agent (7.68 MPa). However, the effect of lignin, based on the provided data, has to be taken with care as the significance of the strength effect is small with regard to the scattering of the measurements. In addition, the reported tensile strength values are considerably lower than the expected, considering the commercial PLA used in the study (~4 MPa – value reported in the study vs. 48 MPa – value provided by NatureWorks® Ingeo™ 3051D).

5. Analytical modelling for tailoring the mechanical performance of biocomposites

This section shall provide a brief overview about micromechanics of biocomposites, to offer the reader a well-founded background on the mechanical interaction between the previously mentioned components. Analytical methods can be used to estimate and determine the required raw material properties that are necessary for targeted biocomposite tensile properties or to verify the interfacial interaction between fiber and matrix [119]. For predicting tensile strength and modulus of composite materials in general, the rule of mixture is a common assumption [124,125].

Lignocellulosic fibers are not available as endless, continuous filaments. The length of lignocellulosic plant fibers usually ranges between 1–35 mm and their diameter between 15–30 μm [33]. However, the length also depends on the origin [60] and might be reduced during processing, e.g. compounding [30,126,127]. Furthermore, they can be classified, according to their length, as short fibers (1–5 mm) or long fibers (5–50 mm) [30,33,128].

Lignocellulosic-short-fiber biocomposites can be considered as isotropic, if the fiber orientation is completely random [91]. In composites, external loads are applied to the matrix and transferred to the fibers through the fiber ends and the cylindrical surface close to the ends. The critical-fiber-length of a fiber in a matrix can be regarded as the minimum length in which the maximum fiber strength $\sigma_{f,max}$ can be achieved. The critical-fiber-length l_c is given by the following equation [91]:

$$\frac{l_c}{d} = \frac{\sigma_{f,max}}{2\tau_y} \quad (5.1)$$

In equation (5.1) d describes the fiber diameter and τ_y is the matrix yield strength in shear, which can be set as equal to the interface shear strength along the fiber length, assuming perfect bonding between fiber and matrix. Through single-fiber pull-out tests the actual interfacial shear strength (IFSS value) can be determined by dividing the load at debonding of fiber and matrix by the shell surface of the fiber [129–131]. Lignocellulosic fibers embedded in a thermoplastic matrix usually result in IFSS values between 3 MPa and 25 MPa [132–136]. Other test methods to determine the interfacial shear strength between fiber and matrix are the single-fiber push-out [137], micro-bonding [133,138] or micro-debonding [139,140] tests. If the fiber length of the lignocellulosic short-fibers is much longer than the load-transfer-length, the biocomposite can be regarded as a continuous-fiber biocomposite [91].

Typical fiber lengths and diameters of lignocellulosic fibers, considered in this review, are presented in Table 3. In addition, a

Table 3
Comparison of lignocellulosic fiber types and comparison of a critical-fiber-length for one specific case.

Fiber type	Fiber diameter	Fiber length before compounding	Fiber length after compounding	Theoretically calculated critical-fiber-length
Lignocellulosic fibers	15–30 μm [33]	1–5 mm [47]	~ 500 μm [30, 119, 141]	400–1500 μm (referred to the fiber length after compounding)
Mechanically/enzymatically treated CNF	20–100 nm [142]	> 10 μm [142]	-	0.6–1.8 μm
TEMPO treated CNF	3–5 nm [143]	200–1100 nm [143]	-	282–882 nm
CNC	3–35 nm [143]	200–500 nm [143]	100 nm [144]	529–45300 nm

theoretically calculated critical-fiber-length is given, to compare it to the actual fiber lengths. Equation (5.1) was used to estimate the critical-fiber-length. For each fiber type the maximum fiber strength was taken from literature according to Table 2 [67,71,72]. BioPE was chosen as an exemplary matrix with a tensile strength of 18 MPa according to [119]. The shear strength at yield for BioPE can then be calculated by $\tau = (\sqrt{2}/3) \cdot \sigma$ and results in $\tau = 8.5$ MPa.

The calculated load-transfer-length of all fiber types is, in this assumption, equal to or much longer than their actual fiber length. These biocomposites are thus regarded as short-fiber biocomposites. Note that the calculated critical-fiber-length depends on the fiber strength and assumes a perfect bond between fiber and matrix. With weak fiber-matrix bonding, the reinforcement would thus be regarded in the form of particles rather than fibers.

Moreover, it is important to note that the lignocellulosic fiber lengths reported in Table 3 correspond to the lengths of the fibers after compounding. Compounding reduces the fiber length as demonstrated by [30,119,141]. In addition, one may expect that similar damage may apply for CNFs, meaning that they may be structurally modified after compounding [144]. This could be the case in particular with mechanically produced CNFs due to the coarse structure of the material.

Equation (5.1) further indicates, that the critical-fiber-length is proportional to the fiber diameter. Assuming the fiber has a circular profile, its dimensions can be described by the corresponding aspect ratio (fiber length divided by fiber diameter) [41]. According to equation (5.1), a higher fiber aspect ratio leads to more effective strengthening of the biocomposite until a critical value l_c/d is reached (see equations 5.1 and 5.3). For higher aspect ratios the strength remains approximately constant. However, this assumption does not cover effects of fiber orientation, homogeneous dispersion, fiber shape and interfacial interactions between fiber and matrix.

There are several micromechanical models for short-fiber biocomposites which extend laminate theory [124] by including interfacial adhesion (Hirsch's model), shape fitting factors (Halpin-Tsai model) or the shear-lag parameter (Cox) [145]. Narin [146] modified Cox's shear lag parameter by including the shear modulus of the fibers and an adhesion parameter to create better agreement with experimental values.

Another widely used model to predict the unidirectional tensile modulus E_l and strength σ_l of biocomposites is the modified rule of mixture (Equation (5.2)). An orientation factor x_1 and a length and interface factor of the fibers x_2 is added to the rule of mixture to cover effects caused by un-oriented short-fiber reinforcements [112, 145]:

$$E_l = x_1 x_2 E_f V_f + E_m (1 - V_f) \quad (5.2)$$

$$\sigma_l = x_1 x_2 \sigma_f V_f + \sigma_m (1 - V_f) \quad (5.3)$$

In equation (5.2) and (5.3) the longitudinal fiber tensile modulus and strength are described by E_f and σ_f . The matrix tensile modulus and strength are described by E_m and σ_m . V_f describes the fiber volume fraction in the biocomposite. The length-and-interface factor x_2 is given by $x_2 = l/(2 \cdot l_c)$ for fiber lengths l less than the critical fiber length l_c . If l is equal or greater than l_c , $x_2 = 1 - l_c/(2 \cdot l)$ [147]. The orientation factor x_1 is assumed to be 0.167 for randomly aligned fibers in three dimensions, 0.334 for a random alignment in plane and 1.0 for unidirectional aligned fibers [148]. However, Sanadi [147] reported difficulties in determining an orientation factor due to the difference between the core- and skin-fiber-orientation, according to the melt flow. Furthermore, the topography of lignocellulosic fibers is quite uneven (Fig. 1) and also the fiber length and strength vary greatly.

Furthermore, equation (5.3) is only valid if the fiber strain is similar to the matrix strain. The biocomposites, considered in this review, consist of brittle reinforcing fibers and ductile matrixes. In that case the biocomposite strength σ_f should be lower than the strength of the neat biopolymer, if the fiber volume fraction is below a critical fiber volume fraction $V_{f,crit} = \frac{\sigma_m - \sigma_m'}{\sigma_f + (\sigma_m - \sigma_m')}$ [31,149]:

$$\sigma_1(V_f) = \begin{cases} \sigma_m(1 - V_f) & \text{for } 0 < V_f < V_{f,min} \\ \sigma_f V_f + \sigma_m(1 - V_f) & \text{for } V_f < V_{f,min} \end{cases} \quad (5.4)$$

In Equation (5.4), σ'_m is the matrix strength at the fiber failure strain and $V_{f,min} = \frac{\sigma_m - \sigma_m'}{\sigma_f - \sigma_m}$ is the fiber volume fraction, at which the biocomposite should result in its minimum strength. At a volume fraction below $V_{f,crit}$ the biocomposite can be regarded as a porous matrix, corresponding to the fiber fraction [149]. According to the Kelly-Tyson equation [150] the fiber strength σ_f is given by $\sigma_f = (l \cdot \tau)/d$ for fibers shorter than l_c and $\sigma_f = \sigma_{uf}(1 - (\sigma_{uf} \cdot d)/(4 \cdot l \cdot \tau))$ for fibers equal or longer than l_c , with σ_{uf} is the ultimate tensile strength of the reinforcing fiber [150].

Since σ_{uf} and the orientation factor x_1 are unknown, Bowyer and Bader proposed to assume that σ_{uf} equals the elastic modulus of the fibers times the strain of the composite [148]. They further assume that the orientation factor x_1 is not strain-dependent and equal for all fibers [148]:

$$\sigma_1 = x_1 \cdot \left[\sum \frac{l_i \cdot \tau}{d} V_{fi} + \sum E_j \cdot \varepsilon_c \left(1 - \frac{E_j \cdot \varepsilon_c \cdot d}{4 \cdot l_j \cdot \tau}\right) V_{fj} \right] + E_m \cdot \varepsilon_c (1 - V_f) \quad (5.5)$$

In equation (5.5) the indices i are used for fiber fractions with a length less than l_c and j for fiber fractions with a length equal or greater than l_c . The values required to solve equation (5.4) must be obtained from a tensile test and by determining the fiber lengths experimentally. The detailed procedure is described in [148].

Several studies [112,151–153] show good agreements between analytical and experimental results by using the Bowyer-Bader assumption [148]. However, one must be aware of the effect of fiber agglomeration, which is still not considered and can increase the error of the equation (5.4), especially for higher fiber loadings.

Applying analytical models to CNF- or CNC-reinforced thermoplastic polymers turns out to be insufficient for predicting tensile strength and modulus due to inadequate dispersion, poor fiber matrix bonding and fiber agglomeration [4,154]. Further research on how to adjust the known micromechanical models to be applicable for CNF/CNC biocomposites is required.

6. Bionanocomposites – challenges and opportunities

Biocomposites containing nanocellulose are commonly referred to as bionanocomposites. There are several articles and reports about the potential of nanocellulose as a reinforcement for bionanocomposites [4, 12,47,155], stating their potentially high tensile stiffness and strength [57,67]. However, there are also some growing concerns as to whether nanocellulose is adequate as thermoplastic reinforcement in large quantities [13], which is understandable when aspects such as energy

consumption during production of nanofibers and the potential nanofiber agglomeration during compounding are taken into account.

Since lignocellulosic fibers exhibit high variations of properties related to disturbances during plant growth, climatic conditions, soil types, etc., the idea is to eliminate the fiber defects by deconstruction [69]. Various grinding and homogenization methods from sectors such as food processing, cosmetics or the pharmaceutical industry were used for the preparation of nanocellulose. The main issues with these methods are still that the fibers tend to entangle which can cause fiber damage, plugging of the processing equipment and a high energy consumption during production [47,69].

As described in Section 2.2, chemical pretreatments are necessary to facilitate the deconstruction of the fibers into homogeneous CNFs (Fig. 3B). When considering lignocellulosic pulp fibers in their largest scale as reinforcement for bioplastics, the previous mentioned chemical pretreatments are omitted. Obviously, this saves time, energy, equipment capacity and human resources.

Lignocellulosic pulp fibers also have a lower outer surface area per unit mass compared to nanocellulose. It thus seems more reasonable to consider surface modification on lignocellulosic pulp fibers than on nanocellulose. Less surface area requires less compatibilizer [13,155]. An extensive overview on how the size of cellulose-based reinforcements affects the mechanical properties of a given biocomposite has been provided by Hubbe and Grigsby [13]. The authors compared multiple recent studies dealing with the mechanical performance of cellulose reinforced HDPE to analyze the effect of fiber size on tensile stiffness and strength. They could not find a statistically significant relation between mechanical strength and fiber size, when considering all their collected data. In contrast they found a statistically significant increase of tensile modulus with increasing fiber length from 0.1 to 10 000 μm . It was also shown that the compatibility between fiber and matrix tend to be a much more important factor, regarding tensile strength, than fiber size.

The use of CNFs in thermoplastic bionanocomposites requires to overcome various limitations. One specific challenge is to dry a CNF dispersion (commonly 1-5% in water) without causing agglomeration of the nanofibrils. Although, the relatively high temperatures applied in compounding and injection molding processes are adequate for lignocellulosic fibers ($< 210^\circ\text{C}$), some CNF grades (e.g. TEMPO CNF) may be more exposed to thermal degradation [64], which may potentially limit the mechanical properties of biocomposites containing CNFs. These conditions lead to significant decrease of tensile strength and stiffness in the resulting bionanocomposite [47]. Such limitations should be a main driver in the development of new compounding processes which may facilitate the potential utilization of nanocellulose in relevant bionanocomposites.

One approach to improve the fiber alignment of CNFs is the so called wet-stretching method [14,156]. The wet-stretching method was developed for wet-spun CNFs for biomedical applications. After spinning a specific wet stretching device is used to increase the fiber alignment [156]. The stretching method was also successfully applied on melt spun poly(butylene succinate) and microfibrillated cellulose [157]. Stretching is generally adopted from classic polymer filament spinning methods, such as wet-, dry- or melt spinning. The filament is stretched by down-drawing to enable orientation of the polymer chains along the fiber axis [158].

An advantage for nanocellulose-based reinforcement may be offered by the use of relatively hydrophilic matrixes like epoxy resin or starch, since there is no need of any coupling agents or surface treatments to gain solid adhesion [13]. Heryv et al. [159] performed a life-cycle-analysis (LCA) for nanocellulose reinforced epoxy resin, neat PLA and 30 wt.% glass fiber reinforced polypropylene (GF/PP). The authors concluded that the production and biocomposite manufacturing of CNFs has a higher global warming potential (GWP) and a higher abiotic depletion potential of fossil fuels (ADf) than producing PLA or GF/PP composites. In terms of use phase and end-of-life it was found that only with a fiber loading of > 60 vol.% the GWP and ADf of

CNF/epoxy can be lower than that of neat PLA [159]. However, it is particularly that Hervy et al. [159] compared thermoplastics (PLA, GF/PP) and thermosets (CNF-reinforced epoxy), which are expected to cover different application areas. A relevant study would be to compare e.g. PLA, fiber-reinforced PLA and CNF-reinforced PLA and thus reveal the LCA performance of timely biocomposite materials. Additionally, studies that only take into account the production of CNFs and CNCs have shown that the use of chemicals during the pre-treatment process is the main contributing factor to the environmental impact [160,161].

7. 3D printing of lignocellulosic short-fiber reinforced bioplastics

Biocomposites can be produced with several methods, depending on quantity, size, design, application and the material to be processed. In addition to the material composition, the production process also affects the biocomposite properties. Biocomposite products are mainly manufactured through injection molding, compression molding, extrusion or 3D printing. The latter is the main focus of this review and will be explored further in the following.

7.1. Fused deposition modelling

For prototyping and/or implementation of challenging designs, 3D printing, such as FDM, is a time and resource saving production method for biocomposite products. FDM applies a heated nozzle to deposit thin threads (approx. diameter <math><400\ \mu\text{m}</math>) to construct 3D structures, layer by layer [162]. The dimensions of the layer height and width depend entirely on parameter selection based on nozzle size, printer and 3D slicer capability. This technique is the most affordable and widespread method within additive manufacturing [18].

The characteristics of FDM printed products depend on processing parameters, layer construction and filament properties. Adjustable processing parameters are the extrusion temperature (nozzle temperature), heating plate temperature, possibly heated enclosure (chamber) temperature, extrusion speed and layer height. The temperature settings are mainly referred to the matrix material, but the degradation temperature of lignocellulosic components (which starts at approx. 200°C) is important to consider. The layer construction, including raster width, layer height orientation and gap size between the filament strands, are the main characteristics that affect the mechanical properties of printed parts [18]. The strand shape and gap size are adjustable through extrusion temperature, layer height and speed [163].

Fiber reinforcements in filaments can strengthen a 3D printed part but can in cases promote void formation due to inadequate fiber-matrix interphase and rough fiber surface [18]. A high-quality biocomposite-filament needs to be well compounded, can only contain a limited amount of fibers and a limited fiber size. Otherwise the melt viscosity will increase significantly which can lead to nozzle blockage. In addition, the filament may become relatively brittle, the quality of the surface finish gets worse and the dimensional accuracy can be reduced [22]. Commercial biocomposite filaments contain up to 40 wt.% fiber loading [163]. Increasing the fiber loading in FDM-filaments roughens the surface and increases the probability of void formation [164,165] and shape deviation, caused by irregular swelling or shrinking of lignocellulosic fibers [11,166]. Although, a recent study on nanocellulose reinforced PLA [12] revealed a great reduction of voids for CNF reinforced PLA (1 wt.%) compared to neat PLA. The authors attributed this realization to reduced filament swelling at the nozzle outlet.

Shrinkage and warping of FDM-printed parts are especially critical for highly crystalline polymers, such as PP. However, amorphous polymers, such as amorphous PLA and ABS are affected by warping. Warping is the dimensional change of a solidified 3D printed part, due to residual stresses induced through rapid cooling. In order to reduce warping in FDM 3D printing, process parameter optimization is essential. It has been found that warping of PLA-parts can be reduced significantly by

choosing a relatively high nozzle temperature (220°C) and printing speed (15 mm/s) [167]. It was further observed, that it is beneficial to choose a smoother corner geometry over sharp corners [168], a lower length to width ratio of the overall 3D printed part [169] and a greater layer thickness [170,171]. Warpage is also correlated with the thermal expansion coefficient, the difference between glass transition and heat chamber temperature [169]. Lignocellulosic fillers have also been reported to reduce warping [172]. This was attributed to an increase in viscosity [22,66,173,174]. In Fig. 5 an example of lignocellulosic-filled FDM-filament, tensile test specimens and printed structures are shown.

An FDM-part is generally a layout of melted filament strands, which is comparable to a composite made of lamina ply stocks. Due to imperfect bonding between the strands, the material strength is reduced in both building planes, in contrast to an injection or compression molded part [119]. For simple modelling purpose, the filament-material itself can be roughly described as isotropic, assuming fiber lengths less than the critical fiber length. The fibers are mainly oriented according to the extrusion direction [177]. However, the effect of porosity has a greater impact on tensile properties than fiber orientation [178]. The actual FDM-part can then be regarded as orthotropic [179].

7.2. Micromechanics of FDM-printed parts

The classical laminate theory [124] considers perfect bonding between each lamina, but FDM specimens are composites of imperfectly bonded strands and voids. Therefore, the equations to calculate the elastic constants of a lamina [124] need to be adjusted. Based on the rule of mixture the elastic modulus of a unidirectional FDM-part, printed in flat build orientation [180] can be calculated by the following approaches listed in Table 4 [181]:

The elastic modulus of the filament material and the void densities must be measured experimentally. To calculate the void densities ρ_1 and ρ_2 , microscopic images of the x - y cross section of the unidirectional specimen need to be analyzed. The calculations assume pure geometric shapes (Fig. 6) [181]. The void density ρ_{voids} can be modelled based on a

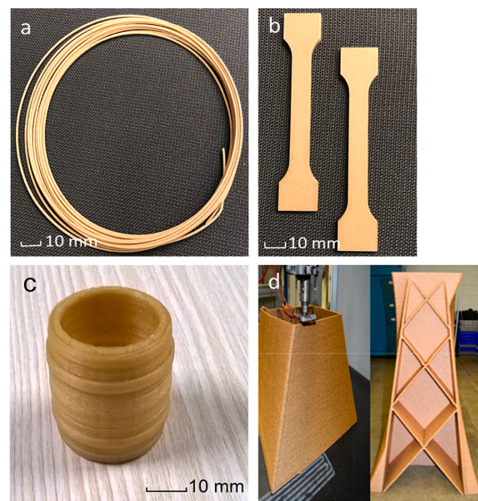


Fig. 5. Example of a lignocellulosic-filled FDM-filament. Image: Chiara Zarna, NTNU. (a), FDM-tensile-test-specimens. Image: Chiara Zarna, NTNU. (b), FDM-printed structure from lignocellulosic-filled/PLA-filament Reprinted from MDPI [175], P. 3]. Copyright (2017) by the authors. (c), building structures printed from poplar/PLA composite. Reprinted with permission from American Chemical Society [176], P. 4560]. Copyright (2019) American Chemical Society. (d).

Table 4
Modelling approaches for analytical estimation of the elastic modulus of FDM printed parts

	Elastic modulus	Nomenclature	Deviation to experiment	Filament material
Longitudinal printing direction, applicable for unidirectional printing [0]	$E_{1,p} = (1 - \rho_1)E_f$ [181]	- E_f : Elastic modulus of filament - ρ_1 : area void density, depended on gap size g , calculated from experimental measurements (Fig. 6)	4%–16%	ABS
	$E_{long} = E_{01}(e^{(1-\rho_{voids})^{C_E}} - \rho_{voids}) + E_{02}(1 - \rho_{voids})$ for an infinite number of layers: $e^{(1-\rho_{voids})^{C_E}} = 1$ [182]	- $E_{01,02}$: Elastic modulus of filament material in longitudinal and transverse direction - ρ_{voids} : area void density - C_E : Sensitivity parameter, needs to be calibrated from experimental results	< 14%	ABS
Transverse printing direction, applicable for unidirectional printing [90]	$E_{2,p} = \xi(1 - \rho_2)E_f$ [181]	- ξ : Empirical factor between 0 and 1 which takes into account the bonding strength between the filaments - ρ_2 : Linear void fraction, $\rho_2 = 1 - ((2y)/(2b - \delta))$, compare Fig. 6	~ 5%	ABS
Applicable for multiple printing lay-ups: [0], [0/90], [±45]	$E_{trans} = \xi E_{long}$ [182] $E_{effective} = \frac{A_{11}A_{22} - A_{12}^2}{A_{22}}$ [183]	- ξ : Empirical factor between 0 and 1 - A_j : Stiffness coefficient of extensional stiffness matrix [183], material parameter obtained from tensile tests on 3D printed parts	< 14 % [0]: 9%–15% [0/90]: 6% - 11% [±45]: 1%–20%	ABS PLA, PLA + carbon black
Applicable for multiple printing lay-ups: [0], [0/90], [15/-75], [30/-60] and [45/-45]	$E_{1,\theta} = \frac{1}{[A^{-1}]_{11}}h$ [181]	- A : Extensional stiffness matrix [124] - h : Thickness of FDM printed part - θ : printing angle (considered by stiffness matrix)	~ 3–7 %, compare Fig. 7	ABS

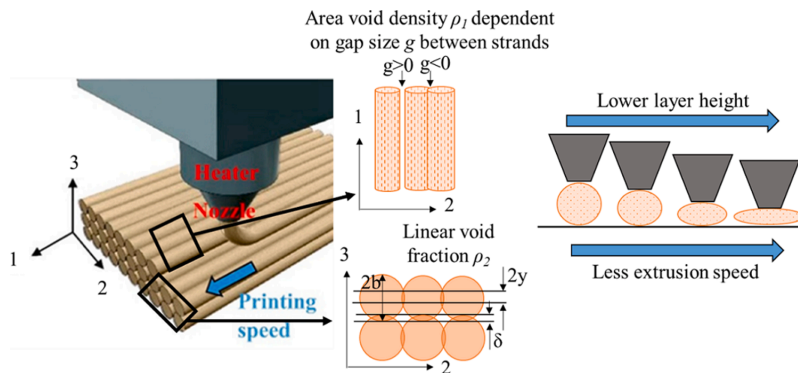


Fig. 6. Schematic illustration of an FDM-printed biocomposite part. Reprinted and modified from MDPI [163], P.3], no permission required. Copyright (2020) by the authors.

thermal model to predict the temperature evolution of the filament and a sintering model based on geometrical considerations. The temperature-dependent viscosity and surface tension of the filament material must be measured experimentally. More detailed information can be found in [182].

According to [182], the tensile strength of an FDM-part can be estimated in the same way as for the elastic modulus, using experimentally obtained material strength data and calibrated sensitivity parameters.

In [181] experiments and theoretical calculations were accomplished with FDM-parts printed in a [0], [0/90], [15/-75], [30/-60] and [45/-45] layup. Laminate theory was used to calculate the tensile modulus in longitudinal loading direction as a function of the printing angle θ . In Fig. 7 the dependency of print direction on elastic modulus of 3D printed parts is shown. Laminate theory was also used in [183] to calculate the elastic modulus for different printing layups. In this study the lowest deviation, of ~1 % between model and experiment was found for a [45/-45] layup, using a PLA- or PLA + carbon black-filament. The highest deviation of ~11 % resulted from the unidirectional [0] layup. Additionally, a bi-material part, printed out of PLA and PLA+carbon black, showed an even higher deviation (< 20 %) between analytical model and experiment in a [45/-45] layup. This was attributed to

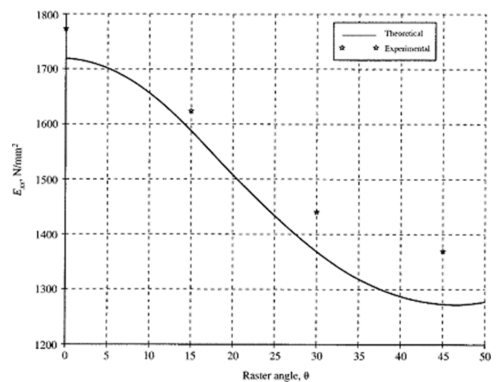


Fig. 7. Comparison between theoretical and experimental values of the elastic modulus at different angled FDM-specimens. Reprinted with permission from Elsevier [181], p. 139], license number: 4965541406639. Copyright (2002), Society of Manufacturing Engineers.

improper adhesion between PLA and PLA + carbon black.

No studies about analytical modeling of 3D printed lignocellulosic fiber reinforced biocomposites could be found, indicating a lack of research in this area. The models presented in Table 4, showed reasonable agreement with experimental results for pure polymer and PLA/carbon black composite FDM-filaments. Since void formation and irregular surface appearance is even more present in filaments containing lignocellulosic reinforcements [11,164,165], the error of the models might be comparatively greater.

7.3. Influence of printing parameters on tensile strength and modulus of lignocellulosic short-fiber biocomposites printed via FDM

Le Duigou et al. [162] presented the influence of gap size between the printing strands and set it in relation to the raster width. The authors showed that printing with less horizontal space between the strands, leads to a greater overlapping area and thus to higher tensile strength and modulus for both, a 0° and 90° printing layout.

Yang and Yeh [163] investigated the effect of extrusion speed on mechanical properties of FDM-printed wood fiber reinforced PLA. Lower extrusion speed with same layer height results in wider layer width. The smoothest surface and greatest overlapping between strands could be produced with the lowest investigated speed of 30 mm/s compared to 50 mm/s and 70 mm/s. The samples were all printed with a 0° layout which means the filament strands were aligned longitudinal to the test direction. This setup did not result in any significant change of tensile strength or modulus for different extrusion speed parameters. Showing, that in a 0° layout the porosity or void formation between the strands has almost no effect on tensile properties longitudinal to the printing direction. In contrast, compressive strength was significantly reduced (~34%) for samples printed with an extrusion speed of 70 mm/s, compared to 30 mm/s. This indicated the improved interaction between the printing strands at lower extrusion speed [163].

Several studies have shown that the overlapping or porosity of printing strands is the main influence parameter with respect to mechanical properties, apart from the layout construction. The porosity can be minimized through optimized extrusion temperature adapted to matrix and filler material [10,184,185], low extrusion speed [163], low raster width [162] and low layer height, resulting in greater layer width [66,185,186] (Fig. 6). Garzon-Hernandez et al. [182] identified the layer height as the main influencing factor on tensile properties. Through adjusting the layer height from 0.3 to 0.1 mm the void density decreased by more than 97 %.

Selected tensile properties of FDM-printed specimens made of different types of lignocellulosic biocomposites are presented in Table 5. Extensive overviews of filament types and tensile properties, including lignocellulosic fiber types for 3D printing have been presented in [21, 165,187,188].

Comparing the mechanical properties of 3D printed specimens for neat and reinforced PLA (presented in Table 5) it appears that neither tensile strength nor modulus have been improved when using fibrillated poplar [189] or lignin [79], as fillers. Using CNF to reinforce PLA increased the strength by ~24% [190] or even ~45% [10]. TMP fibers (20 wt.%) more than doubled the tensile strength and modulus of BioPE [119]. This seems to confirm the ability of wood fibers to reinforce bioplastics for 3D printing applications, compared to wood powder and lignin. Similar conclusions have been drawn by [165].

It can also be observed, that the improvement of almost 45% in tensile strength after adding 30 wt.% freeze-dried CNF to a PLA matrix, is strongly related to adjustments of the FDM-printing parameters. With the first printing setup, almost no tensile strength increment could be gained by increasing the CNF loading. After lowering the extrusion temperature from 215°C to 180°C, increasing the bed temperature from 93°C to 120°C and lowering the speed from 15 mm/s to 7.5 mm/s, a clear strength increment was achieved [10]. The influence of an optimized printing setup becomes obvious and leads to the assumption that

Table 5
Examples of tensile properties of 3D printed biocomposites

Thermoplastic polymer	Biocomposite	Strength [MPa]	Stiffness [GPa]	Elong. at break [%]
PLA [189]	Neat PLA	60	2.9	6.3
	PLA/poplar wood powder (80/20) wt. %	50	3.6	1.6
	PLA/fibrillated poplar fiber (85/15) wt. %	32	2.6	1.5
PLA [190]	Neat PLA	~46	-	~3
	PLA/PEG/CNF (91/4/5) wt.%	~57	-	~4.5
PLA [10]	Neat PLA	~55	~3	~3
	PLA/CNF (70/30) wt.%	~80	~7	~1.5
PLA [79]	Neat PLA	58.5	2.9	2.5
	PLA/Lignin (60/40) wt. %	45.7	2.7	1.9
BioPE [119]	Neat BioPE	10	0.7	10
	BioPE/lignocellulosic fiber (80/20) wt. %	30	1.5	5.5

important effects can be overlaid due to insufficient parameter configurations.

7.4. Stereolithography

Stereo-lithography (SLA) is a 3D printing technology based on photo-polymerization. A stereo-lithography resin was reinforced with CNC (0.5–10% w/w) for the prototyping of 3D objects [191]. The mechanical properties (e.g. tensile strength, young's modulus and flexural modulus) of the biocomposites increased modestly as the CNC content increased from 0.5 to 2%. Increasing the CNC content to 5% reduced the tensile strength and flexural modulus, potentially due to the formation of CNC aggregates that act as stress concentrators. Photo-polymerization is an attractive 3D printing technology that may be adequate for nanofibers and lignin. Potentially these components may be valuable reinforcement and filler candidates provided that the materials can be mixed with the photo-curable ink components.

7.5. Selective laser sintering

In Selective Laser Sintering (SLS) polymer powder is spread in a bead and a selected cross-sectional area is sintered or melted through a laser and forms a solid layer.

Lignocellulosic fiber – thermoplastic SLS parts have low mechanical strength, up to 5 MPa in tensile strength without post-processing and 6–11 MPa with wax-, or epoxy-infiltration [192-194]. To address this issue, a prosopis chilensis wood powder/poly-ethersulfone biocomposite formulation was proposed by [194]. An addition of 10% wood powder to poly-ethersulfone powder was found to be the optimum, regarding bending and tensile strength. In addition, the dimensional accuracy was improved through the filler material.

Lignin has also been introduced as a filler material in SLS to safe costs while maintaining or improving processability [195]. Including lignin in a polyamide (PA) matrix resulted in higher porosity and accordingly a higher elastic modulus and lower tensile strength compared to neat PA. The effect of lignin on the tensile strength and modulus was related to differences in surface roughness and surface energy. However, lignin also enhanced the thermal stability and wettability (for 90° print orientation) of the structure. The wettability was attributed to higher surface roughness, caused by the addition of lignin.

7.6. Applications for 3D printed lignocellulosic biocomposites

Biocomposites are widely applied for structural and nonstructural products, for example in building industry, automotive industry and household items [34,196–198]. As applications for CNF-based biocomposites the paper industry, packaging industry and medical applications are often mentioned in literature [46,47,155,199].

Presently, there are no known structural applications for biocomposites in which CNFs have proven major advantages over lignocellulosic fibers. However, there are some interesting approaches for potential future applications like wind turbine blades [200] or car components [99]. An overview of recent studies on FDM and SLA polymeric input materials containing lignocellulosic components and their applications is provided in [187]. As mentioned above, processing of a given CNF reinforced bionanocomposite is limited by the high polarity and water content of the CNF dispersion. Therefore, water-soluble polymers are the most favorable systems for CNF-based biocomposites, so far [199].

However, the use of biocomposites, primarily composed of PLA as the bioplastic matrix, has gained attention as a filament for FDM, because of its degradability and ease of printing [165]. Advances on the manufacturing of PLA- biocomposite filaments for FDM have been reported, focusing on the appropriate fiber modification for increasing the adhesion to the PLA matrix [116]. Gauss et al. [21] stated in a recent review, that continues efforts have been taken to improve the mechanical and physical performance of PLA as matrix material for biocomposite FDM-filaments, since it is widely applicable and the best tensile performance of cellulose-reinforced biocomposites has been achieved by using PLA as a matrix.

As mentioned above, lignocellulosic material covers lignocellulosic powders, fibers, nanofibrils and lignin. These materials have varying properties, enabling a wide range of different type of 3D printed applications. There exist several published studies about the mechanical properties of 3D printed lignocellulosic biocomposites [11,22,79,116,119,189,201], but there are only a few about CNF [10,11,190,202] or CNC reinforced filaments for FDM [9,11,203]. Suggesting that structural applications for these nanomaterials are still uncertain. In addition, research on long-term behaviour, is currently missing. To assess the suitability of 3D printed lignocellulosic biocomposites for structural applications, studies on durability, fatigue and reproducibility could play a major role.

8. Fatigue of lignocellulosic biocomposites

When studying mechanical properties, the short-term quasi static strength and elastic properties tend to get most attention. However, for many applications the long-term performance is no less important and may be the critical design parameter. Many parameters can influence long-term performance, such as cyclic loading (fatigue), long-term static loads (stress rupture), swelling due to the absorption of fluids and chemical degradation. This paper will just describe one of these aspects, mechanical fatigue.

Fatigue of thermoplastics generally depends on loading rate and temperature as well as on the concentration of absorbed liquids such as water [204,205].

S-N curves (stress – number of fatigue cycle curves) are used to characterize fatigue test results and to predict the remaining fatigue life of a material. Originally S-N curves were presented as Woehler curves in the log-log scale as [206]:

$$\log \Delta \sigma = \log \Delta \sigma_0 + \alpha \cdot \log N_f \quad (8.1)$$

$\Delta \sigma$ is the stress amplitude and $\Delta \sigma_0$ and α are fit parameters. This presentation of fatigue data is used also today in many design codes. However, polymer and composite fatigue material data are often published as in the linear-log scale. A widely used model in composite fatigue is the following fatigue-life-relation [207]:

$$\sigma_{max} = \beta + \alpha \cdot \log N_f \quad (8.2)$$

In equation (8.2) σ_{max} describes the maximum applied stress, β and α are curve fitting parameters and N_f is the number of cycles to failure. The S-N curve is only valid below the yield strength.

This model was used by Haque et al. [208] to analyze the fatigue behavior of PP reinforced with 50 wt.% lignocellulosic flour, 2.5 wt.% CNF and 2.5 wt.% maleic anhydride and peroxide (MAPO). The authors presented a S-N curve for a 95% survivability of neat PP and PP/lignocellulosic flour composites, as seen in Fig. 8.

In general, fiber-reinforced bio-composites offer higher fatigue strength than unreinforced plastics, because the reinforcement hinders the crack propagation in the matrix [208,209]. However, in Fig. 8 the slope of PP/lignocellulosic flour is steeper compared to neat PP. The graphs A-G refer to different temperatures ((120, 140, 160, 180)°C) and mixing time ((5, 10, 20) min.) during twin-screw extrusion of the PP/lignocellulosic flour/CNF/MAPP biocomposite. Furthermore, sample A was composed without MAPP. However, neither mixing temperature nor time variation showed a significant influence on the fatigue properties of the composites. It was also concluded that the effect of molecular degradation of PP, due to the addition of MAPP, had a higher influence on the fatigue properties of the composites compared with the compatibilizing effect of MAPP [208].

Due to the hygroscopic nature of lignocellulosic pulp fibers, the environmental conditions affect its dimensional stability and thus the fatigue behavior [210]. Several recent studies on fatigue behavior of lignocellulosic fiber-reinforced thermoplastic biocomposites can be found in the literature, comparing neat thermoplastics to biocomposites and studying the influence of coupling agents on the corresponding fatigue properties [208,211,212]. Fotouh [212] observed that after water absorption the S-N curve was shifted down on the fatigue-strength-axis about 4–7% compared to the dry composite.

In a recent study from Travieso-Rodriguez, et al. [213] the fatigue behavior of 3D printed lignocellulosic fiber reinforced PLA was investigated. The authors showed an experimental investigation of the influences of different manufacturing parameters. They concluded that the addition of lignocellulosic fibers increases voids between the filament layers and thus decreases their fatigue behavior. The mechanical fatigue properties of 3D printed parts are influenced by the same factors like under static loading: Printing parameters, material and reinforcement and layer construction [214].

Shanmugam et al. [214] presented a review about fatigue behavior

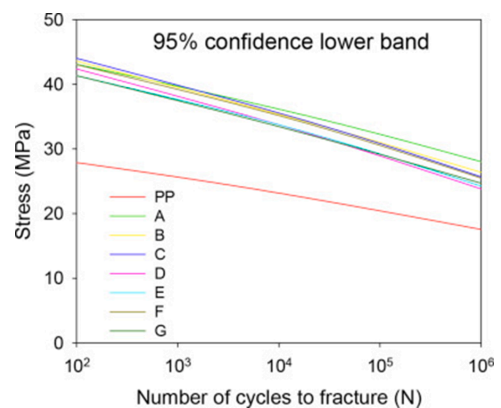


Fig. 8. S-N curve of 95% confidence band of experimental data of neat PP and PP/lignocellulosic flour composites (A-G), prepared under different mixing conditions. Reproduced with permission from Elsevier [[208], P.140], under creative commons license: <https://creativecommons.org/licenses/by-nd/4.0/>. Copyright (2019), Kingfa SCI. & TECH. CO., LTD.

of FDM-3D printed polymeric composites. The authors aim was to evaluate 3D printed polymeric materials' fatigue properties and they emphasize that mechanical fatigue investigations play a major role for enabling the use of FDM-printed products in various structural and load-bearing applications. They further concluded that a +45°/-45° print layout yields to longer fatigue life for PLA-based materials and that process parameter optimizations (regarding void reduction and ink material characteristics) are of high importance for fatigue properties. When it comes to fiber reinforcements the authors indicated the fiber wettability, fiber fraction in the matrix, fiber dimension and properties as crucial factors for determining fatigue life. But also mentioned the lack of such investigations in literature [214]. This seems to apply to biocomposites in general [215].

Studies on the fatigue properties of CNF bionanocomposite materials also lack in literature, so far. Nonetheless, analyzing the fatigue properties are important to evaluate if there are feasible applications for thermoplastic CNF-based bionanocomposites. Since the fatigue properties of biocomposite are strongly dependent on the water absorbing ability of the lignocellulosic reinforcements [210,212] and the interfacial coupling between fiber and matrix, these dependencies might apply for CNF-based bionanocomposites as well.

An investigation of lignocellulosic fiber/PP biocomposites with different aspect ratios of fibers [216] showed, that a higher aspect ratio can lead to a slight improvement of the fatigue performance of the biocomposite. But the effect of aspect ratio on fatigue strength appeared to be quite low (< 5% increased strength with ~ 44% increased aspect ratio) [216]. However, water absorption of lignocellulosic fibers is a known issue regarding to their fatigue performance due to swelling and fiber-matrix de-bonding [212,217].

A deeper understanding of failure mechanism behind the static and dynamic loading condition of 3D printed lignocellulosic biocomposites can help to improve the durability and reliability of such products [214, 215]. Greater research effort is required in this field to drive forward the implementation of (3D printed) lignocellulosic biocomposites in structural applications. Liber-Kneć et al. [218] found accelerated fatigue testing to be a useful tool to recognize basics of fatigue behavior of lignocellulosic fiber reinforced thermoplastic biocomposites or for comparative studies.

9. Conclusions

This review focused on the reinforcing ability of lignocellulosic materials as a component of biocomposites and attempted to shed light on several perspectives in terms of applicability and production challenges. Furthermore, important background information about micro-mechanics of biocomposites was presented to contribute a wider perspective for the reader.

Lignocellulosic fibers are well implemented as a reinforcement for bioplastics and contribute with beneficial properties, such as e.g. higher stiffness and strength increment. Additionally, lignin has shown potential in combination with thermoplastics and may be a plausible addition to fiber and nanocellulose-based biocomposites. However, a main challenge remains to extract and isolate lignin with high purity and reactivity. Moreover, one must find adequate chemical and enzymatic functionalization method for lignin to be further used as a polymeric matrix in thermoplastic wood-based biocomposite materials.

Optimally shaped, individual cellulose nanofibers seem to offer great mechanical properties, according to theoretical estimations. However, the reinforcing ability of nanofibers undergoes a strong reduction during biocomposite production. The most critical factors in this context are agglomeration of the nanofibers and in some cases poor compatibility between nanofiber and matrix. Presently, both of these factors suggest that nanofibers have a limited reinforcing effect in bioplastics and are not well controllable and reproducible, yet.

In 3D printing, inadequate parameter setups may greatly detract the reinforcing ability of lignocellulosic components. This review draws

attention to the deviation between theoretical estimations and physical test results, mainly caused by the poor consideration of fiber-matrix-interaction and strong impact through biocomposite processing on the resulting mechanical properties of the end-product.

Concluding, this review indicates that presently lignocellulosic pulp fibers may be more adequate as component of thermoplastic biocomposites than the corresponding cellulose nanofibers. In addition to their reinforcing properties, they require less production efforts and may perform better in LCA analysis compared to the corresponding nanofibers. This is expected to extend their applicability in a wide variety of industries such as construction, household items, interior design, and automotive. Further, investigations on durability and fatigue of lignocellulosic biocomposites are required. Understanding of production processes and their influence on the mechanical properties of biocomposites, appear to be of high importance to apply biocomposites in conversion processes such as extrusion, injection molding and 3D printing. In addition, a stronger focus on the development of energy-saving production processes could support the attractiveness of biocomposites for large-scale productions.

Declaration of Competing Interests

The authors declare that they have no known competing financial interests or personal relationships that could have appeared to influence the work reported in this paper.

Acknowledgments

The Research Council of Norway and the companies supporting the ALLOC project (Grant no. 282310) are thanked for financial support.

Supplementary materials

Supplementary material associated with this article can be found, in the online version, at [doi:10.1016/j.jcom.2021.100171](https://doi.org/10.1016/j.jcom.2021.100171).

References

- [1] P. Nygård, B.S. Tanem, T. Karlsen, P. Brachet, B. Leinsvang, Extrusion-based wood fibre-PP composites: Wood powder and pelletized wood fibres – a comparative study, *Compos. Sci. Technol.* 68 (15) (2008) 3418–3424, <https://doi.org/10.1016/j.compscitech.2008.09.029>.
- [2] G. Josefsson, F. Berthold, E.K. Gamstedt, Stiffness contribution of cellulose nanofibrils to composite materials, *Int. J. Solids Struct.* 51 (5) (2014) 945–953, <https://doi.org/10.1016/j.jisoistr.2013.11.018>.
- [3] M. Delgado-Aguilar, F. Julián, Q. Tarrés, J.A. Méndez, P. Mutjé, F.X. Espinach, Bio composite from bleached pine fibers reinforced polyolactic acid as a replacement of glass fiber reinforced polypropylene, macro and micro-mechanics of the Young's modulus, *Compos. Part B, Eng.* 125 (2017) 203–210, <https://doi.org/10.1016/j.compositesb.2017.05.058>.
- [4] Y. Aitomäki, K. Oksman, Reinforcing efficiency of nano-cellulose in polymers, reactive and functional polymers 85 (2014) 151–156, <https://doi.org/10.1016/j.reactfunctpolym.2014.08.010>.
- [5] M. Brodin, M. Vallejos, M.T. Opedal, M.C. Area, G. Chinga-Carrasco, Lignocellulosics as sustainable resources for production of bioplastics – a review, *J. Cleaner Prod.* 162 (2017) 646–664, <https://doi.org/10.1016/j.jclepro.2017.05.209>.
- [6] C. Johansson, J. Bras, I. Mondragon, P. Nechita, D. Plackett, P. Simon, D. Gregor Svetec, S. Virtanen, M. Giacinti Baschetti, C. Breen, S. Aucejo, RENEWABLE FIBERS AND BIO-BASED MATERIALS FOR PACKAGING APPLICATIONS – A REVIEW OF RECENT DEVELOPMENTS 7 (2) (2012) 47, 2012.
- [7] E. Fortunati, F. Luzi, A. Janke, L. Häußler, J. Pionteck, J.M. Kenny, L. Torre, Reinforcement effect of cellulose nanocrystals in thermoplastic polyurethane matrices characterized by different soft/hard segment ratio, *Polym. Eng. Sci.* 57 (6) (2017) 521–530, <https://doi.org/10.1002/pen.24532>.
- [8] M. Jonoobi, J. Harun, A.P. Mathew, K. Oksman, Mechanical properties of cellulose nanofiber (CNF) reinforced polyolactic acid (PLA) prepared by twin screw extrusion, *Compos. Sci. Technol.* 70 (12) (2010) 1742–1747, <https://doi.org/10.1016/j.compscitech.2010.07.005>.
- [9] A. Cataldi, D. Rigotti, V.D.H. Nguyen, A. Pegoretti, Polyvinyl alcohol reinforced with crystalline nano-cellulose for 3D printing application, *Mater. Today Commun.* 15 (2018) 236–244, <https://doi.org/10.1016/j.mtcomm.2018.02.007>.
- [10] H.L. Tekinalp, X. Meng, Y. Lu, V. Kunc, L.J. Love, W.H. Peter, S. Ozcan, High modulus biocomposites via additive manufacturing: cellulose nano-fibril

- networks as “microsponges”, *Compos. Part B: Eng.* 173 (2019), 106817, <https://doi.org/10.1016/j.compositesb.2019.05.028>.
- [11] Q. Wang, J. Sun, Q. Yao, C. Ji, J. Liu, Q. Zhu, 3D printing with cellulose materials, *Cellulose* (2018) 25, <https://doi.org/10.1007/s10570-018-1888-y>.
- [12] T. Ambone, A. Torris, K. Shanmuganathan, Enhancing the mechanical properties of 3D printed polylactic acid with nano-cellulose, *Poly. Eng. Sci.* 60 (8) (2020) 1842–1855, <https://doi.org/10.1002/pen.25421>.
- [13] M.A. Hubbe, W. Grisby, From nanocellulose to wood particles: a review of particle size vs. the properties of plastic composites reinforced with cellulose-based entities, *BioResources* 15 (1) (2020) 2030–2081.
- [14] K. Oksman, Y. Aitomäki, A.P. Mathew, G. Siqueira, Q. Zhou, S. Butylina, S. Tanpichai, X. Zhou, S. Hooshmand, Review of the recent developments in cellulose nanocomposite processing, *Compos. Part A, Appl. Sci. Manuf.* 83 (2016) 2–18, <https://doi.org/10.1016/j.compositesa.2015.10.041>.
- [15] A. Gholampour, T. Ozbakkaloglu, A review of natural fibre composites: properties, modification and processing techniques, characterization, applications, *J. Mater. Sci.* 55 (3) (2020) 829–892, <https://doi.org/10.1007/s10853-019-03990-y>.
- [16] S. Yang, B. Wei, Q. Wang, Superior dispersion led excellent performance of wood-plastic composites via solid-state shear milling process, *Compos. Part B: Eng.* 200 (2020), 108347, <https://doi.org/10.1016/j.compositesb.2020.108347>.
- [17] H.N. Chia, B.M. Wu, Recent advances in 3D printing of biomaterials, *J. Biol. Eng.* 9 (2015) 4, <https://doi.org/10.1186/s13036-015-0001-4>.
- [18] T.D. Ngo, A. Kashani, G. Imbalzano, K.T.Q. Nguyen, D. Hui, Additive manufacturing (3D printing): a review of materials, methods, applications and challenges, *Compos. Part B* 143 (2018) 172–196, <https://doi.org/10.1016/j.compositesb.2018.02.012>.
- [19] S. Singh, S. Ramakrishna, F. Berto, 3D Printing of polymer composites: a short review, material design & processing communications 2(2) (2020) e97, <https://doi.org/10.1002/mdp2.97>.
- [20] M. Guvendiren, J. Molde, R.M.D. Soares, J. Kohn, Designing biomaterials for 3D printing, *ACS Biomater. Sci. Eng.* 2 (10) (2016) 1679–1693, <https://doi.org/10.1021/acsbomater.6b00121>.
- [21] C. Gauss, K.L. Pickering, L.P. Muthe, The use of cellulose in bio-derived formulations for 3D/4D printing: a review, *Compos. Part C: Open Access.* 4 (2021), 100113, <https://doi.org/10.1016/j.jcom.2021.100113>.
- [22] V. Mazzanti, L. Malagutti, F. Mollica, FDM 3D printing of polymers containing natural fillers: a review of their mechanical properties, *Polymers* 11 (7) (2019) 1094.
- [23] 3DSourced, Fused deposition modeling: everything you need to know about FDM 3D printing, 2019. https://3dsourced.com/guides/fused-deposition-modeling-fdm/#Advantages_and_Disadvantages_of_FDM. (Accessed 20.08. 2020).
- [24] J.-Y. Lee, J. An, C.K. Chua, Fundamentals and applications of 3D printing for novel materials, *Appl. Mater. Today* 7 (2017) 120–133, <https://doi.org/10.1016/j.apmt.2017.02.004>.
- [25] A. El Mouden, M. Tarfaoui, K. Lafdi, Additive manufacturing of polymer composites: processing and modeling approaches, *Compos. Part B: Eng.* 171 (2019) 166–182, <https://doi.org/10.1016/j.compositesb.2019.04.029>.
- [26] S. Singamneni, R. Velu, M.P. Behera, S. Scott, P. Brorrens, D. Harald, J. Gerrard, Selective laser sintering responses of keratin-based bio-polymer composites, *Mater. Des.* (2019) 138, <https://doi.org/10.1016/j.matdes.2019.108087>.
- [27] R. Velu, A. Feryhough, D.A. Smith, M.J. Le Guen, Selective laser sintering of bio-composite material, *Lasers in Eng.* 0 (2016) 1–14, <https://doi.org/10.1557/jmr.2014.211>.
- [28] H. Eng, S. Maleksaeedi, S. Yu, Y.Y.C. Choong, F.E. Wiria, C.L.C. Tan, P.C. Su, J. Wei, 3D Stereolithography of Polymer Composites Reinforced with Oriented Nanoclay, *Procedia Engineering* 216 (2017) 1–7, <https://doi.org/10.1016/j.proeng.2018.02.080>.
- [29] 3DSourced, Stereolithography: Everything You Need To Know About SLA 3D Printing, 2020. <https://3dsourced.com/guides/stereolithography-sla/>. (Accessed 04.11. 2020).
- [30] T. Joffre, A. Miettinen, F. Berthold, E.K. Gamstedt, X-ray micro-computed tomography investigation of fibre length degradation during the processing steps of short-fibre composites, *Compos. Sci. Technol.* 105 (2014) 127–133, <https://doi.org/10.1016/j.compscitech.2014.10.011>.
- [31] K.L. Pickering, M.G.A. Efendy, T.M. Le, A review of recent developments in natural fibre composites and their mechanical performance, *Compos. Part A, Appl. Sci. Manuf.* 83 (2016) 98–112, <https://doi.org/10.1016/j.compositesa.2015.08.038>.
- [32] C. Neagu, K. Gamstedt, F. Berthold, Stiffness contribution of various wood fibres to composite materials, *J. Compos. Mater.* 40 (2006) 663–699, <https://doi.org/10.1177/0021998305055276>.
- [33] S.R. Djafari Petroudy, 3 - Physical and mechanical properties of natural fibers, in: M. Fan, F. Fu (Eds.), *Advanced High Strength Natural Fibre Composites in Construction*, Woodhead Publishing, 2017, pp. 59–83, <https://doi.org/10.1016/B978-0-08-100411-1.00003-0>.
- [34] D. Dai, M. Fan, 1 - Wood fibres as reinforcements in natural fibre composites: structure, properties, processing and applications, in: A. Hodzic, R. Shanks (Eds.), *Natural Fibre Composites*, Woodhead Publishing, 2014, pp. 3–65, <https://doi.org/10.1533/9780857099228.1.3>.
- [35] S.N. Monteiro, F.P.D. Lopes, A.P. Barbosa, A.B. Bevitori, L.L.A.D. Silva, L.L. D. Costa, Natural lignocellulosic fibres as engineering materials—an overview, *Metall. Mater. Trans. A* 42 (10) (2011) 2963, <https://doi.org/10.1007/s11661-011-0789-6>.
- [36] K.G. Satyanarayana, G.G.C. Arizaga, F. Wypych, Biodegradable composites based on lignocellulosic fibers—an overview, *Prog. Polym. Sci.* 34 (9) (2009) 982–1021, <https://doi.org/10.1016/j.progpolymsci.2008.12.002>.
- [37] H. Dahy, Natural Fibre-Reinforced Polymer Composites (NFRP) fabricated from ligno-cellulosic fibres for future sustainable architectural applications, case studies: segmented-shell construction, acoustic panels, and furniture, *Sensors* 19 (3) (2019), <https://doi.org/10.3390/s19030738> <https://doi.org/>.
- [38] V. Tserki, P. Matzinos, N.E. Zafeiropoulos, C. Panayiotou, Development of biodegradable composites with treated and compatibilized ligno-cellulosic fibers, *J. Appl. Polym. Sci.* 100 (6) (2006) 4703–4710, <https://doi.org/10.1002/app.23240>.
- [39] V.K. Thakur, M.K. Thakur, P. Raghavan, M.R. Kessler, Progress in green polymer composites from lignin for multifunctional applications: a review, *ACS Sustain. Chem. Eng.* 2 (5) (2014) 1072–1092, <https://doi.org/10.1021/sc500087z>.
- [40] A. Farooq, M.K. Patoary, M. Zhang, H. Mussana, M. Li, M.A. Naeem, M. Mushtaq, A. Farooq, L. Liu, Cellulose from sources to nanocellulose and an overview of synthesis and properties of nano-cellulose/zinc oxide nanocomposite materials, *Int. J. Biol. Macromol.* 154 (2020) 1050–1073, <https://doi.org/10.1016/j.ijbiomac.2020.03.163>.
- [41] H. Peltola, E. Laatikainen, P. Jetsu, Effects of physical treatment of wood fibres on fibre morphology and biocomposite properties, *Plast. Rubber Compos* 40 (2) (2011), <https://doi.org/10.1179/174328911X12988622801016>, 86–2.
- [42] G. CHINGA-CARRASCO, Exploring the multi-scale structure of printing paper – a review of modern technology, *J. Microsc.* 234 (3) (2009) 211–242, <https://doi.org/10.1111/j.1365-2818.2009.03164.x>.
- [43] Q. Tarrés, H. Oliver-Ortega, F.X. Espinach, P. Mutjé, M. Delgado-Aguilar, A. M.J., Determination of mean intrinsic flexural strength and coupling factor of natural fiber Reinforcement in Poly(lactic Acid) Biocomposites, *Polymers* (2019) 11.
- [44] F. Serra-Parareda, F. Julián, E. Espinosa, A. Rodríguez, F.X. Espinach, F. Vilaseca, Feasibility of Barley straw fibres as reinforcement in fully bio-based polyethylene composites: macro and micro mechanics of the flexural strength, *Molecules* 25 (9) (2020) 2242, <https://doi.org/10.3390/molecules25092242>.
- [45] F. Serra-Parareda, Q. Tarrés, F.X. Espinach, F. Vilaseca, P. Mutjé, M. Delgado-Aguilar, Influence of lignin content on the intrinsic modulus of natural fibres and on the stiffness of composite materials, *Int. J. Biol. Macromol.* 155 (2020) 81–90, <https://doi.org/10.1016/j.ijbiomac.2020.03.160>.
- [46] M.P. Arrieta, E. Fortunati, N. Burgos, M.A. Peltzer, J. López, L. Peponi, Chapter 7 - Nanocellulose-based polymeric blends for food packaging applications, in: D. Puglia, E. Fortunati, J.M. Kenny (Eds.), *Multifunctional Polymeric Nanocomposites Based on Cellulosic Reinforcements*, William Andrew Publishing, 2016, pp. 205–252, <https://doi.org/10.1016/B978-0-323-44248-0.00007-9>.
- [47] A. Isogai, Wood nanocelluloses: fundamentals and applications as new bio-based nanomaterials, *J. Wood Sci.* 59 (6) (2013) 449–459, <https://doi.org/10.1007/s10086-013-1365-z>.
- [48] R. Alén, Chapter 3A - Pulp and Mill and Wood-Based Biorefineries, in: A. Pandey, R. Höfer, M. Taherzadeh, K.M. Nampoothiri, C. Larroche (Eds.), *Industrial Biorefineries & White Biotechnology*, Elsevier, Amsterdam, 2015, pp. 91–126, <https://doi.org/10.1016/B978-0-444-63453-5.00003-3>.
- [49] R.A. Young, Comparison of the properties of chemical cellulose pulps, *Cellulose* 1 (2) (1994), 107–0, <https://doi.org/10.1007/BF00819662>.
- [50] H. Kargarzadeh, M. Ielovich, I. Ahmad, S. Thomas, A. Dufresne, Methods for extraction of nanocellulose from various sources, *Handb. Nanocellulose and Cellulose Nanocompos.* (2017) 1–49, <https://doi.org/10.1002/9783527689972.ch1>.
- [51] M. Pääkkö, M. Ankerfors, H. Kosonen, A. Nykänen, S. Ahola, M. Österberg, J. Ruokolainen, J. Laine, P.T. Larsson, O. Ikkala, T. Lindström, Enzymatic hydrolysis combined with mechanical shearing and high-pressure homogenization for nano-scale cellulose fibrils and strong gels, *Biomacromolecules* 8 (6) (2007) 1934–1941, <https://doi.org/10.1021/bm061215p>.
- [52] N. Lavoine, I. Desloges, A. Dufresne, J. Bras, Micro-fibrillated cellulose - its barrier properties and applications in cellulosic materials: a review, *Carbohydr. Polym.* 90 (2) (2012) 735–764, <https://doi.org/10.1016/j.carbpol.2012.05.026>.
- [53] J. Shojaeiarani, D. Bajwa, G. Holt, Sonication amplitude and processing time influence the cellulose nanocrystals morphology and dispersion, *Nanocomposites* 6 (1) (2020) 41–46, <https://doi.org/10.1080/20550324.2019.1710974>.
- [54] A. Bhatnagar, M. Sain, Processing of cellulose nano-fiber-reinforced composites, *J. Reinf. Plast. Compos.* 24 (12) (2005) 1259–1268, <https://doi.org/10.1177/0731684405049864>.
- [55] P. Phanthong, P. Reubroycharoen, X. Hao, G. Xu, A. Abudula, G. Guan, Nanocellulose: extraction and application, *Carbon Resour. Convers.* 1 (1) (2018) 32–43, <https://doi.org/10.1016/j.crcon.2018.05.004>.
- [56] M. Islam, A. Patrucco, A. Montarsolo, M. Alam, Preparation of Nano-cellulose: a review, *AATCC J. Res.* 1 (2014) 17–23, <https://doi.org/10.14504/ajr.1.5.3>.
- [57] J. Wang, X. Liu, T. Jin, H. He, L. Liu, Preparation of nanocellulose and its potential in reinforced composites: a review, *J. Biomater. Sci. Polym. Ed.* 30 (11) (2019) 919–946, <https://doi.org/10.1080/09205063.2019.1612726>.
- [58] T. Saito, Y. Nishiyama, J.-L. Putaux, M. Vignon, A. Isogai, Homogeneous suspensions of individualized micro-fibrils from TEMPO-catalyzed oxidation of native cellulose, *Biomacromolecules* 7 (6) (2006) 1687–1691, <https://doi.org/10.1021/bm060154s>.
- [59] L. Wågberg, G. Decher, M. Norgren, T. Lindström, M. Ankerfors, K. Axnäs, The build-up of polyelectrolyte multilayers of micro-fibrillated cellulose and cationic polyelectrolytes, *Langmuir* 24 (3) (2008) 784–795, <https://doi.org/10.1021/la702481v>.

- [60] G. Chinga-Carrasco, Y. Yu, O. Diserud, Quantitative electron microscopy of cellulose nanofibril structures from eucalyptus and pinus radiata kraft pulp fibers, *Microsc. Microanal.* 17 (4) (2011) 563–571, <https://doi.org/10.1017/S1431927611000444>.
- [61] H. Fukuzumi, T. Saito, A. Isogai, Influence of TEMPO-oxidized cellulose nanofibril length on film properties, *Carbohydr. Polym.* 93 (1) (2013) 172–177, <https://doi.org/10.1016/j.carbpol.2012.04.069>.
- [62] H. Lilimäntinen, M. Visanko, J.A. Sirviö, O.E.O. Hormi, J. Niinimäki, Enhancement of the Nano-fibrillation of Wood Cellulose through Sequential Periodate–Chlorite Oxidation, *Biomacromolecules* 13 (5) (2012) 1592–1597, <https://doi.org/10.1021/bm300319n>.
- [63] I. Siró, D. Plackett, M. Hedenqvist, M. Ankerfors, T. Lindström, Highly transparent films from carboxymethylated microfibrillated cellulose: the effect of multiple homogenization steps on key properties, *J. Appl. Polym. Sci.* 119 (5) (2011) 2652–2660, <https://doi.org/10.1002/app.32831>.
- [64] E.B. Heggset, G. Chinga-Carrasco, K. Syverud, Temperature stability of nano-cellulose dispersions, *Carbohydr. Polym.* 157 (2017) 114–121, <https://doi.org/10.1016/j.carbpol.2016.09.077>.
- [65] I. Sacui, R. Nieuwendael, D. Burnett, S. Stranick, M. Jorfi, C. Weder, E.J. Foster, R. Olsson, J. Gilman, Comparison of the Properties of Cellulose Nanocrystals and Cellulose Nanofibrils Isolated from Bacteria, Tunicate, and Wood Processed Using Acid, Enzymatic, Mechanical, and Oxidative Methods, *ACS Appl. Mater. Interfaces* 6 (2014) 6127–6138, <https://doi.org/10.1021/am500359f>.
- [66] A.Le Duigou, D. Correa, M. Ueda, R. Matsuzaki, M. Castro, A review of 3D and 4D printing of natural fiber biocomposites, *Mater. Des.* 194 (2020), 108911, <https://doi.org/10.1016/j.matdes.2020.108911>.
- [67] K.-Y. Lee, Y. Aitomäki, L.A. Berglund, K. Oksman, A. Bismarck, On the use of nano-cellulose as reinforcement in polymer matrix composites, *Compos. Sci. Technol.* 105 (2014) 15–27, <https://doi.org/10.1016/j.compscitech.2014.08.032>.
- [68] H. Yano, S. Nakahara, Bio-composites produced from plant microfiber bundles with a nanometer unit web-like network, *J. Mater. Sci.* 39 (5) (2004) 1635–1638, <https://doi.org/10.1023/B:JMSC.0000016162.43897.0a>.
- [69] K. Spence, Y. Habibi, A. Dufresne, Nanocellulose-based composites, 2011, pp. 179–213. https://doi.org/10.1007/978-3-642-17370-7_7.
- [70] P.P. Gillis, Effect of hydrogen bonds on the axial stiffness of crystalline native cellulose, *J. Polym. Sci. Part A-2: Polym. Phys.* 7 (5) (1969) 783–794, <https://doi.org/10.1002/pol.1969.160070504>.
- [71] F. El-Hosseiny, D.H. Page, The mechanical properties of single wood pulp fibres: theories of strength, *Fibre Sci. Technol.* 8 (1) (1975) 21–31, [https://doi.org/10.1016/0015-0568\(75\)90012-3](https://doi.org/10.1016/0015-0568(75)90012-3).
- [72] P. Bajpai, Chapter 2 - wood and fiber fundamentals, in: P. Bajpai (Ed.), *Biermann's Handbook of Pulp and Paper*, Third Edition, Elsevier, 2018, pp. 19–74, <https://doi.org/10.1016/B978-0-12-814240-0.00002-1>.
- [73] S. Biswas, Q. Ahsan, A. Cenna, M. Hasan, A. Hassan, Physical and mechanical properties of jute, bamboo and coir natural fiber, *Fibers Polym.* 14 (10) (2013) 1762–1767, <https://doi.org/10.1007/s12221-013-1762-3>.
- [74] J. Bras, D. Viet, C. Bruzzese, A. Dufresne, Correlation between stiffness of sheets prepared from cellulose whiskers and nanoparticles dimensions, *Carbohydr. Polym.* 84 (1) (2011) 211–215, <https://doi.org/10.1016/j.carbpol.2010.11.022>.
- [75] A.J. Ragauskas, G.T. Beckham, M.J. Bidy, R. Chandra, F. Chen, M.F. Davis, B. H. Davison, R.A. Dixon, P. Gilna, M. Keller, P. Langan, A.K. Naskar, J.N. Saddler, T.J. Tschaplinski, G.A. Tuskan, C.E. Wyman, Lignin valorization: improving lignin processing in the Biorefinery, *Science* 344 (6185) (2014), <https://doi.org/10.1126/science.1246843>, 1246843–1246843.
- [76] W. Zhao, B. Simmons, S. Singh, A. Ragauskas, G. Cheng, From lignin association to nano-/micro-particle preparation: extracting higher value of lignin, *Green chemistry: an international journal and green chemistry resource: GC* 18(21) (2016) 5693–5700, <https://doi.org/10.1039/c6gc01813k>.
- [77] A. Grossman, W. Vermerris, Lignin-based polymers and nano-materials, *Curr. Opin. Biotechnol.* 56 (C) (2019), <https://doi.org/10.1016/j.copbio.2018.10.009>.
- [78] G. Gellerstedt, P. Tomani, P. Axegård, B. Backlund, CHAPTER 8 Lignin Recovery and Lignin-Based Products, *Integrated Forest Biorefineries: Challenges and Opportunities*, The Royal Society of Chemistry, 2013, pp. 180–210, <https://doi.org/10.1039/9781849735063-00180>.
- [79] M. Tanase-Opedal, E. Espinosa Victor, A. Rodríguez, G. Chinga Carrasco, Lignin: a biopolymer from forestry biomass for bio-composites and 3D Printing, *Materials* 12 (18) (2019) 3006, <https://doi.org/10.3390/ma12183006>.
- [80] D. López Serna, P. Elizondo Martínez, M.A. Reyes González, A.A. Zaldívar Cadena, E.A. Zaragoza Contreras, M.G. Sánchez Anguiano, Synthesis and characterization of a lignin-styrene-butyl acrylate based composite, *Polymers* 11 (6) (2019) 1080, <https://doi.org/10.3390/polym11061080>.
- [81] J. Domínguez-Robles, E. Larrañeta, M.L. Fong, N.K. Martin, N.J. Irwin, P. Mutjé, Q. Tarrés, M. Delgado-Aguilar, Lignin/poly(butylene succinate) composites with antioxidant and antibacterial properties for potential biomedical applications, *Int. J. Biol. Macromol.* 145 (2020) 92–99, <https://doi.org/10.1016/j.ijbiomac.2019.12.146>.
- [82] E. Ten, W. Vermerris, Recent developments in polymers derived from industrial lignin, *J. Appl. Polym. Sci.* 132 (24) (2015), <https://doi.org/10.1002/app.42069>.
- [83] D. Barana, M. Orlandi, L. Zoia, L. Castellani, T. Hanel, C. Bolck, R. Gosselink, Lignin based functional additives for natural rubber, *ACS Sustain. Chem. Eng.* 6 (9) (2018) 11843–11852, <https://doi.org/10.1021/acssuschemeng.8B02145>.
- [84] S. Laurichesse, L. Averous, Chemical modification of lignins: towards bio-based polymers, *Prog. Polym. Sci.* 39 (7) (2014) 1266–1290, <https://doi.org/10.1016/j.progpolymsci.2013.11.004>.
- [85] A. Dufresne, 8 - Cellulose-Based Composites and Nano-composites, in: S. Ebnesajjad (Ed.), *Handbook of Biopolymers and Biodegradable Plastics*, William Andrew Publishing, Boston, 2013, pp. 153–169, <https://doi.org/10.1016/B978-1-4557-2834-3.00008-2>.
- [86] X. Yang, G. Wang, M. Miao, J. Yue, J. Hao, W. Wang, The dispersion of pulp-fiber in high-density polyethylene via different fabrication processes, *Polymers* 10 (2) (2018) 122, <https://doi.org/10.3390/polym10020122>.
- [87] B.V. Kokta, R. Chen, C. Daneault, J.L. Valade, Use of wood fibers in thermoplastic composites, *Polym. Compos.* 4 (4) (1983) 229–232, <https://doi.org/10.1002/pc.750040407>.
- [88] W.G. Glasser, R. Taib, R.K. Jain, R. Kander, Fiber-reinforced cellulosic thermoplastic composites, *J. Appl. Polym. Sci.* 73 (7) (1999) 1329–1340, [https://doi.org/10.1002/\(sici\)1097-4628\(19990815\)73:7<1329::Aid-app26>3.0.Co;2-4](https://doi.org/10.1002/(sici)1097-4628(19990815)73:7<1329::Aid-app26>3.0.Co;2-4).
- [89] J.R. Wagner, E.M. Mount, H.F. Giles, 13 - Screw Design, in: J.R. Wagner, E. M. Mount, H.F. Giles (Eds.), *Extrusion, Second Edition*, William Andrew Publishing, Oxford, 2014, pp. 171–179, <https://doi.org/10.1016/B978-1-4377-3481-2.00013-2>.
- [90] M. Brebu, C. Vasile, Thermal Degradation of Lignin - a Review, 2010.
- [91] B.D. Agarwal, L.J. Broutman, K. Chandrasekhara, *Analysis And Performance Of Fiber Composites*, 3. ed., John Wiley & Sons, Inc, 2006.
- [92] S. Boran, A. Kiziltas, E. Erbas Kiziltas, D.J. Gardner, Characterization of Ultrafine Cellulose-filled High-Density Polyethylene Composites Prepared using Different Compounding Methods 11 (4) (2016) 22, 2016.
- [93] P. Saha, S. Chowdhury, D. Roy, B. Adhikari, J.K. Kim, S. Thomas, A brief review on the chemical modifications of lignocellulosic fibers for durable engineering composites, *Polym. Bull.* 73 (2) (2016) 587–620, <https://doi.org/10.1007/s00289-015-1489-y>.
- [94] A.M. Radzi, S.M. Sapuan, M. Jawaid, M.R. Mansor, Water absorption, thickness swelling and thermal properties of roselle/sugar palm fiber reinforced thermoplastic polyurethane hybrid composites, *J. Mater. Res. Technol.* 8 (5) (2019) 3988–3994, <https://doi.org/10.1016/j.jmrt.2019.07.007>.
- [95] F. Ani, A. Hassan, J.C. Lai, Water absorption of lignocellulosic phenolic composites, *Polym. Polym. Compos.* 16 (2008) 379–387, <https://doi.org/10.1177/09673911080160060605>.
- [96] A. Soroudi, I. Jakubowicz, Recycling of bioplastics, their blends and biocomposites: a review, *Eur. Polym. J.* 49 (10) (2013) 2839–2858, <https://doi.org/10.1016/j.eurpolymj.2013.07.025>.
- [97] F. Codari, S. Lazzari, M. Soos, G. Storti, M. Morbidelli, D. Moscatelli, Kinetics of the hydrolytic degradation of poly(lactic acid), *Polym. Degrad. Stab.* 97 (2012) 2460–2466, <https://doi.org/10.1016/j.polydegradstab.2012.06.026>.
- [98] V. Mazzanti, M. Salzano de Luna, R. Pariente, F. Mollica, G. Filippone, Natural fiber-induced degradation in PLA-hemp biocomposites in the molten state, *Composites, Part A* 137 (2020), 105990, <https://doi.org/10.1016/j.compositesa.2020.105990>.
- [99] Y. Igarashi, A. Sato, H. Okumura, F. Nakatsubo, H. Yano, Manufacturing process centered on dry-pul direct kneading method opens a door for commercialization of cellulose nanofiber reinforced composites, *Chem. Eng. J.* 354 (2018) 563–568, <https://doi.org/10.1016/j.cej.2018.08.020>.
- [100] L. Wang, D.J. Gardner, J. Wang, Y. Yang, H.L. Tekinalp, M. Tajvidi, K. Li, X. Zhao, D.J. Neivandt, Y. Han, S. Ozcan, J. Anderson, Towards industrial-scale production of cellulose nano-composites using melt processing: a critical review on structure-processing-property relationships, *Compos- Part B: Eng.* 201 (2020), 108297, <https://doi.org/10.1016/j.compositesb.2020.108297>.
- [101] A. Bourmaud, D. Shah, J. Beaugrand, H. Dhakal, Property changes in plant fibres during the processing of bio-based composites, *Ind. Crops Prod.* 154 (2020), 112705, <https://doi.org/10.1016/j.indcrop.2020.112705>.
- [102] W. Thielemans, E. Can, S.S. Morye, R.P. Wool, Novel applications of lignin in composite materials, *J. Appl. Polym. Sci.* 83 (2) (2002) 323–331, <https://doi.org/10.1002/app.2247>.
- [103] W. Thielemans, R.P. Wool, Kraft lignin as fiber treatment for natural fiber-reinforced composites, *Polym. Compos.* 26 (5) (2005) 695–705, <https://doi.org/10.1002/pc.20141>.
- [104] N. Graupner, Application of lignin as natural adhesion promoter in cotton fibre-reinforced poly(lactic acid) (PLA) composites, *J. Mater. Sci.* 43 (15) (2008) 5222–5229, <https://doi.org/10.1007/s10853-008-2762-3>.
- [105] J. Rao, Y. Zhou, M. Fan, Revealing the interface structure and bonding mechanism of coupling agent treated WPC, *Polymers* 10 (3) (2018) 266, <https://doi.org/10.3390/polym10030266>.
- [106] E.A. Coleman, *Applied plastics engineering handbook*, in: M. Kutz (Ed.), 23 - Plastics Additives, William Andrew Publishing, Oxford, 2011, pp. 419–428, <https://doi.org/10.1016/B978-1-4377-3514-7.10023-6>.
- [107] J. Lu, Q. Wu, H.S. Jr, *Chemical coupling in wood fiber and polymer composites: a review of coupling agents and treatments*, *Wood Fiber Sci.* 32 (2000) 88–104.
- [108] Y. Xie, C.A.S. Hill, Z. Xiao, H. Militz, C. Mai, Silane coupling agents used for natural fiber/polymer composites: A review, *Composites, Part A* 41 (7) (2010) 806–819, <https://doi.org/10.1016/j.compositesa.2010.03.005>.
- [109] K. Oloniasakin, M. fan, Z. Xin-Xiang, L. Ran, W. Lin, W. Zhang, Y. Wenbin, Key improvements in interfacial adhesion and dispersion of fibers/fillers in polymer matrix composites; focus on PLA Matrix Composites, *Compos. Interfaces* (2021) 1–50, <https://doi.org/10.1080/09276440.2021.1878441>.
- [110] M.E. González-López, J.R. Robledo-Ortiz, R. Manríquez-González, J.A. Silva-Guzmán, A.A. Pérez-Fonseca, Poly(lactic acid) functionalization with maleic anhydride and its use as coupling agent in natural fiber biocomposites: a review, *Compos. Interfaces* 25 (5–7) (2018) 515–538, <https://doi.org/10.1080/09276440.2018.1439622>.

- [111] S. Cichosz, A. Masek, A. Rylski, Cellulose modification for improved compatibility with the polymer matrix: mechanical characterization of the composite material, *Materials* 13 (23) (2020) 5519.
- [112] F. Serra-Parareda, Q. Tarrés, M. Delgado-Aguilar, F.X. Espinach, P. Mutjé, F. Vilaseca, Bio-based composites from bio-based-polyethylene and barley thermo-mechanical fibers: micro-mechanics of composites, *Materials* (Basel) 12 (24) (2019), <https://doi.org/10.3390/ma12244182>.
- [113] 1-Natural fibers and their composites in: N. Chand, M. Fahim (Eds.), *Tribology of Natural Fiber Polymer Composites*, Woodhead Publishing Series in Composites Science and Engineering 2008, pp. 1-58. <https://doi.org/10.1533/9781845695057.1>.
- [114] N.V. Ehmman, D. Ita-Nagy, F.E. Felissia, M.E. Vallejos, I. Luispe, M.C. Area, G. Chinga-Carrasco, Bio-composites of Bio-Polyethylene Reinforced with a Hydrothermal-Alkaline Sugarcane Bagasse Pulp and Coupled with a Bio-Based Compatibilizer, *Molecules* 25 (9) (2020) 2158, <https://doi.org/10.3390/molecules25092158>.
- [115] J. Lan, J. Lin, Z. Chen, G. Yin, Transformation of 5-Hydroxymethylfurfural (HMF) to Maleic Anhydride by Aerobic Oxidation with Heteropolyacid Catalysts, *ACS Catal.* 5 (4) (2015) 2035–2041, <https://doi.org/10.1021/cs501776n>.
- [116] D. Filgueira, S. Holmen, J.K. Melbø, D. Moldes, A.T. Echtermeyer, G. Chinga-Carrasco, Enzymatic-assisted modification of thermo-mechanical pulp fibers to improve the interfacial adhesion with Poly(lactic acid) for 3D Printing, *ACS Sustain. Chem. Eng.* 5 (10) (2017) 9338–9346, <https://doi.org/10.1021/acsschemeng.7b02351>.
- [117] A. Sato, D. Kabusaki, H. Okumura, T. Nakatani, F. Nakatsubo, H. Yano, Surface modification of cellulose nanofibers with alkenyl succinic anhydride for high-density polyethylene reinforcement, *Compos., Part A* 83 (2016) 72–79, <https://doi.org/10.1016/j.compositesa.2015.11.009>.
- [118] A. Lepetit, R. Drolet, B. Tolnai, D. Montplaisir, R. Lucas, R. Zerrouki, Microfibrillated cellulose with sizing for reinforcing composites with LDPE, *Cellulose* 24 (10) (2017) 4303–4312, <https://doi.org/10.1007/s10570-017-1429-0>.
- [119] Q. Tarrés, J.K. Melbø, M. Delgado-Aguilar, F.X. Espinach, P. Mutjé, G. Chinga-Carrasco, Bio-polyethylene reinforced with thermomechanical pulp fibers: Mechanical and micromechanical characterization and its application in 3D-printing by fused deposition modelling, *Compos. Part B: Eng.* 153 (2018) 70–77, <https://doi.org/10.1016/j.compositesb.2018.07.009>.
- [120] F. Dong, M. Yan, C. Jin, S. Li, Characterization of Type-II Acetylated cellulose nano-crystals with various degree of substitution and its compatibility in PLA Films, *Polymers* 9 (8) (2017) 346.
- [121] M. Jonoobi, A.P. Mathew, M.M. Abdi, M.D. Makeinejad, K. Oksman, A Comparison of Modified and Unmodified Cellulose Nanofiber Reinforced Poly(lactic Acid) (PLA) Prepared by Twin Screw Extrusion, *J. Polym. Environ.* 20 (4) (2012) 991–997, <https://doi.org/10.1007/s10924-012-0503-9>.
- [122] J.L. Orellana, D. Wichhart, C.L. Kitchens, Mechanical and optical properties of poly-lactic acid films containing surface-modified cellulose nano-crystals, *J. Nanomater.* 2018 (2018), 7124260, <https://doi.org/10.1155/2018/7124260>.
- [123] I. Anugwom, V. Lahtela, M. Kallioinen, T. Kärki, Lignin as a functional additive in a bio-composite: influence on mechanical properties of poly(lactic acid) composites, *Ind. Crops Prod.* 140 (2019), 111704, <https://doi.org/10.1016/j.indcrop.2019.111704>.
- [124] R.F. Gibson, *Principles of Composite Material Mechanics*, McGraw-Hill, New York, London, 1994.
- [125] D. Richardson, *The Fundamental Principles of Composite Material Stiffness Predictions*, University of the West of England, UWE Bristol.
- [126] J. Olson, *Fibre length fractionation caused by pulp screening, slotted screen plates*, *J. Pulp Paper Sci.* 27 (2001).
- [127] O. Ferritsius, R. Ferritsius, M. Rundlöf, Average fibre length as a measure of the amount of long fibres in mechanical pulps – ranking of pulps may shift, *Nord. Pulp Pap. Res. J.* 33 (3) (2018) 468–481, <https://doi.org/10.1515/npprj-2018-3058>.
- [128] A. Miettinen, C.L. Luengo Hendriks, G. Chinga-Carrasco, E.K. Gamstedt, M. Kataja, A non-destructive X-ray microtomography approach for measuring fibre length in short-fibre composites, *Compos. Sci. Technol.* 72 (15) (2012) 1901–1908, <https://doi.org/10.1016/j.compscitech.2012.08.008>.
- [129] P.J. Herrera-Franco, A. Valadez-González, A study of the mechanical properties of short natural-fiber reinforced composites, *Compos. Part B: Eng.* 36 (8) (2005) 597–608, <https://doi.org/10.1016/j.compositesb.2005.04.001>.
- [130] O. Adekomaya, T. Majosi, Compatibility of Natural Fiber and Hydrophobic Matrix in Composite Modification (2020) 1–20, <https://doi.org/10.1016/j.978-3-030-11155-7.181-1>.
- [131] C. DiFranca, T. C. Ward, R.O. Claus, The single-fibre pull-out test. 1: review and interpretation, *Composites, Part A* 27 (8) (1996) 597–612, [https://doi.org/10.1016/1359-835X\(95\)00069-E](https://doi.org/10.1016/1359-835X(95)00069-E).
- [132] D.C. Nguyen, A. Makke, G. Montay, A Pull-out Fiber/Matrix Interface characterization of vegetal fibers reinforced thermoplastic polymer composites: the influence of the processing temperature, engineering and technology, *Int. J. Chem., Mol., Nucl., Mater. Metall. Eng., World Acad. Sci.* 9 (2015) 732–736.
- [133] N. Graupner, J. Rößler, G. Ziegmann, J. Müssig, Fibre/matrix adhesion of cellulose fibres in PLA, PP and MAPP: A critical review of pull-out test, microbond test and single fibre fragmentation test results, *Composites, Part A* 63 (2014) 133–148, <https://doi.org/10.1016/j.compositesa.2014.04.011>.
- [134] H. Wang, G. Tian, H. Wang, W. Li, Y. Yu, Pull-out method for direct measuring the interfacial shear strength between plant fibers and thermoplastic polymer composites (TPC), *Holzforschung* (2014) 68, <https://doi.org/10.1515/hf-2013-0052>.
- [135] M. Sain, K.O. Niska, M. Institution of, Metallurgy, Wood-polymer composites, Woodhead Publ. and Maney Publ. on behalf of the Institute of Materials, Minerals & Mining, Cambridge, 2008.
- [136] J.L. Thomason, J.L. Rudeiros-Fernández, Characterization of interfacial strength in natural fibre – polyolefin composites at different temperatures, *Compos. Interfaces* (2021) 1–22, <https://doi.org/10.1080/09276440.2021.1913901>.
- [137] C. Medina M, J.M. Molina-Aldareguía, C. González, M.F. Melendrez, P. Flores, J. Llorca, Comparison of push-in and push-out tests for measuring interfacial shear strength in nano-reinforced composite materials, *J. Compos. Mater.* 50 (12) (2015) 1651–1659, <https://doi.org/10.1177/0021998315595115>.
- [138] L. Yang, J.L. Thomason, Development and application of micromechanical techniques for characterising interfacial shear strength in fibre-thermoplastic composites, *Polym. Test.* 31 (7) (2012) 895–903, <https://doi.org/10.1016/j.polymertesting.2012.07.001>.
- [139] A.Le Duigou, C. Baley, Y. Grohens, P. Davies, J.-Y. Cognard, R. Créach'cadec, L. Sohier, A multi-scale study of the interface between natural fibres and a biopolymer, *Composites, Part A* 65 (2014) 161–168, <https://doi.org/10.1016/j.compositesa.2014.06.010>.
- [140] J.F. Mandell, J.H. Chen, F.J. McGarry, A microbonding test for in situ assessment of fibre/matrix bond strength in composite materials, *Int. J. Adhes. Adhes.* 1 (1) (1980) 40–44, [https://doi.org/10.1016/0143-7496\(80\)90033-0](https://doi.org/10.1016/0143-7496(80)90033-0).
- [141] M. Hietala, K. Oksman, Pelletized cellulose fibres used in twin-screw extrusion for biocomposite manufacturing: Fibre breakage and dispersion, *Composites, Part A* 109 (2018) 538–545, <https://doi.org/10.1016/j.compositesa.2018.04.006>.
- [142] G. Albornoz-Palma, F. Betancourt, R.T. Mendonça, G. Chinga-Carrasco, M. Pereira, Relationship between rheological and morphological characteristics of cellulose nanofibrils in dilute dispersions, *Carbohydr. Polym.* 230 (2020), 115588, <https://doi.org/10.1016/j.carbpol.2019.115588>.
- [143] O. Nechyporchuk, M.N. Belgacem, J. Bras, Production of cellulose nano-fibrils: a review of recent advances, *Ind. Crops Prod.* 93 (2016) 2–25, <https://doi.org/10.1016/j.indcrop.2016.02.016>.
- [144] A. Dufresne, Nanocellulose: From Nature to High Performance Tailored Materials, *De Gruyter*, 2017, <https://doi.org/10.1515/9783110254600>.
- [145] O. Das, N.K. Kim, D. Bhattacharyya, The mechanics of biocomposites, Second edition ed., Duxford, 2017 <https://doi.org/10.1016/B978-0-08-100752-5.00017-2>.
- [146] J.A. Nairn, Generalized shear-lag analysis including imperfect interfaces, *Adv. Compos. Lett.* 16 (6) (2004), <https://doi.org/10.1177/096369350401300601>.
- [147] A.R. Sanadi, R.A. Young, C. Clemons, R.M. Rowell, Recycled newspaper fibers as reinforcing fillers in thermoplastics: part i-analysis of tensile and impact properties in polyethylene, Reinforced Plast. Compos. (1994) 13, <https://doi.org/10.1177/073168449401300104>.
- [148] W.H. Bowyer, M.G. Bader, On the re-inforcement of thermoplastics by imperfectly aligned discontinuous fibres, *Mater. Sci.* 7 (1972) 1315–1321, <https://doi.org/10.1007/BF00550698>.
- [149] A. Lotfi, H. Li, D.V. Dao, G. Prusty, Natural fiber-reinforced composites: a review on material, manufacturing, and machinability, *J. Thermoplast. Compos. Mater.* 34 (2019), 089270571984454, <https://doi.org/10.1177/0892705719844546>.
- [150] A. Kelly, W.R. Tyson, Tensile properties of fibre-reinforced metals: Copper/tungsten and copper/molybdenum, *J. Mech. Phys. Solids* 13 (1965) 329, [https://doi.org/10.1016/0022-5096\(65\)90035-9](https://doi.org/10.1016/0022-5096(65)90035-9), in1, 339.
- [151] N.K. Kim, R.J.T. Lin, D. Bhattacharyya, Extruded short wool fibre composites: mechanical and fire retardant properties, *Composites, Part B* 67 (2014) 472–480, <https://doi.org/10.1016/j.compositesb.2014.08.002>.
- [152] G. Kalaprasad, K. Joseph, S. Thomas, C. Pavithran, Theoretical modelling of tensile properties of short sisal fibre-reinforced low-density polyethylene composites, *J. Mater. Sci.* 32 (16) (1997) 4261–4267, <https://doi.org/10.1023/A:1018651218515>.
- [153] G.W. Beckermann, K.L. Pickering, Engineering and evaluation of hemp fibre reinforced polypropylene composites: Micro-mechanics and strength prediction modelling, *Composites, Part A* 40 (2) (2009) 210–217, <https://doi.org/10.1016/j.compositesa.2008.11.005>.
- [154] J. Agarwal, S. Mohanty, S.K. Nayak, Influence of cellulose nano-crystal/sisal fiber on the mechanical, thermal, and morphological performance of polypropylene hybrid composites, *Polym. Bull.* 78 (3) (2021) 1609–1635, <https://doi.org/10.1007/s00289-020-03178-4>.
- [155] A. Sharma, M. Thakur, M. Bhattacharya, T. Mandal, S. Goswami, Commercial application of cellulose nano-composites – A review, *Biotechnol. Rep.* 21 (2019) e00316, <https://doi.org/10.1016/j.btre.2019.e00316>.
- [156] J.G. Torres-Rendon, F.H. Schacher, S. Ifuku, A. Walthner, Mechanical Performance of Macro-fibers of Cellulose and Chitin Nanofibrils Aligned by Wet-Stretching: a critical comparison, *Biomacromolecules* 15 (7) (2014) 2709–2717, <https://doi.org/10.1021/bm500566m>.
- [157] M. Zhou, M. Fan, Y. Zhao, T. Jin, Q. Fu, Effect of stretching on the mechanical properties in melt-spun poly(butylene succinate)/microfibrillated cellulose (MFC) nanocomposites, *Carbohydr Polym* 140 (2016) 383–392, <https://doi.org/10.1016/j.carbpol.2015.12.040>.
- [158] Y. Imura, R.M.C. Hogan, M. Jaffe, 10 - Dry spinning of synthetic polymer fibers, in: D. Zhang (Ed.), *Advances in Filament Yarn Spinning of Textiles and Polymers*, Woodhead Publishing, 2014, pp. 187–202, <https://doi.org/10.1533/9780857099174.2.187>.
- [159] M. Hery, S. Evangelisti, P. Lettieri, K.-Y. Lee, Life cycle assessment of nanocellulose-reinforced advanced fibre composites, *Compos. Sci. Technol.* 118 (2015) 154–162, <https://doi.org/10.1016/j.compscitech.2015.08.024>.
- [160] R. Arvidsson, D. Nguyen, M. Svanström, Life Cycle Assessment of Cellulose Nanofibrils production by mechanical treatment and two different pretreatment

- processes, *Environ. Sci. Technol.* 49 (11) (2015) 6881–6890, <https://doi.org/10.1021/acs.est.5b00888>.
- [161] H. Gu, R. Reiner, R. Bergman, A. Rudie, LCA Study for Pilot Scale Production of Cellulose Nano Crystals (CNC) from Wood Pulp (2015) 33–42.
- [162] A. Le Duigou, M. Castro, R. Bevan, N. Martin, 3D printing of wood fibre biocomposites: from mechanical to actuation functionality, *Mater. Des.* 96 (2016) 106–114, <https://doi.org/10.1016/j.matdes.2016.02.018>.
- [163] T.-C. Yang, C.-H. Yeh, Morphology and Mechanical Properties of 3D Printed wood fiber/poly(lactic acid) composite parts using Fused Deposition Modeling (FDM): the effects of printing speed, *Polymers* 12 (6) (2020) 1334, <https://doi.org/10.3390/polym12061334>.
- [164] M. Kariz, M. Sernek, M. Obucina, M. Kuzman, Effect of wood content in FDM filament on properties of 3D printed parts, *Mater. Today Commun.* (2017) 14, <https://doi.org/10.1016/j.jmtcomm.2017.12.016>.
- [165] M.E. Lamm, L. Wang, V. Kishore, H. Tekinalp, V. Kunc, J. Wang, D.J. Gardner, S. Ozcan, Material extrusion additive manufacturing of wood and Lignocellulosic filled composites, *Polymers* 12 (9) (2020) 2115.
- [166] R. Kumari, H. Ito, M. Takatani, M. Uchiyama, T. Okamoto, Fundamental studies on wood/cellulose-plastic composites: effects of composition and cellulose dimension on the properties of cellulose/PP composite, *Journal of Wood Science* 53 (6) (2007) 470–480, <https://doi.org/10.1007/s10086-007-0889-5>.
- [167] M. Alsoufi, A. El-Sayed, Warping deformation of desktop 3D printed parts manufactured by open source Fused Deposition Modeling (FDM) System, *Int. J. Mech. Mechatron. Eng.* 17 (2017) 7–16.
- [168] P. Sreejith, K. Kannan, K.R. Rajagopal, A thermodynamic framework for additive manufacturing, using amorphous polymers, capable of predicting residual stress, warpage and shrinkage, *Int. J. Eng. Sci.* 159 (2021), 103412, <https://doi.org/10.1016/j.jengsci.2020.103412>.
- [169] A. Armillotta, M. Bellotti, M. Cavallaro, Warpage of FDM parts: experimental tests and analytic model, *Rob. Comput. Integr. Manuf.* 50 (2018) 140–152, <https://doi.org/10.1016/j.rcim.2017.09.007>.
- [170] H. Li, T. Wang, Q. Li, Z. Yu, N. Wang, A quantitative investigation of distortion of poly(lactic acid) (PLA) part in FDM from the point of interface residual stress, *Int. J. Adv. Manuf. Technol.* 94 (1) (2018) 381–395, <https://doi.org/10.1007/s00170-017-0820-1>.
- [171] B.N. Panda, K. Shankhwar, A. Garg, Z. Jian, Performance evaluation of warping characteristic of fused deposition modelling process, *Int. J. Adv. Manuf. Technol.* 88 (5) (2017) 1799–1811, <https://doi.org/10.1007/s00170-016-8914-8>.
- [172] M.A. Morales, C.L. Atencio Martinez, A. Maranon, C. Hernandez, V. Michaud, A. Porras, Development and characterization of rice husk and recycled polypropylene composite filaments for 3D Printing, *Polymers* 13 (7) (2021) 1067.
- [173] B. Huang, H. He, S. Meng, Y. Jia, Optimizing 3D printing performance of acrylonitrile-butadiene-styrene composites with cellulose nanocrystals/silica nanohybrids, *Polym. Int.* 68 (7) (2019) 1351–1360, <https://doi.org/10.1002/pi.5824>.
- [174] D. Filgueira, S. Holmen, J.K. Melbo, D. Moldes, A.T. Echtermeyer, G. Chingacarrasco, 3D printable filaments made of bio-based polyethylene bio-composites, *Polymers* 10 (3) (2018) 314.
- [175] Y. Tao, H. Wang, Z. Li, P. Li, S.Q. Shi, Development and application of wood filled poly(lactic acid) composite filament for 3D Printing, *Materials* 10 (4) (2017) 339, <https://doi.org/10.3390/ma10040339>.
- [176] X. Zhao, H. Tekinalp, X. Meng, D. Ker, B. Benson, Y. Pu, A.J. Ragauskas, Y. Wang, K. Li, E. Webb, D.J. Gardner, J. Anderson, S. Ozcan, Poplar as bio-fiber reinforcement in composites for large-scale 3D Printing, *ACS Appl. Bio. Mater.* 2 (10) (2019) 4557–4570, <https://doi.org/10.1021/acsbm.9b00675>.
- [177] J. Gardan, D.C. Nguyen, L. Roucoules, G. Montay, Characterization of wood filament in additive deposition to study the mechanical behavior of reconstituted wood products, *J. Eng. Fibers Fabr.* 11 (4) (2016), <https://doi.org/10.1177/155892501601100408>.
- [178] H.L. Tekinalp, V. Kunc, G.M. Velez-Garcia, C.E. Duty, L.J. Love, A.K. Naskar, C. A. Blue, S. Ozcan, Highly oriented carbon fiber-polymer composites via additive manufacturing, *Compos. Sci. Technol.* 105 (2014) 144–150, <https://doi.org/10.1016/j.compscitech.2014.10.009>.
- [179] R. Sayre, A Comparative Finite Element Stress Analysis of Isotropic and Fusion Deposited 3D Printed Polymer, *Mechanical Engineering, Rensselaer Polytechnic Institute, Hartford, Connecticut*, 2014.
- [180] M. Somireddy, A. Czekanski, C.V. Singh, Development of constitutive material model of 3D printed structure via FDM, *Mater. Today Commun.* 15 (2018) 143–152, <https://doi.org/10.1016/j.jmtcomm.2018.03.004>.
- [181] L. Li, Q. Sun, C. Bellehumeur, P. Gu, Composite modeling and analysis for fabrication of FDM prototypes with locally controlled properties, *J. Manuf. Processes* 4 (2) (2002) 129–141, <https://doi.org/10.1016/j.jmpt.2002.02.002>.
- [182] S. Garzon-Hernandez, D. Garcia-Gonzalez, A. Jerusalem, A. Arias, Design of FDM 3D printed polymers: an experimental-modelling methodology for the prediction of mechanical properties, *Mater. Des.* 188 (2020), 108414, <https://doi.org/10.1016/j.matdes.2019.108414>.
- [183] P. Kumar Mishra, P.S., Prediction of in-plane stiffness of multi-material 3D printed laminate parts fabricated by FDM process using CLT and its mechanical behavior under tensile load, *Mater. Today Commun.* 23 (2020), 100955, <https://doi.org/10.1016/j.jmtcomm.2020.100955>.
- [184] T.-C. Yang, Effect of Extrusion Temperature on the Physico-Mechanical Properties of Unidirectional Wood Fiber-Reinforced Poly(lactic Acid) Composite (WFRPC) Components Using Fused Deposition Modeling, *Polymers* 10 (9) (2018) 976, <https://doi.org/10.3390/polym10090976>.
- [185] F. Ning, W. Cong, Y. Hu, H. Wang, Additive manufacturing of carbon fiber-reinforced plastic composites using fused deposition modeling: Effects of process parameters on tensile properties, *J. Compos. Mater.* 51 (4) (2017) 451–462, <https://doi.org/10.1177/0021998316646169>.
- [186] N. Ayrlimis, M. Kariz, J.H. Kwon, M. Kitek Kuzman, Effect of printing layer thickness on water absorption and mechanical properties of 3D-printed wood/PLA composite materials, *Int. J. Adv. Manuf. Technol.* 102 (5) (2019) 2195–2200, <https://doi.org/10.1007/s00170-019-03299-9>.
- [187] A. Ji, S. Zhang, S. Bhagia, C.G. Yoo, A.J. Ragauskas, 3D printing of biomass-derived composites: application and characterization approaches, *RSC Adv.* 10 (37) (2020) 21698–21723, <https://doi.org/10.1039/D0RA03620J>.
- [188] L. Jiang, X. Peng, D. Walczyk, 3D printing of biofiber-reinforced composites and their mechanical properties: a review, *Rapid Prototyp. J.* 26 (2020) 1113–1129, <https://doi.org/10.1108/RPJ-08-2019-0214>.
- [189] S. Bhagia, R.R. Lowden, D. Erdman, M. Rodriguez, B.A. Haga, I.R.M. Solano, N. C. Gallego, Y. Pu, W. Muchero, V. Kunc, A.J. Ragauskas, Tensile properties of 3D-printed wood-filled PLA materials using poplar trees, *Appl. Mater. Today* 21 (2020), 100832, <https://doi.org/10.1016/j.apmt.2020.100832>.
- [190] Q. Wang, C. Ji, L. Sun, J. Sun, J. Liu, Cellulose Nanofibrils Filled Poly(Lactic Acid) Bio-composite Filament for FDM 3D Printing, *Molecules* 25 (10) (2020) 2319, <https://doi.org/10.3390/molecules25102319>.
- [191] S. Kumar, M. Hofmann, B. Steinmann, E.J. Foster, C. Weder, Reinforcement of Stereolithographic Resins for Rapid Prototyping with Cellulose Nano-crystals, *ACS Appl. Mater. Interfaces* 4 (10) (2012) 5399–5407, <https://doi.org/10.1021/am301321v>.
- [192] H. Zhang, Y. Guo, K. Jiang, D. Bourell, D. Zhao, Yu Yueqiang, P. Wang, Z. Li, A Review of Selective Laser Sintering of Wood-plastic Composites (2016).
- [193] K. Jiang, Y. Guo, D.L. Bourell, W. Zeng, Z. Li, Study on selective laser sintering of Eucalyptus/PES blend and investment casting technology, *Procedia CIRP* 6 (2013) 510–514, <https://doi.org/10.1016/j.procir.2013.03.039>.
- [194] A.B. Idriss, J. Li, Y. Wang, Y. Guo, E.A. Elfaki, S.A. Adam, Selective Laser Sintering (SLS) and Post-Processing of Prosopis Chilensis/Polyethersulfone Composite (PCPC), *Materials* 13 (13) (2020) 3034.
- [195] R. Ajdari, N. Kretzschmar, H. Baniasadi, J. Trifol, J. Seppala, J. Partanen, O. Rojas, Selective laser sintering of lignin-based composites, *ACS Sustain. Chem. Eng.* (2021) 9, <https://doi.org/10.1021/acscuschemeng.0c07996>.
- [196] P.K. Mallick, 5 - Thermoplastics and thermoplastic-matrix composites for lightweight automotive structures, in: P.K. Mallick (Ed.), *Materials, Design and Manufacturing for Lightweight Vehicles*, Woodhead Publishing, 2010, pp. 174–207, <https://doi.org/10.1533/9781845697822.1.174>.
- [197] D.F. Caulfield, C. Clemons, R.M. Rowell, *Wood Thermoplast. Compos.* (2010) 141–161.
- [198] M. Biron, 8 - Application Examples, in: M. Biron (Ed.), *Industrial Applications of Renewable Plastics*, William Andrew Publishing, 2017, pp. 463–518, <https://doi.org/10.1016/B978-0-323-48065-9.00008-X>.
- [199] H. Kargarzadeh, M. Mariano, J. Huang, N. Lin, I. Ahmad, A. Dufresne, S. Thomas, Recent developments on nano-cellulose reinforced polymer nano-composites: a review, *Polymer* (2017), <https://doi.org/10.1016/j.polymer.2017.09.043>.
- [200] N.D. Sanandiya, Y. Vijay, M. Dimopoulou, S. Dritsas, J.G. Fernandez, Large-scale additive manufacturing with bio-inspired cellululosic materials, *Sci. Rep.* 8 (1) (2018) 8642, <https://doi.org/10.1038/s41598-018-26985-2>.
- [201] W. Ahmed, F. Alnajjar, E. Zanelidin, A. Al-Marzouqi, M. Gochoo, S. Khalid, Implementing FDM 3D printing strategies using natural fibers to produce biomass composite, *Materials* 13 (2020) 4065, <https://doi.org/10.3390/ma13184065>.
- [202] Z. Wang, J. Xu, Y. Lu, L. Hu, Y. Fan, J. Ma, X. Zhou, Preparation of 3D printable micro/nanocellulose-poly(lactic acid) (MNC/PLA) composite wire rods with high MNC constitution, *Ind. Crops Prod.* 109 (2017) 889–896, <https://doi.org/10.1016/j.indcrop.2017.09.061>.
- [203] A. Giubilini, G. Siqueira, F.J. Clemens, C. Sciancalepore, M. Messori, G. Nyström, F. Bondioli, 3D-Printing Nano-cellulose-Poly(3-hydroxybutyrate-co-3-hydroxyhexanoate) Biodegradable Composites by Fused Deposition Modeling, *ACS Sustain. Chem. Eng.* 8 (27) (2020) 10292–10302, <https://doi.org/10.1021/acscuschemeng.0c03385>.
- [204] M.N. Riddell, G.P. Koo, J.L. O'Toole, Fatigue mechanisms of thermoplastics, *Polym. Eng. Sci.* 6 (4) (1966) 363–368, <https://doi.org/10.1002/pen.760060414>.
- [205] A.E. Krauklis, A.I. Gagani, A.T. Echtermeyer, Hygrothermal aging of amine epoxy: reversible static and fatigue properties, *Open Eng.* 8 (1) (2018) 447–454, <https://doi.org/10.1515/eng-2018-0050>.
- [206] A. Wöhler, Über die Festigkeitsversuche mit Eisen und Stahl, *Ernst & Korn* (1870).
- [207] I. Burhan, H.S. Kim, S-N Curve models for composite materials characterization: an evaluative review, *J. Compos. Sci.* 2 (3) (2018) 38, <https://doi.org/10.3390/jcs2030038>.
- [208] M.M.-U. Haque, K. Goda, S. Ogoe, Y. Sunaga, Fatigue analysis and fatigue reliability of polypropylene/wood flour composites, *Adv. Ind. Eng. Polym. Res.* 2 (3) (2019) 136–142, <https://doi.org/10.1016/j.aiepr.2019.07.001>.
- [209] A. Gaurav, K.K. Singh, Fatigue behavior of FRP composites and CNT-Embedded FRP composites: a review, *Polym. Compos.* 39 (6) (2018) 1785–1808, <https://doi.org/10.1002/polp.24177>.
- [210] G.H. Kyanka, Fatigue properties of wood and wood composites, *Int. J. Fract.* 16 (6) (1980) 609–616, <https://doi.org/10.1007/BF02265220>.
- [211] M. Mejri, L. Toubal, J.C. Cuillière, V. François, Fatigue life and residual strength of a short-natural-fiber-reinforced plastic vs Nylon, *Compos. Part B: Eng.* 110 (2017) 429–441, <https://doi.org/10.1016/j.compositesb.2016.11.036>.
- [212] A. Foutouh, J.D. Wolodko, M.G. Lipsett, Fatigue of natural fiber thermoplastic composites, *Compos. Part B: Eng.* 62 (2014) 175–182, <https://doi.org/10.1016/j.compositesb.2014.02.023>.

- [213] J.A. Travieso-Rodriguez, M.D. Zandi, R. Jerez-Mesa, J. Lluma-Fuentes, Fatigue behavior of PLA-wood composite manufactured by fused filament fabrication, *J. Mater. Res. Technol.* 9 (4) (2020) 8507–8516, <https://doi.org/10.1016/j.jmrt.2020.06.003>.
- [214] V. Shanmugam, O. Das, K. Babu, U. Marimuthu, A. Veerasimman, D.J. Johnson, R.E. Neisiany, M.S. Hedenqvist, S. Ramakrishna, F. Berto, Fatigue behavior of FDM-3D printed polymers, polymeric composites and architected cellular materials, *Int. J. Fatigue* 143 (2021), 106007, <https://doi.org/10.1016/j.ijfatigue.2020.106007>.
- [215] B.P. Chang, A.K. Mohanty, M. Misra, Studies on durability of sustainable bio-based composites: a review, *RSC Adv.* 10 (31) (2020) 17955–17999, <https://doi.org/10.1039/C9RA09554C>.
- [216] M. Haque, K. Goda, H. Ito, S. Ogoe, M. Okamoto, T. Ema, K. Kagawa, H. Nogami, Fatigue performance of wet and dry pulverized wood flour reinforced PP composites, *J. Compos. Sci.* 3 (2019) 20, <https://doi.org/10.3390/jcs3010020>.
- [217] D. Djeghader, B. Redjel, Effect of water absorption on the Weibull distribution of fatigue test in jute-reinforced polyester composite materials, *Adv. Compos. Lett.* 28 (2019), 0963693519853833, <https://doi.org/10.1177/0963693519853833>.
- [218] A. Liber-Kneć, P. Kuźniar, S. Kuciel, Accelerated fatigue testing of biodegradable composites with flax fibers, *J. Polym. Environ.* 23 (3) (2015) 400–406, <https://doi.org/10.1007/s10924-015-0719-6>.







A. II Publication II

Influence of compounding parameters on the tensile properties and fibre dispersion of injection moulded poly(lactic acid) and thermomechanical pulp fibre biocomposites



Article

Influence of Compounding Parameters on the Tensile Properties and Fibre Dispersion of Injection-Moulded Polylactic Acid and Thermomechanical Pulp Fibre Biocomposites

Chiara Zarna ^{1,*}, Sandra Rodríguez-Fabià ², Andreas T. Echtermeyer ¹ and Gary Chinga-Carrasco ^{2,*}

¹ Department of Mechanical and Industrial Engineering, NTNU, Richard Birkelandsvei 2B, 7491 Trondheim, Norway

² RISE PFI AS, Høgskoleringen 6b, 7491 Trondheim, Norway

* Correspondence: chiara.zarna@ntnu.no (C.Z.); gary.chinga.carrasco@rise-pfi.no (G.C.-C.)

Abstract: Thermomechanical pulp (TMP) fibres can serve as renewable, cost-efficient and lightweight reinforcement for thermoplastic polymers such as poly(lactic acid) (PLA). The reinforcing ability of TMP fibres can be reduced due to various factors, e.g., insufficient dispersion of the fibres in the matrix material, fibre shortening under processing and poor surface interaction between fibres and matrix. A two-level factorial design was created and PLA together with TMP fibres and an industrial and recyclable side stream were processed in a twin-screw microcompounder accordingly. From the obtained biocomposites, dogbone specimens were injection-moulded. These specimens were tensile tested, and the compounding parameters statistically evaluated. Additionally, the analysis included the melt flow index (MFI), a dynamic mechanical analysis (DMA), scanning electron microscopy (SEM) and three-dimensional X-ray micro tomography (X- μ CT). The assessment provided insight into the microstructure that could affect the mechanical performance of the biocomposites. The temperature turned out to be the major influence factor on tensile strength and elongation, while no significant difference was quantified for the tensile modulus. A temperature of 180 °C, screw speed of 50 rpm and compounding time of 1 min turned out to be the optimal settings.

Keywords: biocomposite; wood fibres; compounding; material characterisation



Citation: Zarna, C.; Rodríguez-Fabià, S.; Echtermeyer, A.T.; Chinga-Carrasco, G. Influence of Compounding Parameters on the Tensile Properties and Fibre Dispersion of Injection-Moulded Polylactic Acid and Thermomechanical Pulp Fibre Biocomposites. *Polymers* **2022**, *14*, 4432. <https://doi.org/10.3390/polym14204432>

Academic Editor: Marcin Maslowski

Received: 23 September 2022

Accepted: 17 October 2022

Published: 20 October 2022

Publisher's Note: MDPI stays neutral with regard to jurisdictional claims in published maps and institutional affiliations.



Copyright: © 2022 by the authors. Licensee MDPI, Basel, Switzerland. This article is an open access article distributed under the terms and conditions of the Creative Commons Attribution (CC BY) license (<https://creativecommons.org/licenses/by/4.0/>).

1. Introduction

Biocomposites from wood-fibre-reinforced thermoplastic polymer have shown potential to be a replacement for fossil-based short-fibre-reinforced composites, such as glass-fibre-reinforced polyolefins. PLA is a biobased and biodegradable thermoplastic polymer and thermomechanical pulp (TMP) fibres have proven their ability to reinforce PLA [1]. Additionally, recycled wood particles obtained from sawmill side streams can be used as a cost-efficient filler material, as a stiffness enhancement and as a potential MFI enhancement [2] that could be beneficial for biocomposites processed by injection moulding, and reused side streams can help to improve circularity and waste management [3,4]. The overall purpose is to create more sustainable, lightweight and cost-efficient products. Such biocomposites, mainly processed by injection moulding, compression moulding or extrusion can serve as nonstructural parts in the automotive sector, in building and construction, for furniture and household items as well as sports and leisure equipment [5]. However, the poor compatibility between hydrophilic fibres and the hydrophobic matrix may hinder the full potential of wood-fibre-reinforced biocomposites. Additionally, the relatively low degradation temperature of wood fibres (200 °C) limits the processibility of such biocomposites [6–8]. Natural raw materials generally show a greater variety in their properties than man-made materials. This might negatively affect the reproducibility and consistency of biocomposite parts.

For preparing biocomposites, one common procedure is to mix dry polymer and possibly a compatibiliser powder before adding wood fibres, e.g., TMP fibres. Additionally, it can be necessary to dry the raw materials prior to processing to eliminate moisture that evaporates during the heat treatment and might cause inclusions and defects. Furthermore, moisture can affect the dimensional stability of TMP fibres and disturb the fibre–matrix interface [9]. In addition, some polymers (e.g., PLA) degrade in the presence of water [10,11].

The dried and mixed biocomposite components can either be fed directly into a melt extruder, or processed into pellets beforehand by melt compounding, pressing and chopping. Through melting and mechanical shearing, the mixture is then compounded and homogenised. The compounding process can be repeated several times, but fibre damage and polymer degradation must be considered. Drying TMP fibres makes them brittle and fragile. This causes fibre damage and shortening during compounding [7,10]. Wet TMP fibres are not that susceptible to damage development, but they agglomerate and cannot be dispersed properly. As shown by Yang et al. [12], to some extent, fibre agglomeration may affect the flexural properties of the biocomposite more negatively than fibre shortening. This was true for compounding wet pulp and high-density polyethylene. However, when oven drying and pelleting of the fibres was done prior to compounding, a reduction in fibre length resulted in an improvement of fibre dispersion and thus a lower flexural strength of the biocomposite [12]. Wood fibres generally have shown to change their mechanical properties and morphology during melt processing. The property changes were mainly related to temperature and exposure time [9,13]. High temperature and long residence times were also found to have a negative impact on the tensile strength of neat polypropylene due to thermal degradation and hydrolysis due to the presence of moisture [14]. On the other hand, to some extent, a higher screw speed could have a positive effect on the tensile strength [15] and fibre dispersion [16,17].

It can be differentiated between continuous and discontinuous melt compounding. In continuous compounding there is a continuous material flow along different mixing elements, e.g., kneading blocks, conveying elements or tooth mixing elements that are connected in series to accomplish certain objectives. The duration of the treatment is dependent on the feeding rate [18,19]. In discontinuous compounding the biocomposite components remain in the barrel and are mixed by two conveying screws for a certain duration of time after being released [20]. Discontinuous microcompounding is especially beneficial if small batches are required for early material development. However, using different processing equipment might lead to different biocomposite properties even when the same parameter settings are used. This applies for upscaling from a discontinuous batch compounder to a continuous compounder for larger quantities or when switching to a similar machine from another manufacturer due to specific dimensions of the barrel and the screws [21].

When compounding TMP fibres and biopolymers, the aim is to achieve a homogeneous dispersion of fibres in the matrix while maintaining the fibre length. To take full advantage of TMP fibre reinforcements, it is of major importance to select suitable processing parameters [9]. The discontinuous compounding process is controlled by the compounding time, screw rotation speed, compounding temperature and the screw design [22]. Adjusting these parameters may affect the mechanical properties of the resulting biocomposites [19] and is a trade-off between sufficient dispersion and material degradation or damage. Increasing the temperature, screw speed and compounding time decreases the viscosity of the polymer, accelerates the process and increases the probability of homogeneous dispersion, respectively. However, elevated temperatures may cause a degradation of the biocomposite components. Elevated screw speed increases the shear and friction forces which can cause fibre damage and uncontrolled internal heating. A longer compounding time results in longer exposure duration of the biocomposite components to heat and mechanical forces. Thus, thermal, and mechanical damage can evolve more significantly. Therefore, studies to optimise the compounding process and gain information on how each compounding

parameter influences the biocomposite properties are crucial [23]. The parameters might not only be optimised towards desired biocomposite properties but also towards other goals such as minimum energy consumption or time efficiency [24].

In this work, a design of experiments (DoE) approach is used to find optimal parameters for compounding TMP fibres, an industrial side stream (S) from fibre boards and PLA in a twin-screw microcompounder. However, it should be noted that the presented results are not only limited to the biocomposite formulation used in this study but can serve as a baseline for other formulations of lignocellulosic fibres and polymers having a similar processing temperature as PLA. The purpose of the study was to provide a method for performing a parameter optimisation for biocomposite processing using a microcompounder and highlighting the impact of exposure time, temperature and screw speed on the biocomposite properties. Importantly, we hypothesised that wax-containing side stream could be used to tailor the MFI. It was thus important to verify whether the compounding variables affected the performance of the side stream as an MFI modifier. Further, microcompounding is greatly used for research purposes [25–28] because of the possibility of producing small batch sizes below 50 g. However, to the best of our knowledge there is a lack of comprehensive studies addressing the effect of microcompounding parameters on the biocomposite properties. The interaction of temperature and residence time and the sensitivity of natural fibre biocomposites on these factors was investigated and reviewed [9,29]. The presented DoE approach aims to clarify whether and how exposure time, temperature and screw speed affect the biocomposite tensile properties and morphology.

2. Materials and Methods

2.1. Raw Materials

The PLA used in this study was an Ingeo 4043D grade (NatureWorks, Minnetonka, MN, USA). The side stream was collected from the production plant at Alloc AS (Lyngdal, Norway). A chemical characterisation of this side stream can be found in [2]. The purpose of introducing this industrial side stream was to enhance the usage of waste material and further explore its beneficial effect on the MFI [2]. Spruce TMP fibres were prepared by Norske Skog Saugbrugs (Halden, Norway). The pulp was granulated to a size of <8 mm as described in [2]. The research method of the present study is illustrated using a flow chart (Figure 1).

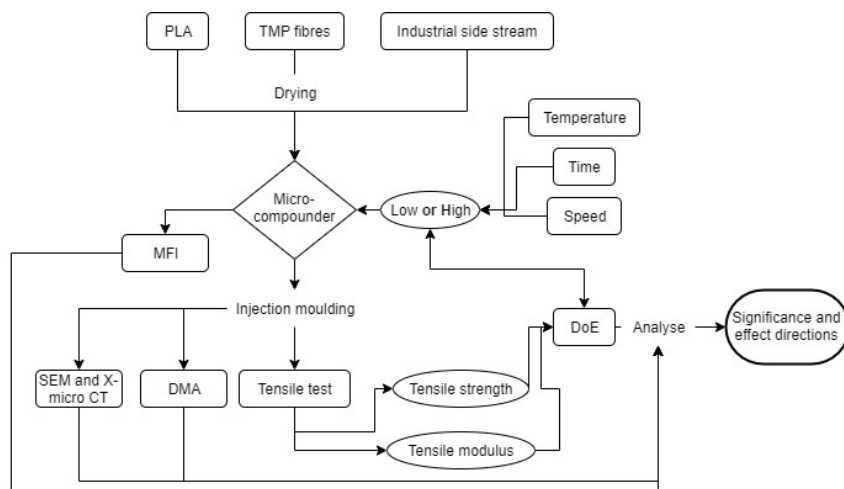


Figure 1. Flow chart to illustrate the research method.

2.2. Compounding

The side stream (S) was ground using a 30-mesh sieve in a Thomas Wiley Mini-Mill cutting mill (Thomas Scientific, Swedesboro, NJ, USA). The side stream powder and TMP fibres were dried for 1 h at 105 °C. PLA was dried for 4 h at 50 °C. The raw materials were compounded in an Xplore twin-screw microcompounder (Xplore Instruments BV, Sittard, The Netherlands). Eight series of biocomposites were compounded using different parameter settings by adjusting the compounding time, the screw rotation speed and the compounding temperature (Table 1). The chosen temperature range was restricted by the minimum processing temperature of PLA (180 °C) [30] recommended by the manufacturer and the degradation temperature of the TMP fibres (200 °C) [7]. The screw rotation speed and compounding time were chosen as low as possible to prevent harming the biocomposite raw materials by excessive mechanical shear forces and exposure to elevated temperatures. The goal was to maximise fibre dispersion while minimising thermal degradation and mechanical damages of the biocomposite components. The formulation of 70 wt.% PLA/20 wt.% TMP/10 wt.% S was equal for every batch. For each series three independent batches were prepared with the microcompounder and mixed randomly before further processing.

Table 1. Compounding parameters to prepare biocomposites from 70 wt.% PLA/20 wt.% TMP/10 wt.% S.

Series Designation	Time (min)		Speed (rpm)		Temperature (°C)	
	Low	High	Low	High	Low	High
1/25/180	1		25		180	
2/25/180		2	25		180	
1/50/180	1			50	180	
2/50/180		2		50	180	
1/25/200	1		25			200
2/25/200		2	25			200
1/50/200	1			50		200
2/50/200		2		50		200

2.3. Injection Moulding

An Xplore injection moulding system (Xplore Instruments BV, Sittard, The Netherlands) was used to form tensile test specimens for mechanical tensile testing. Eight test specimens per series were prepared. The injection temperature was 190 °C and the mould temperature was 30 °C.

2.4. Tensile Tests

The injection-moulded dogbone specimens were mechanically tensile-tested with an MTS Criterion 42 503E testing machine (MTS, Eden Prairie, MN, USA) and a load cell of 5 kN, using an extensometer (MTS 632.29F-30) with 5 mm gauge length. The test speed was 2 mm/min. The modulus was calculated from the linear slope between two points on the stress–strain curves at a strain of 0.25% and 0.5% according to ISO 527-2:2012.

2.5. Statistical Analysis

The effect of compounding parameters on the tensile properties of injection-moulded specimens was assessed as part of a 2³ full factorial design, i.e., three factors (compounding parameters from Table 1) at two levels (low and high from Table 1) with five repetitions per series. As a response, the tensile strength and tensile modulus were assigned. The statistical analysis of the standardised effects and interactions was done using Minitab® 19.2020.1 software. Prior to the analysis of variance (ANOVA) a normality test (Shapiro–Wilk) and a

homoscedasticity test (Levene) was performed to ensure the data sets were following the normal distribution and the variances were equal. To compare each series to each other and assess the statistical difference between groups, a post hoc test (Tukey method) was used. It was determined which factors had a statistically significant influence on the tensile properties and which series were significantly different from each other. A significance level of 0.05 was chosen. Additionally, interaction plots were used to show how the relationship between one compounding parameter and the tensile properties depended on the value of another compounding parameter [31]. To find the p -value, the F -test from the analysis of variance was used:

$$F = \frac{\text{Effect variance}}{\text{Error variance}} \quad (1)$$

The procedure for performing the F -test is explained in [32]. The F -ratio (Equation (1)) was obtained by dividing the mean squares between the factors by the mean squares within the groups (factors). The p -value could then be found in F tables for desired probabilities (here 5%) and degrees of freedom [32].

2.6. Melt Flow Index

The melt flow index (MFI) of samples from series 1/50/180 and 2/50/200 was measured with a Melt Flow Index-Deluxe (model no: MFI—DX, Presto Stantest Private Limited, Faridabad, India). These samples were chosen because they resulted in the highest and lowest tensile strength, respectively. A temperature of 190 °C was applied, the preheating of a sample was 5 min and a weight of 2.16 kg was used. Ten measurements were undertaken for each sample, and this was repeated two times on different batches. There is a significant difference in sample mass when the sample is taken right after the beginning or towards the end of the material extrusion. The results presented here were obtained from samples taken right after starting the test.

2.7. Scanning Electron Microscopy

The fracture surfaces of injection-moulded samples from series 1/50/180 and 2/50/200 were assessed with scanning electron microscopy (SEM). The fracture area was coated with a layer of gold and visualised in secondary electron mode. SEM was conducted with a Hitachi scanning electron microscope (SU3500, Hitachi High-Tech Corporation, Tokyo, Japan). The acceleration voltage and working distance were 5 kV and 5–10 mm, respectively.

2.8. Dynamic Mechanical Analysis

A dynamic mechanical analysis (DMA) was performed on injection-moulded dog-bone specimens of series 1/50/180 and 2/50/200. The tests were performed in accordance with ISO 6721-11:2019 (method A) on a Gabo Eplexor 1500 N test machine from NETZSCH (Selb, 95100, Germany). The dog-bone specimens were used in axial tension mode in a temperature range of 25 °C to 100 °C. The tests were performed at a constant frequency of 10 Hz, a static strain of 0.2%, a dynamic strain of 0.1% and a heat rate of 5 K/min.

2.9. X-ray Micro-Computed Tomography

The fibre dimensions were assessed on injection-moulded samples from series 1/50/180 and 2/50/200 with X- μ CT [33]. The samples were imaged with a Xradia MicroXCT-400 tomograph (XRadia, Concord, CA, USA) with a 1.1 μ m pixel size. The X-ray tube voltage was set to 30 kV and the power to 3 W. A total of 1881 projections were acquired with 8 s exposure time and 10 \times magnification. Three-dimensional volume images were constructed using an algorithm from [34]. A cropped region of the image was edited by bilateral and high-pass filtering [35]. Fibres, matrix and voids were segmented by thresholding according to [36]. To segment the agglomerates, individual fibres were erased with a morphological opening filter, and the pores in the agglomerates were closed by a morphological closing filter. The fibre lengths were determined using the constrained path transform [37] and the fibre orientation using the structure tensor method [38]. By applying the approach of

Miettinen et al. [33], the fibre length and orientation were combined into fibre property distributions. With the local thickness algorithm [39], agglomerates were characterised by measuring the volume and the surface area.

3. Results and Discussion

3.1. Tensile Tests

The tensile test results of injection-moulded dog bones, prepared by using eight different compounding parameter combinations (Table 1) are presented in Figure 2. Additionally, groups of responses with similar characteristics could be identified using the Tukey method. Four groups named A, B, C and D were identified. The series means that do not share a group letter were significantly different.

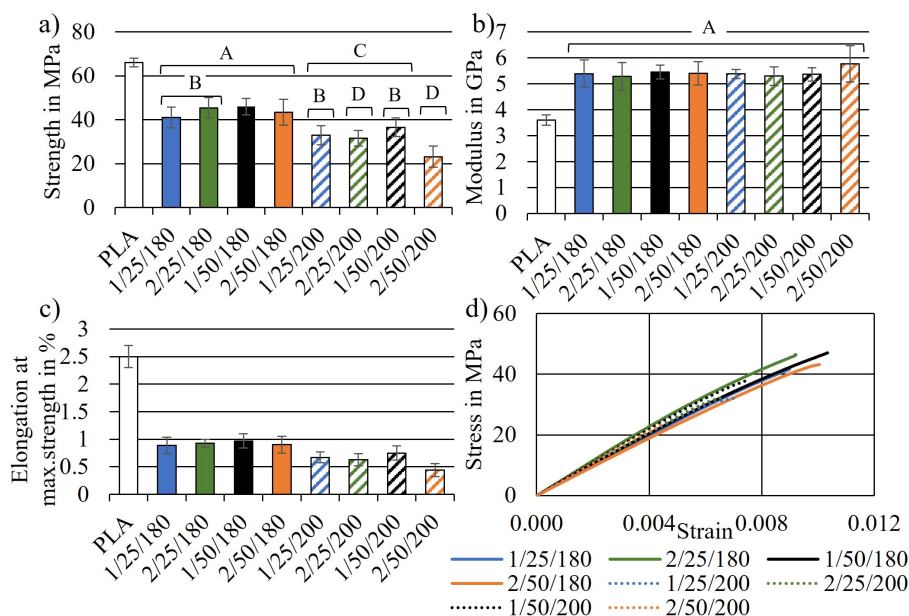


Figure 2. Results from tensile tests of the biocomposite series. (a) Tensile strength with indication of homogeneous groups A–D, (b) tensile modulus, (c) elongation at maximum stress and (d) representative stress–strain curve of each series.

The tensile modulus was similar for all eight biocomposite series, as seen in Figure 2b. No significant effect could be observed, as indicated by the grouping information. All series means were assigned to the same group A. Regarding the tensile strength, four data groups were identified. Series compounded at 180 °C (group A) generally showed a higher tensile strength than the series compounded at 200 °C (group C and D). The same trend was observed for the elongation at maximum strength. The highest tensile strength was found for series 1/50/180 with (45.96 ± 3.68) MPa and the lowest for series 2/50/200 with (23.16 ± 4.77) MPa. Additionally, series 2/50/200 (Group D) showed a significantly lower tensile strength than the other series compounded at 200 °C (Group C). The combined average tensile modulus of all series was found to be (5416 ± 143) MPa. Series 1/50/180 and 1/50/200 resulted in the highest tensile strength inside their data group. Both were compounded for 1 min at 50 rpm. Thus, for achieving the highest possible tensile strength, this setting seemed to be more appropriate than the others. The strength of all series was lower than the one of neat PLA. This was most probably related to the presence of waxes in S. The waxes might have disturbed the interfacial adhesion between PLA and the fibres and thus acting as a defect rather than a reinforcement [2]. Additionally, the addition of stiff

fibres and particles to a ductile matrix such as PLA restricts the mobility and deformation of the matrix leading to a reduced strain to failure [40].

In biocomposites, the modulus is mainly influenced by the fibre and matrix modulus, the fibre volume fraction and orientation but only to a much lesser degree by the fibre length [41]. The tensile modulus of a TMP-fibre-reinforced biocomposite can be calculated as suggested by Thomason [42]:

$$E = V_m E_m \eta_1 + V_f E_f \eta_0 \quad (2)$$

In Equation (2), V_i and E_i are the volume fraction and elastic modulus. $i = m, f$ refers to the matrix or the fibres. η_1 is obtained by the shear lag theory developed by Cox and refers to the morphology of the fibres. η_0 is an orientation factor [42]. For injection-moulded short-fibre composites, the fibre orientation is mostly considered as being random due to the different orientations of the fibres in the midplane and close to the mould surface [43]. According to Equation (2), the modulus gets reduced with lower fibre length. The factor of fibre length is eliminated when using a model for particulate-reinforced composites [44]:

$$E = \frac{V_f^{0.67} E_m}{1 - V_m^{0.33} (1 - \frac{E_m}{E_f})} + (1 - V_f^{0.67}) E_m \quad (3)$$

The tensile strength is more sensitive to the fibre length or length-to-width ratio. If the fibre length is below the critical load transfer length, the fibre might rather act as a defect than a reinforcement [10,45]. The tensile strength can be predicted by:

$$\sigma = V_f \sigma_f x_1 x_2 + V_m \sigma_m \quad (4)$$

For illustrating the effect of fibre length or particle volume fraction on the tensile modulus and strength with the proposed models, the parameters according to Table 2 were applied and plotted in Figure 3. The values in Table 2 refer to the biocomposite used in this study. The material properties of the matrix (PLA) were taken from the above-presented measurements and the TMP fibre properties were taken from the literature, as indicated in Table 2. The fibre morphology was assessed using X- μ CT. The fibre orientation was considered random [43] and the corresponding factors were taken from the literature [10,42,45]. The experimentally obtained data points (cross markers) of the series resulting in the lowest (2/50/200) and the highest (1/50/180) tensile strength are plotted in each model graphic. Additionally, the tensile strength and stiffness values for the corresponding biocomposite predicted by the model are indicated by a rhombus marker. The grey graph is a plot of the Equations (2)–(4) over the fibre length or fibre volume fraction. All parameters were kept constant except for the fibre length l in η_1 (Figure 3a,c) or the fibre volume fraction V_f (Figure 3b).

Table 2. Parameters used for the analytical models.

Parameter	Value	Unit	Clarification
V_m	0.7	-	Matrix volume fraction
V_f	0.3	-	Fibre volume fraction
E_m	3.6	GPa	Matrix tensile modulus
E_f	2	GPa	Fibre tensile modulus [46]
η_0	0.375	-	Fibre orientation factor [42]
η_1	$1 - \frac{\tanh(\beta l/2)}{\beta l/2}$	-	Fibre length factor [42]
β	$\frac{2}{d} \left[\frac{2G_m}{E_f \ln(\sqrt{\pi/X_i/V_f})} \right]^{1/2}$	-	- [42]

Table 2. Cont.

Parameter	Value	Unit	Clarification
X_i	4.0	-	Squared packing value [42]
G_m	$\frac{E_m}{2(1+\nu)}$	MPa	Matrix shear modulus
ν	0.3	-	Poisson's ratio of matrix
σ_m	66	MPa	Matrix's ultimate tensile strength
σ_f	500	MPa	Fibre's ultimate tensile strength [10]
τ_m	$\frac{\sqrt{2}}{5}\sigma_m$	MPa	Matrix shear strength
d	0.02	mm	Fibre diameter (measured with X- μ CT)
l_c	$\frac{\sigma_f}{2\tau_m}d$	mm	Critical load transfer length [45]
x_1	0.167	-	Fibre orientation factor [10]
x_2	$\frac{l}{2l_c}; l < l_c$ $1 - \frac{l}{2l_c}; l \geq l_c$	-	Length factor [10]

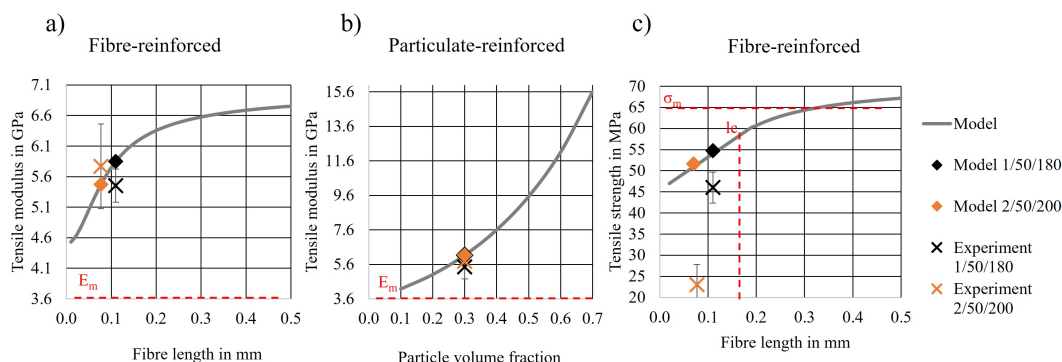


Figure 3. Micromechanical models for (a) Tensile modulus for short-fibre-reinforced composites (Cox) with varying fibre length, (b) tensile modulus for particulate-reinforced composites (Mital) with varying particle volume fraction and (c) tensile strength of short-fibre-reinforced composites (Bowyer and Bader) with varying fibre length.

According to the micromechanical model in Equation (2) (Figure 3a), longer fibres are expected to stiffen the matrix to some extent. However, this was not true for the biocomposites presented here. As indicated by the rhombus marker, the modulus of both series was similar despite the difference in fibre length. Regarding the effect of the volume fraction (Figure 3b) of particulate reinforcements, it can be observed that the fibre or particle volume fraction had a much greater impact on the composite stiffness. Since in the biocomposites presented here, the volume fraction of the TMP fibres and S particles was the same in all series, it is understandable that the effect of marginally different fibre lengths was negligible. Both models predicted the modulus fairly well with an error of about 10%. However, the error was the least when applying the model for particulate reinforcements (Equation (3)) to series 2/50/200 and the one for fibre reinforcements (Equation (2)) to series 1/50/180, indicating that the TMP fibres in series 2/50/200 were probably broken down to a particle-like shape.

Figure 3c shows the modelled and experimentally obtained tensile strength of the biocomposite in relation to the TMP fibre length. Although the model (Equation (4)) over-estimated the experimental results from both series 1/50/180 and 2/50/200, the measured and modelled tensile strengths of series 1/50/180 deviated by only 14% when applying

the micromechanical model for fibre lengths below the critical load transfer length ($l < l_c$). However, in the case of 2/50/200, the analysis showed that not only the fibre length reduction caused the comparatively low tensile strength of biocomposites from this series, but porosity and insufficient fibre–matrix interaction probably also contributed to the major reduction of tensile strength. Importantly, the higher temperature in combination with a higher screw speed and compounding time might have led to the thermal degradation of matrix and fibres, fibre shortening due to elevated shear forces and probably the evaporation of moisture and volatilisation contributing to void formations and a reduced fibre–matrix interaction [1,13,47].

3.2. Statistical Analysis

The p -values obtained from the test for normality and homoscedasticity were greater than the confidence level of 0.05 for all tested sets of data. Thus, the data of the tensile strength and modulus followed the normal distribution for each series and the variances between the two levels of each factor were equal for both responses. The p -values found for the influence of the compounding parameters on the tensile properties with a confidence level of 0.05 are provided in Table 3.

Table 3. p -values for the influence of the compounding parameters on the tensile properties with a significance level of 0.05.

Factor	p -Value	
	Tensile Strength Response	Tensile Modulus Response
Temperature	$\ll 0.05$	0.683
Speed	0.695	0.110
Time	0.250	0.898
Time \times Speed	0.065	0.940
Time \times Temperature	0.175	0.962
Speed \times Temperature	0.162	0.133
Time \times Speed \times Temperature	0.785	0.321

The only p -value less than 0.05 was found for the influence of temperature on the tensile strength. As already indicated by the bar graph in Figure 2b, no significant influence of any compounding parameter on the tensile modulus was found. The combined effects of two or all three parameters were not significant either. A Pareto chart of standardised effects and main effect plots for the tensile strength and modulus are presented in Figure 4.

Figure 4b and d show whether a factor had a significant effect on the response or not. If the red dashed line is crossed by a bar, the corresponding factors had a significant effect on the response. This was only valid for the effect of compounding temperature on the tensile strength. The combined factors showed a relatively similar effect magnitude on the tensile strength. The screw speed had the least effect, but it became more prominent in combination with time or temperature. Regarding the effect plot for the tensile strength (Figure 4a), it can be observed that the higher value or level of each factor had a negative effect on the tensile strength, meaning that an elevated compounding time, screw speed and temperature led to a lower tensile strength of the biocomposite. An opposite but not significant effect can be observed for the tensile modulus (Figure 4c). The screw speed had the largest effect on the tensile modulus followed by the combined effect of temperature and screw speed. The temperature and combination of screw speed and temperature and time and temperature had the least effect on the tensile modulus. The screw speed most probably contributed to the fibre dispersion and potential fibre damage or shortening. It was previously shown that the fibre or particle size had no significant effect on the tensile modulus [40]. However, a slight trend of decreasing modulus with increasing particle size was observed [40], consistent with the results presented here. Since no significance was

found for the tensile modulus response, interaction plots are only shown and discussed for the tensile strength response (Figure 5).

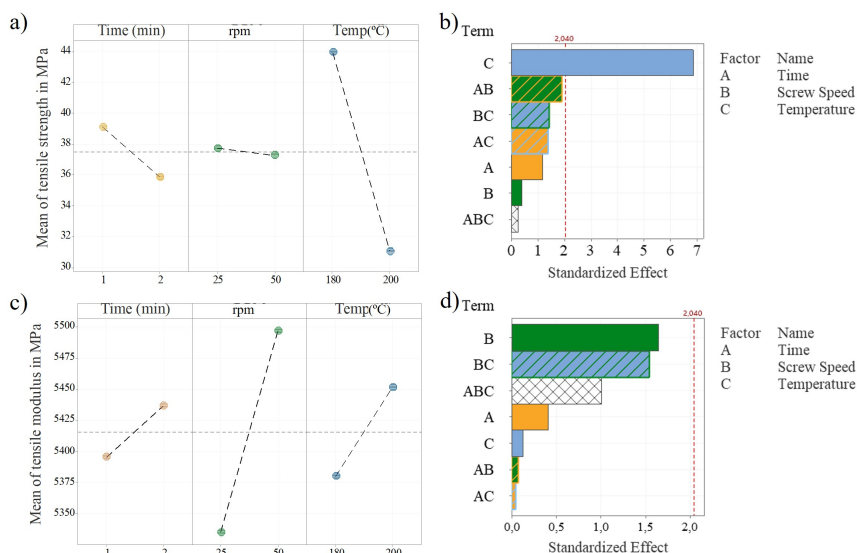


Figure 4. Main effect plots for the response of (a) tensile strength and (c) tensile modulus and Pareto charts of standardised effects for (b) tensile strength and (d) tensile modulus.

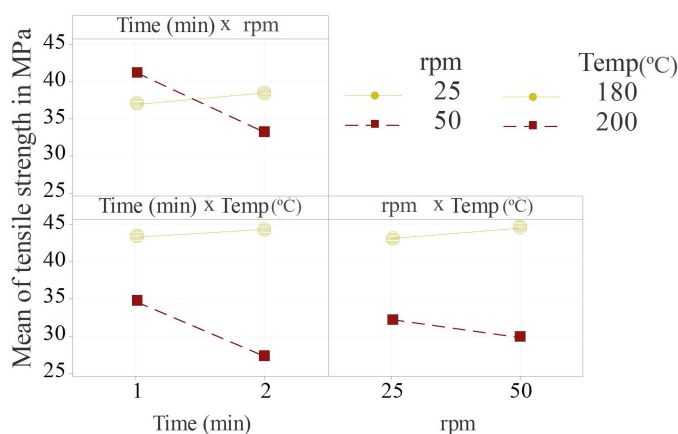


Figure 5. Interaction plots for the tensile strength.

The upper left plot in Figure 5 shows the combined effect direction of compounding time and screw speed on the tensile strength. The yellow data points correspond to the lower level of speed and the red data points to the higher level of speed. It can be concluded that when a lower screw speed (25 rpm) was applied, the effect of the compounding time was very little. When a higher screw speed (50 rpm) was applied, the effect of time became more prominent. The same trends can be observed for the combined effects of compounding time and temperature and screw speed and temperature. This shows that the effects intensified each other.

From the tensile test results and the statistical analysis, it can be concluded that a 180 °C compounding temperature, 50 rpm screw speed and 1 min compounding duration were the optimal parameter settings for achieving the highest tensile strength of the tested

biocomposite. Similar compounding parameters were suggested by Lu et al. [48] for a wood fibre high-density polyethylene composite. The results of the present study can serve as a baseline for compounding similar lignocellulosic-reinforced biocomposites. Instead of 50 rpm and 1 min (series 1/50/180), 25 rpm and 2 min (series 2/25/180) resulted in a very similar average tensile strength (Figure 2). However, this was not valid when applying a higher compounding temperature of 200 °C. Here, the maximum tensile strength could only be obtained by applying 50 rpm and 1 min (series 1/50/200). Not-dried biocomposite components may (inter)act differently. Wet lignocellulosic fibres might be less brittle and sensitive to shear forces, but the fibre–matrix surface interaction may be disturbed by the presence of water [12]. Varying the processing procedure [12] or applying these compounding parameters to other compounding equipment, especially to large-scale continuous extruders might lead to different mechanical properties than the ones presented here. This is due to potentially different screw shapes and dimensions leading to different mechanical shear forces, internal friction, etc. [21]. However, it can be assumed that the effect directions of the compounding parameters also remain similar when different equipment is used.

3.3. Melt Flow Index

Based on the results obtained from the tensile tests and the statistical analysis, an MFI analysis is presented for the series with the highest (1/50/180) and the lowest tensile strength (2/50/200). The biocomposite from series 1/50/180 was measured to have an MFI of (4.73 ± 1.79) g/10 min. Series 2/50/200 was not measurable because the biocomposite was not able to exit the nozzle of the MFI measurement equipment even when higher forces (5 kg) were applied. The MFI tester nozzle was clogged, and volatilisation was visible. The other three series compounded at 200 °C (1/25/200, 2/25/200, 1/50/200) were also not measurable, and a similar volatilisation was observed. Neat PLA has an MFI of 6 g/10 min, according to its technical data sheet [30]. Incorporating TMP fibres into a PLA matrix typically reduces the MFI [4]. However, the side stream in the biocomposite formulation presented here contained waxes [2] that may have contributed to reducing the interfacial adhesion between the PLA and the side stream particles. The side stream may, on the one hand, contribute to an increased MFI but on the other hand, to a reduction of tensile strength [2,49]. An increased MFI is beneficial with respect to the further processing of the biocomposite, e.g., injection moulding [2]. Typically, the MFI rises when harsher heat treatment or multiple cycles of heat treatment are applied due to chain scission [50]. It was therefore unexpected that the MFI of series 2/50/200 was lower than the MFI of series 1/50/180. The waxes might have been partially volatilised during the harsher heat treatment of series 2/50/200 thus eliminating the beneficial contribution of the waxes for increasing the MFI.

3.4. Dynamic Mechanical Analysis

Injection-moulded dog-bone samples of series 1/50/180 and 2/50/200 were subjected to a DMA temperature sweep test to investigate their viscoelastic behaviour and glass transition temperature (T_g). The resulting storage modulus E' , loss modulus E'' and $\tan(\delta)$ are presented in Figure 6.

The storage modulus corresponds to the ability of a material to store energy elastically, while the loss modulus is the viscous response to stress and is related to the energy dissipated per cycle of sinusoidal deformation. The ratio of loss and storage modulus is $\tan(\delta)$, also called loss factor.

The loss factor $\tan(\delta)$ of series 1/50/180 was higher than the $\tan(\delta)$ of series 2/50/200, meaning that series 1/50/180 behaved more viscous and series 2/50/200 more elastically. The TMP fibres generally lead to a reduction of chain mobility, thus more energy is required for the transition from the glassy to the rubbery state [51]. This indicated a reduced chain mobility of series 2/50/200 compared to series 1/50/180. Fillers with a lower surface area per volume or insufficient fibre–matrix surface interaction are known for allowing a greater

mobility of the biocomposite, leading to increased heat dissipation under deformation through applied stress to the biocomposite. This results in a higher loss modulus, as seen for series 1/50/180 [52–54]. The greater chain mobility observed for series 1/50/180 was already indicated by its comparatively high MFI, thus confirming the presented results.

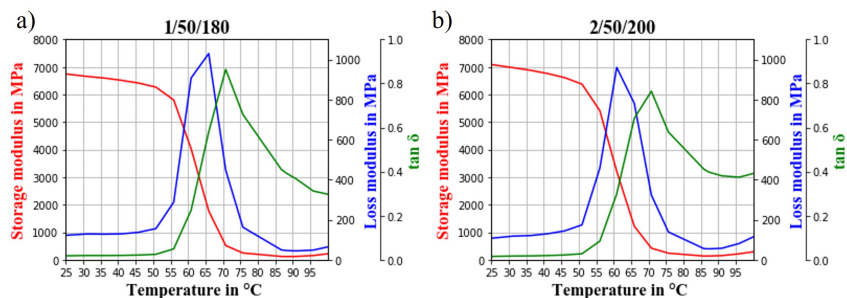


Figure 6. Storage modulus, loss modulus and $\tan\delta$ obtained from DMA temperature sweep test of (a) series 1/50/180 and (b) series 2/50/200.

Further, an increased storage modulus can be an indication of a uniform dispersion of fillers in a matrix material. This is related to the assumption that agglomerates or nonuniformly dispersed fibres would not restrict the movement of polymer chains as much as uniformly dispersed ones [12,52]. The storage modulus of series 2/50/200 was higher than the one of series 1/50/180, indicating more uniformly dispersed fibres in samples of series 2/50/200. This is expected since series 2/50/200 was compounded for a longer time and at higher temperature than series 1/50/180. The restriction in chain mobility due to uniform fibre dispersion and a potentially improved fibre–matrix surface interaction due to the volatilisation of waxes most probably explains the lower MFI of series 2/50/200 compared to 1/50/180 [55].

According to ISO 6721-11:2019, the glass transition temperature can be read from the peak of the loss modulus curve, at the inflection point of storage modulus or at the peak of the $\tan(\delta)$ curve. A reduction in molecular weight due to polymer degradation under processing might lead to a lower T_g. Generally, the processing of PLA might increase crystallinity leading to a reduced mobility and an increased T_g [56]. When read from the peak of E'' and the inflection point of E' , series 1/50/180 had a higher T_g (66 °C or 63 °C) than series 2/50/200 (61 °C or 60 °C). The peak of $\tan(\delta)$ was at 71 °C for both series.

3.5. Scanning Electron Microscopy

Fractured tensile test specimens from the series 1/50/180 and 2/50/200 were investigated more closely. The fracture surfaces of the samples from series 1/50/180 (left) and one from series 2/50/200 (right) are shown in Figure 7.

In Figure 7 left, some fibre agglomerates are visible in the form of areas where fibres are accumulating without being surrounded by matrix material. Series 1/50/180 showed the highest tensile strength and elongation at maximum stress. However, the dispersion of fibres was not fully achieved as already indicated by the lower storage modulus of 1/50/180 compared to 2/50/200.

In Figure 7 right, the fracture surface of series 2/50/200 appears to be rougher and rugged compared to series 1/50/180. Fibre fragments and pores in the matrix are visible and it can clearly be seen that both fibres and matrix were damaged under compounding. The agglomerations visible on the fracture surface of 1/50/180 probably initiated the failure of the specimen. However, the matrix surrounding the agglomerates seems smoother and not as porous as the fracture surfaces of 2/50/200. This observation highlights the trade-off between homogeneous fibre dispersion and material degradation when compounding wood fibre biocomposites. As 1/50/180 was stronger and tougher than 2/50/200, it might

be more beneficial to maintain the raw materials' morphology to a certain extent at the expense of some fibre agglomerations.

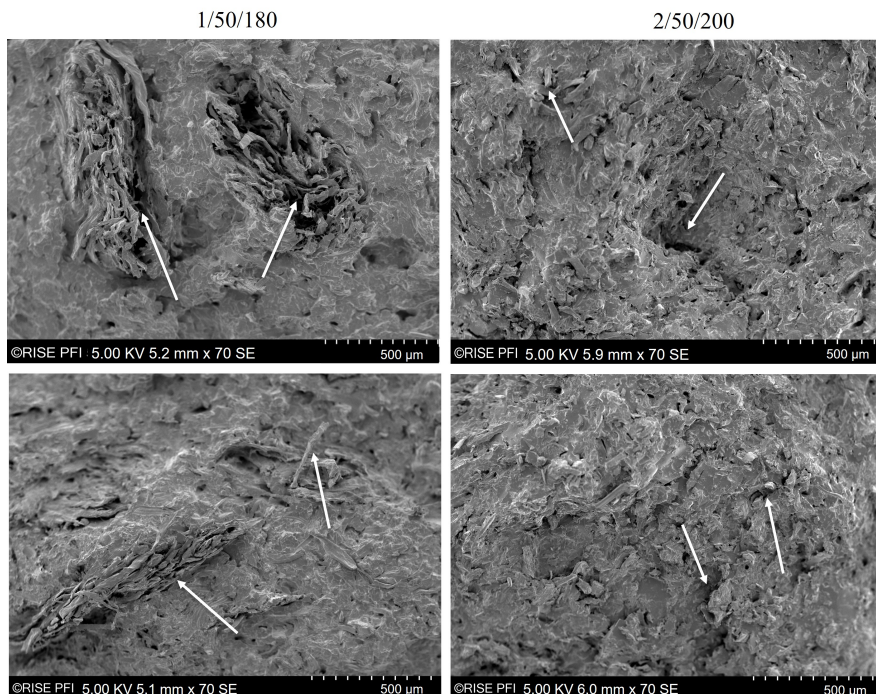


Figure 7. SEM images with 70× magnification of fractured surfaces of a tensile test specimens from series 1/50/180 (left) and series 2/50/200 (right).

3.6. X-ray Micro-Computed Tomography

The fibre length distribution of series 1/50/180 and 2/50/200 was investigated on injection-moulded specimens using X- μ CT (Figure 8).

As seen in Figure 8b, series 1/50/180 showed a higher probability for the presence of longer fibres than series 2/50/200. This agrees with the micromechanical modelling and tensile test results presented in Figure 3c. Since longer fibres were present in the biocomposites of series 1/50/180, more fibres could potentially transfer the load applied to the biocomposite. Although the TMP fibres were not fully dispersed in series 1/50/180 (as indicated by SEM images Figure 7 and DMA Figure 6), the applied compounding parameters were considered to be optimal. Based on the presented results from tensile tests and statistical analysis, it is not expected that either increasing compounding time, temperature or screw speed would contribute to a significantly higher tensile strength of the biocomposite. It was shown that a longer or stronger mixing may potentially improve the fibre dispersion but may damage the biocomposite components at the same time, resulting in a nonsignificant improvement of tensile strength. Potentially, other feeding techniques or mixing and pelletising prior to compounding could contribute to a more uniform dispersion [12,57].

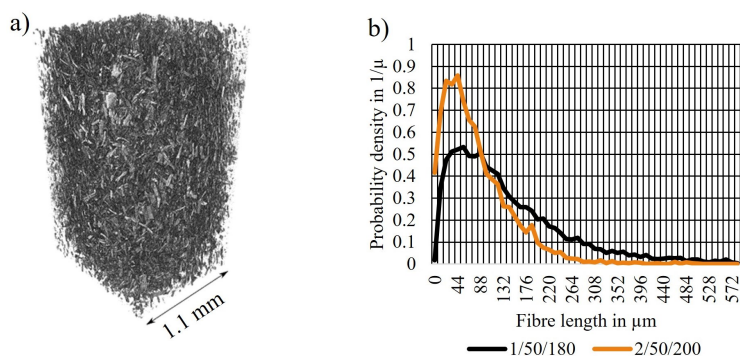


Figure 8. Results from X- μ CT. (a) Visualisation of series 1/50/180, (b) fibre length distribution of series 1/50/180 and 2/50/200.

4. Conclusions

An analysis of variance revealed that the compounding parameters had no influence on the tensile modulus. In terms of tensile strength, only the compounding temperature had a significant influence. Compounding the biocomposite at 200 °C led to a significantly lower tensile strength than compounding at 180 °C. Applying the high levels of all three factors yielded the biocomposite with the lowest tensile strength with a significant difference from all other data groups. The combined effects of parameters were not significant. However, when applying a screw speed of 50 rpm the influence of time became more prominent. A similar trend was observed for both applied temperatures.

The MFI revealed a severe difference in flow properties of series 1/50/180 (highest tensile strength) and 2/50/200 (lowest tensile strength). Series 2/50/200 was not measurable while series 1/50/180 had a similar MFI as neat PLA, most probably due to the wax-containing industrial side stream. In DMA, series 1/50/180 showed to be more viscous than series 2/50/200. Inhibited chain mobility in series 2/50/200 was an indicator for a more uniform filler dispersion. This was confirmed by SEM images that showed a rugged and porous fracture surface of biocomposites from series 2/50/200. Both, fibres and matrix were damaged, resulting in the low tensile strength. Biocomposites from series 1/50/180 showed a smoother surface but some fibre agglomerations were found. An X- μ CT analysis confirmed the conclusions drawn from the previous analysis. The fibre lengths in the biocomposites from series 2/50/200 were generally shorter than those from series 1/50/180.

Finally, a micromechanical analysis was applied to explain, discuss and support the outcome of this study based on existing modelling approaches. The strong impact of degradation and porosity due to a higher compounding temperature and longer exposure time on the tensile strength was highlighted. We demonstrated that optimising the compounding process for biocomposites is crucial. The mechanical properties, microstructure and appearance of the biocomposite are highly dependent on the compounding parameters, especially the compounding temperature. For lignocellulosic-reinforced biocomposites, a temperature of 180 °C, screw speed of 50 RMP and a compounding time of 1 min can be suggested.

Author Contributions: Conceptualisation, G.C.-C.; methodology, G.C.-C. and C.Z.; software, C.Z.; validation, C.Z.; formal analysis, C.Z.; investigation, C.Z.; resources, G. C.-C., S.R.-F. and A.T.E.; data curation, C.Z. and S.R.-F.; writing—original draft preparation, C.Z.; writing—review and editing, G.C.-C., S.R.-F. and A.T.E.; visualisation, C.Z.; supervision, G.C.-C. and A.T.E.; project administration, G.C.-C. and A.T.E.; funding acquisition, G.C.-C. All authors have read and agreed to the published version of the manuscript.

Funding: This research was funded by the Research Council of Norway, grant number 282310.

Institutional Review Board Statement: Not applicable.

Informed Consent Statement: Not applicable.

Data Availability Statement: Not applicable.

Acknowledgments: The Research Council of Norway and the companies supporting the ALLOC project (Grant no. 282310) are thanked for their funding. Thanks to Joni Tanttú and Arttu Miettinen (University of Jyväskylä, Finland) for performing the X- μ CT analyses included in this work.

Conflicts of Interest: The authors declare no conflict of interest.

Abbreviations

The following abbreviations are used in this manuscript:

ANOVA	Analysis of variance
DMA	Dynamic mechanical analysis
DoE	Design of experiments
PLA	Poly(lactic acid)
S	Industrial side stream
SEM	Scanning electron microscopy
Tg	Glass transition temperature
TMP	Thermomechanical pulp
X- μ CT	X-ray microtomography

References

- Peltola, H.; Laatikainen, E.; Jetsu, P. Effects of physical treatment of wood fibres on fibre morphology and biocomposite properties. *Plast. Rubber Compos.* **2011**, *40*, 86–92. [[CrossRef](#)]
- Chinga-Carrasco, G.; Zarna, C.; Rodríguez-Fabià, S.; Leirset, I.; Tanase-Opedal, M.; Molteberg, D.; Echtermeyer, A.; Hindersland, L.K. Side streams from flooring laminate production—Characterisation and recycling in biocomposite formulations for injection moulding. *Compos. Part A Appl. Sci. Manuf.* **2022**, *153*, 106723. [[CrossRef](#)]
- Tao, Y.; Wang, H.; Li, Z.; Li, P.; Shi, S.Q. Development and Application of Wood Flour-Filled Poly(lactic acid) Composite Filament for 3D Printing. *Materials* **2017**, *10*, 339. [[CrossRef](#)] [[PubMed](#)]
- Pilla, S.; Gong, S.; O'Neill, E.; Yang, L.; Rowell, R.M. Poly(lactide)-recycled wood fiber composites. *J. Appl. Polym. Sci.* **2009**, *111*, 37–47. [[CrossRef](#)]
- Tarrés, Q.; Melbø, J.K.; Delgado-Aguilar, M.; Espinach, F.X.; Mutjé, P.; Chinga-Carrasco, G. Micromechanics of Tensile Strength of Thermo-mechanical Pulp Reinforced Poly(lactic acid) Biodegradable Composites. *J. Nat. Fibers* **2022**, 1–14. [[CrossRef](#)]
- Dufresne, A. 8-Cellulose-Based Composites and Nanocomposites. In *Plastics Design Library*; Ebnesajjad, S.B.T.H.o.B., Eds.; William Andrew Publishing: Boston, MA, USA, 2013; pp. 153–169. [[CrossRef](#)]
- Joffre, T.; Miettinen, A.; Berthold, F.; Gamstedt, E.K. X-ray micro-computed tomography investigation of fibre length degradation during the processing steps of short-fibre composites. *Compos. Sci. Technol.* **2014**, *105*, 127–133. [[CrossRef](#)]
- Stanciu, M.D.; Teodorescu Draghicescu, H.; Tamas, F.; Terciú, O.M. Mechanical and Rheological Behaviour of Composites Reinforced with Natural Fibres. *Polymers* **2020**, *12*, 1402. [[CrossRef](#)]
- Bourmaud, A.; Shah, D.U.; Beaugrand, J.; Dhakal, H.N. Property changes in plant fibres during the processing of bio-based composites. *Ind. Crop. Prod.* **2020**, *154*, 112705. [[CrossRef](#)]
- Zarna, C.; Opedal, M.T.; Echtermeyer, A.T.; Chinga-Carrasco, G.; Ngo, T.D.; Kashani, A.; Imbalzano, G.; Nguyen, K.T.Q.; Hui, D.; Shahrubudin, N.; et al. Reinforcement ability of lignocellulosic components in biocomposites and their 3D printed applications—A review. *Compos. Part C Open Access* **2019**, *143*, 100171. [[CrossRef](#)]
- Codari, F.; Lazzari, S.; Soos, M.; Storti, G.; Morbidelli, M.; Moscatelli, D. Kinetics of the hydrolytic degradation of poly(lactic acid). *Polym. Degrad. Stab.* **2012**, *97*, 2460–2466. [[CrossRef](#)]
- Yang, X.; Wang, G.; Miao, M.; Yue, J.; Hao, J.; Wang, W. The Dispersion of Pulp-Fiber in High-Density Polyethylene via Different Fabrication Processes. *Polymers* **2018**, *10*, 122. [[CrossRef](#)] [[PubMed](#)]
- Yang, T.C. Effect of Extrusion Temperature on the Physico-Mechanical Properties of Unidirectional Wood Fiber-Reinforced Poly(lactic acid) Composite (WFRPC) Components Using Fused Deposition Modeling. *Polymers* **2018**, *10*, 976. [[CrossRef](#)] [[PubMed](#)]
- Van de Voorde, B.; Katalagarianakis, A.; Huysman, S.; Toncheva, A.; Raquez, J.M.; Duretek, I.; Holzer, C.; Cardon, L.; Bernaerts, K.V.; Van Hemelrijck, D.; et al. Effect of extrusion and fused filament fabrication processing parameters of recycled poly(ethylene terephthalate) on the crystallinity and mechanical properties. *Addit. Manuf.* **2022**, *50*, 102518. [[CrossRef](#)]
- Hasook, A.; Muramatsu, H.; Tanoue, S.; Iemoto, Y.; Unryu, T. Preparation of nanocomposites by melt compounding poly(lactic acid)/polyamide 12/organoclay at different screw rotating speeds using a twin screw extruder. *Polym. Compos.* **2008**, *29*, 1–8. [[CrossRef](#)]

16. Pötschke, P.; Villmow, T.; Krause, B. Melt mixed PCL/MWCNT composites prepared at different rotation speeds: Characterization of rheological, thermal, and electrical properties, molecular weight, MWCNT macrodispersion, and MWCNT length distribution. *Polymer* **2013**, *54*, 3071–3078. [CrossRef]
17. Mayoral, B.; Lopes, J.; McNally, T. Influence of Processing Parameters During Small-Scale Batch Melt Mixing on the Dispersion of MWCNTs in a Poly(propylene) Matrix. *Macromol. Mater. Eng.* **2014**, *299*, 609–621. [CrossRef]
18. Feldmann, M.; Heim, H.P.; Zarges, J.C. Influence of the process parameters on the mechanical properties of engineering biocomposites using a twin-screw extruder. *Compos. Part A Appl. Sci. Manuf.* **2016**, *83*, 113–119. [CrossRef]
19. Irfan, M.S.; Umer, R.; Rao, S. Optimization of Compounding Parameters for Extrusion to Enhance Mechanical Performance of Kenaf-Polypropylene Composites. *Fibers Polym.* **2021**, *22*, 1378–1387. [CrossRef]
20. De Santis, F.; Pantani, R. Melt compounding of poly (Lactic Acid) and talc: assessment of material behavior during processing and resulting crystallization. *J. Polym. Res.* **2015**, *22*, 242. [CrossRef]
21. Ruppel, A.; Wolff, S.; Oldemeier, J.P.; Schöppner, V.; Heim, H.P. Influence of Processing Glass-Fiber Filled Plastics on Different Twin-Screw Extruders and Varying Screw Designs on Fiber Length and Particle Distribution. *Polymers* **2022**, *14*, 3113. [CrossRef]
22. Peltola, H.; Pääkkönen, E.; Jetsu, P.; Heinemann, S. Wood based PLA and PP composites: Effect of fibre type and matrix polymer on fibre morphology, dispersion and composite properties. *Compos. Part A Appl. Sci. Manuf.* **2014**, *61*, 13–22. [CrossRef]
23. Muthuraj, R.; Misra, M.; Defersha, F.; Mohanty, A.K. Influence of processing parameters on the impact strength of biocomposites: A statistical approach. *Compos. Part Appl. Sci. Manuf.* **2016**, *83*, 120–129. [CrossRef]
24. Gamon, G.; Evon, P.; Rigal, L. Twin-screw extrusion impact on natural fibre morphology and material properties in poly(lactic acid) based biocomposites. *Ind. Crop. Prod.* **2013**, *46*, 173–185. [CrossRef]
25. Huda, M.S.; Drzal, L.T.; Misra, M.; Mohanty, A.K. Wood-fiber-reinforced poly(lactic acid) composites: Evaluation of the physicomechanical and morphological properties. *J. Appl. Polym. Sci.* **2006**, *102*, 4856–4869. [CrossRef]
26. Asadollahzadeh, M.; Mahboubi, A.; Taherzadeh, M.J.; Åkesson, D.; Lennartsson, P.R. Application of Fungal Biomass for the Development of New Polylactic Acid-Based Biocomposites. *Polymers* **2022**, *14*, 1738 [CrossRef] [PubMed]
27. Hijazi, N.; Le Moigne, N.; Rodier, E.; Saucéau, M.; Vincent, T.; Benezet, J.C.; Fages, J. Biocomposite films based on poly(lactic acid) and chitosan nanoparticles: Elaboration, microstructural and thermal characterization. *Polym. Eng. Sci.* **2019**, *59*, E350–E360. [CrossRef]
28. Krishnaprasad, R.; Veena, N.R.; Maria, H.J.; Rajan, R.; Skrifvars, M.; Joseph, K. Mechanical and Thermal Properties of Bamboo Microfibril Reinforced Polyhydroxybutyrate Biocomposites. *J. Polym. Environ.* **2009**, *17*, 109. [CrossRef]
29. Vandi, L.J.; Chan, C.M.; Werker, A.; Richardson, D.; Laycock, B.; Pratt, S. Extrusion of wood fibre reinforced poly(hydroxybutyrate-co-hydroxyvalerate) (PHBV) biocomposites: Statistical analysis of the effect of processing conditions on mechanical performance. *Polym. Degrad. Stab.* **2019**, *159*, 1–14. [CrossRef]
30. Nature Works. Ingeo™ Biopolymer 4043D Technical Data Sheet. 2022. Available online: https://www.natureworksilc.com/~media/Files/NatureWorks/Technical-Documents/Technical-Data-Sheets/TechnicalDataSheet_4043D_3D-monofilament_pdf.pdf (accessed on 15 September 2022).
31. Minitab. Minitab 19 Support. 2022. Available online: <https://support.minitab.com/en-us/minitab/21/> (accessed on 4 October 2022).
32. Turner, J.R. *Introduction to Analysis of Variance: Design, Analysis, & Interpretation*; SAGE: Thousand Oaks, CA, USA, 2001.
33. Miettinen, A.; Luengo Hendriks, C.L.; Chinga-Carrasco, G.; Gamstedt, E.K.; Kataja, M. A non-destructive X-ray microtomography approach for measuring fibre length in short-fibre composites. *Compos. Sci. Technol.* **2012**, *72*, 1901–1908. [CrossRef]
34. Feldkamp, L.A.; Davis, L.C.; Kress, J.W. Practical cone-beam algorithm. *J. Opt. Soc. Am.-Opt. Image Sci. Vis.* **1984**, *1*, 612–619. [CrossRef]
35. Tomasi, C.; Manduchi, R. Bilateral filtering for gray and color images. In Proceedings of the 6th International Conference on Computer Vision (IEEE Cat. No. 98CH36271), Bombay, India, 7 January 1998; pp. 839–846. [CrossRef]
36. Otsu, N. A threshold selection method from gray level histograms. *IEEE Trans. Syst. Man, Cybern.* **1979**, *9*, 62–66. [CrossRef]
37. Hendriks, C.L.L. Constrained and Dimensionality-Independent Path Openings. *Trans. Img. Proc.* **2010**, *19*, 1587–1595. [CrossRef] [PubMed]
38. Jahne, B. *Practical Handbook on Image Processing for Scientific and Technical Applications*; CRC Press: Boca Raton, FL, USA, 2004.
39. Hildebrand, T.; Rüegeth, P. A new method for the model-independent assessment of thickness in three-dimensional images. *J. Microsc.* **1997**, *185*, 67–75. [CrossRef]
40. Fu, S.Y.; Feng, X.Q.; Lauke, B.; Mai, Y.W. Effects of particle size, particle/matrix interface adhesion and particle loading on mechanical properties of particulate-polymer composites. *Compos. Part B Eng.* **2008**, *39*, 933–961. [CrossRef]
41. Thomason, J.L. The influence of fibre length and concentration on the properties of glass fibre reinforced polypropylene: 5. Injection moulded long and short fibre PP. *Compos. Part A Appl. Sci. Manuf.* **2002**, *33*, 1641–1652. [CrossRef]
42. Thomason, J.L.; Vlug, M.A. Influence of fibre length and concentration on the properties of glass fibre-reinforced polypropylene: 1. Tensile and flexural modulus. *Compos. Part A Appl. Sci. Manuf.* **1996**, *27*, 477–484. [CrossRef]
43. Mallick, P.K. Chapter 5—Thermoplastics and thermoplastic-matrix composites for lightweight automotive structures. In *Woodhead Publishing in Materials; Manufacturing for Lightweight Vehicles (Second Edition)*; Woodhead Publishing: Cambridge, UK, 2021; pp. 187–228. [CrossRef]

44. Mital, S.K.; Murthy, P.L.N.; Goldberg, R.K. Micromechanics for Particulate-Reinforced Composites. *Mech. Compos. Mater. Struct.* **1997**, *4*, 251–266. [[CrossRef](#)]
45. Ariawan, D.; Surojo, E.; Triyono, J.; Purbayanto, I.F.; Pamungkas, A.F.; Prabowo, A.R. Micromechanical analysis on tensile properties prediction of discontinuous randomized zalacca fibre/high-density polyethylene composites under critical fibre length. *Theor. Appl. Mech. Lett.* **2020**, *10*, 57–65. [[CrossRef](#)]
46. Neagu, C.; Gamstedt, K.; Berthold, F. Stiffness Contribution of Various Wood Fibers to Composite Materials. *J. Compos. Mater.* **2006**, *40*, 663–699. [[CrossRef](#)]
47. Chan, C.M.; Vandi, L.J.; Pratt, S.; Halley, P.; Richardson, D.; Werker, A.; Laycock, B. Composites of Wood and Biodegradable Thermoplastics: A Review. *Polym. Rev.* **2018**, *58*, 444–494. [[CrossRef](#)]
48. Lu, J.Z.; Wu, Q.; Negulescu, I.I. Wood-fiber/high-density-polyethylene composites: Compounding process. *J. Appl. Polym. Sci.* **2004**, *93*, 2570–2578. [[CrossRef](#)]
49. Viksne, A.; Rence, L.; Kalnins, M.; Bledzki, A.K. The effect of paraffin on fiber dispersion and mechanical properties of polyolefin–sawdust composites. *J. Appl. Polym. Sci.* **2004**, *93*, 2385–2393. [[CrossRef](#)]
50. Fazelinejad, S.; Åkesson, D.; Skrifvars, M. Repeated Mechanical Recycling of Polylactic Acid Filled with Chalk. *Prog. Rubber, Plast. Recycl. Technol.* **2017**, *33*, 1–16. [[CrossRef](#)]
51. Renstad, R.; Karlsson, S.; Albertsson, A.C. Influence of processing parameters on the molecular weight and mechanical properties of poly(3-hydroxybutyrate-co-3-hydroxyvalerate). *Polym. Degrad. Stab.* **1997**, *57*, 331–338. [[CrossRef](#)]
52. Panwar, V.; Pal, K. Chapter 12—Dynamic Mechanical Analysis of Clay–Polymer Nanocomposites; Elsevier: Amsterdam, The Netherlands, 2017; pp. 413–441. [[CrossRef](#)]
53. Saba, N.; Jawaid, M.; Alothman, O.Y.; Paridah, M.T. A review on dynamic mechanical properties of natural fibre reinforced polymer composites. *Constr. Build. Mater.* **2016**, *106*, 149–159. [[CrossRef](#)]
54. Muck, D.; Tomc, H.G.; Elesini, U.S.; Ropret, M.; Leskovšek, M. Colour Fastness to Various Agents and Dynamic Mechanical Characteristics of Biocomposite Filaments and 3D Printed Samples. *Polymers* **2021**, *13*, 3738. [[CrossRef](#)]
55. Shenoy, A.; Saini, D. Melt flow index: More than just a quality control rheological parameter. Part II. *Adv. Polym. Technol.* **1986**, *6*, 125–145. [[CrossRef](#)]
56. Baker, G.L.; Vogel, E.B.; Smith, M.R. Glass Transitions in Polylactides. *Polym. Rev.* **2008**, *48*, 64–84. [[CrossRef](#)]
57. Boran, S.; Kiziltas, A.; Kiziltas, E.; Gardner, D. Characterization of Ultrafine Cellulose-filled High-Density Polyethylene Composites Prepared using Different Compounding Methods. *BioResources* **2016**, *11*, 8178–8199. [[CrossRef](#)]

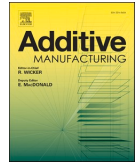


A. III Publication III

Preparation and characterisation of biocomposites containing thermo-mechanical pulp fibres, poly(lactic acid) and poly(butylene-adipate-terephthalate) or poly(hydroxyalkanoates) for 3D and 4D printing







Preparation and characterisation of biocomposites containing thermomechanical pulp fibres, poly(lactic acid) and poly(butylene-adipate-terephthalate) or poly(hydroxyalkanoates) for 3D and 4D printing

Chiara Zarna^{a,*}, Sandra Rodríguez-Fabià^b, Andreas T. Echtermeyer^a, Gary Chinga-Carrasco^{b,*}

^a Department of Mechanical and Industrial Engineering, NTNU, Richard Birkelandsvei 2B, 7491 Trondheim, Norway

^b RISE PFI, Høgskoleringen 6b, 7491 Trondheim, Norway

ARTICLE INFO

Keywords:

Biocomposites
4D printing
Wood fibres
Material extrusion
Mechanical characterization

ABSTRACT

Wood fibres are hygroscopic and swell when immersed in water. This effect can be used to create shape-changing structures in 3D printing. Hence, wood fibre reinforced filaments have the potential to be used in four-dimensional (4D) printing. In this work, biocomposites based on granulated or milled thermomechanical pulp (TMP) fibres and poly(lactic acid) (PLA) were prepared and evaluated based on their tensile properties. Poly(hydroxyalkanoates) (PHA) or poly(butylene-adipate-terephthalate) (PBAT) were included in the biocomposite recipes to assess their effect on the melt flow index (MFI) and tensile properties. Clear effects of the TMP fibre morphology on MFI were quantified. Biocomposites containing 20 wt% PBAT turned out to be stronger and tougher than the ones containing PHA. Based on that, filaments for 3D and 4D printing were manufactured. Interestingly, the tensile strength of 3D printed specimens containing milled TMP (TMPm) fibres was about 33% higher compared to those containing TMP fibre granulate (TMPg). Using hot water as the stimulus, the 3D printed specimens containing TMPg showed a greater reactivity and shape change compared to TMPm specimens.

1. Introduction

Wood fibres, including TMP fibres, became an attractive material for creating more sustainable short-fibre reinforced composites, i.e., biocomposites. TMP fibres can serve as mechanical reinforcement, as cost and weight-efficient filler material, for design purposes and for enhancing dimensional stability [1]. TMP fibres might have the potential to act as reinforcement in PLA without using any compatibilizers. This has been suspected to be due to the presence of lignin on the TMP fibre surface [2].

Currently, biocomposites are used as packaging material [3–5], to

construct furniture and to replace conventional short-fibre reinforced composite materials for non-structural applications [6–10]. Several wood fibre reinforced filaments for 3D printing are commercially available under the brand names Woodfill® from ColorFabb, EasyWood™ from 3DJAKE, etc.

One of the most used polymer matrices for wood fibre biocomposites in material extrusion is the biopolymer PLA. However, PLA generally has a relatively low toughness, depending on its crystallinity. Introducing wood fibres to PLA additionally reduces the toughness by creating local defects [11–13]. 3D printing filaments with low fracture toughness are likely to break during printing causing a fatal error in the

Abbreviations: DSC, Differential scanning calorimetry; MFI, Melt flow index; PBAT, Poly(butylene-adipate-terephthalate); PHA, Poly(hydroxyalkanoates); PLA, Poly(lactic acid); SEM, Scanning electron microscopy; TGA, Thermogravimetric analysis; TMP, Thermomechanical pulp; TMPg, TMP(Thermomechanical pulp) fibre granulates; TMPm, Milled TMP¹ fibres; B+TMPg, Biocomposite from 65wt.% PLA/20wt.% PBAT/15wt.% TMPg; B+TMPm, Biocomposite from 65wt.% PLA/20wt.% PBAT/15wt.% TMPm; P + PHA+TMPg, Biocomposite from 50wt.% PLA/20wt.% PHA/30wt.% TMPg; P + PHA+TMPm, Biocomposite from 50wt.% PLA/20wt.% PHA/30wt.% TMPm; P + PBAT+TMPg, Biocomposite from 50wt.% PLA/20wt.% PBAT/30wt.% TMPg; P + PBAT+TMPm, Biocomposite from 50wt.% PLA/20wt.% PBAT/30wt.% TMPm; X-μCT, X-ray micro-computed tomography.

* Corresponding authors.

E-mail addresses: chiara.zarna@ntnu.no (C. Zarna), sandra.fabia@rise-pfi.no (S. Rodríguez-Fabià), andreas.echtermeyer@ntnu.no (A.T. Echtermeyer), gary.chinga.carrasco@rise-pfi.no (G. Chinga-Carrasco).

<https://doi.org/10.1016/j.addma.2022.103166>

Received 26 June 2022; Received in revised form 1 September 2022; Accepted 21 September 2022

Available online 24 September 2022

2214-8604/© 2022 The Authors. Published by Elsevier B.V. This is an open access article under the CC BY license (<http://creativecommons.org/licenses/by/4.0/>).

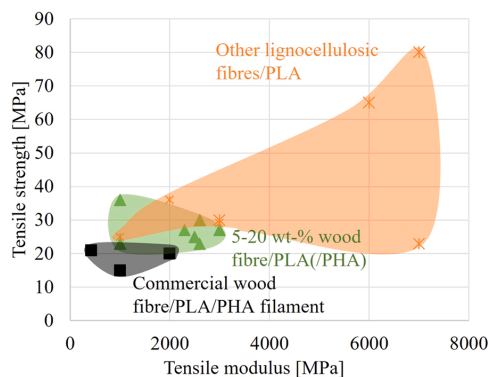


Fig. 1. Tensile strength and modulus of 3D printed parts from lignocellulosic fibre/PLA(PHA) biocomposite collected from literature [14,15,25–27,32,34,38–44].

process. To enhance the toughness of wood fibre reinforced PLA filaments, aliphatic polyesters such as PHA are commonly introduced to the biocomposite [14–17]. Amorphous PHA shows rubbery behaviour and commonly has a lower tensile strength and stiffness, but higher elongation than PLA [14,18].

PBAT, a biodegradable aliphatic/aromatic copolyester, was also found to enhance the fracture toughness and processability of PLA [19–21]. It was further stated that PBAT might not lead to a drastic loss in tensile strength and stiffness [19] and showed to increase the melt flow index (MFI) of neat PLA [21]. The MFI can be used to assess the ability of a material to flow through a nozzle at a certain temperature. Ensuring a sufficient material flow during 3D printing is crucial [22]. Wang et al. [22] recommended a minimum MFI of 10 g/min to obtain an acceptable quality of 3D printed parts. The addition of 20–30 wt% of PHA or PBAT to PLA seems to be beneficial when used as a toughness enhancer [14,19–21].

3D printing with wood fibre biocomposites can be challenging due to potential nozzle clogging, filament breakage, relatively low and non-uniform melt flow, relatively rough surface finish and more prominent porosity than in neat polymer parts [1,13,23]. These challenges restrict the wood fibre fraction in the biocomposite as well as the wood fibre size. Mostly wood fibre fractions from 5 to 20 wt% are used, with 20 wt% already showing stick-slip effects under extrusion through a 1 mm nozzle [23]. Tensile strength and modulus of 3D printed parts were shown to decrease with fibre fractions above 10 wt% due to a significant increase in porosity [24]. Other lignocellulosic fillers considered for 3D printing are for example cork [25], cellulose networks [26], cellulose nanofibrils [27], lignin [28–30], flax [31], jute [32,33], bamboo [34,35] and hemp fibres [36–38]. Typical values of lignocellulosic reinforced PLA(PHA) 3D printed parts found in the literature are presented in Fig. 1.

3D printing nozzle outlets usually have diameters in the range of 0.2–0.8 mm. The fibres or particles must be smaller than the nozzle size to prevent clogging [24]. Therefore, recycled fibres in form of flour or particles are used rather than higher aspect ratio fibres to produce 3D printing filaments [1,23,42,45]. Since wood particles are more or less randomly shaped with dimensions similar in all directions, they do not contribute to any tensile strength increase of the matrix polymer [1]. The usage of larger nozzle diameters for the printing of large-scale parts, for example in the building and construction or automotive sector, could be a promising application perspective for reinforcement by wood fibres having a higher aspect ratio [24,31,46]. 15 wt% kraft pulp fibres with a relatively high aspect ratio (lengths of 2.4 mm and widths of 0.03 mm) together with PLA and PHA were successfully processed into filament for commercial 3D printers [14]. Compared to kraft pulp fibres, TMP fibres

use fewer chemicals, and fewer fossil fuels, but require more electricity during production [47]. In Norway electricity is generated from hydropower which is an environmentally sound clean energy source. Additionally, TMP fibres are less costly than kraft pulp fibres. TMP fibres are thus considered a good alternative to kraft pulp fibres for biocomposite production. TMP fibres together with bio polyethylene were used to prepare filament with a TMP fibre weight fraction of 10 and 20 wt% [48].

4D printing is a method of adding a fourth dimension to 3D printed parts in form of actuation through an external stimulus. This can include moisture, water, temperature, light, etc. Wood fibres absorb water and swell accordingly [23,49–52].

Water absorption usually leads to unwanted deformations, optical defects, and degradation of the mechanical properties of a biocomposite. However, the self-shaping effect of wood fibres can be used to create hygromorph biocomposites [15]. Hygromorph biocomposites can be applied as e.g. ventilation valves, self-aligning solar panels [53], multiple hinges folds and curls of flat sheets and sensors [52].

Warping of wood fibre-reinforced composite parts can be controlled through a bilayer structure, which is exposed to environmental changes. The anisotropy of 3D printed parts and wood fibre swelling can be used to design shape morphing structures mainly through different raster angle orientations [1,15,54]. Wood fibre fraction and orientation in the filament and porosity of the 3D printed parts highly influence the shape change and response rate. To some extent, a greater wood fibre fraction leads to greater shape changes and response rates. A greater porosity can contribute to a faster response but might reduce the maximum deflection because of the inability to transfer swelling strains [54].

Combining two materials which respond differently to water exposure is another option to induce warping. Similar effects are well known from bimetal materials used in thermometers or circuit breakers, for example [15,55].

Wood fibres generally swell the most in the tangential direction and the least in the longitudinal direction [56,57]. This is caused by the almost longitudinally aligned cellulose microfibrils in the S₂ cell wall layer. The stiff microfibrils hinder the wood fibre from expanding longitudinally through water absorption [57]. Differences in tangential and radial swelling are mostly attributed to the arrangements of cells [57]. Untreated, dry TMP fibres take up 1–2 g of water per gram of TMP fibres, depending on the temperature [58].

After being immersed in hot water, the tensile strength and modulus of lignocellulosic fibre reinforced biocomposites typically decrease (about 5–15%) [59–61]. This is due to the swelling of the fibres which can induce microcracks in the fibre-matrix-interface and fibre-matrix debonding. On the other hand, 15 wt% wood flour/Polypropylene composite was immersed in boiling water and the tensile strength increased slightly. This was most probably related to an additional process of annealing which increased the degree of crystallinity of the matrix and thus the tensile strength [27,59]. It was also suspected that the swollen particles led to an increase in interfacial shear strength between the wood flour and the matrix. Additionally, the wet strength of wood fibres might be higher than the dry strength because of better interaction between microfibrils [62]. Concerning 3D printed wood fibre/PLA biocomposite, the water absorption increased with increasing layer thickness while the tensile properties decreased accordingly [63].

The purpose of this study is to design biocomposite formulations for 3D printing objects that could react to external stimuli, thus introducing shape changing capabilities (4D printing). Due to the hygroscopic behaviour of TMP fibres, the fibres were used as the components that react to an external stimulus, i.e., humidity. PHA and PBAT were used as toughness enhancers. The effect on the corresponding tensile strength and stiffness and MFI was assessed.

Table 1
Sample composition and designation. TMPg indicates TMP granulate and TMPm milled TMP fibres.

Sample designation	PLA [wt%]	PHA [wt%]	PBAT [wt%]	TMPg [wt%]	TMPm [wt%]	Compounding time [min.]
PLA	100	–	–	–	–	–
P + PHA_1	80	20	–	–	–	1
P + PBAT_1	80	–	20	–	–	1
P + PHA+TMPg_1	50	20	–	30	–	1
P + PHA+TMPm_1	50	20	–	–	30	1
P + PHA+TMPg_3	50	20	–	30	–	3
P + PHA+TMPg_3	50	20	–	–	30	3
P + PBAT+TMPg_1	50	–	20	30	–	1
P + PBAT+TMPm_1	50	–	20	–	30	1
P + PBAT+TMPg_3	50	–	20	30	–	3
P + PBAT+TMPm_3	50	–	20	–	30	3

Table 2
3D printing parameters used for sample preparation.

Extrusion temperature [°C]	Bed temperature [°C]	Layer height [mm]	Line width [mm]	Extrusion speed [mm/s]	Flow [%]	Infill [%]
210	60	0.15	0.6	60	110	100

2. Materials and methods

2.1. Materials

PLA Ingeo 4043D with a density of 1.24 g/cm³ [64] and molecular weight of 67 kDa [65], was purchased from NatureWorks (Minnetonka, MN 55345, USA). PHA with a density of 1.23 g/cm³ [66] and a molecular weight of 50–100 kDa [67] was purchased from GoodFellow Cambridge Limited (Huntingdon, PE29 6WR, United Kingdom). PBAT with a density of 1.25 g/cm³ [68] and a molecular weight of 52 kDa [69] (ecoflex® from BASF) was purchased from B-Plast2000 (26605, Aurich, Germany). PLA filament for 3D printing was purchased from Prusa Research a.s. (17000, Prague, Check Republic). Spruce TMP fibres were prepared by Norske Skog Saugbrugs (Halden, Norway). The chemical composition and processing history of the TMP fibres were previously provided by [7,70]. The TMP fibre morphology was assessed with a FiberTester Plus device. Before measurement, the fibres were diluted (0.1 g in 300 ml water), the TMPg fibre length was (1.41 ± 0.05) mm and the width was (32.6 ± 0.3) µm. Some of the TMPg granules (diameter < 8 mm) were further processed in a Thomas Wiley Mini-Mill with a 30 mesh (TMPm). The resulting TMPm fibre length was (0.43 ± 0.01) mm and the width was (38.2 ± 0.3) µm.

2.2. Compounding

The polymers and fibres were dried before compounding in an Xplore twin-screw micro compounder (Xplore Instruments BV, Sittard, The Netherlands) as described in [7]. From the samples containing TMP fibres, two batches were prepared and compounded for 1 or 3 min. Table 1 provides the sample formulations and corresponding designations.

2.3. Melt flow index (MFI), thermo-gravimetric analysis (TGA) and differential scanning calorimetry (DSC)

A Netzsch Jupiter F3 equipment, operating in a nitrogen environment was used for simultaneous DSC and TGA analyses. The scans were performed from 35 °C to 800 °C with a heating rate of 10 °C/min. The onset temperature of the DTG curve was considered as decomposition temperature. The melt flow index was measured with a Melt Flow Index - Deluxe (Model No: MFI – DX, Presto Stantest Private Limited, Faridabad, India) at 195 °C, as described in more detail in [7,14].

2.4. Injection moulding, mechanical testing, and scanning electron microscopy

Tensile test specimens (4 per series) were injection moulded with an Xplore injection moulding system (Xplore Instruments BV, Sittard, The Netherlands). An injection moulding temperature of 190 °C and a mould temperature of 30 °C was applied. The specimens have a dogbone shape with an overall length of 50 mm and a length of the narrow parallel-sided portion of 18 mm. The cross-sectional area is 4 mm × 2 mm (width × thickness).

Unidirectional tensile tests were conducted on a dynamic mechanical analysis test machine Gabo Eplexor® 150 from NETZSCH (Selb, 95100, Germany) with a maximum axial force of 1500 N. The test speed was 2 mm/min., and the gauge length was 33 mm. An integrated optical strain measurement system was used.

Scanning electron microscopy (SEM) images were taken from the fracture surfaces of tensile test specimens as described in [14].

2.5. Filament manufacturing and X-ray micro-computed tomography (X-µCT) analysis

Based on the results from mechanical testing, the compounds P + PBAT+TMPg_3 and P + PBAT+TMPm_3 were selected to be processed into a 3D printing filament. The filament was manufactured as described in [14].

To secure a filament with constant thickness and good printability, the compounds had to be diluted with PLA and PBAT to a composition of 65 wt% PLA+ 20 wt% PBAT+ 15 wt% TMPg (B+TMPg) and 65 wt% PLA+ 20 wt% PBAT+ 15 wt% TMPm (B+TMPm). The biocomposites were undertaken a second round of compounding using the same parameters as mentioned earlier.

The fibre spatial distribution and fibre dimensions were assessed with X-ray microtomography [71]. Filament pieces with an approximate length of 5 mm were imaged with an Xradia MicroXCT-400 tomograph (XRadia, Concord, California, USA) with a 1.1 µm pixel size. X-ray tube voltage was set to 30 kV and the power to 3 W. 1881 projections were acquired with 8 s exposure time and 10x magnification. 3D volume images were constructed using an algorithm from [72]. A cropped region of the image was edited by bilateral and high pass filtering [73]. Fibres, matrix, and voids were segmented by thresholding according to [74]. To segmentate agglomerates, individual fibres were erased with a morphological opening filter, and the pores in the agglomerates were closed by a morphological closing filter. The fibre lengths were determined using the constrained path transform [75], and fibre orientation

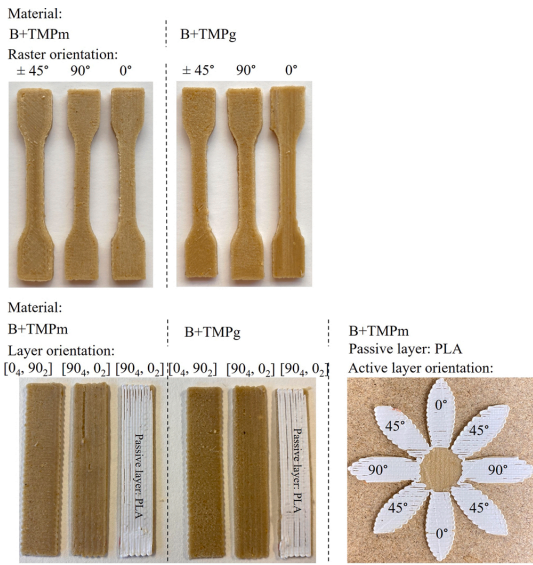


Fig. 2. 3D printed dogbone specimens from B+TMPm (top left) and B+TMPg (top right) with raster orientations of $\pm 45^\circ$, 0° , and 90° . Samples to demonstrate shape changes after water immersion: Bilayer sheets in mono- and bi-material configurations (bottom left) and blooming flower example with different raster orientations and bi-material petals (bottom right).

Table 3

Active and passive layer orientation of samples for evaluation of the filament's response to water absorption. B+TMPg or B+TMPm indicate a biocomposite of 65 wt% PLA, 20 wt% PBAT and 15 wt% TMP fibre granulate or milled TMP fibres, respectively.

Active layer material	Passive layer material	Layup
B+TMPg	B+TMPg	$[0_4/90_2]$
B+TMPm	B+TMPm	$[0_4/90_2]$
B+TMPg	B+TMPg	$[90_4/0_2]$
B+TMPm	B+TMPm	$[90_4/0_2]$
B+TMPg	PLA	$[90_4/0_2]$
B+TMPm	PLA	$[90_4/0_2]$

using the structure tensor method [76]. By applying the approach of Miettinen et al. [77], the fibre length and orientation were combined into fibre property distributions. With the local thickness algorithm [78] agglomerates were characterised by measuring the volume and the surface area.

Table 4

Thermal properties of biocomposites, neat polymers and TMP fibres.

Sample	Compounding time [min.]	Melting temperature [°C]	Decomposition temperature [°C]	Residual mass [%]
PLA	–	146.4	348.7	0.57
PHA	–	–	281.8	1.53
PBAT	–	97.2	384.7	5.14
TMP	–	–	313.7	17.5
P + PHA+TMPg_3	3	148.8	288.7	7.23
P + PHA+TMPm_3	3	144	288.8	7.33
P + PBAT+TMPg_3	3	147.1	319.3	10.28
P + PBAT+TMPm_3	3	148.9	324.4	9.81
P + PHA+TMPg_1	1	147.4	282.9	7.67
P + PHA+TMPm_1	1	144	287.2	7.54
P + PBAT+TMPg_1	1	148.2	320.9	11.02
P + PBAT+TMPm_1	1	147.1	322.5	8.45

2.6. 3D/4D printing

An Original Prusa i3 MK3 (Prusa, Prague, Czech Republic) with a 0.6 mm nozzle was used for 3D printing. Additional printing parameters can be found in Table 2 Ultimaker Cura 4.13.1 slicer software was used to prepare the g-code. Before printing the filaments were dried at 50°C for 4 h.

3D printed samples were oven dried at 80°C for 24 h and immersed in a 60°C tempered water bath. The samples were weighted, and dimensional changes were measured using a digital microscope (RH-2000 from Hirox, Tokyo, Japan) after 0 h, 24 h and 48 h. The measurements were used to calculate swelling strains according to Eq. (2.4). The 3D printed samples were flat printed squares (10×10) mm^2 and 0.6 mm thick. This corresponds to 4 printed layers with a layer thickness of 0.15 mm. The raster orientation was unidirectional. Four samples per specimen type were considered.

Dogbone specimens, with the same shape as the injection moulded ones, were printed for mechanical tensile testing. The dogbones were printed in three different raster orientations: $\pm 45^\circ$, 0° , and 90° , as seen in Fig. 2.

To demonstrate the applicability of the filaments in 4D printing, rectangular sheets ($10 \times 50 \times 0.9$) mm^3 were printed with different raster orientation lay-ups. The samples consist of 6 layers (thereof 2/3 active and 1/3 passive [79,80]) and no outer walls. The active layers are supposed to swell longitudinal to the shape morphing axis, while the passive layers should remain more or less constant. Constructing the active and passive layers in different raster orientations and/or materials with different swelling coefficients should induce warping towards the passive layer under water absorption. The layup of the here presented biocomposite samples were either $[90_4/0_2]$ or $[0_4/90_2]$

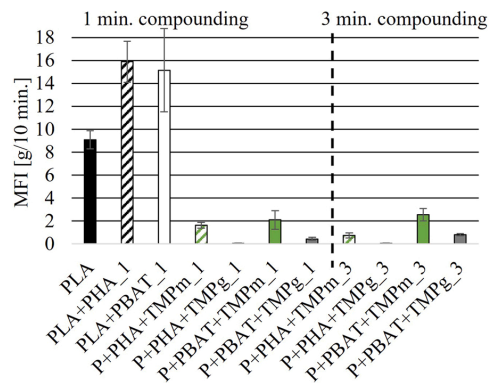


Fig. 3. MFI of PLA, PLA+PHA, PLA+PBAT and biocomposites after 1 min and 3 min compounding time.

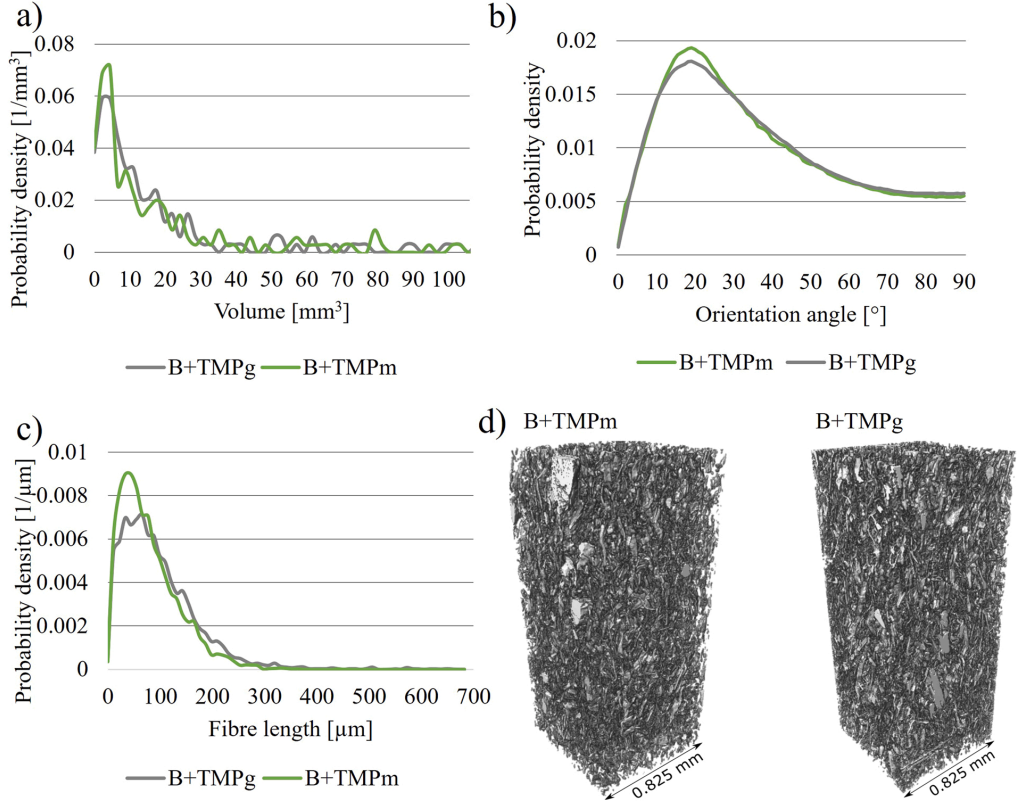


Fig. 4. Results from X-μCT analysis. a) fibre volume distribution in b) fibre orientation angle, c) fibre length, d) visualisation of X-μCT scans of B+TMPm and B+TMPg.

(Table 3). Layers printed in 90° raster orientation were considered active and with 0° raster orientation as passive.

An object in the shape of a blooming flower was used to investigate the effect of raster orientations of the active layer at 0°, 90° and 45° simultaneously. The samples to demonstrate 4D printing were dried at 80 °C for 24 h and afterwards immersed in 60 °C tempered water. The change of shape in form of warping and the difference in weight was captured after 24 h. To quantify the deflection the chord length and height of deflection was measured with a caliper. The curvature was then calculated according to Eq. (2.1) and the water absorption according to Eq. (2.5).

3. Theory and calculation

3.1. Curvature assessment

For calculating the curvature κ of 3D printed sheet samples (Fig. 2) the centre of the deflection h and chord length L was measured. The measurement was done after 24 h of water immersion. The curvature was calculated by [81]:

$$\kappa = \frac{8 \times h}{L^2 + 4 \times h^2} \quad (2.1)$$

To design hygromorph biocomposites Le Duigou et al. [15,80] proposed the analytical solution for the analysis of bi-metal thermostats from Timoschenko [82]. The curvature of a beam can be calculated by:

$$\kappa_T = \frac{\Delta\beta \times \Delta M \times f(m, n)}{t} \quad (2.2)$$

$$f(m, n) = \frac{6(1+m)^2}{3(1+m)^2 + (1+mn) \times (m^2 + \frac{1}{mn})} \quad (2.3)$$

In Eqs. 2.2 and 2.3 $m = t_p/t_a$, where t_p is the thickness of the passive layer (0° raster orientation), t_a is the thickness of the active layer (90° raster orientation) and t the total thickness. Further, $n = E_p/E_a$, where E_p and E_a are the elastic moduli of the passive and active layer, respectively. The swelling coefficient $\Delta\beta$ is the difference between the swelling coefficient of the active and the passive layer. ΔM describes the difference in water content between immersed and dried samples. The swelling coefficient and water content was calculated by:

$$\beta_{a,p} = \frac{\epsilon_{a,p}}{\Delta M} \quad (2.4)$$

$$\Delta M = \frac{m_0 - m_1}{m_0} \quad (2.5)$$

In Eq. 2.4 $\epsilon_{a,p}$ is the swelling strain along 0° raster orientation (active layer) and 90° raster orientation (passive layer). The weighted mass of the dried specimen before water immersion is described by m_0 and m_1 after 24 h of water immersion.

Regarding the 3D printed biocomposite part as construction of laminate plies, laminate theory including the effect of expansional strains due to moisture swelling can be applied [83,84]. Orthotropic material behaviour is assumed for the 3D printed laminate plies. The

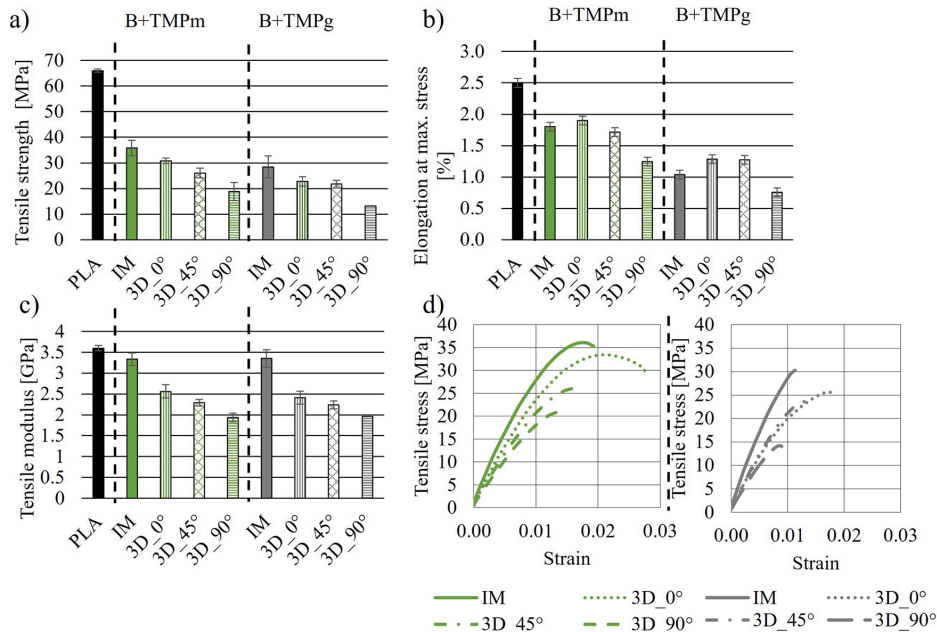


Fig. 5. Tensile properties of injection moulded PLA, injection moulded (IM) and 3D printed (3D) biocomposites. a) Ultimate strength, b) Elongation at ultimate strength, c) Elastic modulus and d) Stress-strain curves of B+TMPm (green) and B+TMPg (grey).

plane stress moisture swelling relation is described by:

$$\sigma' = Q' \times (\epsilon^0 + z\kappa - \Delta\beta\Delta M) \quad (2.6)$$

In Eq. (2.6) Q' is the reduced stiffness matrix of the 3D printed biocomposite part, ϵ^0 are the midplane strains, and z is the distance from the midplane to the top surface of the ply. Taking into account different raster (ply) orientations the constitutive relations for a laminate subjected to swelling loads (N_{sw}) and moments (M_{sw}) can be written as:

$$\begin{bmatrix} N_{sw} \\ M_{sw} \end{bmatrix} = \begin{bmatrix} A & B \\ B & D \end{bmatrix} \begin{bmatrix} \epsilon^0 \\ \kappa \end{bmatrix} \quad (2.7)$$

In Eq. (2.7) $[A]$ is the laminated extensional stiffness matrix, $[B]$ is the bending-stretching coupling and $[D]$ is the laminate bending stiffness. Detailed explanations of laminate theory and the corresponding stiffness matrix can be found in [84,85]. No external forces were applied to the here considered 3D printed parts and were therefore considered equal to zero.

3.2. Statistical analysis

The effect of the biocomposite formulations on the mechanical properties of injection moulded specimens was assessed as part of a 2^3 full factorial design, i.e., three variables at two levels. The three variables were: TMP fibre type (granulate or milled), plasticizer type (PBAT or PHA) and compounding time (1 min or 3 min). The statistical analysis of the main effects was done using Minitab® 19.2020.1 software.

4. Results and discussion

4.1. TGA and DSC

The thermal properties of PLA and the here presented biocomposites are shown in Table 4. The melting temperature of the biocomposites was ranging between 144 °C and 149 °C. The decomposition temperature is

the highest for neat PLA (349 °C) and lowest for PHA containing biocomposites (289 °C), as also reported in previous studies [86]. The addition of PBAT to the biocomposites reduces the decomposition temperature of PLA just slightly to 329–324 °C, as similarly reported in [87]. The addition of TMP fibres resulted in an increase in the residual mass of the biocomposite samples from 0.57% for PLA to 7.23%–10.28%. This is due to the comparatively high residual mass of the TMP fibres themselves. For the TMP fibres two decomposition temperature ranges could be identified. One between 35.1 °C and 176.2 °C with a mass loss of 4.29% and one between 313.7 °C and 779.4 °C with a mass loss of 78.65%. Hemicellulose and cellulose typically degrade in a range from 200 °C to 350 °C and lignin starts degrading from 250 °C [88,89]. Additionally, aromatic rings in lignin are expected to decompose above 500 °C and after heating to 800 °C fractions of the lignin forms highly condensed aromatic structures [90], which explain the relatively high residual mass of the TMP fibres (17.5%). An influence of compounding time on the thermal properties of the biocomposites could not be identified.

4.2. Melt flow index (MFI)

Both, PHA and PBAT increased the MFI of neat PLA by about 80%. However, the MFI turned out to be relatively low (< 3 g/min.) for all biocomposite formulations (Fig. 3). This is related to the addition of TMP fibres. It was previously shown that an addition of 30 wt% TMP fibres reduces the MFI of PLA and polyethylene drastically to an MFI below 1 g/10 min [7,48]. As seen in Fig. 3, the addition of TMPm results in higher MFI than TMPg. The longer TMPg fibres are more likely to entangle than the shorter particle-like TMPm fibres. The fibre entanglement and the resulting formation of agglomerates most probably led to a reduced ability of the biocomposite to flow. The MFI of PBAT containing biocomposites was slightly higher than the ones containing PHA. Main effect plots for the MFI can be found in Appendix B. A clear difference between the shorter or longer compounding time could not be

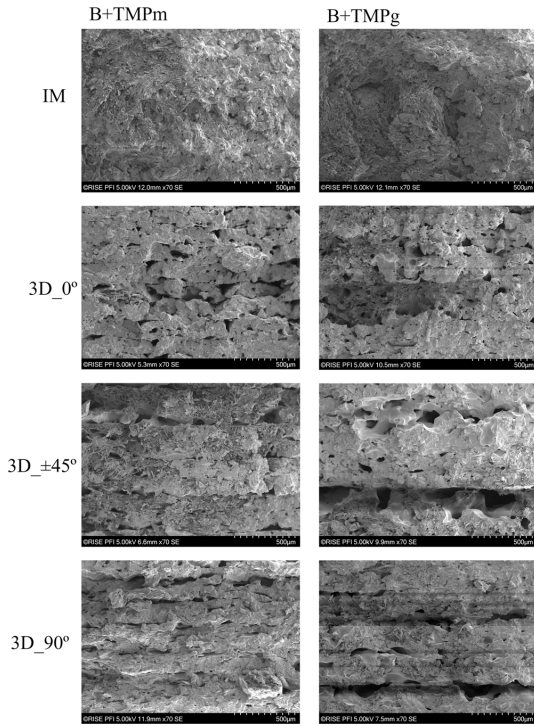


Fig. 6. SEM images of the fracture surfaces in 70x magnification of injection moulded (IM) and 3D-printed (3D) biocomposites having different raster orientations: 0°, ± 45° and 90°.

pointed out.

4.3. Tensile tests of injection moulded biocomposites

Comparing the ultimate tensile strengths of the here investigated biocomposites (Appendix A, Fig. A a-d), it can be observed that the biocomposites containing PBAT (35.8–41.8 MPa) resulted in higher ultimate tensile strengths than those containing PHA (29.9–35.5 MPa). The same applies to the elongation at maximum stress (1.52–1.94% for PBAT and 1.12–1.43% for PHA containing biocomposites). The elastic modulus of the biocomposites containing PBAT (4.0–4.2 GPa) was lower

compared to the ones containing PHA (4.1–4.6 GPa). The plasticiser had a significant effect ($P < 0.05$) on the tensile properties of the investigated biocomposites. In Fig. 4 d stress-strain curves of biocomposites compounded for 3 min, neat PLA, P + PHA_1 and P + PBAT_1 are shown. Biocomposites containing PBAT showed a slightly less steep initial gradient in the elastic region and a higher strain at ultimate strength compared to PHA. Introducing TMP fibres to PLA, without adding plasticisers, typically increases the stiffness and reduces the strain to failure [7,14]. PBAT-containing biocomposites almost maintained the stiffness (+ 14%) and reduced the strain at maximum stress of neat PLA slightly (–20%). However, a greater non-linearity and drastically reduced ultimate strength must be considered (–36%).

The factors fibre type and compounding time did not result in significant effects on the tensile properties. However, trends could be observed. Generally, the TMPg fibres resulted in a slightly higher ultimate tensile strength, elongation and modulus when compounded for just one minute. After a longer compounding time of three minutes, the

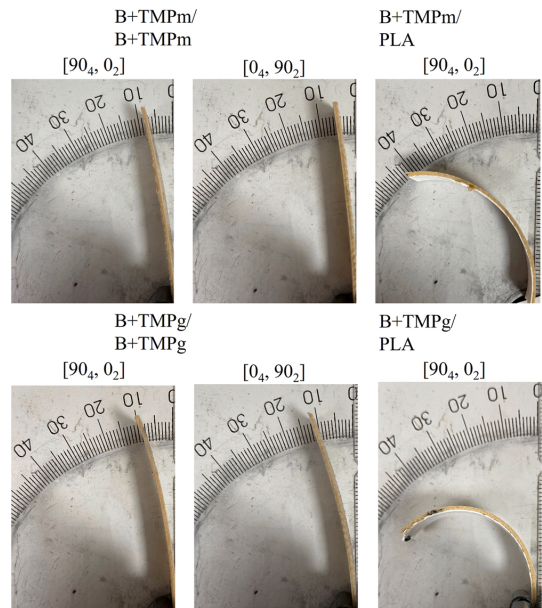


Fig. 8. Deflection of biocomposites with different active layer orientations after 24 h water immersion.

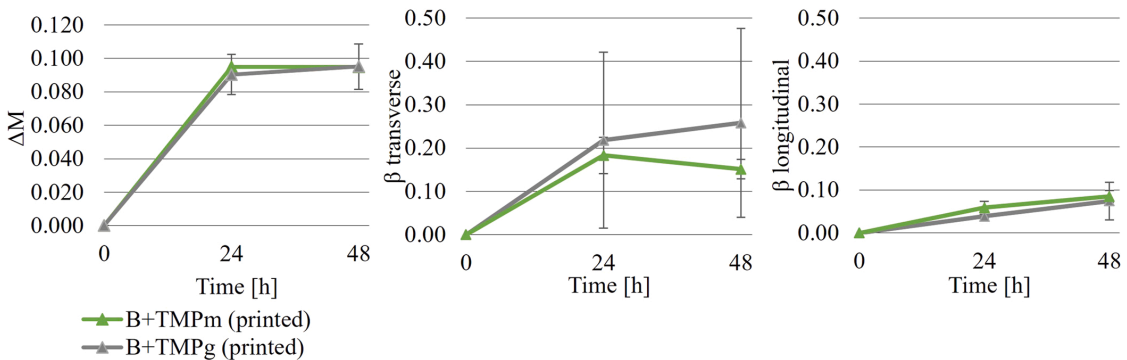


Fig. 7. Weight change and swelling coefficient in transverse and longitudinal direction after water immersion for 24 h and 48 h of 3D printed specimens.

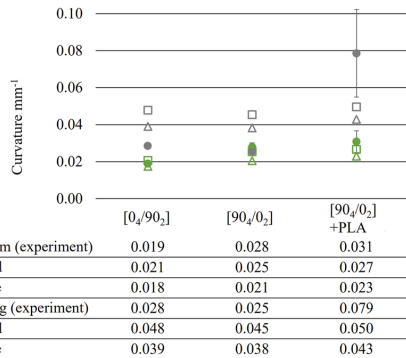


Fig. 9. Experimentally measured and theoretically calculated curvature of biocomposite sheets after water immersion.

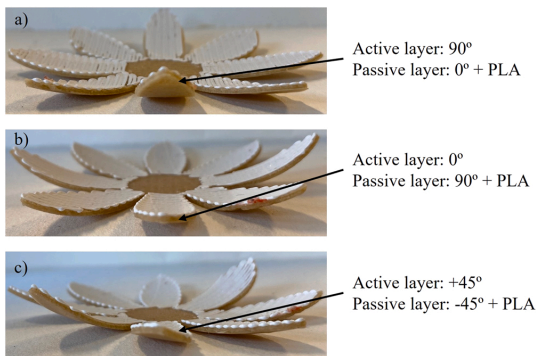


Fig. 10. Blooming flower 4D printing example for investigation of deformations with different layer orientations simultaneously. a) view on active layers oriented in 90° , b) view on active layers oriented in 0° and c) view on active layers oriented in $+45^\circ$.

tensile properties were nearly identical for both fibre types. The longer the biocomposite components remain in the compounder, the more they are exposed to external forces and high temperatures which might damage and shorten the fibres and contribute to polymer degradation. Main effect plots for the tensile strength and modulus can be found in Appendix B.

Based on the obtained tensile test results, the materials P + PBAT+TMPg₃ and P + PBAT+TMPm₃ were chosen for further investigation and production of biocomposite filament for 3D and 4D printing.

4.4. X- μ CT analysis of biocomposite filaments and tensile tests of 3D printed parts

X- μ CT analysis revealed that both fibres TMPg and TMPm got significantly shortened during compounding. The initial fibre lengths of TMPg and TMPm got reduced to $(105.1 \pm 82.5) \mu\text{m}$ and $(85.8 \pm 51.7) \mu\text{m}$, respectively (Fig. 4c).

According to X- μ CT analysis results, B+TMPm filaments had more oriented fibres along the filament axis and lower volumes of agglomerations than B+TMPg filaments (Fig. 4a, b).

Dogbone specimens were 3D printed from both filaments B+TMPg and B+TMPm. Additionally, injection moulded dogbones were prepared since the biocomposite formulation had to be adjusted to be able to

produce good quality filaments. The results of the tensile tests are presented in Fig. 5.

The initial tensile properties of the injection moulded specimens (Appendix A) got reduced in tensile strength about 12% for P + PBAT+TMPm and 32% for P + PBAT+TMPg compared to the new formulations B+TMPm and B+TMPg, respectively. Further, the elastic modulus was reduced by about 19% for both materials. The elongation of P + PBAT+TMPg got particularly reduced (43%) when compared to B+TMPg. Thus, the fracture toughness was significantly reduced although the TMPg fibre fraction got halved. With lowering the fibre fraction an increase in fracture toughness was expected. Fibre damage and thermal degradation of the polymer matrix due to the second compounding round must be considered and contributed most probably to the reduced tensile strength and elongation [91,92].

The 3D printed samples with different raster orientations resulted in slightly lower tensile strengths and stiffnesses than the injection moulded ones. This was expected, because of the presence of voids in the printed parts which form under the 3D printing process [93,94]. Void formations can be seen in the fracture surfaces presented in Fig. 6. Relatively large voids and irregularities can especially be observed on the fracture surface of B+TMPg. The fibre accumulations of relatively large volumes in B+TMPg may have hindered the polymer flow through the 3D printer extrusion nozzle resulting in a relatively porous part. Fibre agglomerations and porosity may have reduced the tensile strength and elongation of the biocomposites since the single fibres were not able to transfer loads and rather acted like local defects. Additionally, the inter-layer fusion bond might not be as strong as in a moulded part. This typically leads to reduced tensile properties of parts printed in 90° and partially of those printed in $\pm 45^\circ$ raster orientation due to inter-layer fusion bond failure [15,95]. The slightly increased elongation for parts printed in 0° or $\pm 45^\circ$ raster orientation might be related to increased crystallinity of the 3D printed parts compared to the injection moulded ones [93,94]. Dogbones printed from P + PBAT + 15TMPm in $\pm 45^\circ$ had a tensile strength of $(26.2 \pm 1.1) \text{MPa}$, an elastic modulus of $(2.3 \pm 1.6) \text{GPa}$ and elongation at maximum stress of $(1.72 \pm 0.13) \%$. These tensile properties are comparable to parts 3D printed from commercially available wood fibre reinforced PLA/PHA [15,40] and also from wood fibre/PLA filaments presented in other studies [14,25,39,41–44]. Eventually, PBAT did only contribute to a slightly improved tensile strength in the 3D printed parts.

In Fig. 6b, an orientation angle of 0° refers to perfectly aligned fibres along the filament axis. Most of the fibres are oriented about $10^\circ - 20^\circ$ off from the filament axis. There is a slightly higher probability for TMPm fibres to have an orientation angle of $\sim 20^\circ$ than for TMPg. The TMPg fibres may be more entangled and thus less oriented in the filament than the TMPm fibres. This may have contributed to the measured higher MFI (Fig. 3).

Additionally, it can be suspected that the greater presence of larger TMPg fibre agglomerations contributed to the comparatively low tensile strength and elongation of injection moulded and 3D printed parts from B+TMPg. Regarding Fig. 6, relatively large voids and irregularities can especially be observed on the fracture surface of B+TMPg. The fibre agglomerations of relatively large volumes in B+TMPg may have hindered the polymer flow through the 3D printer extrusion nozzle resulting in a relatively porous part. Fibre agglomerations and porosity may reduce the tensile strength and elongation of a composite since the single fibres are not able to transfer loads and rather act like local defects.

4.5. Water absorption and swelling of 3D printed parts containing TMP fibres

3D printed samples of the materials B+TMPg and B+TMPm were immersed in tempered water to investigate their water absorption and swelling behaviour. TMP fibre agglomerations and increased surface roughness could also be observed in 3D printed samples after water immersion. A roughened surface was particularly visible for B+TMPg.

This might be related to greater swelling strains induced through the larger TMPg fibre agglomerations. Pictures of 3D printed specimens before and after water immersion are presented in [Appendix C](#).

[Fig. 7](#) presents the weight change and swelling coefficient in transverse (90° raster orientation) and longitudinal direction (0° raster orientation) of 3D printed biocomposites. B+TMPm seemed to absorb water slightly faster than B+TMPg. B+TMPm was almost saturated after 24 h in the water bath while P + PBAT+ 15TMPg showed a slight increase in weight also after 48 h in water ([Fig. 7](#) (left)). [Fig. 7](#) (right) shows that B+TMPg resulted in greater dimensional changes than B+TMPm. The swelling coefficient β is higher in the transverse direction (up to 26% for B+TMPg and 18% for B+TMPm) than in the longitudinal (up to 9.5% for B+TMPg and 7.5% for B+TMPm), which is related to the anisotropic swelling behaviour of wood fibres [56,57]. Additionally, it is assumed that the TMP fibres are oriented longitudinally to the filament axis [38]. Measuring the swelling of B+TMPg was particularly challenging because irregular swelling of the 3D printed strands was more prominent than in B+TMPm. This was most probably related to the greater presence of TMP fibre agglomerations and resulted in a higher deviation of the transverse swelling coefficient for B+TMPg.

4.6. 4D printing of biocomposites

The deflection of 3D printed samples from B+TMPm and B+TMPg with different active and passive layer orientations after water immersion is shown in [Fig. 8](#). Besides two mono-material configurations, one bi-material with a passive layer of PLA-filament was investigated. As seen in [Fig. 8](#), bi-material configurations warped far more than mono-material configurations. Samples printed with a $[90_4/0_2]$ layout deflected slightly more than those with a $[0_4/90_2]$ layout. This observation agrees with previous investigations on printed square samples presented in Section 3.5.

The experimentally measured and theoretically calculated curvature is presented in [Fig. 9](#). Input parameters used for the analytical models are given in [Appendix D](#). Comparing the models, values obtained from laminate theory are generally lower than those obtained from bi-metal theory. Especially for the bi-material configurations (“+PLA”), the measured curvature was up to 90% higher than estimated by the models. Considering the mono-material configurations with B+TMPm, the bi-metal model deviates about 8%, while values obtained by laminate theory deviate about 22%. Curvatures of the configurations with B+TMPg were greatly (30–40%) overestimated by the analytical models. This was related to the measured water uptake ΔM , which was comparatively high for B+TMPg. It can be assumed that the greater presence of fibre agglomerations and porosity led to more diffuse swelling and therefore a less significant curvature in relation to the amount of absorbed water. Greater porosity could additionally hinder stress transfer in the sample and hence shape change [15]. The porosity was calculated based on weight measurements and is given in [Appendix E](#).

Other sources of error might have been the swelling strain measurement and the measurement of h and L of the 3D printed sheet samples. Irregularities in the 3D printing process and in the filament material itself must also be considered. Additionally, the ratio between active and passive layer thickness might have been affected by the printing sequence. The first layers are generally more compressed than the upper layers of a 3D sample, which means that in the $[90_4/0_2]$ layout the active layer might be denser than the in the $[0_4/90_2]$ layout [80]. The curvature is expected to be less prominent for more compressed samples [15].

Concludingly, both models are considered suitable for comparative assessment of the direction and to some extent also intensity of the effect of raster orientation and layer thickness on the curvature. Both models and the measurements indicated similar trends of curvature when comparing the different configurations. However, the models were barely capturing the strong curvature of the bi-material samples. It is

expected that thermal effects contribute to the strong curvature of the bi-material samples. Due to immersion in 60°C temperate water, PLA is heated to its glass transition temperature. During printing, the amorphous structure of PLA transformed into relatively large crystals due to rapid cooling. Heating PLA above its crystallisation temperature and below its glass transition temperature (T_g), after it was processed into a 3D printed, part is called annealing [27,59]. The crystals formed after cooling are not in equilibrium. When PLA is heated to temperatures close to T_g , there is an increase in the mobility of polymeric chains (of the amorphous region) and therefore an increase in viscous behaviour and decrease in elastic behavior [27,96]. The internal stresses induced during fabrication can then be relieved and cause shape changes. Since the water temperature is close to T_g this might cause a difference in theoretical and experimental results. [97,98]. The swelling coefficient, in this case, could have been negative and amplified the effect of the shape change.

Since the bi-material construction resulted in greater deflections, a blooming flower with different raster orientations in the petals was printed for demonstration of the shape morphing effect of different raster orientations. After being immersed in 60°C water for 24 h a raster orientation of 90° of the active layers results in the greatest shape morphing effect, as seen in [Fig. 10 a](#)). The petals bent upwards with a rotational axis longitudinal to the active layer orientation. In [Fig. 10 b](#)) the shape morphing effect is less compared to [Fig. 10 a](#)). A $[90_4/0_2]$ layout only led to minor shape changes. In the case of $[45_4/-45_2]$, a twist in the petals was observed. As expected, the twist formed around an axis longitudinal to the active layer orientation.

These results show the applicability of both biocomposite materials (B+TMPm and B+TMPg) for 4D printing using water as a stimulus. The shape morphing behaviour was highly dependent on the raster orientation and the material combination.

5. Conclusion

In this study biocomposites from PLA, PHA or PBAT and TMP fibres were prepared and evaluated based on mechanical, thermal, and rheological properties. The goal was to optimise a biocomposite formulation suitable for 3D and 4D printing. Two materials were chosen to be processed into 3D printing filament: B+TMPm and B+TMPg. The decision was based on PBAT containing biocomposites showing higher tensile strength, elongation at ultimate strength and MFI than PHA containing formulations. Both chosen biocomposites were well printable. However, B+TMPg turned out to be comparatively brittle and more porous.

Importantly, tensile tests of 3D printed dogbones showed that B+TMPm outperforms B+TMPg concerning tensile strength and elongation. The tensile properties of 3D printed dogbones of B+TMPm are comparable to commercially available wood fibre reinforced PLA filaments.

X- μ CT analysis revealed the presence of greater fibre agglomerations and less aligned fibres along the filament axis in B+TMPg compared to B+TMPm filament. That may have contributed to reduced flow properties of B+TMPg under 3D printing leading to greater printing defects and lower tensile properties.

To demonstrate the applicability of B+TMPg and B+TMPm filaments for 4D printing, water absorption and swelling strains were measured on 3D printed parts. B+TMPg showed greater swelling strains than B+TMPm, especially transverse to the filament axis. This was most probably attributed to the anisotropic swelling behaviour of TMP fibres and that the TMP fibres are oriented longitudinally to the 3D printed strands. Additionally mono- and bi-material parts were 3D printed to demonstrate the design of shape morphing effects. Bi-material samples deformed greatly, while mono-material samples warped just slightly after being immersed in water for 24 h.

Finally, a blooming flower was 3D printed with B+TMPm and PLA in a bi-material construction to investigate the shape morphing effects of different raster orientations simultaneously. Again, the greatest shape

morphing effect was observed transversely to the filament strands (90° active layer orientation).

The biocomposite B+TMPm showed to be well suited for 3D and 4D printing. Concluding, B+TMPm had greater tensile strength, was less brittle and had a higher MFI as B+TMPg and showed reasonable shape morphing effects using water as stimulus.

CRedit authorship contribution statement

Rodríguez-Fabià Sandra: Writing – review & editing, Resources, Investigation, Conceptualization. **Zarna Chiara:** Writing – original draft, Visualization, Validation, Software, Methodology, Investigation, Formal analysis, Data curation, Conceptualization. **Chinga-Carrasco Gary:** Writing – review & editing, Supervision, Resources, Project administration, Methodology, Funding acquisition, Conceptualization. **Echtermeyer Andreas T.:** Writing – review & editing, Supervision, Resources, Funding acquisition, Conceptualization.

Declaration of Competing Interest

The authors declare the following financial interests/personal

relationships which may be considered as potential competing interests: Gary Chinga-Carrasco reports financial support was provided by Research Council of Norway, Grant no. 282310.

Data Availability

Data will be made available on request.

Acknowledgement

The Research Council of Norway and the companies supporting the ALLOC project (Grant no. 282310) are thanked for the funding. Thanks to Joni Tantt and Arttu Miettinen (University of Jyväskylä, Finland) for performing X-μCT analyses included in this work.

Appendix. A: Tensile test results of injection moulded PLA, PLA+PHA, PLA+PBAT and biocomposites

See Fig. A1.

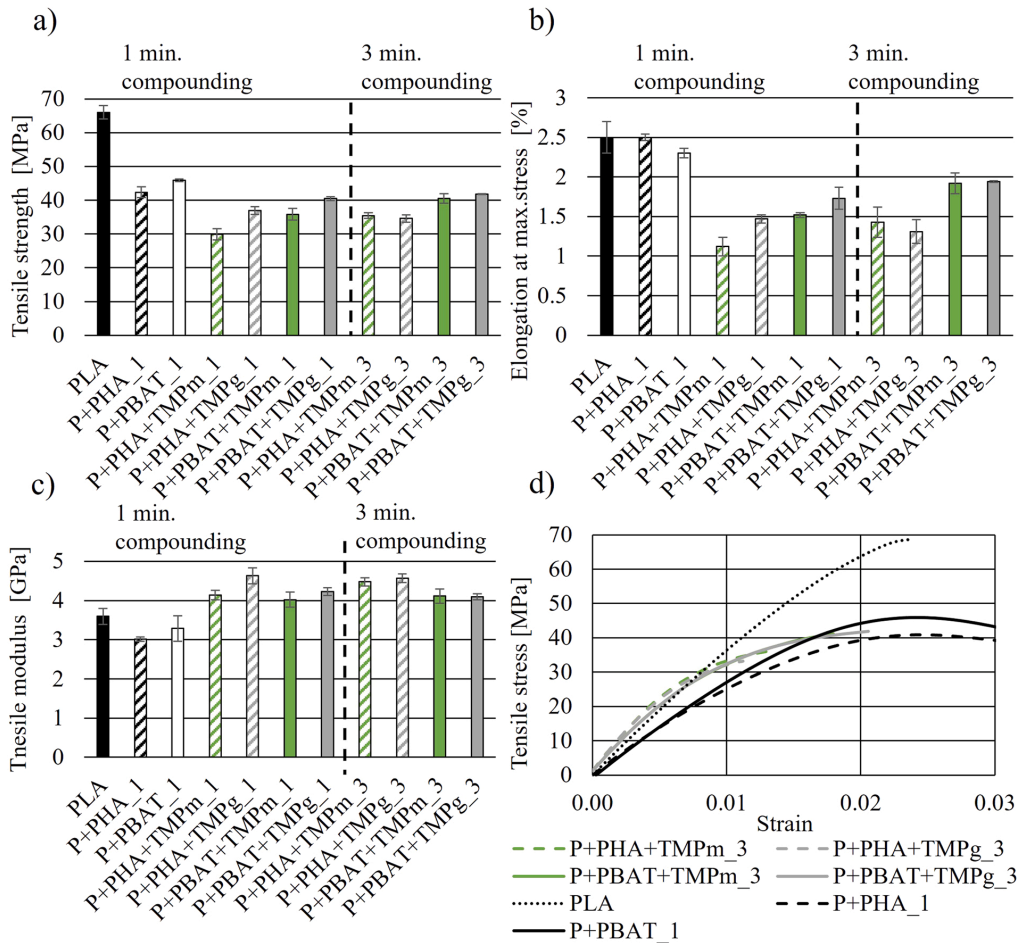


Fig. A1. Tensile properties of injection moulded PLA, PLA+PHA_1, PLA+PBAT_1 and biocomposites. a) Ultimate tensile strength, b) Elongation at ultimate strength, c) Young's modulus, d) Stress-strain graph of biocomposites compounded for 3 min.

Appendix B. : Main effect plots

See Fig. B1.

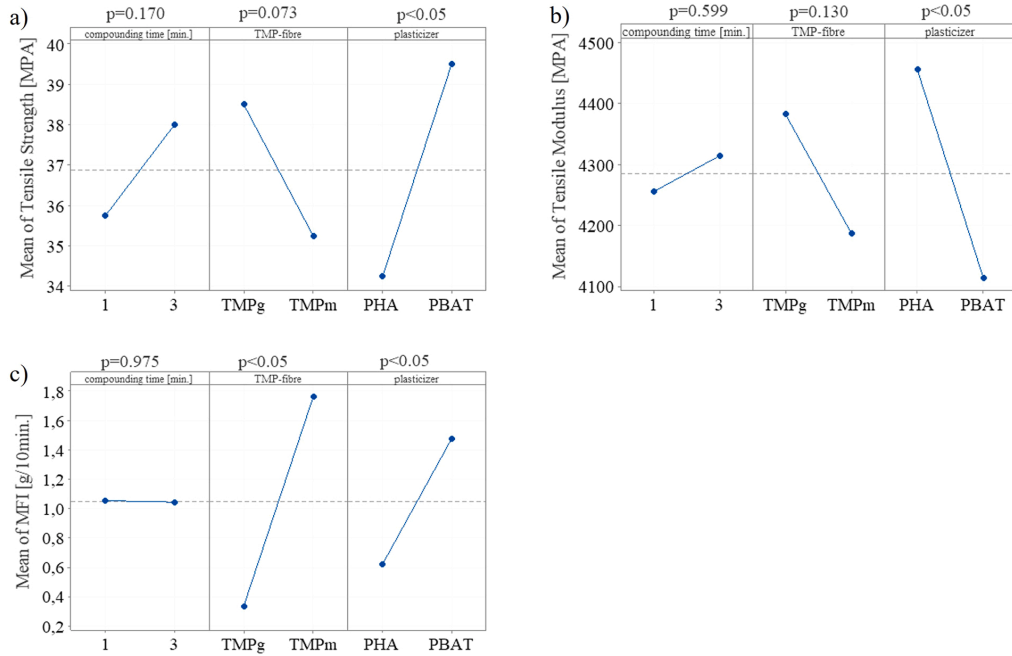


Fig. B1. Main effect plots of a) tensile strength, b) tensile modulus and c) MFI.

Appendix C. : 3D printed biocomposite specimens before and after water immersion

See Fig. C1.

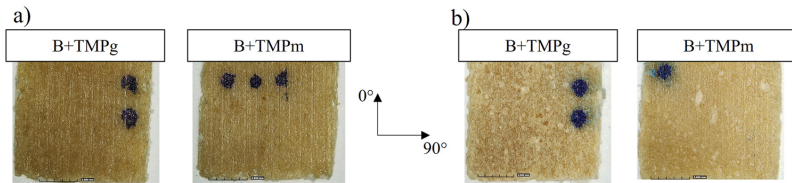


Fig. C1. a) 3D printed squares before water immersion in 20x magnification. b) 3D printed squares after water immersion of 48 h in 20x magnification.

Appendix D. : Warping of 3D printed biocomposite specimens after 24 h in water

See Table D1.

Table D1
Parameters used for the Bi-metal model and laminate theory model.

Material Active/passive	Layup	β_a	β_p	ΔM	E_a [MPa]	E_p [MPa]	t_a [mm]	t_p [mm]
B+TMPm/ B+TMPm	[0 ₄ / 90 ₂]	0.183	0.039	0.092	1937	2562	0.3	0.6
B+TMPm/ B+TMPm	[90 ₄ / 0 ₂]	0.183	0.039	0.102	1937	2562	0.6	0.3
B+TMPm/ PLA	[90 ₄ / 0 ₂]	0.183	0.003 ¹	0.088	1937	2200 ¹	0.6	0.3
B+TMPg/ B+TMPg	[0 ₄ / 90 ₂]	0.249	0.059	0.159	1957	2405	0.3	0.6
B+TMPg/ B+TMPg	[90 ₄ / 0 ₂]	0.249	0.059	0.140	1957	2405	0.6	0.3
B+TMPm/ PLA	[90 ₄ / 0 ₂]	0.249	0.003 ¹	0.120	1957	2200 ¹	0.6	0.3

With:
 β_a : Transverse swelling coefficient (90° raster orientation) obtained from 3D printed square samples
 β_p : Longitudinal swelling coefficient (0° raster orientation) obtained from 3D printed square samples
 ΔM : Difference in water content obtained from weight measurements on the corresponding 3D printed sheet sample.
 E_a : Elastic modulus obtained from tensile tests on 3D printed dogbone specimens with a raster orientation of 90°.
 E_p : Elastic modulus obtained from tensile tests on 3D printed dogbone specimens with a raster orientation of 0°.
 t_a : Theoretical thickness of the active layer according to the slicer software.
 t_p : Theoretical thickness of the passive layer according to the slicer software.
¹: Values for PLA filament as a passive layer were taken from the technical datasheet:
<https://www.prusa3d.com/product/prusament-pla-vanilla-white-1-kg/#/downloads>

Appendix E. : Porosity of 3D printed samples

See Table E1.

Table E1
Porosity of 3D printed biocomposite samples.

Sample type	Material	Layup	Porosity [%]	
Sheet (4D printing)	B+TMPm/ B+TMPm	[0 ₄ / 90 ₂]	16.86 ± 3.08	
	B+TMPm/ B+TMPm	[90 ₄ / 0 ₂]	21.90 ± 1.69	
	B+TMPg/ B+TMPg	[0 ₄ / 90 ₂]	40.06 ± 2.14	
	B+TMPg/ B+TMPg	[90 ₄ / 0 ₂]	38.86 ± 0.18	
	Dogbone (mechanical testing)	B+TMPm	[0]	18.95 ± 4.04
		B+TMPm	[+ 45/ - 45]	11.28 ± 4.76
		B+TMPm	[90]	24.11 ± 2.20
		B+TMPg	[0]	19.86 ± 6.66
	B+TMPg	[+ 45/ - 45]	24.55 ± 7.90	
	B+TMPg	[90]	28.60 ± 2.77	

Porosity was calculated from:

$$Porosity = \left(1 - \frac{\rho_{specimen}}{\rho_{material}}\right) \times 100\% \quad (F.1)$$

With:
 $\rho_{specimen}$: Density of the specimen considering the specimens theoretical volume.

$\rho_{material}$: Density of the material measured on injection moulded dogbones under the assumption of neglectable porosity of the injection

moulded parts compared to the 3D-printed ones.

References

- [1] D. Krapež Tomec, M. Kariž, Use of wood in additive manufacturing: review and future prospects, *Polymers* 14 (6) (2022), <https://doi.org/10.3390/polym14061174>.
- [2] H. Peltola, E. Laatikainen, P. Jetsu, Effects of physical treatment of wood fibres on fibre morphology and biocomposite properties, *Plast., Rubber Compos.* 40 (2) (2011) 86–92, <https://doi.org/10.1179/174328911X12988622801016>.
- [3] B.M. Trinh, E.O. Ogunsona, T.H. Mekonnen, Thin-structured and compostable wood fiber-polymer biocomposites: Fabrication and performance evaluation, *Compos. Part A Appl. Sci. Manuf.* 140 (2021), 106150, <https://doi.org/10.1016/j.compositesa.2020.106150>.
- [4] M. Duhovic, S. Peterson, K. Jayaraman, 9 - Natural-fibre-biodegradable polymer composites for packaging, in: K.L. Pickering (Ed.), *Properties and Performance of Natural-Fibre Composites*, Woodhead Publishing 2008, pp. 301–329.
- [5] H.P.S. Abdul Khalil, Y. Davoudpour, C.K. Saurabh, M.S. Hossain, A.S. Adnan, R. Dungani, M.T. Paridah, M.Z. Islam Sarker, M.R.N. Fazita, M.I. Syakir, M.K. M. Haafiz, A review on nanocellulosic fibres as new material for sustainable packaging: process and applications, *Renewable and Sustainable Energy Reviews* 64 (2016) 823–836, <https://doi.org/10.1016/j.rser.2016.06.072>.
- [6] T. Lindström, C. Aulin, Market and technical challenges and opportunities in the area of innovative new materials and composites based on nanocellulosics, *Scand. J. For. Res.* 29 (4) (2014) 345–351, <https://doi.org/10.1080/02827581.2014.928365>.
- [7] G. Chinga-Carrasco, C. Zarna, S. Rodríguez-Fabià, I. Leirset, M. Tanase-Opedal, D. Molteberg, A. Echtermeyer, L.K. Hindersland, Side streams from flooring laminate production – Characterisation and recycling in biocomposite formulations for injection moulding, *Compos. Part A Appl. Sci. Manuf.* 153 (2022), 106723, <https://doi.org/10.1016/j.compositesa.2021.106723>.
- [8] S.S. Raj, Wood-plastic composite processing and mechanical characteristics—a brief literature review, in: S.K. Natarajan, R. Prakash, K. Sankaranarayananasamy (Eds.), *Recent Advances in Manufacturing, Automation, Design and Energy Technologies*, Springer, Singapore, Singapore, 2022, pp. 269–276.
- [9] J.W. Kaczmar, J. Pach, R. Kozłowski, Use of natural fibres as fillers for polymer composites, *Int. Polym. Sci. Technol.* 34 (6) (2007) 45–50, <https://doi.org/10.1177/0307174X0703400610>.

- [10] C. Chan, L.-J. Vandi, S. Pratt, P. Halley, D. Richardson, A. Werker, B. Laycock, Composites of wood and biodegradable thermoplastics: a review, 00-00, *Polym. Rev.* 58 (2017), <https://doi.org/10.1080/15583724.2017.1380039>.
- [11] M.S. Huda, L.T. Drzal, M. Misra, A.K. Mohanty, Wood-fiber-reinforced poly(lactic acid) composites: Evaluation of the physicomechanical and morphological properties, *J. Appl. Polym. Sci.* 102 (5) (2006) 4856–4869, <https://doi.org/10.1002/app.24829>.
- [12] L.W. Gallagher, A.G. McDonald, The effect of micron sized wood fibers in wood plastic composites, 2013.
- [13] C. Zarna, M.T. Opedal, A.T. Echtermeyer, G. Chinga-Carrasco, Reinforcement ability of lignocellulosic components in biocomposites and their 3D printed applications – A review, *Compos. Part C Open Access* 6 (2021), 100171, <https://doi.org/10.1016/j.jcomc.2021.100171>.
- [14] S. Rodríguez-Fabiá, G. Chinga-Carrasco, Effects of a poly(hydroxyalkanoate) elastomer and kraft pulp fibers on biocomposite properties and three-dimensional (3D) printability of filaments for fused deposition modelling, *J. Biosour. Bioprod.* (2022), <https://doi.org/10.1016/j.jobab.2022.03.002>.
- [15] A. Le Duigou, M. Castro, R. Bevan, N. Martin, 3D printing of wood fibre biocomposites: from mechanical to actuation functionality, *Mater. Des.* 96 (2016) 106–114, <https://doi.org/10.1016/j.matdes.2016.02.018>.
- [16] V. Kumar, R. Sehgal, R. Gupta, Blends and composites of polyhydroxyalkanoates (PHAs) and their applications, *Eur. Polym. J.* 161 (2021), 110824, <https://doi.org/10.1016/j.eurpolymj.2021.110824>.
- [17] N. Ehman, A. Ponce De León, F. Felissia, M. Vallejos, M.C. Area, G. Chinga-Carrasco, Biocomposites of Polyhydroxyalkanoates and Lignocellulosic Components: A Focus on Biodegradation and 3D Printing, in: M. Kuddus, Roohi (Eds.), *Bioplastics for Sustainable Development*, Springer Singapore, Singapore, 2021, pp. 325–345.
- [18] J.V. Ecker, I. Burzic, A. Haider, S. Hild, H. Renhoffer, Improving the impact strength of PLA and its blends with PHA in fused layer modelling, *Polym. Test.* 78 (2019), 105929, <https://doi.org/10.1016/j.polymertesting.2019.105929>.
- [19] V. Gigante, I. Canesi, P. Cinelli, M.B. Coltelli, A. Lazzari, Rubber toughening of polylactic acid (PLA) with poly(butylene adipate-co-terephthalate) (PBAT): mechanical properties, fracture mechanics and analysis of ductile-to-brittle behavior while varying temperature and test speed, *Eur. Polym. J.* 115 (2019) 125–137, <https://doi.org/10.1016/j.eurpolymj.2019.03.015>.
- [20] J. Andrzejewski, J. Cheng, A. Anstey, A.K. Mohanty, M. Misra, Development of toughened blends of poly(lactic acid) and poly(butylene adipate-co-terephthalate) for 3D printing applications: compatibilization methods and material performance evaluation, *ACS Sustain. Chem. Eng.* 8 (17) (2020) 6576–6589, <https://doi.org/10.1021/acsschemeng.9b04925>.
- [21] P. Chaiwutthinan, S. Chuayjittijit, S. Srasomsub, A. Boonmahithisud, Composites of poly(lactic acid)/poly(butylene adipate-co-terephthalate) blend with wood fiber and wollastonite: Physical properties, morphology, and biodegradability, *J. Appl. Polym. Sci.* 136 (21) (2019) 47543, <https://doi.org/10.1002/app.47543>.
- [22] S. Wang, L. Capoen, D.R. D'hooge, L. Cardon, Can the melt flow index be used to predict the success of fused deposition modelling of commercial poly(lactic acid) filaments into 3D printed materials? *Plast., Rubber Compos.* 47 (1) (2018) 9–16, <https://doi.org/10.1080/14658011.2017.1397308>.
- [23] A. Le Duigou, D. Correa, M. Ueda, R. Matsuzaki, M. Castro, A review of 3D and 4D printing of natural fibre biocomposites, *Mater. Des.* 194 (2020), 108911, <https://doi.org/10.1016/j.matdes.2020.108911>.
- [24] M. Kariz, M. Sernek, M. Obućina, M.K. Kuzman, Effect of wood content in FDM filament on properties of 3D printed parts, *Mater. Today Commun.* 14 (2018) 135–140, <https://doi.org/10.1016/j.mtcomm.2017.12.016>.
- [25] S.P. Magalhães da Silva, T. Antunes, M.E.V. Costa, J.M. Oliveira, Cork-like filaments for additive manufacturing, *Addit. Manuf.* 34 (2020), 101229, <https://doi.org/10.1016/j.addma.2020.101229>.
- [26] H.L. Tekinalp, X. Meng, Y. Lu, V. Kunc, L.J. Love, W.H. Peter, S. Ozcan, High modulus biocomposites via additive manufacturing: cellulose nanofibril networks as “microspores”, *Compos. Part B: Eng.* 173 (2019), 106817, <https://doi.org/10.1016/j.compositesb.2019.05.028>.
- [27] J. Dong, M. Li, L. Zhou, S. Lee, C. Mei, X. Xu, Q. Wu, The influence of grafted cellulose nanofibers and postextrusion annealing treatment on selected properties of poly(lactic acid) filaments for 3D printing, *J. Polym. Sci. Part B Polym. Phys.* 55 (11) (2017) 847–855, <https://doi.org/10.1002/polb.24333>.
- [28] M. Tanase-Opedal, E. Espinosa, A. Rodríguez, G. Chinga-Carrasco, Lignin: a biopolymer from forestry biomass for biocomposites and 3D printing, *Materials* 12 (18) (2019), <https://doi.org/10.3390/ma12183006>.
- [29] J.O. Obielodan, K. Vergeniz, D. Agil, J. Wu, L.J.M. Ellistrem, Characterization of PLA/Lignin Biocomposites for 3D Printing, *International Solid Freeform Fabrication Symposium, Texas*, 2019, <https://doi.org/10.26153/tsw/17335>.
- [30] M.E. Lamm, L. Wang, V. Kishore, H. Tekinalp, V. Kunc, J. Wang, D.J. Gardner, S. Ozcan, Material extrusion additive manufacturing of wood and lignocellulosic filled composites, *Polymers* 12 (2020), <https://doi.org/10.3390/polym12092115>.
- [31] A. Le Duigou, A. Barbé, E. Guillou, M. Castro, 3D printing of continuous flax fibre reinforced biocomposites for structural applications, *Mater. Des.* 180 (2019), 107884, <https://doi.org/10.1016/j.matdes.2019.107884>.
- [32] A.R. Torrado, C.M. Shemelya, J.D. English, Y. Lin, R.B. Wicker, D.A. Roberson, Characterizing the effect of additives to ABS on the mechanical property anisotropy of specimens fabricated by material extrusion 3D printing, *Addit. Manuf.* 6 (2015) 16–29, <https://doi.org/10.1016/j.addma.2015.02.001>.
- [33] R. Matsuzaki, M. Ueda, M. Namiki, T.-K. Jeong, H. Asahara, K. Horiguchi, T. Nakamura, A. Todoroki, Y. Hirano, Three-dimensional printing of continuous-fiber composites by in-nozzle impregnation, *Sci. Rep.* 6 (1) (2016) 23058, <https://doi.org/10.1038/srep23058>.
- [34] H. Long, Z. Wu, Q. Dong, Y. Shen, W. Zhou, Y. Luo, C. Zhang, X. Dong, Mechanical and thermal properties of bamboo fiber reinforced polypropylene/poly(lactic acid) composites for 3D printing, *Polym. Eng. Sci.* 59 (s2) (2019) E247–E260, <https://doi.org/10.1002/pen.25043>.
- [35] N. Gama, S. Magina, A. Ferreira, A. Barros-Timmons, Chemically modified bamboo fiber/ABS composites for high-quality additive manufacturing, *Polym. J.* 53 (12) (2021) 1459–1467, <https://doi.org/10.1038/s41428-021-00540-9>.
- [36] D. Stooß, K. Pickering, Sustainable composite fused deposition modelling filament using recycled pre-consumer polypropylene, *Compos. Part B: Eng.* 135 (2018) 110–118, <https://doi.org/10.1016/j.compositesb.2017.10.005>.
- [37] B. Coppola, E. Garofalo, L.D. Maio, P. Scarfato, L. Incarnato, Investigation on the use of PLA/hemp composites for the fused deposition modelling (FDM) 3D printing, *AIP Conf. Proc.* 1981 (1) (2018), 020086, <https://doi.org/10.1063/1.5045948>.
- [38] V. Mazzanti, L. Malagutti, F. Mollica, FDM 3D printing of polymers containing natural fillers: a review of their mechanical properties, *Polymers* 11 (7) (2019), <https://doi.org/10.3390/polym11071094>.
- [39] S. Guessasma, S. Belhabib, H. Nouri, Microstructure and mechanical performance of 3D printed Wood-PLA/PHA using fused deposition modelling: effect of printing temperature, *Polymers* 11 (11) (2019) 1778.
- [40] Y. Dong, J. Milentis, A. Pramanik, Additive manufacturing of mechanical testing samples based on virgin poly(lactic acid) (PLA) and PLA/wood fibre composites, *Adv. Manuf.* 6 (1) (2018) 71–82, <https://doi.org/10.1007/s40436-018-0211-3>.
- [41] J.V. Ecker, A. Haider, I. Burzic, A. Huber, G. Eder, S. Hild, Mechanical properties and water absorption behaviour of PLA and PLA/wood composites prepared by 3D printing and injection moulding, *Rapid Prototyp. J.* 25 (4) (2019) 672–678, <https://doi.org/10.1108/RPJ-06-2018-0149>.
- [42] Y. Tao, H. Wang, Z. Li, P. Li, S.Q. Shi, Development and application of wood flour-filled polylactic acid composite filament for 3D printing, *Materials* 10 (4) (2017) 339, <https://doi.org/10.3390/ma10040339>.
- [43] S. Kain, J.V. Ecker, A. Haider, M. Musso, A. Petutschnigg, Effects of the infill pattern on mechanical properties of fused layer modeling (FLM) 3D printed wood/poly(lactic acid) (PLA) composites, *Eur. J. Wood Wood Prod.* 78 (1) (2020) 65–74, <https://doi.org/10.1007/s00107-019-01473-0>.
- [44] J. Tian, R. Zhang, Y. Wu, P. Xue, Additive manufacturing of wood flour/polyhydroxyalkanoates (PHA) fully bio-based composites based on micro-screw extrusion system, *Mater. Des.* 199 (2021), 109418, <https://doi.org/10.1016/j.matdes.2020.109418>.
- [45] R. Guo, Z. Ren, H. Bi, Y. Song, M. Xu, Effect of toughening agents on the properties of poplar wood flour/poly(lactic acid) composites fabricated with Fused Deposition Modeling, *Eur. Polym. J.* 107 (2018) 34–45, <https://doi.org/10.1016/j.eurpolymj.2018.07.035>.
- [46] R. Wimmer, B. Steyrer, J. Woess, T. Koddenberg, N. Mundigler, 3D Printing and Wood, *International Conference "Wood Science and Engineering in the Third Millennium" - ICWSE, Brasov, Romania*, 2015, <https://doi.org/10.13140/RG.2.1.2483.6563>.
- [47] A. Ghose, G. Chinga-Carrasco, Environmental aspects of Norwegian production of pulp fibres and printing paper, *J. Clean. Prod.* 57 (2013) 293–301, <https://doi.org/10.1016/j.jclepro.2013.06.019>.
- [48] Q. Tarrés, J.K. Melbo, M. Delgado-Aguilar, F.X. Espinach, P. Mutjé, G. Chinga-Carrasco, Bio-polyethylene reinforced with thermomechanical pulp fibers: Mechanical and micromechanical characterization and its application in 3D-printing by fused deposition modelling, *Compos. Part B: Eng.* 153 (2018) 70–77, <https://doi.org/10.1016/j.compositesb.2018.07.009>.
- [49] F. Momeni, S. M. Mehdi Hassani, N. X. Liu, J. Ni, A review of 4D printing, *Mater. Des.* 122 (2017) 42–79, <https://doi.org/10.1016/j.matdes.2017.02.068>.
- [50] D.-G. Shin, T.-H. Kim, D.-E. Kim, Review of 4D printing materials and their properties, *Int. J. Precis. Eng. Manuf. Green Technol.* 4 (3) (2017) 349–357, <https://doi.org/10.1007/s40684-017-0040-z>.
- [51] Y. Jiang, J. Leng, J. Zhang, A high-efficiency way to improve the shape memory property of 4D-printed polyurethane/poly(lactide) composite by forming in situ microfibrils during extrusion-based additive manufacturing, *Addit. Manuf.* 38 (2021), 101718, <https://doi.org/10.1016/j.addma.2020.101718>.
- [52] A. Mitchell, U. Lafont, M. Holyńska, C. Semprinoschnig, Additive manufacturing — A review of 4D printing and future applications, *Addit. Manuf.* 24 (2018) 606–626, <https://doi.org/10.1016/j.addma.2018.10.038>.
- [53] M. Rüggeberg, I. Burgert, Bio-inspired wooden actuators for large scale applications, *PLoS One* 10 (4) (2015), e0120718, <https://doi.org/10.1371/journal.pone.0120718>.
- [54] D. Krapež Tomec, A. Straže, A. Haider, M. Kariz, Hygromorphic response dynamics of 3D-printed wood-PLA composite bilayer actuators, *Polymers* 13 (19) (2021), <https://doi.org/10.3390/polym13193209>.
- [55] E. Reyssat, L. Mahadevan, Hygromorphs: from pine cones to biomimetic bilayers, *J. R. Soc. Interface* 6 (39) (2009) 951–957, <https://doi.org/10.1098/rsif.2009.0184>.
- [56] N.M. Nurazzi, M.R.M. Asyraf, S. Fatimah Athiyah, S.S. Shazleen, S.A. Rafiqah, M. Harussani, S.H. Kamarudin, M.R. Razman, M. Rahmah, E.S. Zainudin, R. A. Ilyas, H.A. Aisyah, M.N.F. Norrahim, N. Abdullah, S.M. Sapuan, A. Khalina, A review on mechanical performance of hybrid natural fiber polymer composites for structural applications, *Polymers* 13 (13) (2021), <https://doi.org/10.3390/polym13132170>.
- [57] X. Arzola-Villegas, R. Lakes, N.Z. Plaza, J.E. Jakes, Wood moisture-induced swelling at the cellular scale—Ab Intra, *Forests* 10 (11) (2019), <https://doi.org/10.3390/f10110996>.

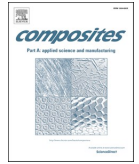
- [58] I. Eriksson, I. Haglund, O. Lidbrandt, L. Sahnén, Fiber swelling favoured by lignin softening, *Wood Sci. Technol.* 25 (2) (1991) 135–144, <https://doi.org/10.1007/BF00226813>.
- [59] A. Orue, J. Anakabe, A.M. Zaldua-Huici, A. Eceiza, A. Arbelaz, The importance of fiber/matrix adhesion and annealing process in water uptake of PLA/PMMA matrix composites reinforced with sisal fibers: the effect of coupling agent addition, *J. Nat. Fibers* (2022) 1–12, <https://doi.org/10.1080/15440478.2022.2028211>.
- [60] H. Ventura, J. Claramunt, M.A. Rodríguez-Pérez, M. Ardanuy, Effects of hydrothermal aging on the water uptake and tensile properties of PHB/flux fabric biocomposites, *Polym. Degrad. Stab.* 142 (2017) 129–138, <https://doi.org/10.1016/j.polydegradstab.2017.06.003>.
- [61] S. Kuciel, K. Mazur, M. Hebda, The influence of wood and basalt fibres on mechanical, thermal and hydrothermal properties of PLA composites, *J. Polym. Environ.* 28 (4) (2020) 1204–1215, <https://doi.org/10.1007/s10924-020-01677-z>.
- [62] Q. Lin, X. Zhou, G. Dai, Effect of hydrothermal environment on moisture absorption and mechanical properties of wood flour-filled polypropylene composites, *J. Appl. Polym. Sci.* 85 (14) (2002) 2824–2832, <https://doi.org/10.1002/app.10844>.
- [63] N. Ayralmis, M. Kariz, J.H. Kwon, M. Kitek Kuzman, Effect of printing layer thickness on water absorption and mechanical properties of 3D-printed wood/PLA composite materials, *Int. J. Adv. Manuf. Technol.* 102 (5) (2019) 2195–2200, <https://doi.org/10.1007/s00170-019-03299-9>.
- [64] Ingeo™ Biopolymer 4043D Technical Data Sheet, 2022. (https://www.natureworksllc.com/~/_/media/Files/NatureWorks/Technical-Documents/Technical-Data-Sheets/TechnicalDataSheet_4043D_3D-monofilament.pdf?la=en).
- [65] X. Meng, N.A. Nguyen, H. Tekinalp, E. Lara-Curzio, S. Ozcan, Supertough PLA-silane nanohybrids by in situ condensation and grafting, *ACS Sustain. Chem. Eng.* 6 (1) (2018) 1289–1298, <https://doi.org/10.1021/acsschemeng.7b03650>.
- [66] Polyhydroxyalkanoate - Biopolymer - Granule, 2022. (<https://www.goodfellow.com/uk/en-gb/displayitemdetails/p/ph32-gl-000101/polyhydroxyalkanoate-biopol-ymcr-granule>).
- [67] C.S.K. Reddy, R. Ghai, Rashmi V.C. Kalita, Polyhydroxyalkanoates: an overview, *Bioresour. Technol.* 87 (2) (2003) 137–146, [https://doi.org/10.1016/S0960-8524\(02\)00212-2](https://doi.org/10.1016/S0960-8524(02)00212-2).
- [68] ecoflex® F Blend C1200, 2013. (https://download.basf.com/p1/8a8082587fd4b608017fd63230bf39c4/en/ecoflex%3Csup%3E%3Csup%3E%3Csup%3E_F_Blen_d.C1200_Product_Data_Sheet_English.pdf?view).
- [69] S. Su, R. Kopitzky, C. Berrenrath, Experimental determination of molecular weight-dependent miscibility of PBAT/PLA blends, *Polymers* 13 (21) (2021), <https://doi.org/10.3390/polym13213686>.
- [70] D. Filgueira, S. Holmen, J.K. Melbo, D. Moldes, A.T. Echtermeyer, G. Chinga-Carrasco, 3D printable filaments made of biobased polyethylene biocomposites, *Polymers* 10 (3) (2018) 314, <https://doi.org/10.3390/polym10030314>.
- [71] A. Miettinen, C.L. Luengo Hendriks, G. Chinga-Carrasco, E.K. Gamstedt, M. Kataja, A non-destructive X-ray microtomography approach for measuring fibre length in short-fibre composites, *Compos. Sci. Technol.* 72 (15) (2012) 1901–1908, <https://doi.org/10.1016/j.compscitech.2012.08.008>.
- [72] L.A. Feldkamp, L.C. Davis, J.W. Kress, Practical cone-beam algorithm, *J. Opt. Soc. Am. A* 1 (6) (1984) 612–619, <https://doi.org/10.1364/JOSAA.1.000612>.
- [73] C. Tomasi, R. Manduchi, Bilateral filtering for gray and color images, Sixth International Conference on Computer Vision (IEEE Cat. No.98CH36271), 1998, pp. 839–846. 10.1109/ICCV.1998.710815.
- [74] N. Otsu, A threshold selection method from gray-level Histograms, *IEEE Trans. Syst. Man, Cybern.* 9 (1) (1979) 62–66, <https://doi.org/10.1109/TSMC.1979.4310076>.
- [75] C.L. Hendriks, Constrained and dimensionality-independent path openings, *IEEE Trans. Image Process* 19 (6) (2010) 1587–1595, <https://doi.org/10.1109/tip.2010.2044959>.
- [76] B. Jahne, *Practical Handbook on Image Processing for Scientific and Technical Applications*, CRC Press, 2004.
- [77] A. Miettinen, A. Ojala, L. Wikström, R. Joffe, B. Madsen, K. Nättinen, M. Kataja, Non-destructive automatic determination of aspect ratio and cross-sectional properties of fibres, *Compos. Part A Appl. Sci. Manuf.* 77 (2015) 188–194, <https://doi.org/10.1016/j.compositesa.2015.07.005>.
- [78] T. Hildebrand, P. Rügsegger, A new method for the model-independent assessment of thickness in three-dimensional images, *J. Microsc.* 185 (1) (1997) 67–75, <https://doi.org/10.1046/j.1365-2818.1997.1340694.x>.
- [79] E. Vazquez, B. Gursoy, J. Duarte, DESIGNING FOR SHAPE CHANGE: A Case study on 3D Printing Composite Materials for Responsive Architectures, 2019.
- [80] A. Le Duigou, T. Fruleux, R. Matsuzaki, G. Chabaud, M. Ueda, M. Castro, 4D printing of continuous flax-fibre based shape-changing hygromorph biocomposites: Towards sustainable metamaterials, *Mater. Des.* 211 (2021), 110158, <https://doi.org/10.1016/j.matdes.2021.110158>.
- [81] P.P. Parlevliet, H.E.N. Bersee, A. Beukers, Residual stresses in thermoplastic composites—A study of the literature—Part II: Experimental techniques, *Compos. Part A Appl. Sci. Manuf.* 38 (3) (2007) 651–665, <https://doi.org/10.1016/j.compositesa.2006.07.002>.
- [82] S. Timoshenko, Analysis of Bi-metal thermostats, *J. Opt. Soc. Am.* 11 (3) (1925) 233–255, <https://doi.org/10.1364/JOSA.11.000233>.
- [83] J. Varna, 15 - Modelling natural-fibre composites, in: K.L. Pickering (Ed.), *Properties and Performance of Natural-Fibre Composites*, Woodhead Publishing, 2008, pp. 503–542.
- [84] J. Whitney, *Structural Analysis Of Laminated Anisotropic Plates*, 2018.
- [85] M.M. Shokrieh, S.M. Kamali Shahri, 6 - Modeling residual stresses in composite materials, in: M.M. Shokrieh (Ed.), *Residual Stresses in Composite Materials*, Second edition., Woodhead Publishing, 2021, pp. 193–213.
- [86] A. Muhr, E.M. Rechberger, A. Salerno, A. Reiterer, M. Schiller, M. Kwiecień, G. Adamus, M. Kowalczyk, K. Strohmeier, S. Schober, M. Mittelbach, M. Koller, Biodegradable latexes from animal-derived waste: biosynthesis and characterization of mcl-PHA accumulated by *Ps. citronellolis*, *React. Funct. Polym.* 73 (10) (2013) 1391–1398, <https://doi.org/10.1016/j.reactfunctpolym.2012.12.009>.
- [87] Y. Fu, G. Wu, X. Bian, J. Zeng, Y. Weng, Biodegradation behavior of poly(Butylene Adipate-Co-Terephthalate) (PBAT), poly(Lactic Acid) (PLA), and their blend in freshwater with sediment, *Molecules* 25 (17) (2020), <https://doi.org/10.3390/molecules25173946>.
- [88] H. Jeske, A. Schirp, F. Cornelius, Development of a thermogravimetric analysis (TGA) method for quantitative analysis of wood flour and polypropylene in wood plastic composites (WPC), *Thermochim. Acta* 543 (2012) 165–171, <https://doi.org/10.1016/j.tca.2012.05.016>.
- [89] H. Yang, R. Yan, H. Chen, D.H. Lee, C. Zheng, Characteristics of hemicellulose, cellulose and lignin pyrolysis, *Fuel* 86 (12) (2007) 1781–1788, <https://doi.org/10.1016/j.fuel.2006.12.013>.
- [90] A. Tejado, C. Peña, J. Labidi, J.M. Echeverria, I. Mondragon, Physico-chemical characterization of lignins from different sources for use in phenol-formaldehyde resin synthesis, *Bioresour. Technol.* 98 (8) (2007) 1655–1663, <https://doi.org/10.1016/j.biortech.2006.05.042>.
- [91] V. Taubner, R. Shishoo, Influence of processing parameters on the degradation of poly(L-lactide) during extrusion, *J. Appl. Polym. Sci.* 79 (12) (2001) 2128–2135, [https://doi.org/10.1002/1097-4628\(20010321\)79:12](https://doi.org/10.1002/1097-4628(20010321)79:12).
- [92] A.F. Rojas-Gonzalez, J.L. Carrero-Mantilla, Thermal degradation kinetic of polylactic acid in multiple extrusions, *Ingeniería y Universidad* 19(1) (2015) 189–206. <https://doi.org/10.11144/Javeriana.iyu19-1.tdkp>.
- [93] M. Lay, N.L.N. Thajudin, Z.A.A. Hamid, A. Rusli, M.K. Abdullah, R.K. Shuib, Comparison of physical and mechanical properties of PLA, ABS and nylon 6 fabricated using fused deposition modeling and injection molding, *Compos. Part B Eng.* 176 (2019), 107341, <https://doi.org/10.1016/j.compositesb.2019.107341>.
- [94] L. Wang, W.M. Gramlich, D.J. Gardner, Improving the impact strength of Poly (lactic acid) (PLA) in fused layer modeling (FLM), *Polymer* 114 (2017) 242–248, <https://doi.org/10.1016/j.polymer.2017.03.011>.
- [95] H. Gonabadi, Y. Chen, A. Yadav, S. Bull, Investigation of the effect of raster angle, build orientation, and infill density on the elastic response of 3D printed parts using finite element microstructural modeling and homogenization techniques, *Int. J. Adv. Manuf. Technol.* 118 (5) (2022) 1485–1510, <https://doi.org/10.1007/s00170-021-07940-4>.
- [96] J. Dong, C. Mei, J. Han, S. Lee, Q. Wu, 3D printed poly(lactic acid) composites with grafted cellulose nanofibers: Effect of nanofiber and post-fabrication annealing treatment on composite flexural properties, *Addit. Manuf.* 28 (2019) 621–628, <https://doi.org/10.1016/j.addma.2019.06.004>.
- [97] S. Singh, A. Rajeshkannan, S. Feroz, A.K. Jeevanantham, Effect of normalizing on the tensile strength, shrinkage and surface roughness of PLA plastic, *Mater. Today Proc.* 24 (2020) 1174–1182, <https://doi.org/10.1016/j.matpr.2020.04.431>.
- [98] B. Wijnen, P. Sanders, J.M. Pearce, Improved model and experimental validation of deformation in fused filament fabrication of polylactic acid, *Prog. Addit. Manuf.* 3 (4) (2018) 193–203, <https://doi.org/10.1007/s40964-018-0052-4>.

A. IV Publication IV

Bending properties and numerical modelling of cellular panels manufactured from wood fibre/PLA biocomposite by 3D printing







Bending properties and numerical modelling of cellular panels manufactured from wood fibre/PLA biocomposite by 3D printing

Chiara Zarna^{a,*}, Gary Chinga-Carrasco^b, Andreas T. Echtermeyer^a

^a Department of Mechanical and Industrial Engineering, NTNU, Richard Birkelandsvei 2B, 7491 Trondheim, Norway

^b RISE PFI, Høgskoleringen 6b, 7491 Trondheim, Norway

ARTICLE INFO

Keywords:

Biocomposites
3-D printing
Sandwich structures
Finite element analysis (FEA)

ABSTRACT

The major advantage of cellular structures is the saving of material, energy, cost, and weight. Biocomposites are strong, lightweight materials and offer a high degree of design freedom. The purpose of this study was to characterise and compare the bending properties of various cellular structures for utilisation in panels made of a wood fibre/PLA biocomposite. Material extrusion (MEX) 3D printing is a highly flexible manufacturing method and well-suited for prototyping. Hence, MEX was applied to manufacture five different cell configurations that were mechanically tested. Additionally, numerical simulations were carried out to present a tool for optimising the structures for future requirements. Two material modelling approaches, a hyperelastic and a linear elastic, bimodular model were created and validated based on 3-point-bending tests. It is shown that a linear elastic, bimodular and perfectly plastic material model can adequately capture the elastic/plastic bending behaviour of the corresponding 3D-printed sandwich panels.

1. Introduction

1.1. Wood fibre-reinforced biocomposites for 3D printing

Wood fibres as reinforcement of thermoplastic biopolymers are considered as having potential for many products, such as furniture and car components [1–4]. Wood fibre-reinforced biocomposites are mainly manufactured by injection moulding, extrusion, and 3D printing [5–7]. Wood fibres, primarily thermomechanical pulp fibres (TMP), have been successfully used as reinforcement of biobased thermoplastics, such as PLA and bio-polyethylene [8–11]. Additionally, recycled wood particles were compounded with PLA, but are considered fillers rather than reinforcement [12–14]. Window frames, deckings and sidings are commercially available products, that are partially made of recycled wood fibre composites [15]. Lightweight cellular panels from wood fibre-reinforced thermoplastic were also manufactured by 3D printing. A biocomposite from PLA and wood fibres is mostly considered a model material due to PLA's moisture sensitivity. One potential industrial application could be floor or wall coverings. LX Hausys produces floor and wall coverings based on PLA composites with the tradename ZEA-Maru [16].

Material extrusion (MEX) 3D printing (ISO/ASTM 52900) is a

resource-saving production method, most suitable for prototyping. This is due to the high degree of flexibility in terms of the part design and the printing materials [17,18]. Filaments for 3D printing, filled with wood particles were used to save resources and reinforce neat polymers [17,19–28].

Voids in 3D-printed parts are usually formed between the deposited filament strands during the printing process. Such voids are one of the main reasons for the comparatively low tensile strength of 3D-printed parts and contribute to their anisotropy [29,30]. Wood fibre fillings in filaments may contribute to void formations [23,31]. However, Filgueira et al. and Tarres et al. [8,19,20] showed that TMP fibres can facilitate the deposition of strands during printing and lead to a more stable 3D-printed structure. Commercially available biocomposite filaments usually contain 10 wt% to 40 wt% fibre loading. Higher fibre contents may increase the risk of nozzle blockage, void formations, and fracture during printing due to a rougher filament surface and a higher brittleness of the filament [23,28,32].

1.2. Cellular structures

Cellular structures are often inspired by nature. Honeycomb cells are the most widely used ones and provide maximum cell space using

* Corresponding author.

E-mail address: chiara.zarna@ntnu.no (C. Zarna).

<https://doi.org/10.1016/j.compositesa.2022.107368>

Received 27 September 2022; Received in revised form 29 November 2022; Accepted 4 December 2022

Available online 8 December 2022

1359-835X/© 2022 The Author(s). Published by Elsevier Ltd. This is an open access article under the CC BY license (<http://creativecommons.org/licenses/by/4.0/>).

minimal material [33]. They are particularly strong and stiff when loaded in the out-of-plane direction since the cell walls support each other and prevent themselves from buckling. The out-of-plane compressive and shear strengths are highly dependent on the relative density of the honeycomb [34], as well as the material used to construct the cells [35].

Honeycomb and other cellular structures are commercially available in many different material types, e.g., paper, metal, ceramic, plastics, and composites and are present in a wide range of applications, including transportation, architecture, construction, chemical, mechanical and environmental engineering, biotechnology and medicine [35–37].

The in-plane properties [38] of a cellular structure are additionally dependent on the geometric cell type [35,39,40]. Besides the hexagonal honeycomb, common cellular shapes appear as triangular, square, or circular [35,39]. These structures are commonly orientated vertically to the skin sheets.

To investigate and compare different structure types, the relative density ρ_{rel} is a crucial parameter. Relative density is the ratio of the density of a structured or porous material and the corresponding solid

material density [39]. It can be calculated considering geometric unit cells. The area of the struts is then divided by the full cell area (Fig. 1) [35,41]. The relative density has a high impact on the bending properties of structured panels. Araújo et al. [39] demonstrated that a lower relative density ($\rho_{rel, low} = 0.25$ compared to $\rho_{rel, high} = 0.6$) can result in lower flexural strength, but higher flexural stiffness for in-plane cellular structures.

An overview of common cellular structures, which were investigated in the present study, is shown in Fig. 1. The equation to calculate ρ_{rel} is given for every structure.

1.3. Modelling of biocomposites

Computational modelling is, among others, a useful tool for product optimisation. Finite element analysis (FE-analysis) can be used to simulate experiments virtually by using a numerical method. Recent research on FE-analysis, applied to natural fibre composites, can be found in [42–44]. The reinforcing ability of short fibres in a thermoplastic matrix is highly dependent on the fibre volume fraction, the fibre's length-to-diameter-ratio (fibre aspect ratio), the fibre dispersion,

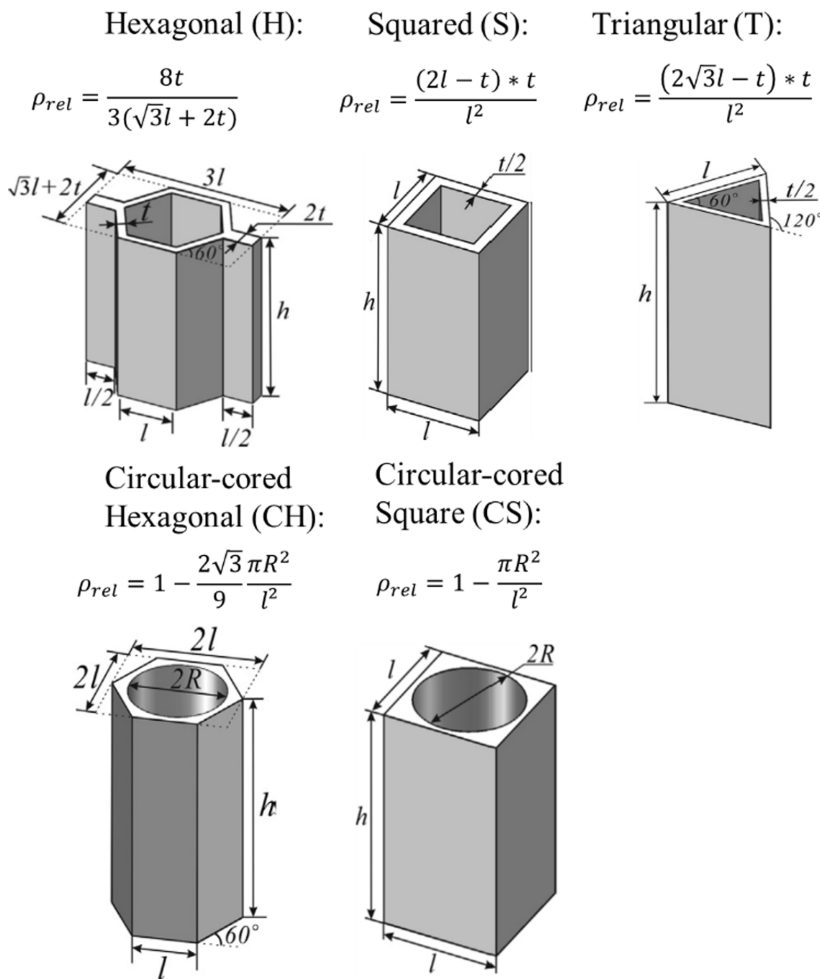


Fig. 1. Potential unit cell shapes for sandwich structures and their relative density. Reprinted and modified with permission from [35, P. 337].

fibre alignment and the fibre–matrix surface interaction. Short-fibre reinforced biocomposites can be considered isotropic when the fibre aspect ratio is below the critical load transfer length, the fibres are evenly distributed in the matrix and the fibre orientation is completely random [45–47]. In this case, the fibres can be regarded as filler material. In 3D printing, most of the wood fibres are probably oriented along the strand deposition direction [48,49]. Additionally, formations of ordered and disordered crystalline forms might occur depending on the cooling rate when depositing the biocomposite material, e.g., low cooling rates yield a higher degree of crystallinity in semicrystalline thermoplastics such as PLA. The polymer chains most likely orientate along the deposition direction. The fibre and polymer chain orientation might enhance the anisotropy of the 3D-printed part. Annealing of the 3D-printed part can be done to overcome this effect [50].

1.4. Purpose of the study

To address rising environmental concerns, especially when it comes to fossil-based raw materials, biocomposites offer potential as a more environmentally friendly alternative compared to conventional composite materials [51–54]. Monteiro et al. [55] stated that the biggest challenges in manufacturing wood fibre composite panels are the reduction of mechanical performance due to reduced relative density, the difficulties in lamination, and low machinability.

The purpose of this study is to explore the potential of 3D-printed biocomposite panels and provide a suitable FE-analysis model for such parts, to be able to optimise the designs of structures more efficiently. The motivation to use 3D printing as a manufacturing method for the presented panels was to limit the manufacturing process to only one single step and material. The use of only one type of material is meant to contribute to the potential recyclability of such panels. In 3D printing, the design could be customised and modified relatively quickly. Therefore, 3D printing might be suitable for design evaluations in the early development stages of such panels. Regarding mass production, extrusion and fusion bonding is considered to be a suitable solution to manufacture sandwich panels in a more efficient way. Using these processes would change the material properties of the here presented 3D-printed panels, but the principles of the structural behaviour of sandwich structures would remain the same.

2. Materials and methods

2.1. Wood fibre-reinforced biocomposite

Recycled pine wood (15 wt%) filled PLA/PHA filament was used to 3D-print all samples presented in this study. The filament is commercially available as woodFill® from Colorfabb BV (Belfeld, The Netherlands). Some material data of woodFill® are presented in Table 1.

The filament material was delivered and stored in vacuum-sealed bags and printing and testing of the specimens were performed within 4 weeks in a dry environment (~30% relative humidity, ~20 °C). Thus, the moisture content of the specimens was considered to be below 1% [56]. The effect on the material strength and stiffness due to ageing was considered to be low and negligible [57,58].

2.2. Test specimen manufacturing

Dogbone, compression and 3-point-bending samples were manufactured with a Prusa i3 MK3 from Prusa research a.s. (Prague, Czech

Republic) with a parameter setup according to Table 2. In this study, no annealing treatment was performed since the focus was placed on a comparative assessment of the different sandwich configurations. The samples were printed under the same environmental conditions and always the same printing parameters. The degree of crystallinity is therefore considered to be similar in all samples. Note, that the dog bone specimens for the tensile test were printed with a 0.4 mm nozzle and the sandwich panels for the 3-point-bending test, as well as compression test specimens, with a 0.6 mm nozzle. The 0.6 mm nozzle was chosen because of nozzle blockage with the 0.4 mm nozzle when printing the relatively large and complex sandwich panels. A [+45/-45] lay-up was chosen because it was shown to yield slightly better printing quality due to a denser packing of the deposited filament strands and reduced anisotropy compared to a [0/90] lay-up [59–62].

The dog bone specimens were printed according to the dimensions of ISO 20753:2018, type A1. The sandwich panels for 3-point-bending tests had dimensions of $50 \times 210 \times 8 \text{ mm}^3$ ($w \times l \times t$), according to EN 310. The skin sheets of the sandwich panels were 1 mm thick each, and the thickness of the core was 6 mm accordingly. To allow the comparability of the structures, all panels were designed to meet a relative density of $\rho_{\text{rel, panel}} = 0.5$. This means, that a biocomposite sandwich panel ($\rho_{\text{rel, panel}} = 0.5$) had half the material volume of a solid panel with the same outer dimensions. The relative density can be calculated by dividing the part density by the material density.

To calculate the relative density of the structures the equations shown in Fig. 1 were used. Note, that the equations in Fig. 1 do not include the skin sheets. Taking an upper and lower skin sheet of 1 mm thickness into account, the relative density of the structured part must be $\rho_{\text{rel, structure}} = 0.33$ to achieve an overall relative panel density of $\rho_{\text{rel, panel}} = 0.5$. The dimensional configurations are presented in Table 3.

Since the structure configurations were based on geometrical considerations, the relative density of the actual specimens was measured and calculated after printing the panels. The average weight of each panel type was measured and divided by the volume of its outer dimensions to calculate the specimen density ρ_{specimen} . The material density ρ_{material} was calculated by dividing the average mass of each specimen type by the volume of the actual panel specimen. The relative panel density can then be calculated by $\rho_{\text{rel, panel}} = \frac{\rho_{\text{specimen}}}{\rho_{\text{material}}}$. Details about the calculations of the relative panel density is provided in the appendix.

2.3. Tensile tests of 3D-printed biocomposite

Ten 3D-printed biocomposite dogbone specimens were tensile tested on an MTS Series 809 Test System (Eden Prairie, MN, United States) with a maximum axial force of 50 kN. The specimens were printed with a raster angle of $\pm 45^\circ$ and following Table 2. The test procedure was following ISO 527–2:2012. The tensile tests were operated with a test speed of 1 mm/min. A dynamic axial clip-on extensometer from Instron with a gauge length of 50 mm was used for axial displacement measurements and strain calculations. Additionally, strain gauges of the type FCA-6–11-3L from TML with a gauge length of 5 mm were used to measure transverse strain and calculate the Poisson's ratio.

2.4. Compression tests of 3D-printed biocomposite

3D-printed biocomposite specimens were tested according to ISO 604:2002 on an MTS Series 809 Test System (Eden Prairie, MN, United States) with a maximum axial force of 50 kN. The specimens had a cylindrical shape with a diameter of 10 mm and a height of $L_m = 50 \text{ mm}$

Table 1
Data for tensile and bending properties of Colorfabb woodFill®.

Product	Tensile strength [MPa]	Tensile stiffness [MPa]	Modulus of rupture [MPa]	Modulus of elasticity [MPa]	Density [kg/m ³]
Colorfabb Woodfill®	46	3290	70	3930	1150

Table 2
Printing set-up for manufacturing dog bone and 3-point-bending specimens from Colorfabb woodFill® filament.

Nozzle diameter	Layup	Infill	Layer height	Extrusion width	Extrusion speed	Extrusion temperature	Bed temperature
0.4/0.6 mm	$\pm 45^\circ$	100 %	0.15 mm	0.65 mm	50 mm/s	200 °C	60 °C

Table 3
Structure configurations of the investigated biocomposite panels for a desired relative density of 0.5.

Specimen code	Wall thickness t [mm]	Side length l [mm]	Radius R [mm]	Actual relative panel density
Hexagonal (H)	1	5.21		0.51
Squared (S)	1	9.02		0.49
Triangular (T)	1	15.60		0.50
Circular-cored hexagonal (CH)	1	8.20	6.10	0.50
Circular-cored squared (CS)	1	26.00	12.00	0.50

and $L_s = 10$ mm, respectively. Eight specimens, with $L_m = 50$ mm, were used to determine compressive elastic modulus and five specimens, with $L_s = 10$ mm, were used to determine compressive strength. The compression tests were operated with a test speed of 1 mm/min. A dynamic axial extensometer (MTS 632.29F-30) with a gauge length of 5 mm was used for axial displacement measurements and strain calculations. Additionally, strain gauges of the type FCAB-5-11-3LJB-F from TML (Tokyo, Japan) with a gauge length of 5 mm were used to measure transverse strain. As seen in Fig. 2a, sandpaper was placed between the sample and compression plate surfaces to prevent slipping.

2.5. 3-point-bending tests of 3D-printed honeycomb structures

For each structure type (Fig. 1), three biocomposite panels were 3D printed (Fig. 3a) and 3-point-bending tests were conducted on an AMETEK CS2-225 (Berwyn, Pennsylvania, United States) test machine with a maximum axial force of 889 N. The test speed was 10 mm/min and the gauge length was 180 mm. The supports had a diameter of 5 mm and the punch 10 mm. The flexural strength and stiffness were calculated according to EN 310.

To 3D print the panel specimens in Fig. 3 the filament was following a perimeter path. The perimeter frame was then filled with a $\pm 45^\circ$ raster orientation. For the structure pattern, the filament was again placed as an external and internal perimeter (three parallel filament strands). The patterns CS and CH required an additional infill with $\pm 45^\circ$

raster orientation to fill the gaps between the structure perimeters (Fig. 3b). To print the upper surface sheet, one layer of bridge infill with a unidirectional 0° raster orientation was placed.

2.6. Modelling and simulations

FE analysis was carried out in Abaqus/Standard 2017 from Dassault Systèmes (Vélizy-Villacoublay, France). All sample geometries were modelled as a solid and 3D deformable part and meshed with a CD3D8R-element with a global size of 0.67 mm for the structure and 2 mm for the skin sheets. No mesh convergence analysis was performed but it was ensured to use at least three elements over the cell wall and skin sheet thickness. The mesh was considered to be sufficient based on previous modelling experience of traditional composites and no global stress concentrations were present. An implicit analysis was performed, based on an isotropic, linear elastic, perfectly plastic and bimodular material model. In this case, bimodular means an asymmetry in the compression and tension behaviour of the material. Since the specimens to determine material properties for the numerical model are printed in an $[45/-45]$ layup, the here presented isotropic model is limited to loading conditions only along the axis to which the 3D-printed strands are oriented in $\pm 45^\circ$. Applying loads along other directions might yield less accurate results due to the anisotropy of the material. In the present study, the focus is placed on the different material behaviour in tension and compression and how this affects the flexural stiffness and strength of 3D-printed biocomposite sandwich panels. The material properties, used to simulate 3-point-bending tests are presented in Table 4. The values were fitted based on tensile and compression tests (Fig. 5 and Fig. 6).

To implement the two different moduli for tension and compression in Abaqus 2017 the field variable function together with a user subroutine (UMAT) was used. The UMAT is used to switch the field variable depending on the hydrostatic strain output of every increment. For negative hydrostatic strains, the field variable $FV = 0$ is applied and refers to E_C and σ_C (compression mode). For positive hydrostatic strains, the field variable $FV = 1$ is applied and refers to E_T and σ_T (tension mode).

Additionally, a hyper-elastic (Marlow Model) and perfectly plastic material model, fitted on tensile test data only, was applied. Both models were validated based on 3-point-bending tests and compared to each

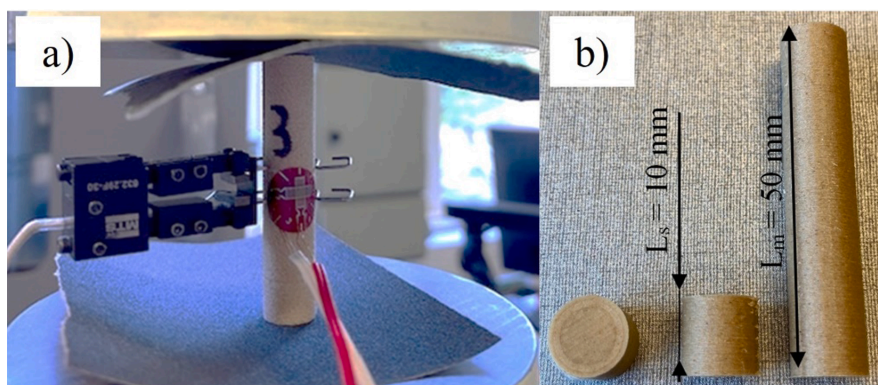


Fig. 2. (a) Experimental setup of compression tests and (b) compression test specimens for measuring compressive strength ($L_s = 10$ mm) and determining compressive modulus ($L_m = 50$ mm).

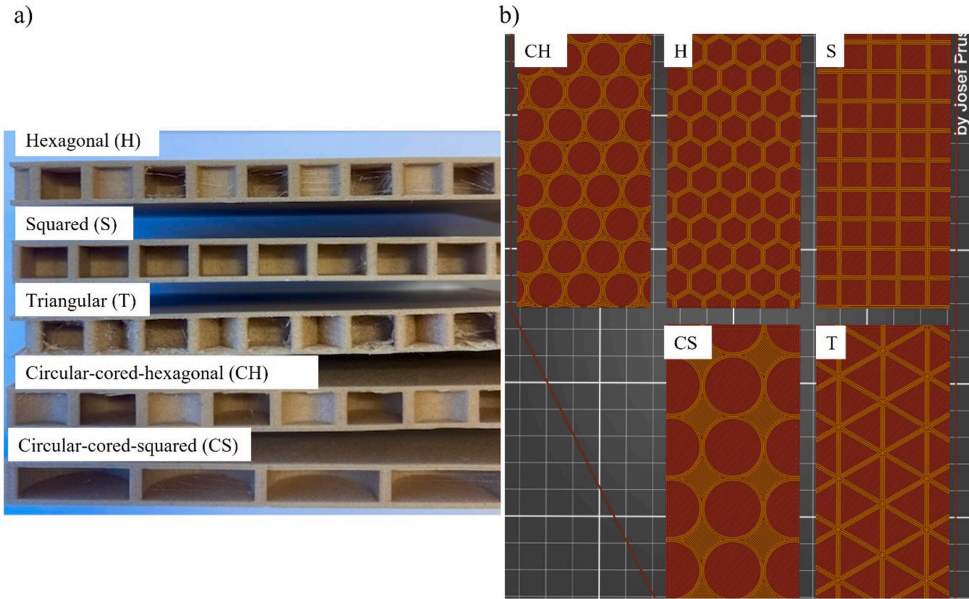


Fig. 3. 3D-printed 3-point-bending specimens (a) printed from wood fibre-reinforced PLA and (b) 3D-slicer preview for each structure panel at an out-of-plane printing height of 6.20 mm.

Table 4

Input data for the material models used in this study.

Material model input variable	Values
Density, ρ	1,15 g/cm ³
Young's modulus in tension, E_T	2500 MPa
Young's modulus in compression, E_C	1800 MPa
Poisson's ratio, ν	0.35
Yield stress in tension σ_T	28.4 MPa
Yield stress in compression σ_C	26.5 MPa

other.

3. Results and discussion

3.1. Tensile tests of 3D printed wood fibre-reinforced PLA

The tensile-tested dogbone specimens are shown in Fig. 4. As seen in Fig. 4a, brittle fracture occurred, and transverse matrix cracks were visible. The crack formation was partially visible along the printing

raster orientation ($\pm 45^\circ$) but failure did not occur at the fusion bond between the layers as it usually does in 3D-printed samples from neat PLA [63]. This emphasises that the interlayer adhesion was sufficiently strong and that the wood fibre particles might have acted as stress concentrations and initiated crack formations. It was assumed that local defects due to the wood fibre filling were more prone to failure than the fusion bond between the layers.

In Fig. 5a, the force–displacement curves, obtained from tensile tests are shown. The sudden drop in force at a displacement of 17 mm, was related to stress relaxation during the extensometer removal. To detach the extensometer from the specimen, the strain was held constant for the removal time. A decrease in stress under constant strain is a typical phenomenon for polymer materials and is related to viscoelasticity. Fig. 5b shows the corresponding stress–strain curves.

The average tensile strength from the experiment was $\sigma_{T,e} = (28.4 \pm 1.0)$ MPa. Tensile strength was taken as the maximum stress from the stress–strain curves in Fig. 5b. An average Young's modulus of $E_{T,e} = (2899 \pm 121)$ MPa and an average Poisson's ratio of $\nu_{T,e} = 0.35 \pm 0.06$ were calculated. All calculations were carried out according to ISO 527–2:2012.

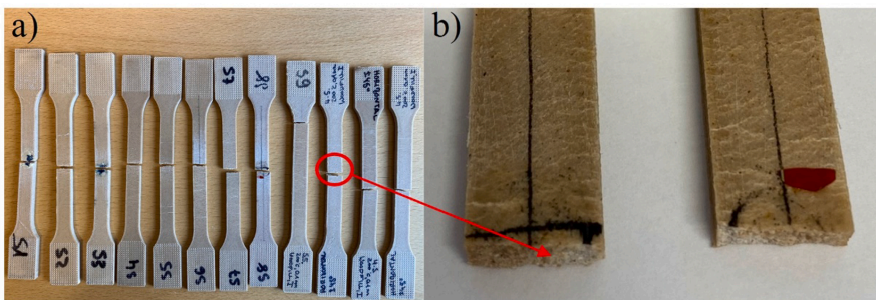


Fig. 4. (a) Biocomposite dogbone specimens after tensile testing and (b) fracture surface showing brittle fracture.

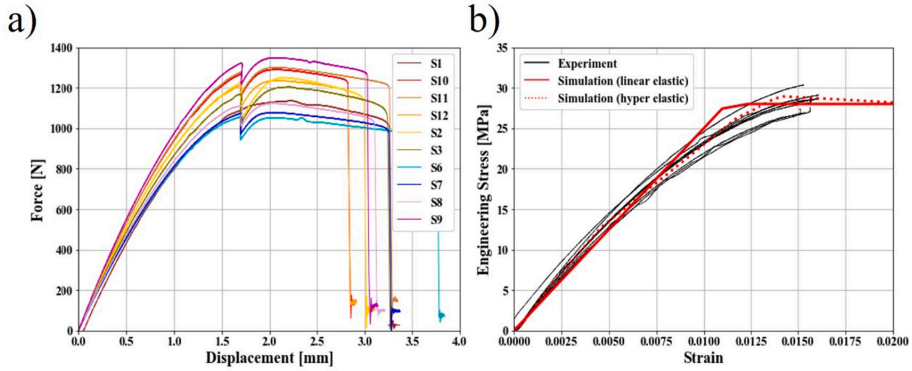


Fig. 5. Results from tensile tests of biocomposite dogbone specimens. a) Force-displacement curves and b) stress-strain curves and simulations of the corresponding tensile test.

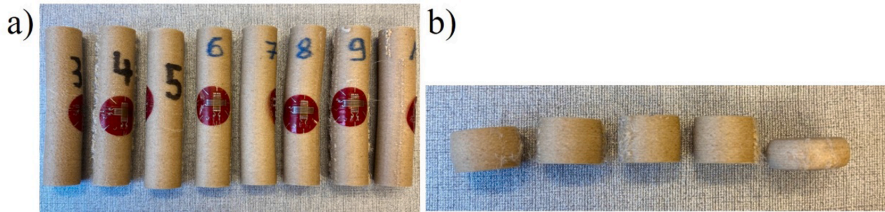


Fig. 6. Compression-tested specimens a) with $L_m = 50$ mm for estimating the compression modulus and b) with $L_s = 10$ mm for measuring the compressive strength.

The red, solid, and dotted curves show the numerical simulations performed in Abaqus 2017. The linear elastic material model (illustrated as the red, solid curve in Fig. 5) was fitted to the physical tests by adjusting Young’s modulus and the tensile yield strength to E_T and σ_T (Table 4). A hyperelastic material model, in this case, the Marlow-Model, was additionally created to describe the elastic tensile properties of the 3D printed biocomposite material more accurately. The hyperelastic model was built based on the stress–strain data of sample S3 since it represented a reasonable average of all stress–strain data. According to [64,65] the Marlow-Model is well applicable to semi-crystalline thermoplastic polymer materials.

3.2. Compression tests of 3D-printed wood fibre-reinforced PLA

Specimens of the length L_s (Fig. 6b) were used to measure

compressive strength and were compressed to different levels of deformation. Lateral bulging was selected as the failure criterion for the material’s compressive strength.

The compression-tested specimens are shown in Fig. 6. The samples with the length L_m were only used to extract information about the elastic material behaviour. As the buckling of the samples became noticeable, the compression test was stopped. The specimens with the length.

In Fig. 7a the corresponding stress–strain curves are shown. Here, only the elastic section of the stress–strain curves was of interest. As Pastor-Artigues et al. [66] already showed, an increase in strength can be seen as plastic deformation occurs. This is because of the reduction of voids and increase of material density under compression.

The average compressive modulus from the experiment was estimated (based on ISO 604:2002) to be $E_{c,e} = (2011 \pm 294)$ MPa. The

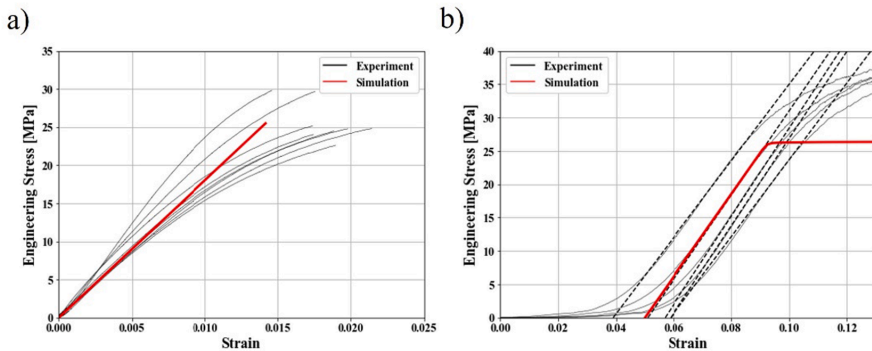


Fig. 7. Results of compression tests of 3D-printed biocomposite specimens with a) a length of $L_m = 50$ mm and b) $L_s = 10$ mm.

compressive strength was read from the stress–strain curves in Fig. 7b, which were obtained by compressing the short cylinder specimens shown in Fig. 6 (right). As illustrated by the black, dashed lines the compressive strength was read at a point where the stress–strain-slope declines and becomes significantly non-linear. The average compressive strength from the experiment was $\sigma_{C,e} = (27.9 \pm 1.2)$ MPa.

The red curves in Fig. 7a and b show the stress–strain curves obtained by simulating the compression tests in Abaqus 2017. An isotropic, linear elastic and perfectly plastic material model was used. The curves were fitted by adjusting Young's modulus and the compressive yield strength to E_C and σ_C (Table 4).

3.3. 3-point-bending tests of 3D printed sandwich structures

Some fracture surfaces of selected 3-point-bended specimens are shown in Fig. 8. Regarding the 3D-printed biocomposite specimens, the crack propagated through short, irregular zig-zag paths with some openings between the stacked layer strands. This is typical for 3D printed materials with a horizontal $\pm 45^\circ$ build-up [59,63]. Additionally, the upper and lower sandwich sheets seemed to slightly peel off under bending and formed a crack pattern according to the structure (Fig. 8a-c). It was previously observed that in 3D-printed parts the crack growth planes delaminate under bending loads [62]. Especially the squared specimens (S) showed a quite even crack surface, leading to the assumption that the interlayer adhesion was sufficient and the printing parameter, chosen to manufacture the specimens, was suitable for this material.

In Fig. 9, the force–displacement curves of all 3-point-bending tested specimens are shown. Comparing the five different biocomposite panel types, the H and triangular T structures were less stiff than the other ones. Regarding the flexural strength, the CS structure was the weakest one, probably due to the less homogeneous material distribution, caused by the specific CS pattern. CH showed the highest average flexural strength and stiffness.

However, all structure types with an out-of-plane orientated pattern, yield quite similar results of flexural stiffness and strength (Table 5). Flexural stiffness and strength were measured and calculated according to EN 310.

3.4. Numerical simulations of different cellular structured panels

Numerical simulations of 3-point-bending tests were performed for all structured biocomposite panels, presented in this study. Both material models hyperelastic and bimodular linear elastic were applied and

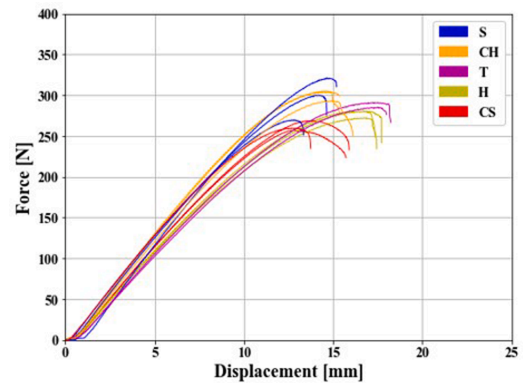


Fig. 9. Results of 3-point-bending tests of different cellular structures, 3D-printed from a biocomposite filament.

Table 5

Average values for flexural modulus and strength for the different structured biocomposite panels tested in this study.

Sample designation	Average flexural modulus E_m [MPa]	Average flexural strength f_m [MPa]
S	1529 \pm 86	24.3 \pm 2.1
CH	1568 \pm 71	24.9 \pm 0.8
T	1375 \pm 49	24.4 \pm 0.7
H	1295 \pm 36	22.5 \pm 0.5
CS	1456 \pm 35	21.5 \pm 0.6

compared. The simulation result for the hexagonal structure (H), using the bimodular linear elastic material model, is presented in Fig. 10. The x-axis symmetry was used to reduce calculation time. The boundary condition XSYMM was used to constrain the cut surface of the panel along the x-axis and rotation around the y- and z-axis. Due to the x-axis symmetry, the sandwich panel is not moveable along the x-axis. The support and punch were modelled as rigid, non-deformable shell bodies. The support was fully in-build having zero degrees of freedom and the punch was constrained to be only moveable along the y-axis. Support and punch were contact pairs with the upper and lower specimen surface, respectively. As contact properties “hard contact” was chosen for the normal behaviour and the friction formulation “penalty” with a

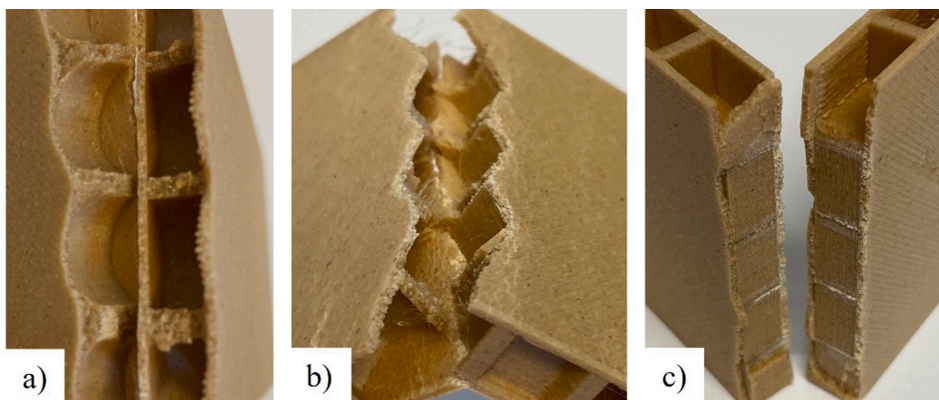


Fig. 8. Failure surface of some selected 3D-printed specimens after they got 3-point-bending tested. a) Circular-cored-hexagonal (CS), b) Hexagonal (H), c) Squared (S).

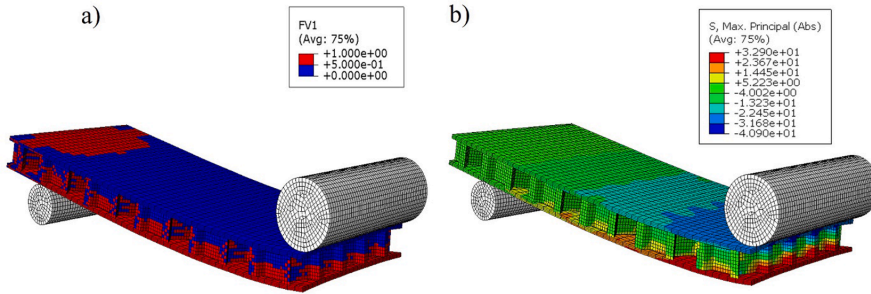


Fig. 10. Simulation results at the last increment of time of the 3-point-bending test of the specimen (H), using the bimodular material model. a) visualization of the field variable (FV) with elements subjected to compressive loads in blue (FV = 0) and elements subjected to tensile loads in red (FV = 1) and b) visualization of the maximum principal stress distribution. (For interpretation of the references to colour in this figure legend, the reader is referred to the web version of this article.)

friction coefficient of 0.3 [67,68]. An implicit, quasi-static simulation was performed where a negative displacement of -20 mm was applied to the punch along the y-axis. As history output, the relative displacement and reaction force in the y-direction was selected.

Fig. 10a shows the distribution between elements, which were identified to be subjected to negative (blue) or positive (red) strains. In Fig. 10b the maximum principal stress distribution is shown for the last time increment. Principal stresses describe the eigenvalues of the Cauchy stress tensor which act in the three principal directions because of projecting the Cauchy stress tensor onto an orientation where all shear stresses are equal to zero. The maximum principal stress describes the maximum normal stress at a point. The maximum principal stress theory states, that failure occurs when the maximum principal stress exceeds the ultimate yield strength of a material [69].

In Fig. 12, the simulation results in form of force–displacement curves are plotted together with the corresponding physical tests of each panel structure type. The bimodular, linear elastic simulation results and force–displacement curves obtained through physical tests showed an error in flexural strength of max. -5% for the CS structure and -8% in flexural modulus for the CH structure. When using the hyperelastic material model the maximum error in flexural modulus was found to be +24 % for the CS structure. The results for flexural strength turned out to be quite similar for both material models. This was expected due to the relatively small difference of 1.9 MPa between the tensile and compressive yield strength values used for the simulations.

In Fig. 11, bar graphs are used to visualize the deviation of flexural modulus and strength obtained from physical tests and simulations. The

least error of 1–2 % between the simulation and the physical test was found for the structures T and H.

In contrast to the hyperelastic material model, the linear elastic, bimodular model slightly underestimated the flexural modulus for S, CH, and CS.

A lower elastic modulus under compression than under tension can be expected for 3D-printed parts [66,70]. One reason for this might be voids, created by the 3D printing process, which will be reduced under compression and let the material behave softer. Pastor-Artigues et al. [66] and Tomás Vukasovic et al. [70] analysed this behaviour and concluded that an elastic bimodular material model should be considered when simulating 3-point-bending tests of 3D-printed structures.

For investigating various design configurations, the linear elastic, bimodular and perfectly plastic material model is representing the elastic/plastic 3-point-bending behaviour sufficiently, if the previously defined 3D printing set-up is maintained. One additional source of error could be the strain rate sensitivity of PLA [71]. In this study, the strain rate of tensile tests for creating the material model was approximately 10^{-4} s^{-1} while the sandwich panels were tested with a strain rate of approximately $2 \times 10^{-4} \text{ s}^{-1}$ [72]. Thus, the model could be expected to be slightly softer and less strong than the experiment. However, the slight difference in strain rate was considered negligible since the strain rate sensitivity of 3D-printed PLA was shown to get more prominent at higher strain rates ($>10^{-3} \text{ s}^{-1}$) [71,73]. This model is considered to be useful for further design developments, and it could be interesting to validate the model on other load cases and structures.

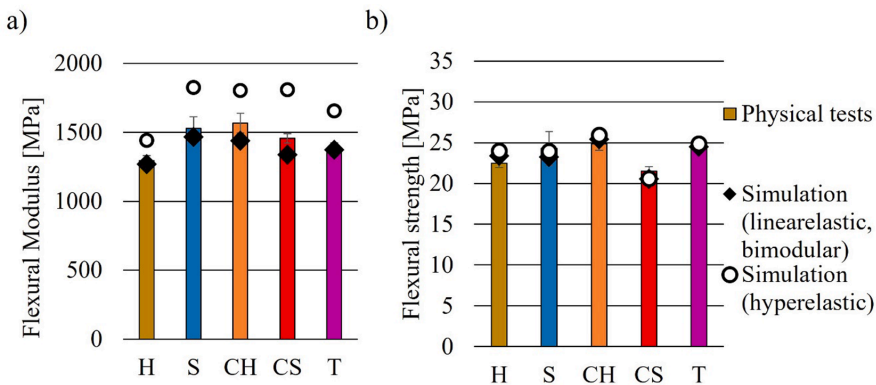


Fig. 11. Bar graphs of the a) flexural modulus and b) strength of 3D-printed, biocomposite sandwich panels. Black rhombuses show the results of flexural modulus and strength obtained from simulations using a linear elastic and bimodular material model and circles show simulation results using a hyperelastic material model.

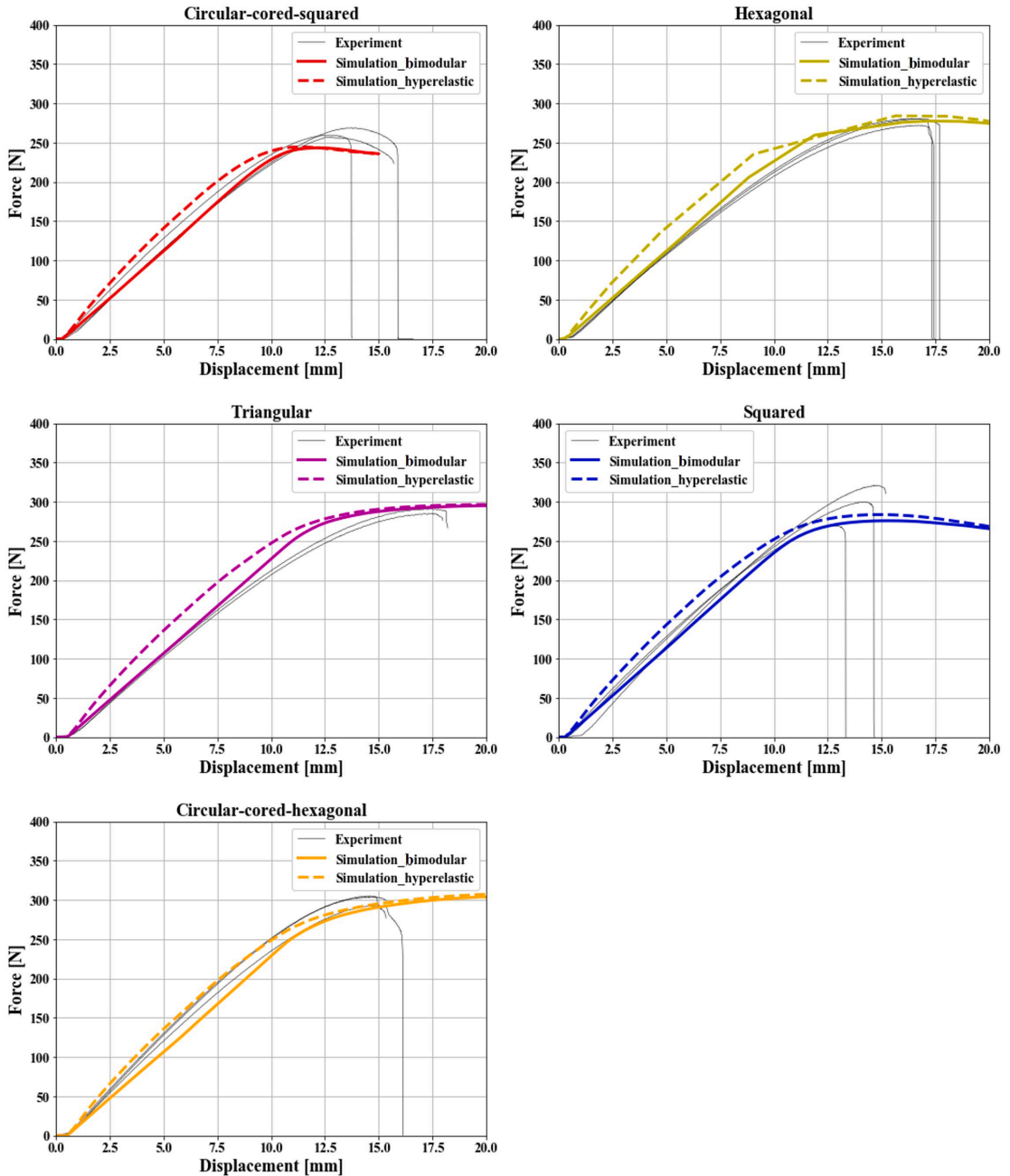


Fig. 12. Simulation results (coloured curves) and physical test results (black curves).

4. Conclusions

This work presented a comparative study of 3-point-bending properties of sandwich panels, having different structures and were simulated based on two different material modelling approaches, a hyperelastic and a linear elastic, bimodular model. The panel specimens were manufactured by MEX printing with a commercial wood fibre-

reinforced PLA filament.

Tension and compression tests were performed on 3D printed, wood fibre-reinforced biocomposite material. The 3-point-bending tests were used for validation of the two modelling approaches. The linear elastic, bimodular model yielded sufficient results and underestimated the flexural strength by only 5% and the flexural stiffness by 8% referring to the CS and CH structure, respectively. The hyperelastic model

overestimated the flexural stiffness by up to 24 %.

The structures with an out-of-plane orientated pattern showed similar bending properties when having the same relative density of 0.5. However, the CH structure yielded the highest flexural strength and stiffness compared to the other investigated structures. The linear elastic, bimodular and perfectly plastic material model, provided in this work, is suitable for predicting the 3-point-bending properties of 3D-printed wood fibre biocomposite panels. It is a relatively simple model, requiring little computing effort and time as well as reasonable experimental effort.

To take this research further, it could be interesting to use the bimodular material model to optimise designs of 3D-printed parts and to adapt the model to other test scenarios and other 3D-printed materials.

CRedit authorship contribution statement

Chiara Zarna: Conceptualization, Methodology, Software, Validation, Formal analysis, Investigation, Data curation, Writing – original draft, Visualization. **Gary Chinga-Carrasco:** Resources, Supervision, Project administration, Funding acquisition, Conceptualization, Writing – review & editing. **Andreas Echtermeyer:** Conceptualization, Methodology, Resources, Writing – review & editing, Supervision.

Declaration of Competing Interest

The authors declare that they have no known competing financial interests or personal relationships that could have appeared to influence the work reported in this paper.

Data availability

Data will be made available on request.

Acknowledgements

The Research Council of Norway and the companies supporting the ALLOC project (Grant no. 282310) are thanked for funding.

Appendix A. Supplementary material

Supplementary data to this article can be found online at <https://doi.org/10.1016/j.compositesa.2022.107368>.

References

- [1] Biron M. 8 - Application Examples. In: Biron M, editor. *Industrial Applications of Renewable Plastics*. William Andrew Publishing; 2017. p. 463–518.
- [2] Caulfield DF, Clemons C, Rowell RM. Wood thermoplastic composites. 2010. p. 141–61.
- [3] Mallick PK. 5 - Thermoplastics and thermoplastic–matrix composites for lightweight automotive structures. In: Mallick PK, editor. *Materials, Design and Manufacturing for Lightweight Vehicles*: Woodhead Publishing; 2010. p. 174–207.
- [4] Dai D, Fan M. 1 - Wood fibres as reinforcements in natural fibre composites: structure, properties, processing and applications. In: Hodzic A, Shanks R, editors. *Natural Fibre Composites*. Woodhead Publishing; 2014. p. 3–65.
- [5] Stenvall E, Flodberg G, Petterson H, Hellberg K, Hermansson L, Wallin M, et al. Additive Manufacturing of Prostheses Using Forest-Based Composites. *Bioengineering (Basel)* 2020;7(3).
- [6] Nygård P, Tanem BS, Karlsen T, Brachet P, Leinsvang B. Extrusion-based wood fibre-PP composites: Wood powder and pelletized wood fibres – a comparative study. *Compos Sci Technol* 2008;68(15):3418–24.
- [7] Arifur Rahman M, Parvin F, Hasan M, Hoque ME. Introduction to Manufacturing of Natural Fibre-Reinforced Polymer Composites. In: Salit MS, Jawaid M, Yusoff NB, Hoque ME, editors. *Manufacturing of Natural Fibre Reinforced Polymer Composites*. Cham: Springer International Publishing; 2015. p. 17–43.
- [8] Tarrés Q, Melbo JK, Delgado-Aguilar M, Espinach FX, Mutjé P, Chinga-Carrasco G. Bio-polyethylene reinforced with thermomechanical pulp fibers: Mechanical and micromechanical characterization and its application in 3D-printing by fused deposition modelling. *Compos B Eng* 2018;153:70–7.
- [9] Filgueira D, Holmen S, Melbo JK, Moldes D, Echtermeyer AT, Chinga-Carrasco G. 3D Printable Filaments Made of Biobased Polyethylene Biocomposites. *Polymers* 2018;10(3).
- [10] Serra-Parareda F, Vilaseca F, Espinach FX, Mutjé P, Delgado-Aguilar M, Tarrés Q. Stiffening Potential of Lignocellulosic Fibers in Fully Biobased Composites: The Case of Abaca Strands, Spruce TMP Fibers, Recycled Fibers from ONP, and Barley TMP Fibers. *Polymers* 2021;13(4).
- [11] Gregorova A, Hrabalova M, Wimmer R, Saake B, Altaner C. Poly(lactide acid) composites reinforced with fibers obtained from different tissue types of *Picea sitchensis*. *J Appl Polym Sci* 2009;114(5):2616–23.
- [12] Peltola H, Pääkkönen E, Jetsu P, Heinemann S. Wood based PLA and PP composites: Effect of fibre type and matrix polymer on fibre morphology, dispersion and composite properties. *Compos A Appl Sci Manuf* 2014;61:13–22.
- [13] Tao Y, Wang H, Li Z, Li P, Shi SQ. Development and Application of Wood Flour-Filled Poly(lactide acid) Composite Filament for 3D Printing. *Materials (Basel)* 2017;10(4):339.
- [14] Pilla S, Gong S, O'Neill E, Yang L, Rowell RM. Poly(lactide)-recycled wood fiber composites. *J Appl Polym Sci* 2009;111(1):37–47.
- [15] Winandy JE, Stark NM, Clemons CM. Considerations in recycling of wood-plastic composites. 2004.
- [16] Sin LT, Rahmat Abdul R, Rahman Wan AWA. 3 - Applications of Poly(lactide Acid). In: Ebnesajjad S, editor. *Handbook of Biopolymers and Biodegradable Plastics*. Boston: William Andrew Publishing; 2013. p. 55–69.
- [17] Le Duigou A, Castro M, Bevan R, Martin N. 3D printing of wood fibre biocomposites: From mechanical to actuation functionality. *Mater Des* 2016;96:106–14.
- [18] Ngo TD, Kashani A, Imbalzano G, Nguyen KTQ, Hui D. Additive manufacturing (3D printing): A review of materials, methods, applications and challenges. *Compos B Eng* 2018;143:172–96.
- [19] Filgueira D, Holmen S, Melbo JK, Moldes D, Echtermeyer AT, Chinga-Carrasco G. Enzymatic-Assisted Modification of Thermomechanical Pulp Fibers To Improve the Interfacial Adhesion with Poly(lactide acid) for 3D Printing. *ACS Sustain Chem Eng* 2017;5(10):9338–46.
- [20] Filgueira D, Holmen S, Melbo JK, Moldes D, Echtermeyer AT, Chinga-Carrasco G. 3D Printable Filaments Made of Biobased Polyethylene Biocomposites. *Polymers* 2018;10(3):314.
- [21] Tarrés Q, Oliver-Ortega H, Espinach FX, Mutjé P, Delgado-Aguilar M, Méndez JA. Determination of Mean Intrinsic Flexural Strength and Coupling Factor of Natural Fiber Reinforcement in Poly(lactide Acid) Biocomposites. *Polymers* 2019;11(11):1736.
- [22] Azimi P, Zhao D, Pouzet C, Crain NE, Stephens B. Emissions of Ultrafine Particles and Volatile Organic Compounds from Commercially Available Desktop Three-Dimensional Printers with Multiple Filaments. *Environ Sci Tech* 2016;50(3):1260–8.
- [23] Mazzanti V, Malagutti L, Mollica F. FDM 3D Printing of Polymers Containing Natural Fillers: A Review of their Mechanical Properties. *Polymers* 2019;11(7):1094.
- [24] Ji A, Zhang S, Bhagia S, Yoo CG, Ragauskas AJ. 3D printing of biomass-derived composites: application and characterization approaches. *RSC Adv* 2020;10(37):21698–723.
- [25] Gardan J, Nguyen DC, Roucoules L, Montay G. Characterization of Wood Filament in Additive Deposition to Study the Mechanical Behavior of Reconstituted Wood Products. *Journal of Engineered Fibers and Fabrics*. 2016;11(4):155892501601100408.
- [26] Bhagia S, Lowden RR, Erdman D, Rodriguez M, Haga BA, Solano IRM, et al. Tensile properties of 3D-printed wood-filled PLA materials using poplar trees. *Appl Mater Today* 2020;21:100832.
- [27] Ahmed W, Alnajjar F, Zanelidin E, Al-Marzouqi AH, Gochoo M, Khalid S. Implementing FDM 3D Printing Strategies Using Natural Fibers to Produce Biomass Composite. *Materials (Basel)* 2020;13(18):4065.
- [28] Kariz M, Sernek M, Obućina M, Kuzman MK. Effect of wood content in FDM filament on properties of 3D printed parts. *Mater Today Commun* 2018;14:135–40.
- [29] Yang T-C. Effect of Extrusion Temperature on the Physico-Mechanical Properties of Unidirectional Wood Fiber-Reinforced Poly(lactide acid) Composite (WFRPC) Components Using Fused Deposition Modeling. *Polymers (Basel)* 2018;10(9).
- [30] Ayrlimis N, Kariz M, Kwon JH, Kitek KM. Effect of printing layer thickness on water absorption and mechanical properties of 3D-printed wood/PLA composite materials. *Int J Adv Manuf Technol* 2019;102(5):2195–200.
- [31] Lamm ME, Wang L, Kishore V, Tekinalp H, Kunc V, Wang J, et al. Material Extrusion Additive Manufacturing of Wood and Lignocellulosic Filled Composites. *Polymers* 2020;12(9).
- [32] Yang T-C, Yeh C-H. Morphology and Mechanical Properties of 3D Printed Wood Fiber/Poly(lactide acid) Composite Parts Using Fused Deposition Modeling (FDM): The Effects of Printing Speed. *Polymers* 2020;12(6):1334.
- [33] Hales TC. The honeycomb conjecture. *Discret Comput Geom* 2001;25(1):1–22.
- [34] Zhang J, Ashby MF. The out-of-plane properties of honeycombs. *Int J Mech Sci* 1992;34(6):475–89.
- [35] Zhang Q, Yang X, Li P, Huang G, Feng S, Shen C, et al. Bioinspired engineering of honeycomb structure – Using nature to inspire human innovation. *Prog Mater Sci* 2015;74:332–400.
- [36] Wang X, Pan Y, Yuan H, Su M, Shao C, Liu C, et al. Simple fabrication of superhydrophobic PLA with honeycomb-like structures for high-efficiency oil-water separation. *Chin Chem Lett* 2020;31(2):365–8.
- [37] Feng Y, Qiu H, Gao Y, Zheng H, Tan J. Creative design for sandwich structures: A review. *International Journal of Advanced Robotic Systems*. 2020;17(3):1729881420921327.
- [38] Zhu H, Mills NJ. The in-plane non-linear compression of regular honeycombs. *Int J Solids Struct* 2000;37:1931–49.

- [39] Araújo H, Leite M, Ribeiro AR, Deus AM, Reis L, Vaz MF. The effect of geometry on the flexural properties of cellular core structures. *Proceedings of the Institution of Mechanical Engineers, Part L: Journal of Materials: Design and Applications*. 2018; 233(3):338-47.
- [40] Wang AJ, McDowell DL. In-plane stiffness and yield strength of periodic metal honeycombs. *Journal of Engineering Materials and Technology, Transactions of the ASME* 2004;126(2):137-56.
- [41] Han B, Qin K, Yu B, Wang B, Zhang Q, Lu TJ. Honeycomb-corrugation hybrid as a novel sandwich core for significantly enhanced compressive performance. *Mater Des* 2016;93:271-82.
- [42] Alhijazi M, Zeeshan Q, Qin Z, Safaei B, Asmael M. Finite element analysis of natural fibers composites: A review. *Nanotechnol Rev* 2020;9(1):853-75.
- [43] Xiong X, Shen SZ, Hua L, Liu JZ, Li X, Wan X, et al. Finite element models of natural fibers and their composites: A review. *J Reinf Plast Compos* 2018;37(9):617-35.
- [44] Moses DM, Prion HGL. Stress and failure analysis of wood composites: a new model. *Compos B Eng* 2004;35(3):251-61.
- [45] Agarwal BD, Broutman LJ, Chandrashekhara K. *Analysis And Performance Of Fiber Composites*. 3. ed. Inc: John Wiley & Sons; 2006.
- [46] Halpin JC, Karoos JL. Strength of discontinuous reinforced composites: I. Fiber reinforced composites. *Polym Eng Sci* 1978;18(6):496-504.
- [47] Zarna C, Opedal MT, Echtermeyer AT, Chinga-Carrasco G. Reinforcement ability of lignocellulosic components in biocomposites and their 3D printed applications – A review. *Composites Part C: Open Access*; 2021. p. 100171.
- [48] Giani N, Mazzeochetti L, Benelli T, Picchioni F, Giorgini L. Towards sustainability in 3D printing of thermoplastic composites: Evaluation of recycled carbon fibers as reinforcing agent for FDM filament production and 3D printing. *Compos A Appl Sci Manuf* 2022;159:107002.
- [49] Tekinalp HL, Kunc V, Velez-Garcia GM, Duty CE, Love LJ, Naskar AK, et al. Highly oriented carbon fiber-polymer composites via additive manufacturing. *Compos Sci Technol* 2014;105:144-50.
- [50] Liao Y, Liu C, Coppola B, Barra G, Di Maio L, Incarnato L, et al. Effect of Porosity and Crystallinity on 3D Printed PLA Properties. *Polymers (Basel)* 2019;11(9).
- [51] Mohanty AK, Misra M, Drzal LT. Sustainable Bio-Composites from Renewable Resources: Opportunities and Challenges in the Green Materials World. *J Polym Environ* 2002;10(1):19-26.
- [52] Shekar HSS, Ramachandra M. Green Composites: A Review. *Materials Today: Proceedings*. 2018;5(1, Part 3):2518-26.
- [53] Fan M, Fu F. 1 - Introduction: A perspective – natural fibre composites in construction. In: Fan M, Fu F, editors. *Advanced High Strength Natural Fibre Composites in Construction*. Woodhead Publishing; 2017. p. 1-20.
- [54] Rao S, Jayaraman K, Bhattacharyya D. Short fibre reinforced cores and their sandwich panels: Processing and evaluation. *Compos A Appl Sci Manuf* 2011;42(9):1236-46.
- [55] Monteiro S, Martins J, Magalhães FD, Carvalho L. Lightweight Wood Composites: Challenges, Production and Performance. In: Kalia S, editor. *Lignocellulosic Composite Materials*. Cham: Springer International Publishing; 2018. p. 293-322.
- [56] Kariz M, Sernek M, Kuzman M. Effect of humidity on 3D-printed specimens from wood-pla filaments. *Wood Research* 2018;63:917-22.
- [57] Banjo AD, Agrawal V, Auad ML, Celestine A-DN. Moisture-induced changes in the mechanical behavior of 3D printed polymers. *Composites Part C: Open Access*. 2022;7:100243.
- [58] Niaounakis M, Kontou E, Xanthis M. Effects of Aging on the Thermomechanical Properties of Poly(lactic acid). *J Appl Polym Sci* 2011;119:472-81.
- [59] Wang K, Li S, Rao Y, Wu Y, Peng Y, Yao S, et al. Flexure Behaviors of ABS-Based Composites Containing Carbon and Kevlar Fibers by Material Extrusion 3D Printing. *Polymers* 2019;11(11):1878.
- [60] John LK, Murugan R, Singamneni S. Impact of quasi-isotropic raster layout on the mechanical behaviour of fused filament fabrication parts. *High Perform Polym* 2022;34(1):77-86.
- [61] Fatimatuzahraa AW, Farahaina B, Yusoff WAY. The effect of employing different raster orientations on the mechanical properties and microstructure of Fused Deposition Modeling parts. In: 2011 IEEE Symposium on Business, Engineering and Industrial Applications; (ISBEIA)2011.. p. 22-7.
- [62] Ameri B, Taheri-Behrooz F, Aliha MRM. Evaluation of the geometrical discontinuity effect on mixed-mode I/II fracture load of FDM 3D-printed parts. *Theor Appl Fract Mech* 2021;113:102953.
- [63] Ameri B, Taheri-Behrooz F, Aliha MRM. Mixed-mode tensile/shear fracture of the additively manufactured components under dynamic and static loads. *Eng Fract Mech* 2022;260:108185.
- [64] Tobajas R, Elduque D, Javierre C, Ibarz E, Gracia L. A comparative study of hyperelastic constitutive models for an automotive shaft seal material. *International Journal of Service and Computing Oriented Manufacturing* 2018;3: 171.
- [65] Şerban DA, Marşavina L, Silberschmidt V. Behaviour of semi-crystalline thermoplastic polymers: Experimental studies and simulations. *Comput Mater Sci* 2012;52(1):139-46.
- [66] Pastor-Artigues M-M, Roure-Fernández F, Ayneto-Gubert X, Bonada-Bo J, Pérez-Guindal E, Buj-Corral I. Elastic Asymmetry of PLA Material in FDM-Printed Parts: Considerations Concerning Experimental Characterisation for Use in Numerical Simulations. *Materials* 2020;13(1):15.
- [67] Zhiani Hervan S, Altinkaynak A, Hardness PZ. friction and wear characteristics of 3D-printed PLA polymer. *Proceedings of the Institution of Mechanical Engineers, Part J: Journal of Engineering Tribology* 2021;235(8):1590-8.
- [68] Roy R, Mukhopadhyay A. Tribological studies of 3D printed ABS and PLA plastic parts. *Mater Today: Proc* 2021;41:856-62.
- [69] Bertram A, Glüge R. *Solid mechanics: Theory, modeling, and problems* 2015.
- [70] Vukasovic T, Vivanco J, Celentano D, Garcia-Herrera C. Characterization of the mechanical response of thermoplastic parts fabricated with 3D printing. *Int J Adv Manuf Technol* 2019;104:1-12.
- [71] Vidakis N, Petousis M, Velidakis E, Liebscher M, Mechtcherine V, Tzounis L. On the Strain Rate Sensitivity of Fused Filament Fabrication (FFF) Processed PLA, ABS, PETG, PA6, and PP Thermoplastic Polymers. *Polymers (Basel)* 2020;12(12).
- [72] Santos P, Valvez S, Monjon A, Reis P. The hybridisation effect on the viscoelastic properties of polymeric composites 2020.
- [73] Luo J, Luo Q, Zhang G, Li Q, Sun G. On strain rate and temperature dependent mechanical properties and constitutive models for additively manufactured polylactic acid (PLA) materials. *Thin-Walled Struct* 2022;179:109624.

Appendix

Bending properties and numerical modelling of cellular panels manufactured from wood fibre/PLA biocomposite by 3D printing

Chiara Zarna^a, Gary Chinga-Carrasco^b, Andreas Echtermeyer^a

^a Department of Mechanical and Industrial Engineering, NTNU, Richard Birkelandsvei 2B, 7491 Trondheim, Norway

^b RISE PFI, Høgskoleringen 6b, 7491 Trondheim, Norway

Corresponding author: Chiara Zarna (chiara.zarna@ntnu.no)

Table A: Relative density of 3D-printed sandwich panels

Specimen code	Specimen average mass [g]	Specimen volume [cm ³]	Specimen density [g/cm ³]	Mat. Density [g/cm ³]	Specimen relative density
H	46.4	43.40	0.55	1.07	0.51
S	48.3	40.91	0.58	1.18	0.49
T	46.3	41.70	0.55	1.11	0.50
CH	50.5	42.04	0.6	1.20	0.50
CS	50.0	42.08	0.59	1.19	0.50

A. V Publication V

Wood fibre biocomposite sandwich panels with unidirectional core stiffeners - 3-point bending properties and considerations on 3D printing and polymer extrusion as a manufacturing method





Biocomposite panels with unidirectional core stiffeners – 3-point bending properties and considerations on 3D printing and extrusion as a manufacturing method

Chiara Zarna^{a,*}, Gary Chinga-Carrasco^b, Andreas T. Echtermeyer^a

^a Department of Mechanical and Industrial Engineering, NTNU, Richard Birkelandsvei 2B, 7491 Trondheim, Norway

^b RISE PFI, Høgskoleringen 6b, 7491 Trondheim, Norway

ARTICLE INFO

Keywords:

Biocomposites
3D printing
Extrusion
Mechanical properties
Wood fibres

ABSTRACT

Sandwich panels with unidirectional core stiffeners are known for their relatively high bending stiffness at low weight, stability under compressive and shear loads and energy absorption capability. In this study, 3D printing was used to screen biocomposite sandwich panels easily and preliminarily with different unidirectional core stiffener designs. Thermomechanical pulp (TMP) fibre-reinforced poly(lactic acid) (PLA) was used in this study.

A corrugated, trapezoid and arched cell structure were tested experimentally and numerically using a bimodular material model, accounting for different behaviour in tension and compression. The trapezoid structure showed the best flexural properties of the three 3D-printed sandwich beams. It was chosen to be explored further, manufacturing it by extrusion. Extrusion is a production process likely to be used in industry on a larger scale.

Basic material properties of the biocomposites were obtained from injection moulded dogbone specimens. The flexural properties of the extruded panels were measured experimentally and simulated using finite element analysis. Simulations were done with a hyperelastic material model. Predictions and experiments were in adequate agreement, allowing such kind of simulation to be used for extruded biocomposite sandwich panels.

1. Introduction

To address rising environmental concerns, especially when it comes to fossil-based raw materials and waste management, biocomposites offer potential as a more environmentally friendly alternative compared to conventional composite materials [48–51]. The attempt of replacing conventional panels with biocomposite sandwich panels is to increase sustainability by using fewer amounts of material and preferably materials derived from natural resources. Additionally, the use of lightweight materials and structures can contribute to reducing fuel consumption under transportation. Wood fibres, such as TMP fibres, were shown to have the potential to reinforce biobased thermoplastics, such as PLA, bio-polyethene, etc. [1–4]. Besides the potential reinforcing effect, TMP fibres can serve as a cost-efficient and lightweight filler material [5]. Wood fibre-reinforced plastic outdoor and indoor decking and facings can be found in form of extruded panels [6]. One example is RecoDeck®+ from Step on Safety Ltd. PLA is a moisture-sensitive biopolymer [7] and is therefore mainly considered a model material

or for indoor use. For example, indoor floor and wall covering products based on PLA composites are commercially available from LX Hausys under the tradename ZEA-Marú [8]. Additionally, PLA is one of the most used biopolymers in 3D printing because of its great availability [9].

Due to the high degree of design freedom, additive manufacturing is a resource-saving production method, especially for prototyping in early development stages [10,11]. Filaments for material extrusion (MEX), filled with wood particles are commercially available and usually contain 5 wt% to 20 wt% fibres. Higher wood fibre contents may increase the risk of nozzle blockage, void formations, and fracture during printing due to a rougher filament surface and a higher brittleness of the filament [12–15]. MEX 3D printing is not yet widely used in large-scale industrial applications, since the process is more time-consuming than those of conventional moulding techniques, such as injection moulding or extrusion and the mechanical properties of 3D-printed parts are comparatively low [16]. However, the usefulness of 3D printing in early development stages was emphasised and 3D printing is applied in several industrial sectors, e.g., automotive, aerospace, sensor

* Corresponding author.

E-mail address: chiara.zarna@ntnu.no (C. Zarna).

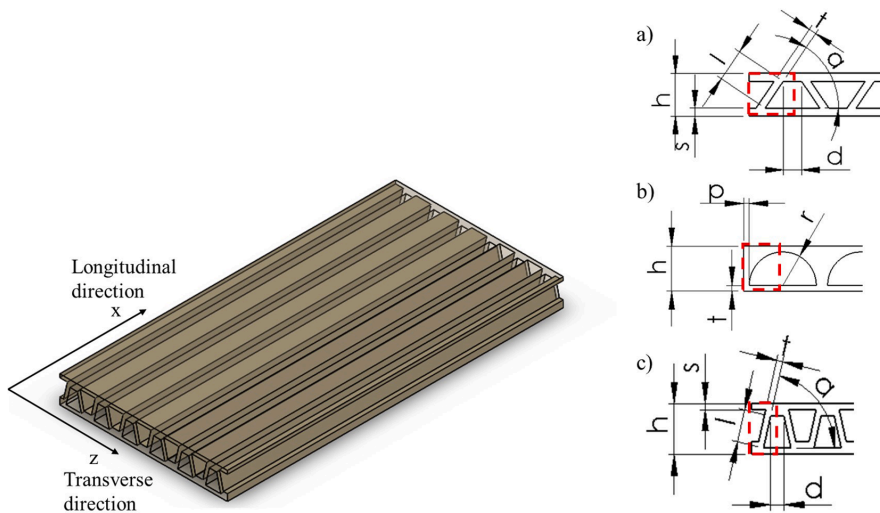


Fig. 1. Directions in a sandwich panel with corrugated unidirectional core stiffeners and unit cell shapes for out-of-plane aligned structures and their relative density: a) trapezoid (TR) unit cell, b) arched (AR) unit cell, c) corrugated (CO) unit cell.

applications and smart textiles [9].

Extrusion of wood-fibre biocomposites is a fast and continuous manufacturing method, most suitable for profiles and panels with unidirectionally aligned structures [17,18]. However, designing and manufacturing an extrusion tool is not trivial and requires extensive consideration of the material flow characteristics, which usually is a time, material and cost-consuming procedure [19]. This might slow down and inhibit efforts to optimise structural designs. Not only the extrusion tool design but also the processing conditions have an impact on the mechanical properties of the extrudate. Especially thermal degradation must be considered when extruding wood-fibre-reinforced biocomposites. Wood fibres usually degrade in temperatures above 200 °C [20]. Luigi-Jules Vandi et al. [21] presented a statistical study on extrusion process parameters for wood-fibre biocomposites and concluded that the extrusion temperature is one of the main influencing parameters regarding the resulting tensile strength of the extrudates and should be kept as low as possible. For Poly(3-hydroxybutyrate-co-3-hydroxyvalerate) with 40 wt.% wood-fibre reinforcement, the optimal extrusion temperature was found to be 170 °C [21]. Other methods to manufacture sandwich panels with unidirectional core stiffeners from biocomposites are hot-pressing [22] or impregnation using a corrugated pre-form [23].

The main application of sandwich designs is to create lightweight and comparatively strong and stiff panels [24]. Sandwich panels with unidirectional core stiffeners, such as corrugated cores, are orthotropic and especially stiff and strong along the core stiffeners [24,25]. Corrugated cores offer a higher bending rigidity in longitudinal than in transverse direction (Fig. 1). Depending on the geometrical configurations of the corrugation, the longitudinal bending rigidity can be about 10^3 times higher than the transverse one [26].

Compared to honeycomb cores the bending strength, stiffness and twisting resistance in corrugated cores can be higher along the longitudinal axis [27,28]. Corrugated sheet structures are known for their high shear strength, energy absorption and load-bearing capacity and are, among other applications, used as cores for panel constructions [29–32]. Another advantage of corrugated cores might be that the open channels are ventable to avoid moisture accumulation, which can be an issue in honeycomb sandwich panels for aircraft construction [27].

Computational modelling, e.g., finite element analysis (FE-analysis) is a useful tool for product optimisation and virtual component testing.

Fibre-reinforced biocomposites manufactured in injection moulding or extrusion are anisotropic. The fibres align according to the flow of the polymer material during the moulding process. Typically, the fibres are aligned unidirectional close to the mould surface and randomly in the centre [33]. Depending on the cooling rate certain formations of ordered and disordered crystalline forms might occur, affecting the mechanical properties of the resulting biocomposite part. During material extrusion, the polymer chains orientate most likely along the extrusion direction, which might enhance the anisotropy of the extruded part [34]. Biocomposites can be considered isotropic, when the fibre aspect ratio is below the critical load transfer length, the fibres are evenly distributed in the matrix and the fibre orientation is completely random [35–37]. There exist several modelling approaches for biocomposites with varying complexity depending on the application [38–40]. 3D-printed wood fibre biocomposites behave differently in tension and compression and exhibit non-linear material behaviour [41,42]. Non-linearity and the difference of elastic behaviour in compression and tension should be considered when using FE-analysis to predict the flexural rigidity of wood fibre composites [41].

The purpose of this study is to explore the potential of biocomposite sandwich panels with an out-of-plane oriented cellular structure using two different manufacturing methods. Here, 3D printing is used for manufacturing of test specimens and to evaluate different geometrical designs, both experimentally and numerically. One panel design was manufactured by profile extrusion and the flexural properties were verified by FE-analysis and compared to the corresponding 3D-printed panel. To the best of our knowledge studies combining 3D printing, material extrusion and numerical predictions, to promote the use of 3D printing for design evaluations of mass products, are still missing in the literature. Although the use of 3D printing for prototyping was emphasized [9,16], 3D-printed biocomposites were so far seldomly used in industrial applications. Since designing and manufacturing new moulds for extrusion requires more recourses than adjusting the part design in 3D printing, the optimisation process of product and mould designs might be restricted. Hence, this study aims to present a methodology to push the proliferation of 3D-printed biocomposites into wider use. The proposed material models might be useful to possibly evaluate more detailed adjustments of the design before manufacturing a mould.

Table 1
Parameter to calculate the flexural strength and stiffness of the 3-point bending tested sandwich panels.

L [mm]	b [mm]	h [mm]	F_1 [N]	F_2 [N]	a_1 [mm]	a_2 [mm]	F_{max} [N]
Gauge length	Panel width	Panel thickness	10% of F_{max}	40% of F_{max}	Deflection at F_1	Deflection at F_2	Fracture load
180	50	8	$0.1 F_{max}$	$0.4 F_{max}$	$a(F_1)$	$a(F_2)$	

2. Theory and calculations

To investigate and compare different sandwich designs, the relative density ρ_{rel} should be considered [42,43]. The relative density can be calculated by considering geometric unit cells [44]. An overview of out-of-plane oriented cellular structures, that were investigated in the present study, is shown in Fig. 1. The red dashed box is framing the unit cell of each geometry.

Equations (1)–(3) were used to calculate ρ_{rel} for trapezoid (TR), arched (AR) and corrugated (CO).

$$\rho_{rel,TR} = \frac{2s}{h} + \frac{t(h-2s)}{h \times (\sin(\alpha) \times (2d + \cos(\alpha) \times l) + t)} \quad (1)$$

$$\rho_{rel,AR} = 1 - \frac{\pi r^2}{4h \times (p+r)} \quad (2)$$

$$\rho_{rel,CO} = 1 - \frac{\sin(\alpha) \times l \times (\cos(\alpha) + d)}{h \times (\cos(\alpha) \times l + d) + \frac{l}{\tan((180^\circ - \alpha)/2)}} \quad (3)$$

The geometrical parameters used in Equations (1)–(3) correspond to the symbols indicated in Fig. 1. To assess the flexural properties of the biocomposite panels, the flexural stiffness E_m and strength f_m were calculated according to Equations (4), (5) and Table 1 which are following the test standard EN 310 for determining the apparent modulus of elasticity in flatwise bending and bending strength of wood-based panels:

$$E_m = \frac{L^3 \times (F_2 - F_1)}{4b \times h^3 (a_2 - a_1)} \quad (4)$$

$$f_m = \frac{3F_{max} \times L}{2b \times h^2} \quad (5)$$

The bending rigidity is linked to the flexural modulus and can be assessed analytically. For TR, CO, and AR sandwich panels with face sheets of equal material and thickness the approximate bending rigidity in a longitudinal direction can be roughly estimated by [25,45]:

$$D_{TR} = \frac{E \times s \times d^2}{2 \times (1 - \nu^2)} \quad (6)$$

$$D_{CO,AR} = \frac{E \times s \times d^2}{2 \times (1 - \nu^2)} + \frac{E \times t^3}{12 \times (1 - \nu^2)} + \frac{E \times t \times (h - 2t)^2}{2} \quad (7)$$

In Equations (6) [45] and (7) [25], E is the elastic modulus of the face sheet material, s is the thickness of the face sheets, d is the distance between the centre of the two face sheets, t is the core wall thickness, h is the panel height and ν is the Poisson's ratio considering isotropic material behaviour. Equation (6) is only valid for cores with neglectable flexural stiffness. This might be true for TR since the core is consisting of single struts which are not connected to each other [45]. CO is comparable to a continuous corrugated sheet and AR has broad solid pillars whose contribution to flexural stiffness may not be negligible.

More accurate predictions of bending modulus and strength can be obtained by FE-analysis. An isotropic, linear elastic, perfectly plastic and

bimodular material model for simulating the bending properties of 3D-printed sandwich panels was previously developed by the authors in [42]. Bimodular means an asymmetry in the compression and tension behaviour of the material.

3. Materials and methods

3.1. Wood fibre-reinforced biocomposites

Recycled pine wood (15 wt.%) filled PLA/PHA filament was used to 3D-print panel specimens for the 3-point bend tests. The filament is commercially available as Colorfabb WoodFill® (Belfeld, The Netherlands).

PLA Ingeo™ 4043D from Nature Works (Minnetonka, MN, USA) was compounded with TMP fibre from Norske Skog Saugbrugs (Halden, Norway) with a granulate size of less than 8 mm. The fibre loadings were 20 and 30 wt.% and the samples were coded P20TMP and P30TMP, respectively. Compounding was done in two rounds in a Copier Werner & Pfleiderer extruder (Stuttgart, Germany). In the first round, PLA and TMP were compounded at an increasing temperature from 170 °C to 195 °C over the extrusion sections. The extrusion screw speed was 300 rpm. The extrudate was granulated in a Schütte-Buffalo Hammernill (Buffalo, NY, USA) and compounded a second time at a decreasing temperature from 170 °C to 160 °C and a screw speed of 500 rpm.

The materials and specimens were stored and tested in a dry environment (~30 % relative humidity, ~20 °C). The moisture content and thereby effects on material strength and stiffness due to ageing were considered negligible [46–48].

3.2. Sandwich panel manufacturing by 3D printing

3-point bending test specimens were manufactured with a Prusa i3 MK3 FDM-printer (Prague, Czech Republic) with a parameter setup according to Table 2. These parameters were shown to be suitable in a previous study [42]. The outer dimensions of the specimens were $50 \times 210 \times 8 \text{ mm}^3$ ($w \times l \times t$), according to EN 310.

To allow the comparability of the structures, all panels were designed to meet a relative density of $\rho_{rel,panel} = 0.5$. The relative density was chosen to design structures that save 50% of the material volume needed to fabricate an equivalent solid panel while offering a reasonable loadbearing capacity along the longitudinal axis. To calculate the relative density of the structures the Equations (1) – (3) were used. The dimensional configurations are presented in Table 3. The three structures were of the same height and CO and AR had the same face sheet and wall or pillar thickness. TR was considered an exception as it is not a sandwich, but the face sheets are supported by single struts. Compared to CO and AR the face sheet thickness of TR was increased to compensate for not having a self-supporting core and the cell width was kept similar to the one of AR. The actual relative panel density was determined by weighting the specimens after printing, as described in [42]. The mass of the specimens and the corresponding relative density are given in Appendix (Table A).

Table 2
Printing set-up for manufacturing 3-point bending test specimens from Colorfabb woodFill® filament [42].

Nozzle diameter	Layup	Infill	Layer height	Extrusion width	Extrusion speed	Extrusion temperature	Bed temperature
0.6 mm	± 45°	100%	0.15 mm	0.65 mm	50 mm/s	200 °C	60 °C

Table 3
Structure configurations of the investigated biocomposite panels for a desired relative density of 0.5.

Specimen code	Wall thickness t [mm]	Side length l [mm]	Width d [mm]	Angle α [°]	Face sheet thickness s [mm]	Actual relative panel density
Trapezoid (TR)	1.4	6.0	1.7	56	1.5	0.50
Corrugated (CO)	1.0	5.1	2.20	77	1.0	0.51
Arched (AR)	Arch radius r [mm]	pillar width p [mm]			1.0	0.48
	6.0	1.0				

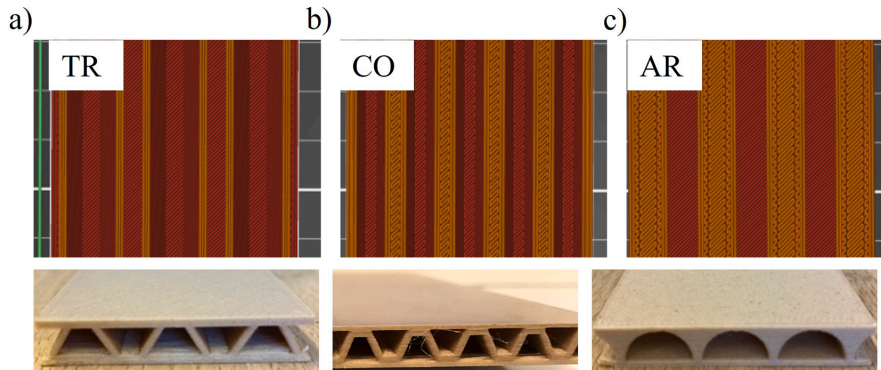


Fig. 2. 3D slicer preview for each structure panel at an out-of-plane printing height of 6.35 mm and 3D-printed 3-point bending test specimens with the a) trapezoid, b) corrugated and c) arched design.

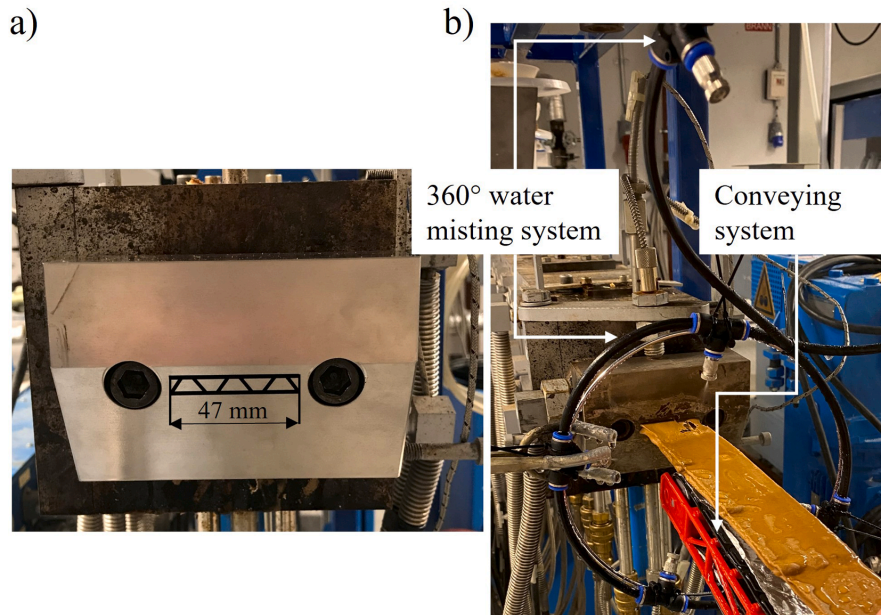


Fig. 3. a) Extrusion tool and b) extrusion line set-up with water cooling system and conveyor.

Table 4
Input data for modelling the here presented 3D-printed biocomposite sandwich panels [42].

Input variables for 3D-printed sandwich panels	Values
Density, ρ	1.15 g/cm ³
Young's modulus in tension, E_T	2500 MPa
Young's modulus in compression, E_C	1800 MPa
Poisson's ratio, ν	0.35
Yield stress in tension σ_T	28.4 MPa
Yield stress in compression σ_C	26.5 MPa

The 3D-printed panel specimens in Fig. 2 were all printed under the same conditions, as described in [42]. One layer of bridge infill with a unidirectional 90° raster orientation was placed to print the upper face sheet.

3.3. Injection moulded dogbones to obtain tensile properties of extruded material

Dogbone specimens of P20TMP and P30TMP were injection moulded with an Xplore micro injection moulder (Sittard, The Netherlands) at an injection temperature of 190 °C and a mould temperature of 30 °C. The dogbone specimen shape is based on ISO 527-2:2012 type A, with modified dimensions resulting in an overall length of 50 mm and a length of the narrow parallel-sided portion of 18 mm. The cross-sectional area is 4 mm × 2 mm (width × thickness). This was restricted by the injection moulding equipment used to manufacture the specimens. Note that valid failure in the gauge section was obtained. Tensile tests were conducted on a Zwick Roell Zmart. Pro (Ulm, Germany) using a load cell of 2.5 kN and an extensometer (Zwick B1089) with a gauge length of 15 mm. The test procedure was based on ISO 527-2:2012 and a test speed of 2 mm/min was chosen. For each material, PLA, P20TMP and P30TMP four specimens were tested. The tensile strength and Young's modulus were calculated according to ISO 527-2:2012.

3.4. Sandwich panel manufacturing by extrusion

An extrusion tool was designed and manufactured to test the concept of extruding such a TR sandwich with biocomposite material. The extrusion tool is shown in Fig. 3a and is designed to fit a Copierion Werner & Pfleiderer laboratory extruder. The mould design is a series of unit cells following the shape and dimensions shown in Fig. 1a and

having an overall width of 47 mm. An experimental extrusion line was built, including water cooling, and a manual conveying system. After extrusion the panels were cut to approximately the same length as the 3D-printed panels, conveying of the extrudate (Fig. 3b). A water misting system was arranged with four nozzles creating a water mist all around the extrudate, directly after leaving the tool. Additional nozzles are placed above the extrudate along the conveying line. P20TMP was extruded at a temperature of 150 °C and P30TMP at 170 °C. The extruded sandwich panels were weighted, and their actual relative density was calculated the same way as for the 3D-printed samples. The actual relative panel density was 0.47 ± 0.05 for both materials.

3.5. 3-point bending tests of 3D-printed and extruded sandwich panels

For each structure type (Fig. 1), three biocomposite panels were 3D-printed (Fig. 2) and the 3-point bending tests were based on the procedure described in the test standard EN 310 and conducted on an Instron Electropulse test machine (Nordwood, United States) with a maximum axial force of 10 kN. The test speed was 10 mm/min and the gauge length was 180 mm. The supports had a diameter of 5 mm and the punch 10 mm. Extruded panels of P20TMP and P30TMP were tested in the same way using the same equipment.

3.6. Modelling and simulation of 3point-bending tests on 3D-printed and extruded sandwich panels

FE analysis was carried out in Abaqus/Standard 2017. All sample geometries were modelled as a solid and 3D deformable part and the panel core and face sheets were meshed with a CD3D8R-element with a global size of 0.67 mm. The x-axis symmetry was used to reduce calculation time. The boundary condition XSYMM was applied to constrain the cut surface of the panel along the x-axis and rotation around the y- and z-axis. The support and punch are modelled as rigid, non-deformable shell bodies. The support is fully in-build having zero degrees of freedom and the punch is only moveable along the y-axis. Support and punch are contact pairs with the upper and lower specimen surface, respectively. As contact properties "hard contact" was chosen for the normal behaviour and the friction formulation "penalty" with a friction coefficient of 0.3 [49,50]. An implicit, quasi-static simulation was performed where a negative displacement of -20 mm was applied to the punch along the y-axis. As history output, the relative displacement and reaction force in the y-direction was selected. The material properties (Table 4) were tested in our lab previously and reported in

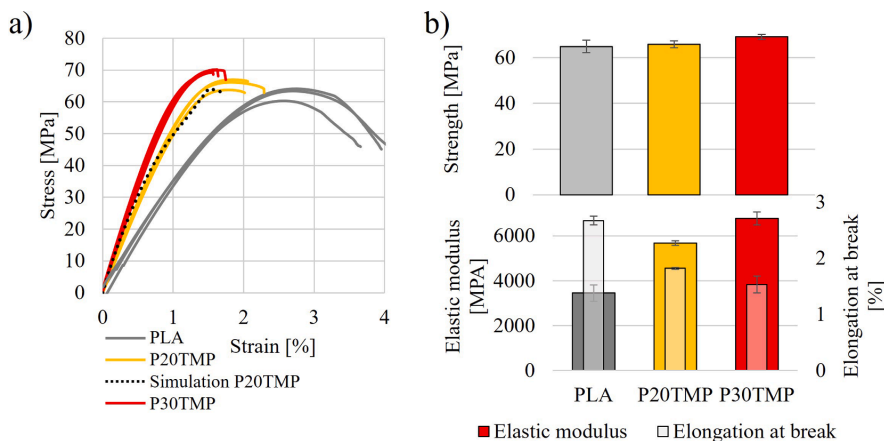


Fig. 4. Tensile test results of injection moulded dogbones from PLA, P20TMP, and P30TMP a) stress–strain curves and b) bar graphs of ultimate tensile strength and modulus. The elongation at break is illustrated as grey-transparent narrow bar graphs together with the elastic modulus in coloured, wider bar graphs.

Table 5
Input variables for modelling extruded sandwich panels from P20TMP.

Input variables for extruded P20TMP sandwich panels	Values
Density, ρ	1.35 g/cm ³
Uniaxial tensile test data	Stress and strain data from one representative test
Poisson's ratio, ν	0.35
Yield stress σ_y	65.9 MPa

[42]. They were obtained through uniaxial tensile and compression tests on 3D-printed specimens, as described in [42].

For simulating the bending properties of extruded P20TMP sandwich panels an isotropic, hyperelastic and perfectly plastic approach was chosen. Only P20TMP was simulated since this material turned out to be more suitable for profile extrusion compared to P30TMP and thus more extruded sandwich panels, suitable for 3-point bending tests, could be obtained from P20TMP. For the hyperelastic response, the Marlow model was applied as it showed good results for non-linear elastic material considerations [51,52]. As input, the stress–strain data set from uniaxial tensile tests on injection moulded dogbones of P20TMP (Fig. 4a) was used. Since in injection moulding and extrusion, the fibres are assumed to orientate along the polymer flow direction, the isotropic material model is considered suitable for the here presented load case. For loading in other or multiple directions, an anisotropic material model might yield more accurate results. The Poisson's ratio of the biocomposite was chosen to be the same as for the 3D-printed biocomposite material from [42]. The actual Poisson's ratio of P20TMP might differ slightly from the assumed value, but should be between 0.3 and 0.4, according to the literature [53–55]. Failure is assumed when the equivalent stress is exceeding the defined yield strength. The defined yield strength is the ultimate tensile strength from the experiment.

Both applied material models are isotropic and therefore limited to loading conditions only along the material axis to which the material was tensile tested. This is because wood fibre-reinforced biocomposites are anisotropic materials due to the alignment of fibres along the

polymer flow direction. Further, strain dependence, damage and plasticity mechanisms are not part of the models.

4. Results and discussion

4.1. Tensile tests and simulation of injection moulded dogbones

The results from tensile tests on injection moulded PLA, P20TMP, and P30TMP dogbones are shown in Fig. 4. There was no significant difference in tensile strength between PLA ((65 ± 3) MPa) and P20TMP ((66 ± 2) MPa) but P30TMP ((69 ± 1) MPa) had a significantly higher tensile strength than PLA and P20TMP. The tensile modulus increased significantly from (3450 ± 362) MPa (PLA) (5669 ± 103) MPa (P20TMP) and (6770 ± 288) MPa (P30TMP), and the elongation at break decreased from (2.67 ± 0.08)% (PLA) to (1.82 ± 0.02)% (P20TMP) and (1.53 ± 0.15)% (P30TMP). The black dotted line is the stress–strain response in uniaxial tension using the material model form Table 5 in FE-analysis. This model was also used to simulate the 3-point bending test of the extruded P20TMP panels.

The reinforcing ability of short fibres in a thermoplastic matrix is highly dependent on the fibre volume fraction, the fibre's length-to-diameter-ratio (fibre aspect ratio), the fibre dispersion, fibre alignment and the fibre–matrix surface interaction. The fibre dispersion and length are affected by the biocomposite processing parameters [56]. The addition of 30 wt.% TMP increased the ultimate strength of the PLA matrix by 6% and the stiffness was almost doubled. The increase in ultimate strength confirmed a suitable choice of compounding parameters for the biocomposite and the partial orientation of the fibres along the vertical axis of the dogbones.

4.2. 3-point bending tests and simulations of 3D-printed sandwich structures

Some fracture surfaces of 3-point bending tested specimens are shown in Fig. 5a. All specimens showed a relatively even crack surface, with a tendency to face sheet peel-off for TR. Since here the face-sheets

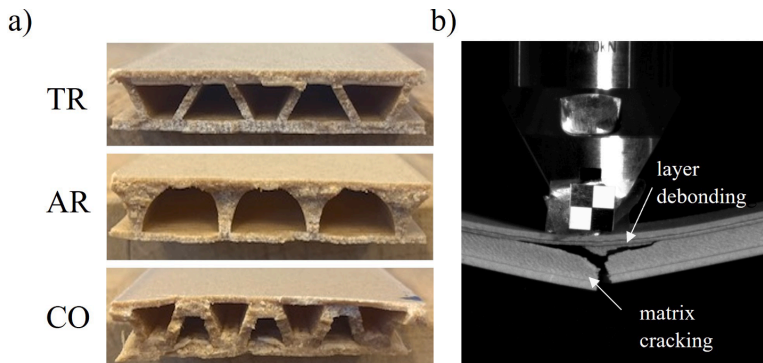


Fig. 5. a) Fracture surface of TR, AR and CO sandwich panels after the 3-point bending test and b) DIC image of sample CO under 3-point bending loading at the time of fracture.

Table 6
Average values of measured flexural modulus and strength and analytically calculated flexural rigidity of the 3D-printed biocomposite sandwich panels assessed in this study.

Sample designation	Flexural modulus from experiment [MPa]	Flexural strength from experiment [MPa]	Calculated flexural rigidity [Nm]	Flexural modulus from simulation [MPa]	Flexural strength from simulation [MPa]
TR	2102 ± 43	34.2 ± 0.8	8.9	1754	34.6
CO	1559 ± 17	29.6 ± 0.8	6.7	1534	29.2
AR	1694 ± 31	27.3 ± 0.3	6.9	1579	28.5

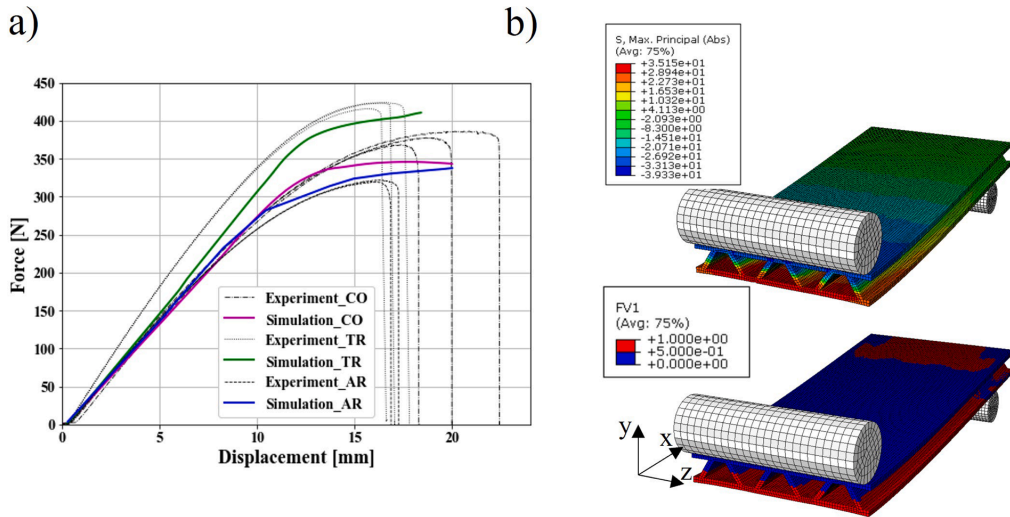


Fig. 6. Results from 3-point bending tests and simulations of 3D-printed panels: a) force–displacement curves using a bi-modular material model (coloured) and experimental results (black), b) visualization of the maximum principal stress distribution and of the field variable (FV) at the last increment of time.

are bonded to a relatively small surface area (1.4 mm strut width), it might be more likely that face-sheet debonding occurs under bending-deformation.

In Fig. 5b a snapshot, taken with a digital image correlation (DIC) camera at the time of the fracture of TR, is shown. The crack was initiated through tensile strains on the bottom side of the specimen caused by matrix cracking. A Mode I fracture due to tensile forces perpendicular to the fracture plane was observed. The crack propagated relatively straight towards the upper face sheet in in-layer mode [57]. Finally, layer debonding occurred close to the upper face sheet.

The average values and standard deviation of flexural strength and stiffness, normalized to a relative density of 0.5, are presented in Table 6. Comparing the three different biocomposite panel types, the TR

structure is outperforming the other structures in terms of flexural strength and stiffness. This is closely related to thicker face sheets used for TR compared to CO and AR. According to Equations (6) and (7), TR is about 33% stiffer than CO and 29% stiffer than AR. Based on physical test data TR is about 35% and 24% stiffer than CO and AR, respectively. The analytically calculated flexural rigidity might be the most accurate for CO since the model was designed for corrugated sheets [25,26].

Simulations of 3-point bending tests were performed for the three panel configurations presented in this study. The bimodular model used in this study was previously developed and presented in [42] and validated on 3D-printed honeycomb-like sandwich panels. The simulation results are presented in Fig. 6. Fig. 6b shows the section cut along the y-z-plane in the middle of the TR panel at the last increment of time of the

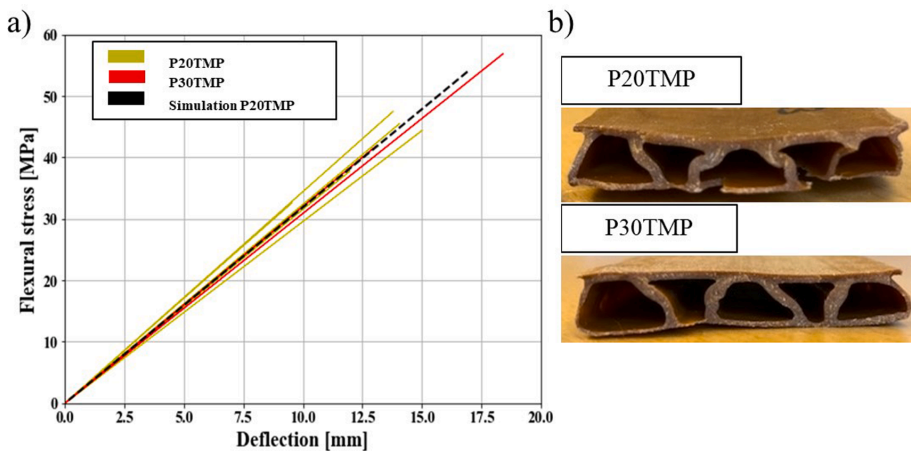


Fig. 7. a) Stress-deflection curve of 3-point bending tested extruded biocomposite sandwich panels and b) the fracture surface of extruded sandwich panels.

3-point bending simulation. The maximum principal stress distribution and the distribution between elements, which were identified to be subjected to negative (blue) or positive (red) strains are shown. The maximum principal stress describes the maximum normal stress at a point. Failure occurs when the maximum principal stress exceeds the yield strength of a material [58].

The error in flexural stress between experiments and simulations amounts to maximal + 8% for AR and -17% in flexural modulus for TR. The deviation between the flexural modulus obtained from simulation and physical test results is less than 5% for CO and AR. However, for TR the flexural modulus is significantly underestimated. This might be related to that the TR struts are constructed out of three parallel filament strands, aligned in 0° orientation. COs and ARs structures are filled with ± 45° oriented strands (Fig. 2). 3D-printed structures are typically stronger and stiffer when the load is applied along the raster orientation compared to 45° off raster orientation. It might also be the case, that the filament alignment in TR is resulting in fewer voids along the loading direction compared to CO and AR and thus leading to a higher overall flexural modulus. Further, TR might be more prone to damage due to the relatively small surface area of the connection between lattices and face sheets compared to CO and AR. Other possible sources of error might be variations in the biocomposite filament, as well as minor changes in environmental conditions during the printing process. Note that the material properties used as input to the FE-analysis were obtained from 3D-printed samples that are already expected to have most of the production-related defects. However, the sufficient agreement between experiments and simulations using the previously presented model from [42] shows that the panels were 3D-printed with reproducible quality.

4.3. 3-point bending tests and simulations of extruded sandwich panels

The relatively simple experimental extrusion line set-up was sufficient to manufacture TR sandwich panels from biocomposite material and prove the concept. P30TMP required a higher extrusion temperature than P20TMP to increase its ability to flow. The ability of a composite melt to flow is typically reduced with increasing fibre fraction [59]. Further, P30TMP was more likely to rip after leaving the extrusion tool, which might be related to a lower melt strength of P30TMP compared to P20TMP. Melt strength is the resistance of a material in a rubbery state to stretching [60]. Additionally higher fibre loadings might increase the friction between melted biocomposite, and the extrusion tool surfaces making the extrudate more likely to stick to the tool surface.

Unfortunately, the here presented experimental extrusion process was poorly controllable, and the panel wall thickness was varying. Variations in wall thickness were even more present in P30TMP compared to P20TMP. This might be improved by implementing a driven and controlled conveying system to draw the extrudate at a constant speed, optimizing the tool design and using lubricants to minimize the friction between the extrudate and extrusion tool. Further, the cooling system could be improved by controlling water temperature and setting up multiple water misting systems in a series or a water bath. Additionally, a second extrusion die could be placed shortly after the tool exit to stabilize the profile shape and smooth the surfaces. Five extruded panels of P20TMP and three of P30TMP could be used for 3-point bending tests. The results are presented in Fig. 7.

Stress-deflection curves are plotted in Fig. 7a as well as simulation results obtained from FE-analysis of P20TMP using the previously described hyperelastic, perfectly plastic material model (Table 5). The model predicts flexural stiffness accurately with an error of about 9%. The flexural strength is overestimated by about 20%, which is most probably related to the varying outer dimensions, wall thicknesses and

Table 7

Flexural strength and stiffness of extruded sandwich panels from P20TMP, P30TMP and simulation of P20TMP normalised to a relative density of 0.5.

Designation	Flexural strength [MPa]	Flexural modulus [MPa]	Actual relative density
P20TMP	41.55 ± 5.54	4374 ± 983	0.47
P30TMP	44.16 ± 9.55	4498 ± 133	0.47
Simulation P20TMP	52.1	4679	0.47

face sheet thicknesses of the extruded panels. Especially the face sheet thickness is tending to be thinner than assumed. The face sheet thickness was considered in the FE-analysis, but local thickness variations were neglected. The flexural strength is assumed at the first sign of yielding since the extruded panels show low toughness. Dimensional inaccuracies, local heterogeneities of the biocomposite material, e.g., fibre agglomerations, voids, etc. and damage mechanisms are not considered in the numerical model. Local defects might induce stress concentration and initiate failure of the biocomposite part at lower strengths than predicted by the homogeneous FE model.

Additionally, there is a slight difference in the strain rate of the tensile tests ($8 \times 10^{-4} \text{ s}^{-1}$) and the bending tests ($2 \times 10^{-4} \text{ s}^{-1}$, calculated according to [61]). Higher strain rates typically result in higher ultimate strength and stiffness of biocomposites. The higher strain rate used for tensile tests compared to the bending tests might have contributed to the overestimation of flexural strength by the simulation. However, this contribution is considered small since it was shown that the strain rate sensitivity of PLA gets more prominent at higher strain rates [62,63]. Due to the water cooling the extruded panels were exposed to higher cooling rates than the injection moulded dogbones which were cooled more slowly. This might have resulted in a higher degree of crystallinity in the dogbones compared to the extruded panels, contributing to a higher ultimate strength obtained from FE-analysis compared to the experiments [64]. However, by comparing the FE-analysis and experimental results, it can be confirmed that polymer extrusion is a suitable method to produce TR sandwich panels from TMP fibre-reinforced PLA. The bending properties of the extruded panels agree with the expected bending properties of such biocomposite material and structure. The fracture surfaces of P20TMP and P30TMP are shown in Fig. 7b. A sudden brittle fracture was initiated from the lower face sheet due to tensile loads. No local buckling was observed in the experiment or simulations.

When normalized to a relative panel density of 0.5, the flexural strength of the extruded P30TMP panel (Table 7) is about 27% higher than the 3D-printed TR panel (Table 6). The flexural stiffness of the extruded sandwich panel is more than doubled compared to the 3D-printed one. The significant differences in flexural strength and stiffness between extruded and 3D-printed panels are closely related to a difference in raw materials and methods used to manufacture the sandwich panels. Both materials (Woodfill® filament and P30TMP), mainly consist of PLA and 30 wt.% wood fibre reinforcement. However, Woodfill® filament also contains an unknown amount of poly-hydroxyalkanoates (PHA), which is a thermoplastic biopolymer, used to enhance printability and reduce the risk of filament breakage under printing. Compared to PLA, it has generally lower tensile strength (10–40 MPa) and stiffness (150–3500 MPa), depending on the composition of monomers [65]. Further, according to the Woodfill® product information recycled fine pinewood is used as the wood fibre component in the filament. P20TMP and P30TMP are compounded with virgin TMP fibres, which are expected to have a greater length-to-width ratio than recycled fibres and thus contribute more to the biocomposite strength

and stiffness [37,66].

Another important aspect is the difference in the manufacturing method. The 3D-printed panels are a structural build-up due to the layer-by-layer construction. Compared to the extruded panels, the 3D-printed ones can be seen as having several initial material defects. Voids form especially between the perimeter and the filling (Fig. 2) as well as between the single strands, depending on the printing parameters. Additionally, the layer-to-layer or strand-to-strand adhesion is considered as being less resistant to external loads than the material itself [37,67]. The difference in tensile as well as flexural strength and stiffness between moulded and 3D-printed parts with $\pm 45^\circ$ raster orientation seems to become even more significant when fibre reinforcements are used. This may be related to differences in fibre orientation. It is assumed that in extruded or moulded parts the fibres orientate along the flow direction [68]. This means that the fibres in the extruded samples are expected to be aligned longitudinally, while in the 3D-printed panels they are mainly aligned in 45° , resulting in lower mechanical properties [68].

It was verified that the material model from [42] can be used to evaluate different 3D printed sandwich designs relatively fast, simply and accurately. After finding a favourable design by FE-analysis, an extrusion tool was built as polymer extrusion might be more suitable for a time and cost-efficient mass production of biocomposite sandwich panels with unidirectional core stiffeners. The bending properties of extruded panels were shown to be predictable with sufficient accuracy by FE-analysis using the hyperelastic and perfectly plastic material model derived from tensile tests on injection moulded dogbones. For future evaluations of e.g., other biocomposite materials and extrusion tool designs, only one set of stress–strain data of the used material might be required to predict the approximate bending properties by FE-analysis.

5. Conclusions

In the present work, three different 3D-printed sandwich designs with unidirectional core stiffeners were physically tested and simulated based on a bimodular material model. Biocomposite material from PLA reinforced with 20 wt.% and 30 wt.% TMP-fibres was produced by compounding. Both biocomposite materials had superior tensile strength and stiffness compared to neat PLA and were used to fabricate the trapezoid panel design in profile extrusion, which has been considered a suitable manufacturing method for sandwich panels with unidirectional core stiffeners.

Comparing the three panel configurations, TR is the strongest and stiffest in bending considering a relative density of 0.5. This was strongly related to the increased face sheet thickness as demonstrated by calculating the panel rigidity analytically. Additionally, the flexural strength and stiffness of the 3D-printed panels could be predicted adequately (minimum and maximum error of + 4% to –17%) using FE-analysis.

Extrusion of TR biocomposite profile panels was successfully demonstrated as a proof of concept in an experimental extrusion line set-

up. Experimental and numerical assessment of the bending properties of extruded sandwich panels from P20TMP further confirmed the suitability of polymer extrusion for such biocomposite sandwich panels. The extruded biocomposite TR sandwich panels were about 27% stronger and 56% stiffer than the corresponding 3D-printed ones.

Sandwich panels with unidirectional core stiffeners were fabricated by 3D printing and profile extrusion from biocomposites. Importantly, in this study two different production methods were combined to bridge different development stages along with testing and prediction of properties of biocomposite materials.

Concludingly, polymer extrusion can be used to mass-produce stiff biocomposite panels with unidirectional core stiffeners and the approximate bending properties of those panels can be sufficiently predicted by using the presented hyperelastic and perfectly plastic material model in FE-analysis. The model required only one set of stress-strain data from a tensile test and the Poisson's ratio of the corresponding biocomposite material to provide satisfactory results. To take this research further and enable a wider applicability of wood fibre-reinforced biocomposites for material extrusion, long-term properties, such as creep, fatigue and environmental durability should be considered and studied to a greater extent.

CRedit authorship contribution statement

Chiara Zarna: Conceptualization, Methodology, Software, Validation, Formal analysis, Investigation, Data curation, Writing – original draft, Visualization. **Gary Chinga-Carrasco:** Resources, Writing – review & editing, Supervision, Project administration, Funding acquisition. **Andreas T. Echtermeyer:** Conceptualization, Methodology, Resources, Writing – review & editing, Supervision, Funding acquisition.

Declaration of Competing Interest

The authors declare that they have no known competing financial interests or personal relationships that could have appeared to influence the work reported in this paper.

Data availability

Data will be made available on request.

Acknowledgements

The Research Council of Norway and the companies supporting the ALLOC project (Grant no. 282310) are thanked for funding.

Appendix:

(See Table A1).

Table A1

Relative density of panels for 3-point bending experiments. The addition of “3D” refers to the 3D-printed panels and “P20TMP” and “P30TMP” to the extruded ones.

Specimen	Average Mass [g]	Approximate volume [cm ³]	Average approx. solid panel volume [cm ³]	Specimen density [g/cm ³]	Material density [g/cm ³]	Specimen relative density [g/cm ³]
CO_3D	52.7	41.6	85.7	0.61	1.27	0.49
AR_3D	49.1	42.0	85.4	0.57	1.17	0.49
TR_3D	51.4	42.1	85.7	0.60	1.22	0.49
TR_P20TMP	39.5	25.5	55.7	0.71	1.55	0.47
TR_P30TMP	36.6	25.5	54.9	0.68	1.43	0.47

References

- [1] Tarrés Q, Melbø JK, Delgado-Aguilar M, Espinach FX, Mutjé P, Chinga-Carrasco G. Bio-polyethylene reinforced with thermomechanical pulp fibers: Mechanical and micromechanical characterization and its application in 3D-printing by fused deposition modelling. *Compos B Eng* 2018;153:70–7.
- [2] Filgueira D, Holmen S, Melbø JK, Moldes D, Echtermeyer AT, Chinga-Carrasco G. 3D Printable Filaments Made of Biobased Polyethylene Biocomposites. *Polymers* 2018;10.
- [3] Serra-Parareda F, Vilaseca F, Espinach FX, Mutjé P, Delgado-Aguilar M, Tarrés Q. Stiffening Potential of Lignocellulosic Fibers in Fully Biobased Composites: The Case of Abaca Strands, Spruce TMP Fibers, Recycled Fibers from ONP, and Barley TMP Fibers. *Polymers* 2021;13.
- [4] Gregorova A, Hrabalova M, Wimmer R, Saake B, Altaner C. Poly(lactide acid) composites reinforced with fibers obtained from different tissue types of Picea sitchensis. *J Appl Polym Sci* 2009;114:2616–23.
- [5] Krapež Tomec D, Kariz M. Use of Wood in Additive Manufacturing: Review and Future Prospects. *Polymers* 2022;14:1174.
- [6] Winandy JE, Stark NM, Clemons CM. Considerations in recycling of wood-plastic composites. 2004.
- [7] Codari F, Lazzari S, Soos M, Storti G, Morbidelli M, Moscatelli D. Kinetics of the hydrolytic degradation of poly(lactide acid). *Polym Degrad Stab* 2012;97:2460–6.
- [8] Sin LT, Rahmat Abdul R, Rahman Wan AWA. 3 - Applications of Poly(lactide Acid). In: Ebnesajjad S, editor. *Handbook of Biopolymers and Biodegradable Plastics*. Boston: William Andrew Publishing; 2013. p. 55–69.
- [9] Tümer EH, Erbil HY. Extrusion-Based 3D Printing Applications of PLA Composites: A Review. *Coatings* 2021;11:390.
- [10] Le Duigou A, Castro M, Bevan R, Martin N. 3D printing of wood fibre biocomposites: From mechanical to actuation functionality. *Mater Des* 2016;96:106–14.
- [11] Ngo TD, Kashani A, Imbalzano G, Nguyen KTQ, Hui D. Additive manufacturing (3D printing): A review of materials, methods, applications and challenges. *Compos B Eng* 2018;143:172–96.
- [12] Yang T-C, Yeh C-H. Morphology and Mechanical Properties of 3D Printed Wood Fiber/Poly(lactide Acid) Composite Parts Using Fused Deposition Modeling (FDM): The Effects of Printing Speed. *Polymers* 2020;12:1334.
- [13] Kariz M, Sernek M, Obućina M, Kuzman MK. Effect of wood content in FDM filament on properties of 3D printed parts. *Mater Today Commun* 2018;14:135–40.
- [14] Mazzanti V, Malagutti L, Mollica F. FDM 3D Printing of Polymers Containing Natural Fillers: A Review of their Mechanical Properties. *Polymers* 2019;11:1094.
- [15] Zama C, Rodríguez-Fabiá S, Echtermeyer AT, Chinga-Carrasco G. Preparation and characterisation of biocomposites containing thermomechanical pulp fibres, poly(lactide acid) and poly(butylene-adipate-terephthalate) or poly(hydroxyalkanoates) for 3D and 4D printing. *Addit Manuf* 2022;59:103166.
- [16] Das AK, Agar DA, Rudolfsson M, Larsson SH. A review on wood powders in 3D printing: processes, properties and potential applications. *J Mater Res Technol* 2021;15:241–55.
- [17] Ghanbari A, Madhoushi M, Ashori A. Wood Plastic Composite Panels: Influence of the Species, Formulation Variables and Blending Process on the Density and Withdrawal Strength of Fasteners. *J Polym Environ* 2014;22:260–6.
- [18] Patil A, Patel A, Purohit R. An overview of Polymeric Materials for Automotive Applications. *Mater Today: Proc* 2017;4:3807–15.
- [19] Soury E, Behravesh AH, Nasrabadi HG, Zolfghari A. Design and Manufacture of an Extrusion Die for Wood—Plastic Composite. *J Reinif Plast Compos* 2008;28:1433–9.
- [20] Tarrés Q, Melbø JK, Delgado-Aguilar M, Espinach FX, Mutjé P, Chinga-Carrasco G. Micromechanics of Tensile Strength of Thermo-mechanical Pulp Reinforced Poly(lactide acid) Biodegradable Composites. *J Nat Fibers* 2022;1–14.
- [21] Vandi L-J, Chan CM, Werker A, Richardson D, Laycock B, Pratt S. Extrusion of wood fibre reinforced poly(hydroxybutyrate-co-hydroxyvalerate) (PHBV) biocomposites: Statistical analysis of the effect of processing conditions on mechanical performance. *Polym Degrad Stab* 2019;159:1–14.
- [22] Mohammadabadi M, Yadama V, Dolan JD. Evaluation of Wood Composite Sandwich Panels as a Promising Renewable Building Material. *Materials (Basel)* 2021;14.
- [23] Dweib MA, Hu B, O'Donnell A, Shenton HW, Wool RP. All natural composite sandwich beams for structural applications. *Compos Struct* 2004;63:147–57.
- [24] Barbirato GHA, Junior WEL, Martins RH, Soriano J, Fiorelli J. Experimental evaluation and numerical modeling of the mechanical performance of OSB sandwich panels manufactured with trapezoidal core. *Constr Build Mater* 2022;326:126721.
- [25] Briassoulis D. Equivalent orthotropic properties of corrugated sheets. *Comput Struct* 1986;23:129–38.
- [26] Wennberg D, Wenhage P, Stichel S. Orthotropic Models of Corrugated Sheets in Finite Element Analysis. *Int Scholarly Res Notices* 2011;2011:1–9.
- [27] Zaid NZM, Rejab MRM, Mohamed NAN. Sandwich Structure Based On Corrugated-Core: A Review. *MATEC Web Conf* 2016;74:00029.
- [28] Le Duigou A, Correa D, Ueda M, Matsuzaki R, Castro M. A review of 3D and 4D printing of natural fibre biocomposites. *Mater Des* 2020;194:108911.
- [29] Yang F, Fei B, Wu Z, Peng L, Yu Y. Selected Properties of Corrugated Particleboards Made from Bamboo Waste (*Phyllostachys edulis*) Laminated with Medium-Density Fiberboard Panels 2014;2014(9):12.
- [30] Kooistra GW, Deshpande V, Wadley HNG. Hierarchical Corrugated Core Sandwich Panel Concepts. *J Appl Mech* 2005;74:259–68.
- [31] Feng Y, Qiu H, Gao Y, Zheng H, Tan J. Creative design for sandwich structures: A review. *International Journal of Advanced Robotic Systems*. 2020;17:1729881420921327.
- [32] Zhang Z, Lei H, Xu M, Hua J, Li C, Fang D. Out-of-plane compressive performance and energy absorption of multi-layer graded sinusoidal corrugated sandwich panels. *Mater Des* 2019;178:107858.
- [33] Bernasconi A, Davoli P, Basile A, Filippi A. Effect of fibre orientation on the fatigue behaviour of a short glass fibre reinforced polyamide-6. *Int J Fatigue* 2007;29:199–208.
- [34] Liao Y, Liu C, Coppola B, Barra G, Di Maio L, Incarnato L, et al. Effect of Porosity and Crystallinity on 3D Printed PLA Properties. *Polymers (Basel)* 2019;11.
- [35] Agarwal BD, Broutman LJ, Chandrashekhara K. *Analysis And Performance Of Fiber Composites*. 3. ed: John Wiley & Sons Inc; 2006.
- [36] Halpin JC, Karoos JL. Strength of discontinuous reinforced composites: I. Fiber reinforced composites. *Polym Eng Sci* 1978;18:496–504.
- [37] Zama C, Opedal MT, Echtermeyer AT, Chinga-Carrasco G. Reinforcement ability of lignocellulosic components in biocomposites and their 3D printed applications – A review. *Composites Part C: Open Access*. 2021;100171.
- [38] Alhijazi M, Zeeshan Q, Qin Z, Safaei B, Asmael M. Finite element analysis of natural fibers composites: A review. *Nanotechnol Rev* 2020;9:853–75.
- [39] Xiong X, Shen SZ, Hua L, Liu JZ, Li X, Wan X, et al. Finite element models of natural fibers and their composites: A review. *J Reinif Plast Compos* 2018;37:617–35.
- [40] Moses DM, Prion HGL. Stress and failure analysis of wood composites: a new model. *Compos B Eng* 2004;35:251–61.
- [41] Soriano J, Fiorelli J, Lopes Junior WE, Barbirato GHA, Deldotti LR. Numerical modeling for adjustment of the equivalent moduli of elasticity of OSB layers estimated from experimental flexural rigidity. *J Mater Res Technol* 2021;14:1630–43.
- [42] Zama C, Chinga-Carrasco G, Echtermeyer A. Bending-properties and numerical modelling of cellular panels manufactured from wood fibre-PLA-biocomposite by 3D-printing. *Composites Part A: Applied Science and Manufacturing*. In press.
- [43] Araújo H, Leite M, Ribeiro AR, Deus AM, Reis L, Vaz MF. The effect of geometry on the flexural properties of cellular core structures. *Proceedings of the Institution of Mechanical Engineers, Part I: J Mater Des Appl* 2018;233:338–47.
- [44] Han B, Qin K, Yu B, Wang B, Zhang Q, Lu TJ. Honeycomb–corrugation hybrid as a novel sandwich core for significantly enhanced compressive performance. *Mater Des* 2016;93:271–82.
- [45] Bitzer T. Sandwich design. In: Bitzer T, editor. *Honeycomb Technology: Materials, Design, Manufacturing, Applications and Testing*. Dordrecht: Springer, Netherlands; 1997. p. 43–69.
- [46] Banjo AD, Agrawal V, Adu ML, Celestine A-DN. Moisture-induced changes in the mechanical behavior of 3D printed polymers. *Composites Part C: Open Access*. 2022;7:100243.
- [47] Niaounakis M, Kontou E, Xanthis M. Effects of Aging on the Thermomechanical Properties of Poly(lactide acid). *J Appl Polym Sci* 2011;119:472–81.
- [48] Kariz M, Sernek M, Kuzman M. Effect of humidity on 3D-printed specimens from wood-pla filaments. *Wood Research* 2018;63:917–22.
- [49] Zhiiani Hervan S, Altunkaynak A, Hardness PZ. friction and wear characteristics of 3D-printed PLA polymer. *Proc Inst Mech Eng, Part J: J Eng Tribol* 2021;235:1590–8.
- [50] Roy R, Mukhopadhyay A. Tribological studies of 3D printed ABS and PLA plastic parts. *Mater Today: Proc* 2021;41:856–62.
- [51] Tobajas R, Elduque D, Javierre C, Ibarz E, Gracia L. A comparative study of hyperelastic constitutive models for an automotive shaft seal material. *Int J Serv Comput Oriented Manuf* 2018;3:171.
- [52] Şerban DA, Marşavina L, Silberschmidt V. Behaviour of semi-crystalline thermoplastic polymers: Experimental studies and simulations. *Comput Mater Sci* 2012;52:139–46.
- [53] Smardzewski J, Wojciechowski K, Pozniak A. Auxetic Lattice Truss Cores Fabricated of LayWood. *BioResources* 2018;13.
- [54] Estakhriahaghghi E, Mirabolghasemi A, Zhang Y, Lessard L, Akbarzadeh A. 3D-Printed Wood-Fiber Reinforced Architected Cellular Composites. *Adv Eng Mater* 2020;22:2000565.
- [55] Carlsson J, Isaksson P. Dynamic crack propagation in wood fibre composites analysed by high speed photography and a dynamic phase field model. *Int J Solids Struct* 2018;144–145:78–85.
- [56] Zama C, Rodríguez-Fabiá S, Echtermeyer AT, Chinga-Carrasco G. Influence of Compounding Parameters on the Tensile Properties and Fibre Dispersion of Injection-Moulded Poly(lactide acid) and Thermomechanical Pulp Fibre Biocomposites. *Polymers* 2022;14:4432.
- [57] Yao T, Ye J, Deng Z, Zhang K, Ma Y, Ouyang H. Tensile failure strength and separation angle of FDM 3D printing PLA material: Experimental and theoretical analyses. *Compos B Eng* 2020;188:107894.
- [58] Bertram A, Glüge R. *Solid mechanics: Theory, modeling, and problems* 2015.
- [59] Wood polymer composites 2015;10:195–249.
- [60] Dean KM, Petinakis E, Meure S, Yu L, Chryst A. Melt Strength and Rheological Properties of Biodegradable Poly(Lactide Acid) Modified with Alkyl Radical-Based Reactive Extrusion Processes. *J Polym Environ* 2012;20:741–7.
- [61] Santos P, Valvez S, Monjon A, Reis P. The hybridisation effect on the viscoelastic properties of polymeric composites 2020.
- [62] Rezzui F, Swistek M, Hiver JM, G'Sell C, Sadoun T. Deformation and damage upon stretching of degradable polymers (PLA and PCL). *Polymer* 2005;46:7370–85.
- [63] Cifuentes SC, Frutos E, Benavente R, Lorenzo V, González-Carrasco JL. Assessment of mechanical behavior of PLA composites reinforced with Mg micro-particles through depth-sensing indentations analysis. *J Mech Behav Biomed Mater* 2017;65:781–90.
- [64] Suryanegara L, Nakagaito AN, Yano H. The effect of crystallization of PLA on the thermal and mechanical properties of microfibrillated cellulose-reinforced PLA composites. *Compos Sci Technol* 2009;69:1187–92.

- [65] Mehrpouya M, Vahabi H, Barletta M, Laheurte P, Langlois V. Additive manufacturing of polyhydroxyalkanoates (PHAs) biopolymers: Materials, printing techniques, and applications. *Mater Sci Eng C* 2021;127:112216.
- [66] Chinga-Carrasco G, Zarna C, Rodríguez-Fabià S, Leirset I, Tanase-Opedal M, Molteberg D, et al. Side streams from flooring laminate production – Characterisation and recycling in biocomposite formulations for injection moulding. *Compos A Appl Sci Manuf* 2022;153:106723.
- [67] Lay M, Thajudin NLN, Hamid ZAA, Rusli A, Abdullah MK, Shuib RK. Comparison of physical and mechanical properties of PLA, ABS and nylon 6 fabricated using fused deposition modeling and injection molding. *Compos B Eng* 2019;176:107341.
- [68] Kaynak C, Varsavas SD. Performance comparison of the 3D-printed and injection-molded PLA and its elastomer blend and fiber composites. *J Thermoplast Compos Mater* 2019;32:501–20.



A. VI List of presentations at international conferences

1. Zarna, Chiara; Carrasco, Gary Chinga; Echtermeyer, Andreas. (2022) Numerical modelling of bending properties of 3D printed biocomposites. ICCS25. A. J. M. Ferreira, Faculty of Engineering, University of Porto, Portugal; Porto, Portugal. 2022-07-19 - 2022-07-22.
2. Zarna, Chiara; Rodriguez Fabia, Sandra; Echtermeyer, Andreas; Chinga Carrasco, Gary. (2022) Influence of compounding parameters on the tensile properties and fibre dispersion of injection moulded polylactic acid (PLA) and TMP fibre biocomposites. CIADICYP 2022. University of Girona; Girona, Spain. 2022-06-28 - 2022-07-01.
3. Zarna, Chiara; Tanase Opedal, Mihaela; Echtermeyer, Andreas; Chinga-Carrasco, Gary. (2021) Micromechanical characterization of wood fibre-reinforced biocomposites. 5th International Conference on Natural Fibres; Online. 2021-05-17 - 2021-05-19.

ISBN 978-82-326-5670-7 (printed ver.)
ISBN 978-82-326-5224-2 (electronic ver.)
ISSN 1503-8181 (printed ver.)
ISSN 2703-8084 (online ver.)



NTNU

Norwegian University of
Science and Technology